Astrocyte cell surface marker phenotyping: Identification of multipotent ACSA-2^{-}/GLAST^{+} cerebellar progenitor cells

I n a u g u r a l – D i s s e r t a t i o n

zur

Erlangung des Doktorgrades

der Mathematisch-Naturwissenschaftlichen Fakultät

der Universität zu Köln

vorgelegt von
Christina Geraldine Kantzer
aus Essen

Köln, 2015

Berichterstatter/in: Prof. Dr. Elena I. Rugarli
Prof. Dr. Thomas Langmann

Tag der mündlichen Prüfung: 19.06.2015

Meiner Mutter

„Die Wege, die wir wählen, machen uns zu den Menschen, die wir sind“

Zusammenfassung

Astrozyten gehören zu den Gliazellen. Sie sind der häufigste Zelltyp im zentralen Nervensystem und besitzen morphologische und funktionelle Divergenz. Astrozyten sind nicht nur wichtige Metabolit Lieferanten, sondern auch ein Bestandteil der Blut-Hirn-Schranke. Sie regulieren Ionenkonzentrationen, sind an der Synaptogenese beteiligt und steuern synaptische Plastizität. Trotz ihrer Diversität sind Astrozytensubpopulationen bisher kaum funktionell charakterisiert. Dies liegt im Wesentlichen an der eingeschränkter Verfügbarkeit von geeigneten Markern. Ziel dieser Studie war die Phänotypisierung von Astrozytensubpopulationen anhand von Zelloberflächenmarkern. Mit Hilfe von magnetischer Zellsortierung sollten die Subtypen isoliert und anschließend funktionell und molekular untersucht werden. Der Astrozytenmarker GLAST ist ein Glutamat Aspartat Transporter, der von Astrozyten im ZNS exprimiert wird. Durch Verwendung eines für GLAST spezifischen Antikörpers können diese Zellen gezielt isoliert werden. Aus diesem Grund wurden GLAST positive Astrozyten als Ausgangspunkt für die Untersuchungen dieser Arbeit definiert. In einem Ansatz wurden GLAST positive Astrozyten isoliert, um mit Hilfe von Hybridomzelltechniken neue Antikörper gegen Astrozytensubpopulationen zu erhalten. Die Generierung von neuen Antikörpern war jedoch nicht erfolgreich. Ein weiterer Ansatz war die Identifikation von neuen Astrozytenzelloberflächenmarkern. Dieser Ansatz basierte auf einem durchflusszytometrischen Screening einer Antikörperbibliothek. Es wurden ingesamt 232 Zelloberflächenmarker auf ihre Expression auf Astrozyten getestet. In diesem Experiment wurden 15 Marker identifiziert, die anschließend mit Hilfe von Immunhistochemie (IHC) und *Multidimensional In Situ Cytometry Survey* (MICS) validiert wurden. In einem Parallelansatz wurde das Expressionsprofil und das Antigen des Anti-ACSA-2 (ACSA: Astrozytenzell-oberflächenantigen) Antikörpers untersucht. In Zusammenarbeit mit der Arbeitsgruppe von Dr. Harold Cremer am Institut de Biologie du Développement de Marseille wurde das Expressionsprofil von ACSA-2 über IHC, Immunzytochemie (ICC), MICS sowie per Durchflusszytometrie untersucht. Durch die Koexpression von ACSA-2 mit diversen Astrozytenmarkern konnte ACSA-2 als Astrozyten spezifischer Marker bestätigt werden, der nicht von Neuronen, Oligodendrozyten oder anderen nicht-astrozytären Zellen exprimiert wird. Western Blot Analysen, Immunprezipitationen und *Deglykosylierungs assays* deuteten darauf hin, dass der Anti-ACSA-2 Antikörper eine Zuckerstruktur auf Astrozyten erkennt. In weiterführenden Untersuchungen wurde das Expressionsprofil von GLAST und ACSA-2 auf embryonalem, neonatalem und adultem Maushirn mittels IHC, ICC und per Durchflusszytometrie getestet. ACSA-2 und GLAST zeigten ein unterschiedliches Expressionsprofil in verschiedenen Hirnregionen, in der Retina und im Rückenmark von neonatalen Mäusen. Es folgten weitere Expressionsanalysen von GLAST und ACSA-2 in Stammzellregionen. Die Expression von ACSA-2 in der subventrikulären Zone (SVZ) wurde anhand von IHC, *in vivo* Elektroporation und Durchflusszytometrie untersucht. Hierbei konnte gezeigt werden, dass GLAST und ACSA-2 in der adulten SVZ koexprimiert vorliegen. Unterschiedliche Expressionsmuster wurden ferner im *rostral migratory stream* und im Hippocampus von adulten Maushirnschnitten detektiert. Jedoch war es nicht möglich, die Unterschiede auf Einzelzellebene zu bestätigen. Signifikante Expressionsunterschiede zwischen GLAST und ACSA-2 wurden im Cerebellum von adulten Maushirnschnitten identifiziert. In anschließenden Untersuchungen wurde die Herkunft dieser Zelltypen in der cerebellaren Entwicklungsphase (E13-P12) analysiert. Hierbei wurde eine ACSA-2^-/GLAST$^+$ und eine ACSA-2^+/GLAST$^{+/-}$ Zellpopulation identifiziert. Die größten Expressionsunterschiede lagen zwischen E17 und P3 vor. Zudem sank die Frequenz an ACSA-2^-/GLAST$^+$ Zellen in der weiteren Entwicklung. Beide Zellpopulationen wurden per magnetischer Zellsortierung mit hoher Reinheit angereichert und anschließend mittels ICC, *Neurosphere assay*, Genexpressionsanalysen und Zelltransplantation untersucht. Zudem wurde ein *in vivo* Zelldifferenzierungs Assay mit isolierten ACSA-2^-/GLAST$^+$ und ACSA-2^+/GLAST$^{+/-}$ Zellen aus dem Cerebellum von β-actin GFP Mäusen durchgeführt. Diese Experimente fanden in Kollaboration mit der Arbeitsgruppe von Dr. Annalisa Buffo am Neuroscienze Institute Cavalieri Ottolenghi in Turin statt. Die Analyse zeigte, dass ACSA-2^-/GLAST$^+$ Zellen in Interneurone, Bergmann glia, Astrozyten and Oligodendrozyten differenzieren konnten. Im Gegenzug, konnten ACSA-2^+/GLAST$^{+/-}$ Zellen nur in Astrozyten und Oligodendrozyten differenzieren. Genexpressionsanalysen beider Zellgruppen zeigten, dass Stammzellfaktoren und Gene für einen GABAergen Phänotyp in den ACSA-2^-/GLAST$^+$ Proben angereichert waren (*Gli1, Wif1, Nestin, Ptf1a, Ascl-1*). Gene, die Zellinteraktion und Zelladhäsion kodieren (*Gjb2, Gjb6, Gja1, Vitronectin*), waren in den ACSA-2^+/GLAST$^{+/-}$ Proben angereichert.

Zusammenfassend zeigt diese Studie eine regionale, funktionale und molekulare Charakterisierung von Astrozyten anhand von Zelloberflächernmarkern. Anhand dieser Charakteristika wurde eine neue ACSA-2^-/GLAST$^+$ multipotente Zellvorläuferpopulation im Cerebellum identifizieren.

Abstract:

Astrocytes, a member of the glial cell family, are the most abundant neural cell type of the central nervous system (CNS) and present functional and morphological heterogeneity. Among other characteristics, astrocytes provide trophic functions, are essential for the formation of the blood-brain barrier, regulate ion homeostasis, synaptogenesis and synaptic plasticity. Despite their diversity astrocyte subpopulations are not well characterized mainly due to the lack of markers that could classify functional subclasses. This study aimed at the phenotyping of astrocyte subpopulations based on cell surface marker expression, their prospective isolation and subsequent molecular and cellular characterization of the identified subsets. The glutamate aspartate transporter (GLAST) is a common astrocyte marker expressed by astrocytes in the CNS. As the GLAST antibody allows for the isolation of astrocytes it was chosen as principal component for the identification of astrocyte subpopulations. One approach, which was not successful, was the generation of novel monoclonal astrocyte subpopulation specific antibodies using GLAST isolated astrocytes and hybridoma techniques. Another approach was the identification of novel astrocyte markers by flow cytometry. 232 cell surface markers were tested for their expression on astrocytes. In total, 15 candidates were identified and subsequently validated by immunohistochemistry (IHC) and the recently established in house technology: Multidimensional *In Situ* Cytometry Survey (MICS). The expression profile and the nature of the target of the novel Anti-ACSA-2 (ACSA: astrocyte cell surface antigen) antibody were addressed. In co-operation with the group of Dr. Harold Cremer at the Institut de Biologie du Développement de Marseille, the expression profile of the ACSA-2 antigen was analyzed systematically using IHC, immunocytochemistry (ICC), MICS and flow cytometry. Co-expression of ACSA-2 with common astrocyte markers such as GFAP, S100β and GLAST and missing expression on neurons, oligodendrocytes validated ACSA-2 as an astrocyte specific marker. Additional Western Blot analysis, immunoprecipitation and deglycosylation assays pointed out the ACSA-2 antibody addresses a glycosylation structure expressed by astrocytes. In the next step, the expression profile of ACSA-2 and GLAST was investigated in comprehensive analyses of embryonal, neonatal and adult mouse brain using IHC, ICC, MICS, and flow cytometry. ACSA-2 and GLAST demonstrated differential marker expression in distinct brain regions, retina and spinal cord of neonatal mice. Additional studies addressed ACSA-2 and GLAST expression on neural stem cells. The expression of ACSA-2 in the subventricular zone (SVZ) was analyzed using IHC, *in vivo* electroporation and flow cytometry. ACSA-2 was demonstrated to be co-expressed with GLAST in the adult SVZ as shown by IHC and flow cytometry. Differences between ACSA-2 and GLAST expression were also identified in the rostral migratory stream (RMS) and hippocampus of the adult mouse brain. However, these differences could not be confirmed on the single cell level by flow cytometry. Cerebellar glia revealed significant differences in GLAST and ACSA-2 expression in the adult mouse brain. To address the origin of these potential subpopulations GLAST and ACSA-2 expression was monitored between E13 and P12 in the developing cerebellum. Thereby, ACSA-2^-/GLAST$^+$ and ACSA-2^+/GLAST$^{+/-}$ cells were identified. Populations were most discriminative between E17 to P3 and frequencies of ACSA-2^-/GLAST$^+$ cells decreased with the onset of development. Both fractions were isolated to high purities by magnetic cell sorting. Cell characteristics were addressed by ICC, neurosphere assay, gene expression profiling and transplantation assay. Cell differentiation *in vivo* was investigated in collaboration with the group of Dr. Annalisa Buffo at the Neuroscienze Institute Cavalieri Ottolenghi in Turin. ACSA-2^-/GLAST$^+$ and ACSA-2^+/GLAST$^{+/-}$ cells were isolated from the cerebellum of P0-P3 β-actin GFP mice and grafted into cerebellum of homochronic wild-type mice. ACSA-2^-/GLAST$^+$ cells were able to differentiate into interneurons (stellate and basket cells), Bergmann glia, astrocytes and oligodendrocytes. In contrast, ACSA-2^+/GLAST$^{+/-}$ cells only differentiated into astrocytes and oligodendrocytes. Gene expression profiling was performed to address differences on the transcriptome level. Genes related to a multipotent and GABAergic phenotyp were enriched in the ACSA-2^-/GLAST$^+$ sample set (*Gli1, Wif1, Nestin, Ptf1a, Ascl-1*). Genes involved in cell-cell interactions as well as cell matrix proteins (*Gjb2, Gjb6, Gja1, Vitronectin*) were enriched in the ACSA-2^+/GLAST$^{+/-}$ sample set.

In conclusion, this study presents a regional, functional and molecular discrimination of astrocyte subpopulations based on specific cell surface markers. As a result it describes the identification of a novel ACSA-2^-/GLAST$^+$ subpopulation of astrocytes which act as multipotent progenitors in the cerebellum.

Abbreviations:

ACSA	Astrocyte cell surface antigen
Aldh1l1	Aldehyde dehydrogenase
BSA	Bovine serum albumin
BLBP	Basic lipid binding protein
BMP	Bone morphogenic protein
CD	Cluster of differentiation
CHO	Chinese Hamster Ovary cell line
CNS	Central nervous system
DAPI	4′,6-Diamidin-2-phenylindol
DMEM	Dulbecco's Modified Eagle's Medium
DMSO	Dimethylsulfoxide
DPBS	Dulbecco's Phosphate Buffered Saline
E	Embryonic day
EGFP	Enhanced green fluorescent protein
EGL	External granule layer (Cerebellum)
EDTA	Ethylen-diamine-tetra-acetate
EGF	Epidermal growth factor
FGF	Fibroblast growth factor
FSC	Forward scatter
Gcl	Granule cell layer
GFAP	Glial fibrillary acidic protein
GLAST (ACSA-1)	Na^+-dependent L-glutamate/L-aspartate transporter
GS	Glutamine synthetase
h	Hour
ipl	Inner plexiform layer (olfactory bulb)
HEPES	4-(2-hydroxyethyl)-1-piperazineethanesulfonic acid
HBSS	Hank's Balanced Salt Solution
IBDM	Institut de Biologie du Développement de Marseille
LB	Luria-Bertani medium
LRC	Ligand receptor capturing
MAP2	Microtubule-associated protein 2
Mcl	Molecular cell layer
mi	Mitral cell layer (olfactory bulb)
min	Minutes
MICS	Multidimensional *in situ* Cytometry Survey
mL	Milliliter
mM	Millimolar
MOPS	3-(*N*-morpholino)propanesulfonic acid
ms	Millisecond
NPC	Neural precusor cell
NSC	Neural stem cell
NTDK (T)	Neural Tissue Dissociation Kit (Trypsin)
NTDK (P)	Neural Tissue Dissociation Kit (Papain)
NTDK (PN)	Neural Tissue Dissociation Kit (Postnatal neurons)
OB	Olfactory bulb
o/n	Over night
P	Postnatal day
PAGE	Polyacrylamid gel elektrophoresis
PB	PBS buffer supplemented with 5%BSA
PC	Purkinje cell
Pcl	Purkinje cell layer
PBS	Phosphate buffered saline
Pen/Strep	Penicillin/Streptomycin
PI	Propidium Iodid
PNS	Peripheral nervous system
PSA-NCAM	Polysialyated cell-adhesion molecule
PVZ	Periventricular Zone
PWM	Prospective white matter
SDS	Sodiumdodecylsulfa

µm	Micrometre
µM	Micromolar
RT	Room temperature
RIN	RNA Integrity number
RMS	Rostral migratory stream
RPMI-1640	Medium composed at the Roswell Park Memorial Institute
SHH	Sonic hedgehog
SSC	Side scatter
SVZ	Subventricular zone
TAE	Tris base; EDTA; acetic acid containing buffer
TBS	Tris Based Saline
v/v	Volume concentration (voume/volume)
VZ	Venricular Zone (4^{th} ventricle)
WGA	Wheat germ agglutinin
wt	wild-type

Table of contents:

1 Introduction

1.1 Function and heterogeneity of astrocytes

During very early embryonic development three primary cell sources, the three germ layers are formed: the ectoderm, mesoderm and endoderm. The central nervous system (CNS) arises from the ectodermal germ layer. In this step of neural induction, organizers trigger the development of the neuro-ectoderm [1]. Further differentiation of the neuro-ectoderm forms the neural plate. In a subsequent step, called neurulation, the lateral edges of the neural plate fold dorsally, fuse and give rise to the neural tube. Through formation of three primary brain vesicles, that give rise to five secondary brain vesicles, various structures of the adult brain are obtained [2].

This work focuses on the most abundant cell type of the CNS: the astrocytes, also named astroglia. They comprise 25-50% of total brain volume and outnumber neurons by the ratio of 10:1 in rodents [3,4]. Astrocytes are non-neuronal cells that compose the subset of glia together with myelin-forming oligodendrocytes and microglia, derivatives of hematopoietic cells also named as macrophages of the brain. Further members of the glial cell family are NG2 cells, and Schwann cells, the oligodendrocyte equivalents of the peripheral nervous system (PNS). Historically, glia have been considered as passive supporters that act like a glue for the brain. At time of their discovery, in the 18th century by Rudolf Virchow, astrocytes were classified as non-excitable cells. Indeed, in comparison to neurons astrocytes are electrically non-excitable [5,6]. However, their excitability is executed by the propagation of calcium signals as a mediator of bi-translational interactions between neurons and glia at the tripartite synapse [7]. Astrocytes are coupled to each other by gap junctions [5]. These gap junctions are permeable for ions, such as potassium, sodium or calcium, small molecules, including nucleotides, cAMP, sugars, and peptides [8]. The flow of small molecules and ions serves as a mean of intercellular communication. Communication between astrocytes is initiated by a calcium influx and propagated to neighboring cells through calcium waves [9,10]. Hippocampal astrocytes were demonstrated to be connected to up to 100,000 synapses [11]. Furthermore, intracellular signaling in astrocytes is triggered by cell-cell contact with neuronal dendrites and synapses [12,13]. Astrocytes also promote synaptogenesis and are an essential element of the tripartite synapse, which is composed of astrocytes, the pre- and the postsynaptic terminal at the synaptic cleft [14,15]. Furthermore, astrocytes have housekeeping functions and are involved in several metabolic pathways. They do not only facilitate the clearance of neurotransmitters at the synaptic cleft [16] but also actively secrete metabolites, called gliotransmitters [17,18] such as D-serine, ATP [18,19], thrombospondins[15] cholesterol[20] as well as growths factors such as

brain-derived neurotrophic factor (BDNF) or nerve growth factor (NGF) [21]. Another important metabolic function is the conversion of glutamate into glutamine catalyzed by the enzyme glutamine synthetase (GS). Astrocytes release glutamine at the presynaptic terminal. Glutamine is subsequently taken up by surrounding neurons and converted into glutamate [22,23]. In addition, astrocytes regulate the pH level and brain homeostasis [24,25,26] through ion channels such as sodium, potassium [27,28] and water channels called aquaporins [11,12]. Furthermore, astrocytes are the major source of extracellular matrix (ECM) proteins and cell adhesion molecules [29]. They secrete different matrix metalloproteases (MMPs) which are important for the remodeling of the ECM [30]. In addition to their functional divergence, astrocytes represent morphological and functional heterogeneity linked to different brain regions or developmental time-points [31]. The most prominent example for morphologically different astrocytes are fibrous astrocytes of the white matter and protoplasmic astrocytes of the gray matter [32]. The functions of astroglia during development were first addressed by Rakic *et al.* [32]. They demonstrated that radial glia, primary progenitors of the developing CNS, a subgroup of astroglia, are essential for the differentiation and guidance of neurons during development [33]. Similar observations were made in the developing cortex and the rostral migratory stream (RMS) [34,35]. In this context it was demonstrated that neuronal guidance is mainly driven by the interaction between members of the Slit family, expressed by astrocytes, and Robo receptors, expressed by neurons [36,37]. Furthermore, astrocytes are an essential element of the blood-brain barrier, a physical barrier around blood-vessels formed by astrocyte perivascular endfeet, endothelial cells and pericytes [38]. In a healthy organism, this barrier separates the blood system from the CNS. Only certain gas molecules such as oxygen or carbon dioxide and small lipophilic agents can pass this barrier by passive diffusion. Some other small molecules such as glucose or amino acids can be selectively transported [38].

Apart from these general properties of astrocytes their functions in the diseased brain were addressed. On the one hand, astrocytes were reported to be mediators of neurodegenerative disorders. On the other hand, astrocytes are considered to be targets for translational or regenerative medicine. Their self-renewing capacities and the possibility to use them for trans-differentiation [39,40] are valuable for clinical approaches. In respect to all the distinct functional properties of astrocytes, it is apparent that astrocytes are not a uniform subset but rather composed of various subpopulations.

1.2 Radial glia

The CNS of vertebrates consists of neurons and glia that derive from multipotent neuroepithelial progenitor cells of the neural tube. During initiation, multipotent neuroepithelial cells of the ectoderm undergo rapid symmetric cell division. They fold and form the neural plate, which then forms the neural tube via Sonic hedgehog (SHH), bone morphogenic protein (BMP) and Wnt signaling [41]. In the next step, neuroepithelial cells polarize and divide asymmetrically. These cells give rise to radial glia a more restricted progenitor population in the early prenatal state [42-44] (Figure (Fig.) 1.1 a). Radial glia are characterized by a long, radial, bipolar shape and span from the ventricular zone towards the pial surface [45]. This cell type was first described by Golgi in 1873. Later, Ramon y Cajal and Magini reported about the significance of radial glia during development [46]. Radial glia belong to the astroglia subset. They express a panel of astrocyte specific markers such as GFAP (absent in rodents) [47], Tenascin C, GLAST [48], glycogen granules [49], and BLBP [50]. Besides, radial glia express neuroepithelial cell markers such as Nestin [51] and the intermediate-filament associated protein RC2 [52,53]. In the first period of development, radial glia serve as scaffold for migrating neuroblasts [54] and as a source for new neurons [55] (Fig. 1.1 b,c). At the end of developmental neurogenesis radial glia disappear or transform into astroglia [56,57]. However, it could be demonstrated that some radial glia subtypes persist as the Bergmann glia in the cerebellum, as Müller glia in the retina and as neural stem cells in the SVZ and hippocampus [58-62].

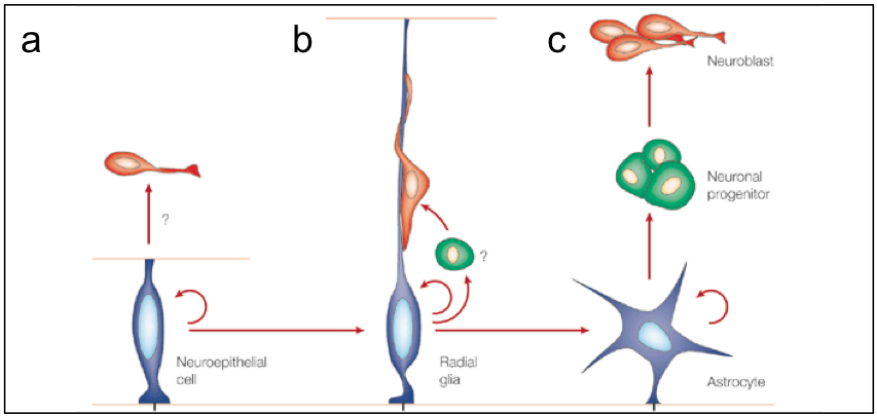

Figure 1.1: Radial glia during development.
Early in development cells of the neuroepithelium, the mutipotent neuroepithelial cells undergo rapid symmetric cell division. During embryonic development and around birth neuroepithelial cells transform into radial glia cells (a). By asymmetric division, radial glia generate pools of transit amplifying cell types or transform into neurons (b). Radial glia postnatally and transform directly into cortical astrocytes. Some radial glia transform intoneuronal stem cells residing in the SVZ and behave as stem cells that can self-renew and give rise to neurons (c). Modified from Alvarez-Buylla *et al*. (2001) [45].

1.3 Neural stem cells

Among the features of astrocytes, their stem cell characteristics are of great interest. Since their discovery in the 1980s [63], research on NSCs has increased dramatically due to the potential of NSCs to cure neurodegenerative diseases. Pioneering studies on neurogenesis were conducted by Altman *et al.* and Kaplan *et al* [64,91]. The classical model of adult neurogenesis is restricted to two neurogenic niches. However, recent studies demonstrated that neurogenesis is not restricted to these two niches and occurs also in other brain areas as demonstrated for the striatum in human brain [65]. One classical neurogenic niche is the subventricular zone (SVZ) of the lateral ventricle. The other one is the dentate gyrus of the hippocampus. Both areas are bilaterally located in the fore- and midbrain. In contrast to other germinal layers, the SVZ of the forebrain persists after birth. In the 1990s several groups discovered multipotent neural stem cells in the developing mouse brain [63,66,67]. In 1999 Doetsch *et al.*[68] characterized these multipotent stem cells of the SVZ as astrocytes based on morphology and marker expression. In a coronal section, the SVZ is shaped like a triangle composed of three walls as depicted in (Fig. 1.2 a). The medial wall contacts the septum. The dorsal wall adjoins the corpus callosum and contacts the lateral wall at the dorsal horn. The lateral wall flanks the striatum. Neural stem cells are commonly isolated from the lateral wall of the SVZ, which is assembled by different cell layers and distinct cell types classified as Type A, B, C, and E cells. The edge of the ventricle is composed of ependymal cells that derive from radial glia [69] (Type E cells), as seen in Figure 1.2 b,c. The ependymal cell layer is tightly connected with slowly proliferating Type B1 cells and a further source of astrocytes [69] the B2 cells that regulate local environment. Type B1 cells are the neural stem cells and are characterized by the expression of common astrocyte markers [70,71]. Since neural stem cells and ependymal cells express mutual astrocyte markers such as epidermal growth factor receptor (EGFR) or GFAP [71] there is a demand to identify a specific stem cell marker. So far, the isolation of neural stem cells is executed using at least two markers in combination, such as GLAST, GFAP, EGFR and Prominin-1 [72,73-75]. *In vivo*, Type B cells of the lateral wall of the SVZ generate transit amplifying precursors (Type C cells), that generate neuroblasts (Type A cells) (Fig. 1.2 b,d). These neuroblasts are characterized by the expression of polysialyted-neural cell adhesion molecule (PSA-NCAM)[76,77]. In the SVZ, neuroblasts are surrounded by Type B and Type C cells. After their generation in the SVZ, neuroblasts follow the RMS along a posterior-anterior axis towards the olfactory bulb [78]. The RMS is composed of 'tunneling astrocytes' that guide the way towards the olfactory bulb. Astrocytes support the migration progress by the secretion of soluble molecules (e.g. growth factors), the expression of matrix proteins, cell-cell contacts as well as

receptor-ligand interactions (e.g. Slit and Robo) [37,79]. In the olfactory bulb neuroblasts migrate to their final location and differentiate into olfactory bulb interneurons.

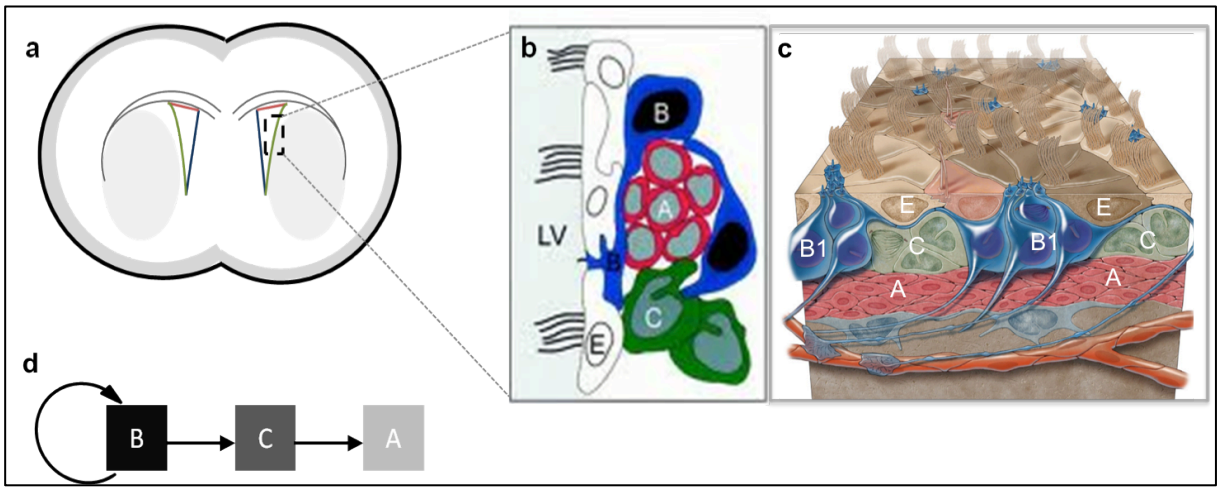

Figure 1.2: The lateral ventricle of the adult mouse brain.
One neurogenic area in the adult brain is the subventricular zone (SVZ). The SVZ is composed of a dorsal (red) a lateral (green) and a medial wall (blue)(a). Cells of the lateral wall are classified as Type A, B, C and E cells (b,c)[80,81]. Type B cells are the neural stem cells that give rise to transit amplifying (Type C cells) that generate migratory neuroblasts (Type A cells) (d). Modified from Alvarez-Buylla *et al.* (2002) and Mizadeh *et al.* (2008) [80,81].

1.4 Identification of astrocyte subpopulation specific markers

Astrocytes are phenotypically diverse and their tasks differ in respect to their localization. Hence, the marker expression profile of astrocytes is strongly correlated to their localization, developmental status and interaction with other cell types. The first sub-classification study was carried out by immunohistochemistry in 1984 [82]. This study was based on morphology, regional distribution and marker expression. The study identified two major astrocyte populations: the protoplasmic astrocytes and the fibrous astrocytes. Protoplasmic astrocytes are located in the grey matter, have short processes, many branches typically ensheath synapses and express the intermediate filament glial fibrillary acidic protein (GFAP) [11,83,84]. Fibrous astrocytes are located in the white matter, have long unbranches processes and are characterized by a weaker expression of GFAP [32]. Besides GFAP, other common astrocyte markers such as glycogen granules, glutamate transporter (GLT-1) and GS were identified [85-87]. In 2008, aldehyde dehydrogenase (Aldh1l1) was identified as a novel astrocyte specific marker by comprehensive microarray analysis [88]. Aldh1l1 is a more robust marker than GFAP, as GFAP is exclusively found on terminally differentiated astrocytes and not expressed by quiescent astrocytes in healthy tissue [89,90]. In addition, first subtype specific markers like calcium-binding protein, S100β, or potassium channel, Kir4.1,

were identified [91-93] using single-cell gene expression profiling [94] or electrophysiological studies [95]. Another subtype marker, Aquaporin-4, a water channel, was identified by transcriptome analysis comparing primary and cultivated astrocytes, neurons and neural stem cells (NSCs) from distinct ages and distinct brain regions [96]. Aquaporin-4 was demonstrated being exclusively expressed on astrocyte endfeet [97]. Unfortunately, the majority of the mentioned markers are intracellular proteins. Therefore, these markers cannot be used for direct isolation and further characterization of living cells. To this aim, several transgenic mouse lines were generated. These mouse lines enable for the isolation of potential astrocyte subpopulations through expression of a reporter gene under an astrocyte specific promoter (e.g. Aldh1L1, BLBP, S100β, GFAP, GLT-1, GLAST [98,99,98,100-103]). The first approach to isolate astrocytes from primary tissue of wild-type (wt) mice was realized in 2012 by the generation of a novel Anti-GLAST antibody [104].

1.5 Reactive Astrocytes

Trauma, neurodegeneration or other CNS insults cause tissue damage which influences neurons and glia and hampers their interaction [105-108]. Upon tissue damage, activated microglia migrate to the affected tissue and initiate first immune response [109-112]. Microglia also produce reactive oxygen species (ROS)[113] and nitric oxide (NO) which cause oxidative stress that leads to damage and aging of cells [114,115]. While NO species can be neutralized by the glutathione metabolites produced by astrocytes, ROS and reactive nitrogen species (RNS) lead to the phosphorylation of STAT6, a stress sensor. This phosphorylation up-regulates expression of cyclooxygenase-2 (COX-2) and induces release of pro-inflammatory cytokines. In addition, the STAT6 phosphorylation induces the release of PGE_2 and prostacyclin. COX-2 activates neighboring cells e.g. astrocytes [116-118]. Activation of astrocytes is called reactive gliosis [119]. Upon reactive gliosis astrocytes undergo biochemical, morphological and physiological changes. They start to proliferate, modify the expression of cellular markers, become hypertrophic [120], increase the production of intermediate filaments [121] and migrate to the side of injury to form a glial scar. This is a cellular attempt to prevent further tissue damage and spread of the disease as the scar separates healthy tissue from injured tissue [122,123].

There is currently no exclusive cell-surface marker is described that allows for the discrimination of reactive astrocytes from non-activated astrocytes in the diseased brain. Furthermore, several markers of reactive astrocyte address intracellular epitopes or transcription factors. Therefore, these markers do not allow for further isolation and characterization of viable reactive astrocytes. The most common marker to study reactive

astrocytes is GFAP [119,121]. Other astrocyte markers, that are upregulated on reactive astrocytes are S100β, BLBP [122], vimentin [124] or Nestin are also used to discriminate reactive astrocytes.

1.6 Cerebellum

1.6.1 Development of the cerebellum

The brain is composed of three main areas named as *Prosencephalon* (Forebrain), *Mesencephalon* (Midbrain) and *Rhombencephalon* (Hindbrain). Each region itself consists of region specifc areas. Major part of this study was performed in the cerebellum, which is part of the *Rhombencephalon* (Hindbrain).

The cerebellum is important for voluntary movement and motor function, as demonstrated in the early 19th century by three neurophysiologists: Luigi Roland, Marie-Jean-Pierre Flourens and John Call Dalton, Jr. [125]. Further reports also showed that the cerebellum has an impact on higher cognitive functions, cognitive progression and behavior [126]. Besides, the cerebellum is affected in several diseases like ataxia, schizophrenia, and autism [127]. In addition, uncontrolled growth of cerebellar precursors results in medullablastoma the most common malignant brain tumor in children [128].

Although the cerebellum comprises only 10% of the total brain volume, granule neurons account for 50% of all brain neurons [129]. The cerebellum is one of the best-studied brain region in respect to circuitry [130], development [54], anatomy and fiber connectivity [131]. During ontogeny the cerebellum arises from the met-mesencephalic junction of the neural tube [132] around embryonic day 9 (E9) in mice [133]. At the initiating phase (E9- E12) the cerebellum conducts a 90° rotation from the anterior-posterior axis towards the medial-lateral axis. This results in a bilateral wing-like morphology [134]. Early developmental steps are driven by specific proteins such as the transcription factors Hoxa2 (posterior) and Oxt2 (anterior) are further accompanied by soluble molecules of the Wnt and FGF families (especially fgf8) [129].

After several structural modification steps, the cerebellum obtains its foliated structure. Anatomically, the mammalian cerebellum is composed of 10 primary lobules (Fig. 1.4 a), first characterized by Olof Larsell (1970) [135,136]. The cardian lobes are formed at embryonic stage while lobules and sub-lobules are formed at postnatal stage [137]. Although the foliation process starts around E14 in mice [138], the maturation of the architecture lasts until adulthood.

1.6.2 Cerebellar progenitors

The progenitor pools of the cerebellum derive from two distinct germinal territories: the ventricular zone of the fourth ventricle and the rhombic lip, as demonstrated by Alvarado-Mallart and Le Dourian [132,139]. It is suggested that cells of the deep cerebellar nuclei (DCN) arise from both germinal matrices. The ventricular zone (VZ) is located at the inner germinal layer, where interneurons arise around E12.5. These interneurons can be distinguished by the expression of Pax-2 [140], and Pft1-a which is exclusively expressed by GABAergic projection neurons [141,142]. Cells of the deep nuclei arise from the cerebellar plate around E10.25 [143]. These cells become post mitotic and form a „mantle“ above the VZ [144,145]. Between E11 and E14.5 cortical precursor cells of the VZ exit the cell cycle. These are Purkinje cell precursors that start to express calbindin [146] and migrate radially along radial glia processes [147], compare Figure 1.3. These precursors pass the „mantle“ of deep cerebellar nuclei and settle down in the prospective white matter just beneath the developing granule cell layer (Gcl) [148]. In this region, Purkinje cell precursors form a multilayer of immature neurons (E14-E17). Then, Purkinje cell precursors differentiate and start to interact with parallel fibers [146]. By maturation, the multilayer disperses and a Purkinje cell monolayer appears (Fig. 1.3 c). Once the Purkinje cell monolayer is formed, interneurons such as stellate, basket and Golgi cells are generated from precursors of the deep (prospective) white matter [129,149].

The second major germinal matrix is the rhombic lip, an external layer located close to the roof plate of the neuroepithelium. This external germinal layer (EGL) arises around E12.5 and gives rise to all types of glutamatergic cells. A pool of migrating cells, which derives from this germinal matrix, contributes to the cerebellar nuclei [37]. The EGL is a highly proliferative cell source, which produces granule neurons [150,151] regulated by SHH and Wnt signaling pathways [152,153]. Cells of the EGL are characterized by the expression of Math1, a helix-loop-helix transcription factor [154]. EGL cells proliferate rapidly between E13 and P15, highest at P8 [143]. Upon birth until P14, cells at the EGL exit cell cycle and start to migrate inwards along Bergmann glia. Migrating granule cells pass through the developing Purkinje cell layer and settle down at the developing internal Gcl [54,146,155,156]. An important molecule involved in this migration process is Reelin [157] and the extracellular protein Astrotactin, which is expressed by migrating neurons in the cerebral cortex and the cerebellum [158-160]. The migration stops soon after the disappearance of the EGL. The final differentiation step of Purkinje cells and granule cells is depending on their interplay and results in the arborisation of Purkinje cells [31,32]. This interaction is also depending on Reelin, BDNF and SHH signaling [161].

Glial cells of the cerebellum were first described by Ramon y Cajal in 1911. The majority of cerebellar glia derives from the ventricular neuroepithelium (VN) [162] and shares a common

ancestor with neurons [163]. The key regulator for glial versus neuronal fate in the VN compartment is considered to be Notch and BMP dependent [164]. Two minor fractions of glial cells originate from the rhombic lip. One is the unipolar brush cell, which migrates towards the white matter [165]. The other fraction migrates tangentially over the cerebellar surface. This cell type is remained postnatally and expresses GFAP [166]. In addition, this cell type expresses Math1 and can differentiate into granule cells [167]. Upon isolation and SHH treatment these progenitors differentiate into astrocytes *in vitro* showing a multipotent potential [168].

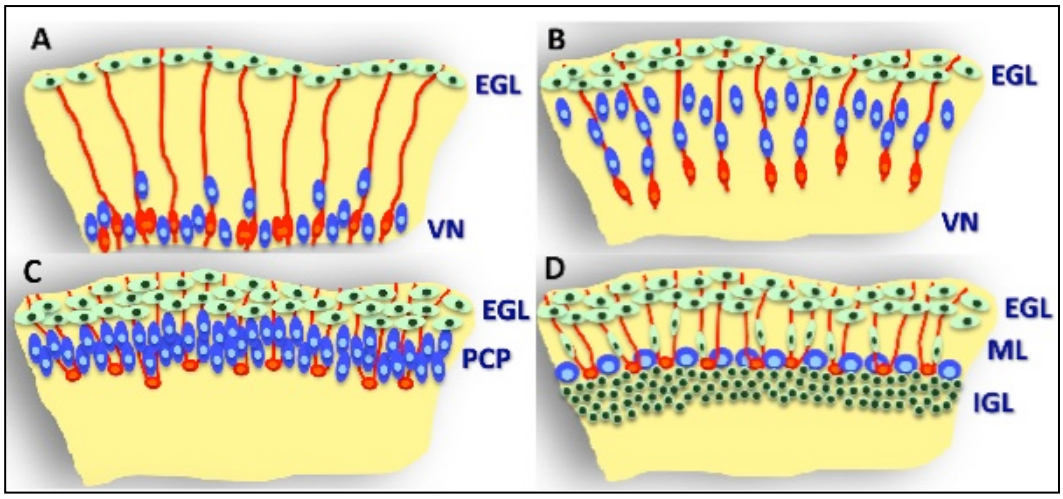

Figure 1.3: Bergmann glia in cerebellar corticogenesis.
Purkinje cells (blue) in the embryonic cerebellum (A) are generated by radial glia (red) in the ventricular neuroepithelium (VN) and migrate along radial glia procresses (red). In the external granular layer (EGL) granule cell precursors (green) are generated. Around birth radial glia transform into Bergmann glia (B). Thereby loosing their connection to the cortex (B). Next, Bergmann glia spread their processes towards the pial surface (B). Purkinje cells cluster in the Purkinje cell plate (PCP) beneath the EGL (C). At postnatal development (D), granule cells migrate inwards along Bergmann glia. Purkinje cells acquire a monolayer arrangement. The interaction between granule cells and Bergmann glia leads to the expansion of the molecular layer (ML) and the internal granule cell layer (IGL). Modified from Buffo *et al.* (2013) [169].

1.6.3 Composition of the cerebellum at adult state

A fully developed cerebellum comprises a four-layer-structure (Fig. 1.4 b) composed of distinct cell types [170]: The inner cell layer of the adult cerebellum is the white matter, which is a myelin-rich area. Above the white matter is the Gcl, where Golgi cells and the most numerous kind of neurons of the brain the granule cells reside. Granule cells are major excitatory neurons, which transmit glutamate [171]. Furthermore, they co-ordinate the afferent excitatory input they receive from mossy fibers. Mossy fibers originate from nuclei in brain stem and spinal cord [172]. These fibers connect granule and Golgi cells and build synaptic complexes, called cerebellar glomeruli (also recognizable as rosettes) [173]. The next cell layer is

the Purkinje cell layer. The cell bodies of the Purkinje cells are surround by Bergmann glia[171]. Purkinje cells are inhibitory and secrete the neurotransmitter GABA. Bergmann glia derive from radial glia and are located around the Purkinje cells soma after maturation. Their processes spread from the Purkinje cell layer towards the subpial basement membrane [174]. During early development, radial glia serve as a scaffold for migrating Purkinje cells (Fig. 1.3). Postnatally, Bergmann glia serve as a scaffold for granule cells [175]. In the superficial layer, the molecular layer, dendrites of the Purkinje cells are located. Furthermore, axons of granule cells (called parallel fibers) but also stellate and basket cells are found in this layer [171]. Parallel fibers of the molecular cell layer (Mcl) derive from the granule cells of the Gcl. Parallel fibers are in contact with stellate and basket cells as well as dendrites of the Purkinje cells. While Purkinje cells are in close contact to Bergmann glia, basket and stellate cells are partially in contact with Bergmann glia whereas Golgi and granule cells are not in contact with Bergmann glia [176]. Cerebellar glia are categorized into different subtypes: glia of the white matter, astrocytes of the Gcl [177], unipolar brush cells [165] and Bergmann glia. Several studies suggest that cerebellar glia of the developing cerebellum have stem cells or progenitor cells characteristics [178,179].

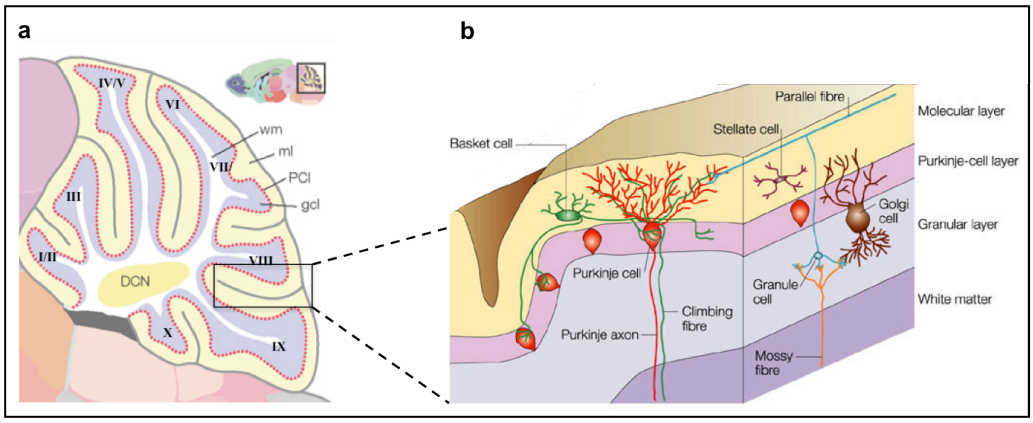

Figure 1.4: The architecture of the cerebellum.
After foliation the cerebellum is composed of 10 lobules (a). The cerebellum is comprised of four layers (b): the white matter, the Gcl, the Purkinje cell layer and the molecular layer. Granule cells and Golgi cells are located in the Gcl. The soma of Purkinje cells and Bergmann glia are located in the Purkinje cell layer. Inhibitory interneurons, stellate and basket cells, the processes of Bergmann glia and dendrites of Purkinje cells are located in the Mcl. Modified from Kobielak *et al.* (2004) and Takana *et al.* (2008) [180,181].

1.8 Aim of this study:

Astrocytes display heterogeneity in morphology and function. Therefore, astrocytes are considered being an inhomogenous cell type that is rather composed of different subpopulations. In the past, several approaches have been performed to classify astrocyte subsets. However, studies based on cell morphology, regional distribution, gene expression profiling, proteomics, electrophysiologic properties or marker expression did not result in functional categorization of astrocyte subpopulations based on marker expression.

Cell surface markers are a powerful tool to classify cell subsets and circumvent the use of transgenic models. They do not only allow for the prospective isolation of cells but also for their subsequent characterization on the single cell level. However, the availability of astrocyte subpopulation specific antibodies is currently limited and this retards further studies. In this study, the astrocyte cell surface marker GLAST, which shows a widespread expression on astrocytes of the CNS, served as basis for the analysis of astrocyte subpopulations. The first aim was to generate novel astrocyte subpopulation specific antibodies or to identify novel subpopulation specific markers. The generation of astrocyte subtype specific antibodies was addressed by immunization approaches. The identification of novel astrocyte markers was performed by cell surface marker screenings using an antibody library. Furthermore, the expression profile of the novel marker ACSA-2 was analyzed to prove its astrocyte specificity. Moreover, the antigen recognized by the ACSA-2 antibody was addressed. Besides, a functional characterization of this marker was performed. In addition, in combination with GLAST this marker was used to identify astrocyte subpopulations.

A further aim of this study was the identification of neural stem cell markers. On the one hand, the subependymal layer of the adult subventricular zone (SVZ) was addressed. One the other hand, stem and progenitor cells of the neonatal cerebellum, a less characterized cell population, were investigated. Although cerebellar stem cells have been well characterized by other studies, the lineage relationship between multipotent stem and lineage restricted precursors in the neonatal cerebellum is not well described. The possibility to identify and isolate stem and precursor cells from neonatal cerebellum would contribute to our understanding of lineage, function and heterogeneity of cerebellar astrocytes.

To address the properties of the astrocyte subpopulations in the developing cerebellum isolation protocols were established and suitable marker combinations were identified. This step was mandatory to proceed with functional studies including cell-based assays, cell transplantation and gene expression profiling. Transplantation studies were chosen to address cell fates, as an *in vivo* model is more reliable than an *in vitro* assay.

Gene expression profiling combined with pathway analysis was further used to address the transcriptome of the multipotent and the precursor cell type. In addition, the lineage relationship between the identified subpopulations was addressed by bioinformatic tools.

2 Materials

2.1.1 Antibodies for immunohistochemistry or immunocytochemistry

Antibody	Clone	Isotype	Provider
Anti-ACSA-2	IH18A3		Miltenyi Biotec
Anti-βIII tubulin	5G8	mouse IgG1	Promega
Anti-Calretinin		rabbit poly.	Swant
Anti-BLBP		rabbit poly	abcam
Anti-EGFR		rabbit poly	Thermo
Anti-GAT-3		rabbit IgG	Millipore
Anti-GFAP		rabbit IgG	Dako
Anti-GFAP	Z334	mouse IgG1	Millipore
Anti-GFP		rabbit poly	Dako
Anti-GLAST	ACSA-1	mouse IgG2a	Miltenyi Biotec
Anti-GS		rabbit poly	abcam
Anti-MAP2		mouse IgG	Chemicon
Anti-MBP		mouse IgG2a	Millipore
Anti-NG2		rabbit IgG	Chemicon
Anti-Parvalbumin		mouse IgG1	Swant
Anti-RC2		mouse IgGM	Millipore
Anti-S100b		rabbit	abcam
Anti-S100b		rabbit poly	abcam
CD24	193- 563	rat IgG	Rougon
CD106	429	rat IgG	BD
Wheat germ agglutinin			sigma

2.1.2 Secondary antibodies and nuclear stain

Invitrogen	A488	A555	A594	A647	Conc.
goat anti mouse IgG1	A-21121	-	A-21125	-	4 µg/mL
goat anti mouse IgG	A-11001	-	A-11032	-	4 µg/mL
goat anti mouse IgG2a	A-21131	-	A-21165	-	4 µg/mL
goat anti mouse IgM	A-21042	-	A-21044	-	4 µg/mL
goat anti rabbit	A-11008	A-31572	A-11012	A-21244	4 µg/mL
goat anti rat IgG	A-11006	-	A-11007	-	4 µg/mL
goat anti rat IgM	A-21212	-	A-21213	-	4 µg/mL
goat anti chicken	A-11039	-	-	-	4 µg/mL

HRP	Provider	Dilution
Anti mouse	Dako	1:20000
Anti goat	stemgent	1:5000
Anti rabbit	Thermo	1:500
Anti rat	BioLegend	1:5000
SA	GE	1:5000
Cy3		
Anti rat	Jackson	1:500

DAPI	Sigma		0.25 µg/mL
DRAQ5™ - Alexa647	abcam	ab108410	5 µM
Hoechst 33342	Sigma		1-10 µM
TOTO-3 -Alexa633	Invitrogen	T3604	1.25 µM

2.1.3 Antibodies for flow cytometry

Antibody	Isotype	Clone	Fluorochrome	Biotin	MicroBeads
Anti-AN2	rat IgG1	1E6.4	PE, APC	x	x
Anti-A2B5	mouse IgM	105-HB2	PE, APC	x	x
Anti-ACSA-2	rat IgG2b	IH3-18A3	PE, APC, FITC	x	x
Anti-GLAST	mouse IgG2a	ACSA-1	PE, APC	x	
Anti-O4	mouse IgM	O-4	PE, APC	x	x
Anti-Prominin	rat IgG1	MB-9-3G8	PE, APC	x	x
Anti-PSA-NCAM	mouse IgM	2-2B	PE, APC	x	x
Anti-Ter119	rat IgG2b	Ter-119	PE, APC, VioBlue	x	x
CD24	rat IgG2bκ	M1/69	PE, APC, VioBlue	x	x
CD31	rat IgG2a	390.1	PE, APC, VioBlue	x	x
CD45	rat IgG2bκ	30F11	PE, APC, VioBlue	x	x
CD51	rat IgG1, κ	RMV-7	PE, APC	x	
CD90.1	rat IgG2bκ	30-H12	PE, APC	x	x
CD140a	rat IgG2aκ	APA5	PE, APC	x	x
CD171	rec.hum IgG1	REA163	PE, APC	x	x

2.1.4 Chemicals

Agarose	Bio Rad; Munich
Agilent Washing buffer	Agilent Techn.; Santa Clara (SA,US)
Barrier Marker (Dako pen)	Dako; Glostrup (Denmark)
Brij35 (30%)	Sigma-Aldrich; St. Louis (MO, US)
Complete EDTA free	Roche; Mannheim
Coomassie	Pierce; Rockford (US)
Cell Trace-Violet Cell Proliferation Kit	Invitrogen; Darmstadt
Disodiumhydrogenphosphate (Na_2HPO_4)	Merck; Darmstadt
Deglycosylation mix	NEB; Hitchin (UK)
DPBS (+ calcium and magnesium)	Lonza; Cologne
Ethanol	Applichem; Darmstadt
Etidium-bromide	Roth; Karlsruhe
Ethylendiaminetetraacetate (EDTA)	Sigma-Aldrich; St. Louis (MO, US)
Fast green (at 1% v/v)	Applichem; Darmstadt
Fetal bovine serum	PAA; Pasching (Austria)
Fetal calf serum- Bichrom	Merck; Darmstadt
Fix and Perm	Miltenyi Biotec; Bergisch Gladbach
Flourescent Mounting Medium	Dako; Glostrup (Denmark)
Glue (Locite 604)	Henkel; Düsseldorf
Glycerin	Roth; Karlsruhe

Goat serum	Dianova; Hamburg
HEPES, 1M	Lonza; Cologne
HBSS -phenol red; calcium; magnesium	Lonza; Cologne
HBSS -phenol red	Lonza; Cologne
Hybond ECL	GE; Fairfield (CT, US)
Hypoxanthine/Azaserin	Sigma-Aldrich; St. Louis (MO, US)
Imaging plates (24, 96 well)	Miltenyi Biotec; Bergisch Gladbach
Isoboa	Roche; Mannheim
L-Glutamine	Invitrogen; Darmstadt
LB Agar	Roth; Karlsruhe
LB Medium	Roth; Karlsruhe
MACSfectin	Miltenyi Biotec; Bergisch Gladbach
Methanol	Applichem; Darmstadt
Nail polish	P2 cosmetics; Neudorf
NeuroBrew-21	Miltenyi Biotec; Bergisch Gladbach
Neuro Basal - Phenol red	Invitrogen; Darmstadt
Not fat dry milk powder	Applichem; Darmstadt
NuPAGE® 4-12% Bis-tris-Gel	Invitrogen; Darmstadt
NuPAGE® MOPS SDS Running Buffer (20X)	Invitrogen; Darmstadt
NuPAGE® Sample reducing agent (10X)	Invitrogen; Darmstadt
NuPAGE® LDS Sample buffer (5X)	Invitrogen; Darmstadt
NP-40 (10%)	NEB; Frankfurt-Höchst
Ketamine hydrochloride/Xylazine hydrochloride	Sigma-Aldrich; St. Louis (MO, US)
Paraformaldehyde-powder	Sigma-Aldrich; St. Louis (MO, US)
Paraformaldehyde (32% Stock)	Science Services; Munich
Penicillin/Streptomycin	Lonza; Cologne
Phytohaemagglutinin (PHA-L)	Sigma-Aldrich; St. Louis (MO, US)
Poly-L-Lysine	Sigma-Aldrich; St. Louis (MO, US)
Polyethylenglycol (PEG 1500)	Sigma-Aldrich; St. Louis (MO, US)
Potassiumchloride (KCl)	Sigma-Aldrich; St. Louis (MO, US)
PageRulerPrestained Protein Ladder	Thermo; Waltham (MA, US)
SDS Running buffer	anamed; Gross-Bieberau
Sodium azide (NaN_3)	Merck; Darmstadt
Sodium chloride	Merck; Darmstadt
Surcrose	Serva Electrophysics; Heidelberg
Sulfo-NHS-Biotin EZ linker	Thermo; Waltham (MA, US)
Tiazovivin	Stemgent; Cambridge (MA US)
Tissue Tack	Polysciences; Eppelheim
Triton-X 100	Sigma-Aldrich; St. Louis (MO, US)
Trizma® hydrochloride	Sigma-Aldrich; St. Louis (MO, US)
Tween-20	Sigma-Aldrich; St. Louis (MO, US)
Tweezerelectrodes CUY650P10	Nepa gene; Ichikawa (Japan)
4′,6-Diamidino-2-phenylindole dihydrochloride	Sigma-Aldrich; St. Louis (MO, US)

2.1.5 Instruments and equipment

Agilent Bioanalyzer 2100	Agilent Techn.; Santa Clara (SA,US)
Brushes	Th. Geyer; Renningen
Centrifuge- Heraeus®	Thermo; Waltham (MA, US)
Cell strainer (70 µm)	BD; Franklin Lakes (NJ,US)
Cell strainer (50 µm)	Miltenyi Biotec; Bergisch Gladbach
Coverslips (12 mm diam.; 25 x 50 mm)	Menzel; Braunschweig
Cryostat (Leica CM1860 UV)	Leica; Solms
Dumont forceps (No.5)	F.S.T; Heidelberg
Electroporation device CUY21	Nepa gene; Ichikawa (Japan)
Falcon tubes (15 mL, 50 mL)	BD; Franklin Lakes (NJ,US)
Filter tips (10, 200, 1000 µL)	Thermo; Waltham (MA, US)
gentleMACS™ Octo Dissociator	Miltenyi Biotec; Bergisch Gladbach
Hamilton Syrige	Hamilton; Bonaduz (CH)
Incubator-Heracell	Thermo; Waltham (MA, US)
LD, LS columns	Miltenyi Biotec; Bergisch Gladbach
Low attachment plates	NOF; New York (US)
MACSMix- Tube Rotator	Miltenyi Biotec; Bergisch Gladbach
MACSQuant	Miltenyi Biotec; Bergisch Gladbach
Microscope	Leica; Solms
Microscope LSM-710	Zeiss; Jena
Microscope slides	Thermo; Waltham (MA, US)
Multiwell plates (96 well; 24 well)	BD; Franklin Lakes (NJ, US)
MS columns	Miltenyi Biotec; Bergisch Gladbach
NanoDrop	PEQLAB; Erlangen
OctoMACS	Miltenyi Biotec; Bergisch Gladbach
Orbital shaker	Heidolph; Schwabach
Pipette (Glas)	VWR; Darmstadt
Pipette	Eppendorf; Hamburg
Pipetboy	Eppendorf; Hamburg
Razor	Wilkinson; Solingen
QuadroMACS	Miltenyi Biotec; Bergisch Gladbach
Razor	Wilkinson; Solingen
Scalpel	B.Braun; Melsungen
Scalpel (22.5°)	F.S.T; Heidelberg
Scissors	F.S.T; Heidelberg
SDS gel chamber	Invitrogen; Darmstadt
Semi Dry Blotter	Biometra; Goettingen
Stripette (5, 10, 25 ,50 mL)	Sarstedt; Nümbrecht
Super Frost Slides	Roth, Karlsruhe
TipOne (10, 100, 1000 µL)	Starlab; Hamburg
TubeOne (0.5, 1.5, 2 mL)	Starlab; Hamburg
Tissue Flasks (T75,T175)	BD; Franklin Lakes (NJ, US)
Tris-Glycerin Gels	anamed; Gross-Bieberau
Tisch centriguge- Heraeus®	Thermo; Waltham (MA, US)
Tris-Glycerin Gels	anamed; Gross-Bieberau

Tweezerelectrodes CUY650P10	Nepa gene; Ichikawa (Japan)
Vibratome (Microm HM 650 V)	Thermo; Waltham (MA, US)
Water bath	Julabo; Seelbach
Whatman paper	Bio Rad; Munich
26 G x 1' canula	B.Braun; Melsungen
30 G x 1/2' canula	B.Braun; Melsungen

Dissociation reagents

Neural Tissue Dissociation Kit (Trypsin) - NTDK(T)	Miltenyi Biotec, Bergisch Gladbach
Neural Tissue Dissociation Kit (Papain) - NTDK(T)	Miltenyi Biotec, Bergisch Gladbach
Neural Tissue Dissociation Kit Postnatal Neurons - NTDK (PN)	Miltenyi Biotec, Bergisch Gladbach

Molecular biological Kits

Agilent Low Input Quick Amp Labeling Kit	Agilent T.; Santa Clara (SA,US)
NucleoBond® PC 500 Kit	Machery-Nagel; Düren
NucleoSpin® plasmid Kit	Machery-Nagel; Düren
Retinal Ganglion Isolation Kit (RGC)	Miltenyi Biotec, Bergisch Gladbach
RNeasy Mini Kit	Quiagen, Hilden

Separation reagents

Anti-ACSA-2 MicroBead Kit	Miltenyi Biotec, Bergisch Gladbach
Anti-GLAST (ACSA-1) MicroBead Kit	Miltenyi Biotec, Bergisch Gladbach
Protein A/G MicroBead Kit	Miltenyi Biotec, Bergisch Gladbach

2.1.6 Reagents

10X PBS pH 7.4

NaCl	138mM
Na_2HPO_4	8.2mM
KCl	2.4mM
KH_2PO_4	1.3mM

Transferbuffer

Tris-Base	48mM
Glycerin	39mM
SDS	1.3mM
Methanol	10%(v/v)

TBS buffer pH 7.6

NaCl	150mM
Tris/HCl	50mM

Lysis buffer

Triton-X-100	1%(v/v)
NaCl	150 mM
Tris HCl	50 mM (pH 8)

2.1.7 Software

Adobe Reader	Abobe; Munich
Axiovision	Zeiss; Jena
Endnote	Thomson Reuter; New York City (NY, US)
FlowJo	Miltenyi; Bergisch Gladbach
MetaCore	Thomson Reuter; New York City (NY, US)
MACSQuantify	Miltenyi; Bergisch Gladbach
Multiple experiment viewer (TM4)	Dana-Farber Cancer Institute; Boston (MA, US)
Prism6	Graph Pad; La Jolla, CA USA
Zen2011	Zeiss; Jena

2.1.8 Animal strains, bacteria strains and cell lines

Cell line		Origin
HM-1	Mouse embryonic stem cell line	Mouse
CM7/1	Mouse embryonic stem cell line	Mouse
OP-9	Mouse embryonic stem cell line	Mouse
L929	Fibroblasts	Mouse
H4 (HTB-148)	Neuroblastoma cell line	Human
LS	Neuroblastoma cell line	Human
1881	B cell lymphoma cell line	Human
BW	B cell line	Human
RPE-1	Retina pigment epithelium	Human
4T-1	Mamacarcinom cell line	Mouse (Xenograft)
HEK (293 T)	Human embyonic kidney cell line	Human
CHO	Chinese hamster ovary cell line	Hamster
Sp2/0-Ag14	Murine myeloma cell line	Mouse

Animals		Background	Supplier
Rat	Wistar	Wild-type	Harlan
Mouse	CD1	Wild-type	Animal facility
Mouse	BALB/c	Wild-type	Harlan
Mouse	C57BL/6	Wild-type	Harlan
Mouse	β-Actin-GFP	Transgene	Animal facility
Mouse	GAD67-GFP	Transgene	Animal facility

Escherichia coli		Supplier
DH5alpha	Competent Cells	Invitrogen

2' Methods

2.2 Cell and biochemical methods

2.2.1 Ethical guidelines for animal research

Animals were maintained under specific pathogen-free conditions according to the recommendations of the Federation of European Laboratory Animal Science Association. All experiments were performed in compliance with the European Communities Council Directive of 24 November 1986 (86/609/EEC)

2.2.2 Tissue dissociation

A single cell suspension from solid tissue is obtained by combination of mechanical and enzymatic treatment. Dissociation protocols are optimized according to tissue type, species and age of the animal. Different parameters such as: Temperature, incubation time and enzymes are carefully chosen to obtain high amounts of vital cells.

2.2.2.1 Dissociation of embryonic brain tissue

Embryonic mouse brain tissue was used to study astrocyte marker expression at early developmental stages. Pregnant CD1 mice purchased from Harlan Laboratories (Rossdorf; Germany) were sacrificed by CO_2 application. Embryonic brains were dissected, collected and dissociated using the Neural Tissue Dissociation Kit – Postnatal Neurons (NTDK (PN)) in combination with trypsin (T) or papain (P). Trypsin is a serine protease that harbors a catalytic triade [182,183] and papain is a cysteine protease. Tissue was incubated in a water bath (37°C) for 5 minutes (min) mixed discontinuously. Tissue was dissociated mechanically using a 1 milliliter (mL) pipette and incubated for another 5 min in a water bath. The cell solution was passed through a 70 µm cell strainer and pelleted by 10 min centrifugation at 300 g at room temperature (RT). The cell pellet was resuspended in Hank's Balanced Salt Solution (HBSS) and processed immediately.

2.2.2.2 Dissociation of neonatal (also referred as postnatal) brain tissue

Neonatal CD1 wt mice aged P0 to P7 were obtained by in-house breeding (Miltenyi Biotec (2.1.8)). Mice were sacrificed by decapitation. Brains were removed and dissociated using the NTDK/ NTDK (PN) plus (T) or (P) in combination with the gentleMACS™ Octo Dissociator according to the manufacturer's instructions (Program: NTDK_1_37°C). For analysis of distinct brain regions olfactory bulb, cortical hemispheres, hippocampus, midbrain/diencephalon and cerebellum were dissected, dissociated and stained separately.

2.2.2.3 Dissociation of adult mouse brain tissue

In contrast to neonatal brain, the adult mouse brain is composed of myelin rich (white matter) and myelin rare areas (grey matter). The isolation of neural cells from the adult brain requires a myelin-removal step, which can either be performed by the depletion of myelin using Myelin Removal Beads or by density gradient centrifugation. Brains from adult CD1 mice (P40) were sliced manually into 8 pieces and dissociated on the gentleMACS Octo Dissociator (Program: ABDK) in the presence of Adult Mouse Brain Dissociation Kit with papain following the manufactuer's protocol. By density gradient centrifugation (10 min, 3.000 g, 4°C), viable cells were separated from myelin, as myelin has a lower density. Neural cells were harvested from the interphase and further processed.

2.2.2.4 Dissociation of SVZ tissue

Adult mice (> P40) (BALB/c, CD1, C57BL/6 (2.1.8)) or neonatal CD1 mice (P2-P5) were sacrificed. Brains were dissected and cut into coronal floating sections (400 µm) using a vibratome. The lateral wall of the SVZ was dissected manually with an ophthalmic scalpel (22.5°). Tissue was collected and incubated at 37°C in pre-heated NTDK(PN) solution 1 and 2 for 15 min under continuous rotation on the MACSmix Tube Rotator. Solution 3 and 4 of the NTDK(PN) were added and tissue was dissociated using a fire polished glass pipette (diameter approx. 0.8 mm), then incubated for another 15 min.

2.2.2.5 Dissociation of retinal tissue

The retina is part of the central nervous system, which develops from the neural tube. Neural retina was harvested from CD1 mice at postnatal day 2 and 6. Mice were decapitated and the eyes were collected. The intra-ocular pressure was reduced by picking the eye with a needle. The lens was cropped using vannas spring scissors, thereby the vitreous humour was exposed and enabled the removal of the retina. The tissue was collected in a 15 mL Falcon™ and processed according to the Retinal Ganglion Cell Isolation Kit, rat (RGC) using 0.05% trypsin for enzymatic treatment. Solutions were applied at RT; centrifugation steps were carried out at 130 g, RT. After sedimentation the supernatant was removed carefully. Solution 1 (RGC) and trypsin were added. Cells were incubated for 15 min at 37°C in the MACSMix, before 30 µL of enzyme mix 2 (RGC) were added. Tissue was then dissociated with a wet 5 mL pipette and incubated for another 10 min at 37°C. Tissue was further dissociated using a fire-polished Pasteur pipette (appr. 0.8 mm diameter). Cells were applied on a cell strainer (70 µm) and resuspended in D-PBS supplemented with BSA.

2.2.2.6 Dissociation of spinal cord

For analyses of spinal cord tissue, CD1 wt mice (P6) were sacrificed by decapitation. The back was opened and the spinal cord was dissected using forceps (Dumont No.5). Tissue was dissociated using NTDK(PN) in combination with trypsin for enzymatic treatment and the gentleMACS Octo Dissociator for mechanical treatment (Program: NTDK_1_37°C).

2.2.3 Cultivation of neural cells

2.2.3.1 Cultivation of primary neural cells

Mixed mouse brain tissue cultures were prepared from the cerebral hemispheres or the midbrain of CD1 wt mice (P0 to P2). The meninges were removed to prevent overgrowth of fibroblasts in the culture. Tissue was dissociated with the NTDK/NTDK(PN)(T) and cells were seeded at a density of 4 x 10^4 to 1 x 10^5 cells on poly-L-lysine coated 1 cm cover slips. The cover slips were incubated with poly-L-lysine for 30 min to o/n, washed with destilled water and dried prior to use. Cells were cultured in MACS Neuro Medium supplemented with 1% NeuroBrew-21, 1% Penicillin/Streptomycin (Pen/Strep) and L-Glutamine (2 mM) for 1 to 14 days.

2.2.3.2 Cultivation of isolated astrocytes

MACS isolated astrocytes (2.6) were seeded at a density of 4 x 10^4 to 1 x 10^5 cells on poly-L-lysine coated 1 cm cover slips or 24-well imaging plates (poly-L-lysine coating according to 2.2.6). Cells were cultured in MACS Neuro Medium supplemented with 1% NeuroBrew-21, 1% Pen/Strep and L-Glutamine (2 mM) for 1 to 14 days.

2.2.3.3 Neurosphere assay

The neurosphere assay addresses the fundamental features of neural stem cells (NSCs). Its principles were first reported by Reynolds and Weiss in 1992 [63]. Self-renewing multipotent stem cells are able to form free-floating spheres in the presence of epidermal growth factor (EGF) and basic fibroblast growth factor (FGF). Upon dissociation and plating in the absence of EGF and FGF these cells differentiate into neurons, astrocytes and oligodendrocytes. The dissociation of primary spheres and further cultivation in FGF and EGF containing medium leads to the generation of secondary neurospheres. By the generation of secondary and tertiary spheres, the self-renewing characteristics of stem cells are examined, as non-stem cells are not

self-renewing and lost during passaging. Cells were seeded at a density of 1,000 cells/µL (500,000 cells/500 µL) in a 24 well low-attachment plate. Cells were grown in MACS Neuro Medium supplemented with 1% NeuroBrew-21, 1% Pen/Strep, 20 ng/mL human FGF and 20 ng/mL human EGF. The medium was prepared fresh and replaced every three days by centrifugation (150 g, 6 min, RT) (Fig. 2.1). If secondary spheres were generated cells were dissociated using trypsin and replaced in a low-attachment dish in the presence of growth factors. Depending on the sphere diameter after 6 or 12 days, cells were seeded on poly-L lysin coated cover slips for final differentiation (coating as decribed in 2.2.3.1) (Fig. 2.1).

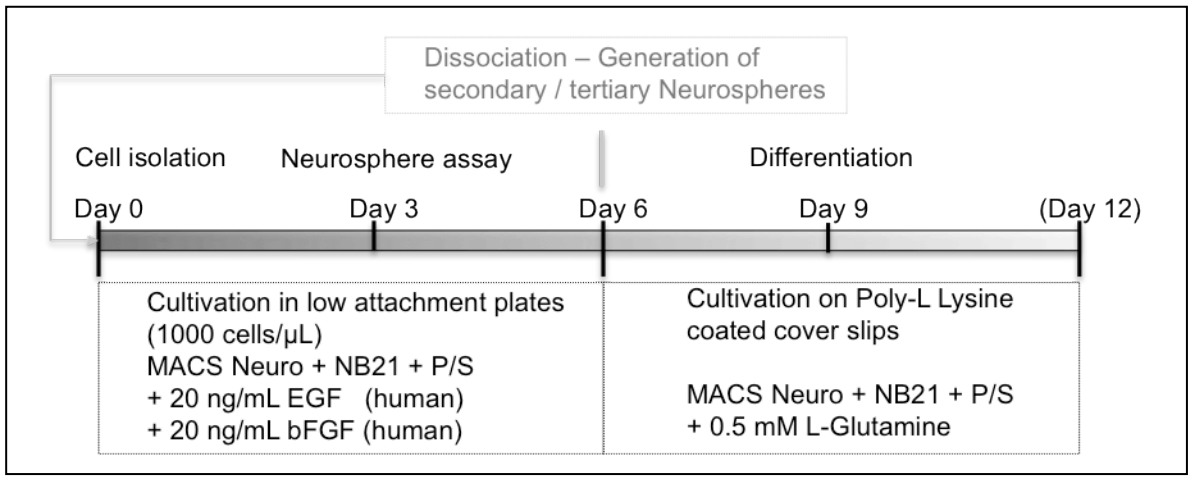

Figure 2.1: A schematic overview of the neurosphere assay
Dissociated cells were cultivated in low attachment plates at a high cell density. For generation of neurospheres human EGF and human FGF were added to the medium. After 6-12 days cells were either dissociated and seeded for final differentiation or re-plated in a low attachment plate for the generation of secondary/tertiary neurospheres.

2.2.4 Cell lines

Frozen cell lines were thawed in pre-warmed medium to dilute the DMSO in the freezing solution. Cells were pelleted by 10 min centrifugation at 300 g, at RT and seeded with fresh medium in a T25 flask. To freeze cells, the cells were harvested from culture at 70% confluence, pelleted using centrifugation and resuspended in FCS. After the addition of DMSO (10% v/v) cells were shock-frozen at -80°C in a freezing container and transferred into liquid nitrogen for long-term storage.

2.2.4.1 Murine myeloma cell line (Sp2/0)

The murine cell line Sp2/0-Ag14 is a myeloma cell line. Myeloma cells are able to fuse with antibody-producing B cells, which result in immortalized hybridoma cells and used for monoclonal antibody production,[184] as demonstrated by Köhler and Milstein in 1975 [185], later awarded Nobel Prize. Sp2/0-Ag14 cells were cultivated in

DMEM (Dulbecco's Modified Eagle's Medium) supplemented with 20 mM HEPES and 2 mM L-Glutamine. After fusion with antibody producing B cells the medium was supplemented with 0.1 mM Hypoxanthine, which induces selection pressure.

2.2.4.2 CHO cells

Chinese Hamster Ovary cells (CHO) are an immortalized adherent growing cell line generated in 1957 [186]. CHO are commonly used for recombinant antibody production [187]. CHO cells were cultivated in CHOMACS CD medium supplemented with 8 mM L-Glutamine in the presence of 1% (v/v) Pen/Strep.

2.2.4.3 HEK 293 cells

This human embryonic kidney cell line is an adherent growing epithelial cell line. It was generated in 1970 by the transformation of human embryonic kidney cells treated with adenovirus 5 DNA [188]. The adherent cell line was cultivated in DMEM supplemented with 10% FCS in the presence of 1% (v/v) Pen/Strep.

2.2.4.4 1881 cells

The 1881 cell line is a mouse B cell line derived from BALB/c bone marrow that was transformed with Abelson murine leukemia virus [189]. The suspension cell line was grown in RPMI-1640 in the presence of 10% FCS and 1% (v/v) Pen/Strep.

2.2.5 Flow cytometric analysis

Single cell suspensions of one million cells from dissociated mouse whole brain tissue or isolated astrocytes were incubated with mouse Fc Receptor (mFcR) blocking reagent ((1:10) Miltenyi Biotec) to block unspecific antibody binding to Fc receptor expressing cells. Cells were subsequently stained with antibodies directed against cell surface marker(s) of interest at a defined titer in PB (Phosphate buffered saline (PBS) supplemented with 5% bovine serum albumin (BSA)) for 10 min at 4°C. After washing and centrifugation (200 g, 5 min, RT), data was acquired on a flow cytometer (MACSQuant) and analyzed using MACSQuantity software.

2.2.5.1 Flow cytometry - Gating strategy

Single suspension cells can be analyzed by flow cytometry. The most common graphs are histograms (one-dimension) or dot plots (two-dimensions). In a dot plot, each event is represented by a dot correlating to the signal intensity of two channels concurrently; see Fig. 2.2 (4,5). A gating strategy allows analyzing subpopulations of cells, independent from the entire sample. The gates are set according to an unstained sample (negative staining control). The first gate excludes all doublets, cells that cluster or stick to each other (Fig. 2.2 (1)). In the next gate, the forward scatter (FSC) is applied against the side scarrer (SSC) to mask the population of interest. In this study neuronal cells were gated, as presented in Fig. 2.2 (2). In the third gate, viable cells are discriminated from dead cells using the cell death marker Propidium-iodide (PI) against PE (Fig. 2.2 (3)). By plotting the FSC against a given fluorescence channel, the frequencies of a marker expressed on a cell population can be determined (Fig. 2.2 (4)). In addition, the percentage of double positive cells can be analyzed if co-stainings were performed. Therefore, two distinct fluorescence channels are assigned against each other (Fig. 2.2 (5)). On the MACSQuant, the spillover was compensated using a matrix that displays all available channels.

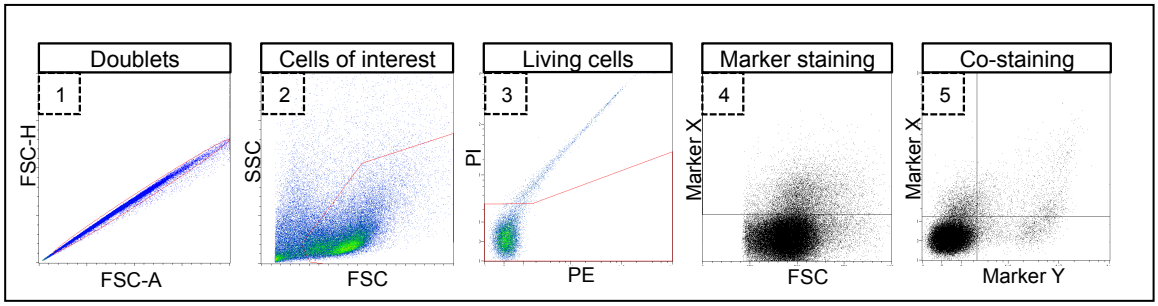

Figure 2.2: Gating strategy for flow cytometry analysis
The first gating step excludes doublets (1). Thereafter the cells of interest are gated (2) and living cells are discriminated by PI labeling (3). The expression of a marker or marker co-expression is further analyzed using dot plots (4,5).

2.2.6 Magnetic cell separation

Magnetic cell separation (MACS) can be used to enrich or deplete cells. Cells are labeled either directly using antibody MicroBead conjugates or indirectly by fluorochrome or biotin conjugates in combination with Anti-fluorochrome or Anti-Biotin MicroBeads. Cells are pre-incubated with mFcR before the antibodies are added according to the manufacturer's instructions. After labeling, cells were washed (Table 1) and applied onto a suitable column: For enrichment an MS or an LS column were used. For depletion, LD columns were used. Columns were placed in a permanent magnet (OctoMACS, QuadroMACS), which induces a

high-gradient magnetic field. The MicroBead labeled cells are retained by the magnetic field within the column. Unlabeled cells run through the column and are collected in the negative fraction (Table 1). In case of a positive enrichment, the target cells are labeled. The column is taken out of the magnet and the labeled fraction can be eluted. In a depletion strategy, non-magnetic cells are magenetically labeled and retained within the magnetic field, whereas target cells are collected in the flow through. For cultivation the separation was performed under a laminar flow with sterile equipment, solutions and filtered buffer. Cells were cultivated as described in 2.2.3.2.

Table 1: MACS separation

Column	Cell amount	Rinse column	Cellsolution	Washing step	Elution
MS	2 x 10^7	500 µL	500 µL	3 x 500 µL	1 mL
LS	4 x 10^7	3 mL	500 µL	3 x 3 mL	5 mL
LD	4 x 10^7	3 mL	500 µL	2 x 1 mL	3 mL

2.2.7 Cell surface marker screen

To perform the cell surface marker screening, single cell suspensions obtained by tissue dissociation were analyzed by flow cytometry. Isolated astrocytes, cells of whole mouse brain tissue or from different brain regions were stained in a 96 well plate with the antibody concentration given in Appendix I. The final antibody titer on the cells was 0.5 µg/mL, as recommended in the protocol of the Mouse Cell surface Marker Screening Panel (BD Lyoplate mouse, BD). Forebrain, midbrain and cerebellum were dissociated separately and labeled with following concentrations of CellTrace™ Violet Cell Proliferation Kit – accoding to the manufactuer's instructions: Forebrain (1.75 µM), midbrain (0.2 µM) and cerebellum (0 µM). Positive markers (>5% on astrocytes) were re-screened (Table 2). For visualization a heat map was generated using the MultiExperiment Viewer (TM4:MeV) using Pearson's Correlation.
For analysis the relative expression was calculated as follows:

$$relative\ expression\ (\ on\ \mathrm{GLAST}^{+} cells) = \frac{\%\ \text{of marker on GLAST}^{+}\ (\mathrm{F+M+C})}{3} \div \frac{\%\ \text{of GLAST}^{+}\text{cells (F+M+C)}}{3} \quad (1)$$

$$relative\ expression\ (on\ \mathrm{ACSA-2}^{+} cells) = \frac{\%\ \text{of marker on ACSA-2}^{+}\text{cells (F+M+C)}}{3} \div \frac{\%\ \text{of ACSA-2}^{+}\text{cells (F+M+C)}}{3} \quad (2)$$

Abbreviations: F: Forebrain, M: Midbrain, C: Cerebellum

Table 2: Antibody clones used for rescreening

Marker	Clone	Conc.
CD3e	145-2C11	1:11
CD24	M1/69	1:11
CD26	H194-112	0.5 µg/mL
CD29	HMß1-1	1:11
CD38	90	1 µg/mL
CD47	DX5	1:11
CD49e	5H10-27	1:11
CD106	429	0.25 µg/mL
CD119	2 E 2	0.5 µg/mL
CD147	RL73	0.25 µg/mL
CD200	OX-90	1:100

2.2.8 Immunization

Lewis rats were immunized by contralateral footpad immunization for the generation of astrocyte subpopulation specific monoclonal antibodies. MACS enriched astrocytes from mice served as immunogen. Another cells pool of murine cells depleted from astrocytes was applied as decoy. Per fraction 0.5 - 2 x 10^6 cells were injected into the hind footpad. The injection was repeated six times, at day 0, 4, 7, 11 and 14. At day -3 only the decoy fraction was injected. In different immunization attempts different immunization strategies were tested:

- Immunogen: Enrichment of GLAST$^+$cells/Decoy: Depletion of GLAST$^+$ cells
- Immunogen: Enrichment of GLAST$^+$cells/Decoy: Depletion of ACSA-2$^+$ cells

Furthermore, different adjuvants such as Phytoheamagglutinin (PHA-L) a lectin derived from *Phaseolus vulgaris* (at a final concentration of 10 µg/mL per boost) or CpG a dinucleotide which addresses Toll-like receptor 9 (at a final concentration of 50 µg per boost) were tested in both settings to increase the immunogenic potential by the activation of the innate immune response. At day 15 the popliteal lymph nodes from the hind footpad of the immunized rats were harvested by dissection. The lymph nodes were minced to obtain the antibody producing B cells. B cells were subsequently fused with murine Sp2/0 hybridoma cells in the presence of Polyethylenglycol (PEG), which enables the fusion of cell membranes. Cells were plated in a 96 well plate in the presence of mouse peritoneal macrophages isolated one day before. Cells were grown in the presence of azaserin and hypoxanthine, based on the HAT system [190]. Azaserine blocks the purine metabolism in unfused cells. In addition, unfused Sp2/0 cells lack the enzyme hypoxanthine-guanine phosphoribosyltransferase (HGPRT) and die. Cells were cultivated in the presence of 9% CO_2 at 37 °C for 5-7 days then fed to enhance cell growth. The hybridoma supernatants were screened on dissociated primary mouse brain tissue (P4-P6)

on a flow cytometer. The supernatant was incubated with 1 x 10^4 cells for 10 min at 4°C. After washing and centrifugation (300 g, 5 min, RT) cells were incubated with a secondary fluorochrome coupled antibody directed against the rat kappa light chain. After washing, cells were stained with the Anti-GLAST or Anti-ACSA-2 antibody to discriminate astrocyte subpopulation specific clones.

2.2.9 *In vivo* electroporation

Electroporation is an effective method to channel small charged molecules like DNA or messenger RNA (mRNA) through the lipid bilayer of cellular membranes, which cannot enter the cell by osmosis. Physically, electroporation induces a shift in the lipid rafts and enables the passage of small molecules [191]. First experiments of *in vivo* electroporation were carried out on mouse muscle tissue [192] and could be translated onto CNS derived tissue including retina [193], embryonic [194] and postnatal brain [195]. The technique is a powerful tool to study developmental processes, cell differentiation and migration processes. *In vivo* electroporation of the periventricular zone of the postnatal brain allows studying the SVZ/RMS/olfactory bulb system. In this study the electroporation technique was used to target stem cells and radial glia in the periventricular zone (PVZ).

Animals were treated according to the guidelines of the French ethics committee. Neonatal mice (P1, P2) were anesthetized by hypothermia and fixed for injection. The injection point was tapped by an ophthalmic scalpel. The injection was performed manually using a glass capillary (200 µm) connected to a Hamilton syringe. The capillary was filled with 2 µL of plasmid solution (5 µg/mL) labeled with 1% (v/v) fast green. For injection the needle was placed to the midpoint between the eye and the lambda, lowered between 2.5 and 3 mm and the DNA was injected. In case of successful injection a labeled ventricle was visible under a light source. By the usage of tweezerelectrodes and conductive gel five electrical pulses (100V, 50 ms, separated by 950 ms intervals) were applied. The electric field was applied horizontally to obtain the electroporation of the dorsal wall and vertically to electroporate the lateral compartment. Animals were resuscitated in an incubator at 37°C and returned to the mother.

2.2.10 Cell transplantation of ACSA-2^+/GLAST$^{+/-}$, ACSA-2^-/GLAST$^+$ cells into the neonatal cerebellum

The progeny of ACSA-2^+/ GLAST$^{+/-}$ and ACSA-2^-/ GLAST$^+$ cells was investigated in an *in vivo* model by cell transplatation. For both transplantation groups cerebelli of β-actin GFP mice (P0-P3) were dissected, dissociated and labeled with mFcR Blocking Reagent. ACSA-2^+/ GLAST$^{+/-}$ cells were isolated using the Anti-ACSA-2 MicroBead Kit. For the

enrichment of ACSA-2$^-$ / GLAST$^+$ cells a two-step separation strategy was applied. Therefore, cells were first labeled with Anti-L1CAM-PE (titer 1:2.5), then labeled with Anti-ACSA-2 MicroBeads (1:2.5), Anti-PE MicroBeads (1:2.5), Anti-CD45 (1:10), Anti-PSA-NCAM (1:10) and Anti-Ter119 MicroBeads and processed over an LD column. Afterwards, ACSA-2$^-$ /GLAST$^+$ were incubated with Anti-GLAST Biotin (1:5) and Anti-Biotin MicroBeads (1:5) and enriched using an MS column. ACSA-2$^+$/GLAST$^{+/-}$ and ACSA-2$^-$/GLAST$^+$ cells were injected into the lateral part of the vermis of P1-P3 hosts (n=9, n=11). Pups were anesthetized by hypothermia. 50,000 cells/µL were injected using a glass micropipette and the pups were returned to the mother. Per condition a cohort of 9 and 11 animals was transplanted. Mice were perfused intracardially with 4% PFA in PBS 30 days after injection and processed as described in 2.3.1/2.3.2. For statistical analysis integrated cells per animal were counted using a representative selection of fractions per animal (15-20 sections). Statistics were calculated with the Prism software using two-tailed unpaired Student's t-test, error bars represent the standard deviation (SD).

2.2.6 Histochemical methods

2.3.1 Preparation of brain tissue

Adult mice were anesthetized with an overdose of xylazin/ketamin (> 10 mg/kg body weight). Neonatal mice were either anesthetized by xylazin/ketamin or by hypothermia (4 min). Mice were perfused intracardically with 2% or 4% paraformaldehyde (PFA) (32% PFA Stock solution diluted with PBS). Brains were post fixed in 2% or 4% PFA for 6 hours (h) or over night (o/n) and then transferred into PBS o/n. For cryoprotection brains were incubated in 30% sucrose o/n.

2.3.2 Immunohistochemistry

For vibratome sectioning, brains were embedded in 3.5% agarose plus 8% sucrose, sectioned into 40-60 µm slices and stained as floating sections. The agarose was removed for staining and unspecific binding sites were blocked for 1 h at RT with 4% goat serum. The primary antibodies were incubated in PBS supplemented with 1% goat serum and 0.0-0.3% Triton-X-100 o/n at 4°C or RT. After washing (3 times, 10 min in PBS), the secondary antibodies were incubated for 1 h at RT. After washing (3 times, 10 min in PBS), cell nuclei were stained by Hoechst 33258 or DAPI. After a final PBS washing step, the sections were mounted (Mowiol or Mounting medium) and monitored by confocal imaging (Zeiss, Leica).

2.3.3 Immunohistochemistry of Afg31l1 d/d Afg3l2 fl/fl GFAP cre mice

Floating sections (30 µm) were dehydrated in PBS containing 4% sucrose (30 min), treated with methanol (30 min) and washed (3 times, 10 min in PBS). Sections were blocked for 45 minutes with 10% goat serum (life technologies). The primary antibodies were incubated over night at 4°C in PBS supplemented with 0.4% Triton-X-100 and 4% goat serum. After washing (3 times, 10 min in PBS), the secondary antibody was applied for 1 h at RT. In the final washing step the nuclei were stained with DAPI and the sections were mounted for visualization.

2.3.4 Immunocytochemistry

Cells were cultivated in a 24 well plate as described before (2.2.3.1/2.2.3.2). Primary neural cells were washed with PBS, fixed with 4% PFA (20 min, RT). After fixation cells were washed again three times with PBS and stored at 4°C in PBS supplemented with 4% sodium azide (NaN_3), which enables long-time storage. For staining, cells were blocked with 5-10% goat serum for 45 minutes. The primary antibodies were incubated over night at 4°C in PBS supplemented with 0.0-0.3% Triton-X-100 and 5% goat serum. After washing (3 times, 10 min in PBS), the secondary antibody was applied for 1 h at RT. After washing (3 times, 10 min in PBS), cell nuclei were stained by Hoechst 33258, DRAQ5 or DAPI. Cover slips were mounted and cells were monitored by confocal imaging.

2.3.5 Live cell staining

Cells were cultivated in a 24 well plate as described before (2.2.3.1/2.2.3.2). Live cell staining was performed to visualize ACSA-2 staining on living astrocytes in mixed mouse brain tissue culture or on isolated astrocytes. The Anti-ACSA-2 antibody was given into the medium of the primary mixed neural cells in a final concentration of 10 µg/mL and incubated o/n at 37°C. After a washing step with medium the secondary antibody [0.4 µg/mL] was incubated for 1 hour at 37°C. Cells were fixed with 4% PFA and stained for further markers as described before (2.3.4).

2.3.6 Multidimensional *in situ* Cytometry Survey (MICS)

Whole mouse brain tissue cells were cultivated in a 24 well imaging plate as described before (2.2.3.1). The Multidimensional *in situ* Cytometry Survey (MICS) allows investigating the expression profile and proteome of 100 markers on the cultivated cells. This is performed by repetitive antibody staining and bleaching cycles [196]. For MICS PE-conjugated antibodies were used. The antibodies were diluted in PB buffer plus 0.2% Triton-X-100 if required. Cells were blocked in an initial step. Each staining cycle starts with 10 min antibody incubation,

then a photo is taken and thereafter the spot is bleached.

2.3.7 Imaging

Sections or cover slips were monitored on Zeiss or Leica confocal microscopes. At the laser-scanning microscope (LSM (Zeiss)) pictures were taken with option 'best compromise'. 'Mosaic pictures' were taken at the Zeiss Z1 Apotome. For the analysis of the transplantation experiments, z-stacks were patially visualized as maximum intensity projections (MIPs) using the AxioVision Software.

2.4 Protein biochemical Methods

2.4.1 Ligand receptor capturing

One approach to identify the ACSA-2 antigen was performed by a so-called ligand receptor capturing (LRC) in co-operation with the ETH Zurich. 100 µm sections of P1 mice brains were obtained by vibratome sectioning. The tissue was shock-frozen in liquid nitrogen and shipped to Zurich. The LRC is a mass-spectrometric approach for the ligand-based identification of antigens [197]. The LRC technology is based on trifunctional linker (TRICEPS), which can be coupled to a ligand of interest and enables the ligand-based capture of receptors. After purification the samples are analyzed by mass spectrometry analysis (MS). In quantitative comparison the identified peptides are compared against a control probe [198].

2.4.2 Western Blot Analysis

Whole mouse brain tissue from adult and neonatal mice (P1, P2) was minced by Ultra-Turrax. Triton-X-100 buffer plus protease inhibition cocktail (P 8340 (Sigma)) was added and incubated for 30 minutes on ice. After centrifugation (4.000 g, 12 min, 4°C), the supernatant was collected. The protein concentration was determined by Bradford assay. 10 µg of protein lysate per sample were incubated with 1x SDS sample buffer on a heating block (70°C, 5 min). Samples and PageRulerPrestained Protein Ladder were loaded onto a 4%-20% Tris-glycin gradient gel. The electrophoresis was run (140 V, 30 mA, 30 Watt for 90 minutes) with electrophoresis or MOPS buffer. Proteins were transferred onto a Hybond ECL membrane® using a semi dry blotter (40 minutes with 23 V, 150 mA, 10 Watt). Prior to primary antibody incubation the membrane was blocked in Tris Based Saline (TBS) plus 0.2% Tween20 and 5% dry milk powder over night at 4°C. The primary antibody Anti-ACSA-2 [10 µg/mL] was applied for 1 hour at RT. The membrane was washed with TBS plus 0.2% Tween20 before the secondary antibody (goat anti rat HRP (Stemgent (1:1000)) was added and incubated for

1 hour at RT. After a washing step with TBS plus 0.2% Tween20 and distilled water, the membrane was treated with Immobilon Western Chemiluminescent HRP Substrat and the photofilm (Hyperfilm ECL) was exposed until a band appeared.

2.4.3 Immunoprecipitation

Cells from postnatal mice were obtained by tissue dissociation of whole mouse brains using the NTDK(P). 1 x 10^7 cells were pelleted by centrifugation and washed with PBS. Cells were lysed in lysis buffer supplemented with protease inhibition cocktail (P 8340 (Sigma)) using a syringe. Cells were incubated on ice for 10-30 minutes and mixed in between. Cells were pelleted by centrifugation (10,000 g, 4°C, 10 min) and the supernatant was collected. For pre-clearing the lysate was incubated with Protein G MicroBeads and incubated for 30 minutes on ice to reduce unspecific signals. The pre-cleared fraction was passed through an µ column and subsequently incubated with 15 µg of the Anti-ACSA-2 pure antibody or the ratIgG2b isotype control antibody. 50 µL of Protein G Beads were added were to both samples and incubated for 30 minutes on ice. The lysate was applied onto µ columns, washed 3 times with low salt buffer and once with high salt buffer. For elution pre-heated 1x SDS sample buffer was used. Samples were analyzed by SDS PAGE and Western Blotting.

2.4.4 Immunoprecipitation upon surface biotinylation

The protocol was kindly provided by Tobias Haas (University of Rome). In brief, the surface of the cell was labeled with a Sulfo-N-Hydroxysulfosuccinimid ester (NHS)-Biotin reagent. The Sulfo-NHS-Biotin is negatively charged and cannot permeate the cell membrane. Instead, it reacts with primary amines and N-termini of polypeptides expressed on the cell surface. In that way, the biotinylation discriminates surface molecules from cellular proteins. The biotinylation step lasted for 30 minutes at 4°C under slightly alkaline conditions (pH 7.4). The reaction was quenched by washing with PBS supplemented with 100 mM glycine. Afterwards the cells were lysed and incubated with pre-clearing Beads (Sepharose + isotype antibody or MicroBeads + isotype antibody) in PBS plus 2.5% BSA to block unspecific binding sides. The pre-clear step was repeated 3 times (3 h, 1 h and 30 minutes). Beads or Sepharose were pelleted after each incubation step. The supernatant was transferred onto the next pre-clearing sample and the pellet was incubated with 1x SDS sample buffer and frozen until anayses. Afterwards, an incubation step with empty Beads was performed. After pelleting the supernatant was incubated with the target antibody (2.5 µg Anti-ACSA-2) over night under continuous rotation. All samples were boiled and loaded onto a MOPS gel. The Western Blot analysis was performed as described before (2.4.2). For detection a Streptavidin HPR antibody was used.

2.4.5 Deglycosylation Assay

The glycosylation pattern of the ACSA-2 antigen was investigated by a deglycosylation assay using the Protein Deglycosylation MIX (NEB). Glycosylation is one of the most common post-translational modifications. Glycosylation pattern can be removed by catalysing enzymes like PNGaseF, *O*-Glycosidase, Neuramidase, Galactosidase and N-Acetylglucoamidase, which are provided in the mixture. 5 µL enzyme mix were applied to 8.3 x 10^4 cells which corresponds to 100 µg glycoprotein. Cells were incubated for 2, 4 and 6 h at 37°C, measured by flow cytometry. Additionally, sorted astrocytes were incubated with the enzyme mix for 4 h, fixed with 2% PFA and stained against ACSA-2 in combination with GFAP, CD81 [5 µg/mL; clone Eat2] as negative control and wheat germ agglutinin (1:300) as positive control. Plated cells were analyzed by immunocytochemistry (2.3.4).

2.5 Molecular Biological Methods

2.5.1 Transformation in *E.coli*

Transformation is used to introduce a DNA-plasmid into a competent recipient (bacteria, yeast, plants) for amplification. Competent cells are obtained by a chemical treatment step using calcium-chloride, which increases the permeability of the cell membrane. The transformation can be performed by heat-shock or by an electric pulse. In this study, the heat competent *Escherichia coli* (DH5alpha) were used. Aliquots were stored at -80°C and thawed on ice prior to use. The DNA-plasmid was pre-diluted to obtain a concentration of 1-10 ng/µL, applied to the bacteria and mixed by soft shaking. Cells were incubated on ice for 5 min. A heat-shock (42°C, 30sec) was applied using a water bath. Cells were resuspended in 250 µL Luria-Bertani (LB) Medium, plated on agar plate with 100 µg/mL ampicillin and cultivated at 37°C for 16 h.

2.5.2 Plasmid preparation

Colonies were picked with a toothpick. Cultures were grown in LB-suspension medium (2 mL) containing 100 µg/mL ampicillin on a shaker (300 rpm) for 16 h at 37°C. Plasmids were either isolated by the NucleoSpin® plasmid Kit or used to inoculate a 200 mL culture. Cells were grown under the given conditions. Plasmids were isolated using the NucleoBond® PC 500-Kit. DNA yield was measured on the NanoDrop. Pure DNA has a quotient E_{260}/E_{280} between 1.8 and 2.0.

2.5.3 Control restriction

Quantitative quality check of the plasmid DNA was performed by control restriction. Restriction enzymes were chosen according to restriction sites indicated on the vector map. The length of vector and insert were calculated using CloneManager. According to the manufacturer's instruction the restriction reaction was incubated for 1 hour at RT.

µL	
X	1 µg DNA
1	Restriction enzyme (10 U/µL)
2	Buffer 10X
20	*ad* aqua dest.

TEA buffer	
40 mM	Tris
20 mM	Acetic acid
1 mM	EDTA
pH 8.0	

Fragments were analyzed on a 1% agarose gel. For the electrophoresis and gel preparation TAE buffer was used. The agarose was dissolved by heating, followed by a cooling-down step in a water bath and supplemented with ethidiumbromide. This reagent binds to nucleic acids and thereby visualizes the DNA fragments under the UV light.

2.5.4 Transfection of mammalian cells

CHO and HEK cells were seeded 24 h before transfection at a density of 50,000 cell/well into a 24 well plate. 6 µL MACSfectin were mixed with 100 µL of medium. 2 µg plasmid DNA were added and incubated for 20 min at RT. The mixture was applied onto the cells. After 24 h the cells were harvested and analyzed by flow cytometry.

2.5.5 Gene expression profiling (Microarray)

ACSA-2^{+}/GLAST^{-}, ACSA-2^{+}/GLAST$^{+/-}$ and ACSA-2^{-}/GLAST^{+} cells were isolated as described in 2.2.10. Each sample group was composed of three to four samples. For each sample 50,000 cells were harvested. RNA was isolated with the RNeasy Mini Kit. Quality was anaylsed on the Agilent 2100 Bioanalyzer platform. The results were visualized as electropherogram and gel image. In addition, the RNA Integrity number (RIN) was calculated to check integrity and over all RNA quality. This value is calculated using a proprietary algorithm, which includes several quality control values, like 28S RNA/18S RNA peak area ratios and unexpected peaks in the 5S region. High RIN values (up to 10) indicate a high quality. Low RIN values (down to 1) indicate low RNA quality. For subsequent gene expression profiling experiments a RIN > 6 is sufficient [199]. In this experiment RIN values were between 3.2 and 10. In the next step 50 ng total RNA was used for the linear T-7 based amplification step. For the production of Cy3-labeled RNA the samples were amplified and labeled according to the manufactuer's protocol (Agilent Low Input Quick Amp Labeling Kit).

Dye-incorporation and yield of cRNA were measured on the NanoDrop. In the subsequent step 600 ng Cy3-labeled fragmented cRNA were hybridized overnight (17h, 65°C) to Agilent Whole Mouse Genome Oligo Microarrays 8 x 60K (Agilent's recommended hybridization chamber and oven). Following samples were processed with less Cy-3 labeled RNA: 1 sample of ACSA-2$^-$/GLAST$^+$ with 470 ng, 1 sample ACSA-2$^-$/GLAST$^+$ with 570 ng and 1 sample ACSA-2$^+$/GLAST$^-$ with 510 ng. The microarrays were washed twice for one minute: First with the Agilent Gene Expression Wash Buffer 1 at RT and second with the Agilent Gene Expression Wash Buffer 2 at 37°C. The detection of hybridized Agilent Microarrays was accomplished using Agilent's Microarray Scanner System. Analyses were performed using MetaCore. Visualization was done in MeV and Prism.

2.5.5.1 Stategies to analyse gene expression profiling data (Microarray)

The raw expression data was pre-processed at the bioinformatics department at Miltenyi Biotec. Statistical properties were equalized by quantile normalization using an R tool. Normalization facilitates comparison between arrays. Data was transformed into log_2. Discriminatory genes analysis was performed testing ACSA-2$^+$/GLAST$^-$, ACSA-2$^+$/GLAST$^+$ and ACSA-2$^-$/GLAST$^+$ genes against each other by analysis of variants (ANOVA). For statistical analysis significance values were calculated using Tukey's range test. For visulatisation heat maps were chosen.

In subsequent analysis, p-values less than 0.05 (Tukey's range test) were considered. In addition, only sample probes with one outlier or less, regarding signal intensity, were considered within the sample set of interest by the applicaton of Flags. Flags prevent usage of genes that are expressed around background level.

In a following step, changes in fold change were included. Fold changes describe the change in the quantile normalization. It is simply calculated as ratio between raw value and final value. Fold changes or log_2 ratios are of value to measure changes in gene expression levels. The log_2 ratios are more stringent as the log_2 ratio of 2/-2 corresponds to a fold change of 4/-4.

In subsequent pathway analysis, gene lists were used to identify bias towards biological processes or pathway. Probabilities of biological processes and pathways were calculated as p-values including multiple testing correction. Categories with p-values lower than 0.05 were considered.

3. Results

3.1 Identification of novel astrocyte cell surface markers by cell surface marker screening

The major bottleneck for the isolation and characterization of astrocyte subpopulations is the limited amount of astrocyte cell surface markers. To overcome this problem, a panel of 232 fluorochrome-coupled antibodies was tested to identify novel astrocyte specific cell surface markers. Flow cytometry and antibody panels are classical immunological tools commonly used to identify and study hematopoietic cells and their subpopulations [200]. The majority of surface markers tested in this approach were annotated according to the nomenclature for clusters of differentiation (CD) [201]. The surface marker screen was performed on single suspensions cells derived from whole mouse brain. These cells were obtained by a combined mechanical and enzymatic treatment as described before (2.2.2) [202]. The proteolytic activity of both enzymes, papain and trypsin, can potentially harm cell surface epitopes. Therefore, markers tested negative in this screen were maybe false negatives due to enzyme sensitivity. In this screen, astrocytes were discriminated from non-astrocytes based on the expression of the astrocyte specific markers ACSA-2 and GLAST (ACSA-1). The screen was performed twice. In total 232 antibodies, including 150 CD annotated antibodies, were tested. All tested antibodies are listed in Appendix I. Markers with a frequency over 5% on astrocytes were further validated in re-screening experiments using whole mouse brain tissue and GLAST sorted astrocytes. In the first screening no novel astrocyte cell surface marker was identified. In a second screening approach the CellSurfaceMarker Panel Mouse (BD) was chosen. Marker expression in different brain regions was addressed by violet staining (CellTrace™ (Invitrogen)). CellTrace™ is internalized by viable cells and cleaved by cellular esterases. Based on different VioDye concentrations cells of forebrain, midbrain and cerebellum were discriminated (2.2.7). Each region was investigated for the co-expression of GLAST/ACSA-2 with markers of the CellSurfaceMarker Panel. The data from this screen was visualized as heat map (Fig. 3.1 a). It represents the frequencies of all tested markers on GLAST and ACSA-2 positive astrocytes in forebrain, midbrain and cerebellum. Markers were clustered by two-dimensional hierarchical clustering using distance matrix of Pearson's correlation (Fig. 3.1). Markers with frequencies higher than 5% on GLAST or ACSA-2 positive astrocytes (regarding whole mouse brain tissue) were considered for subsequent re-screening (Fig. 3.1). Markers known to be commonly expressed by neural cells (CD90.2, CD81, CD9) were not rescreened.

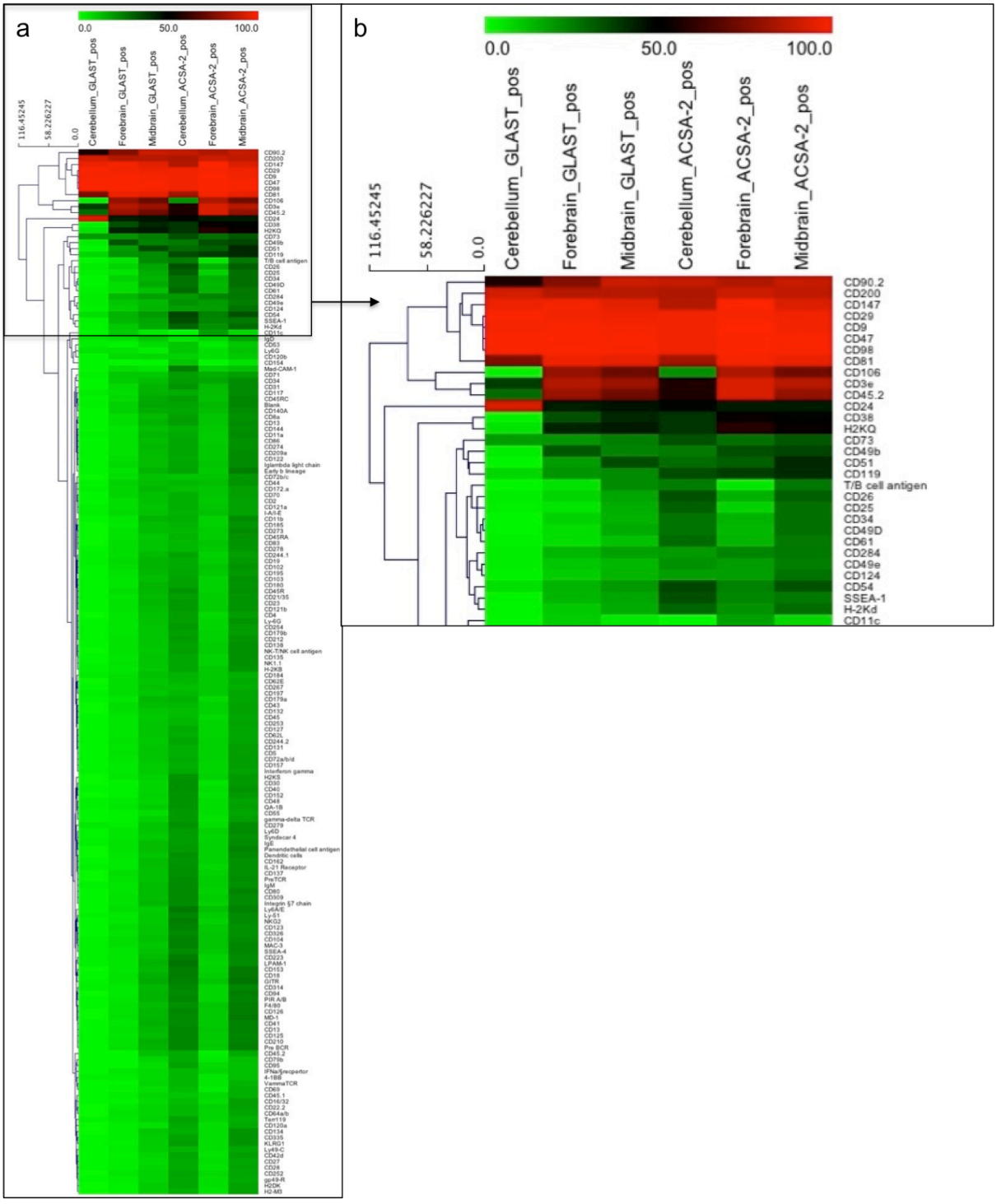

Figure 3.1: Visualization of the cell surface marker screen as heat map.

Mouse brain tissue of forebrain, midbrain and cerebellum was dissociated and discriminated by CellTrace™ labeling. Marker expression on astrocytes was determined by co-labeling with Anti-ACSA-2 and Anti-GLAST (ACSA-1). Markers tested positive on ACSA-2/GLAST expressing astrocytes of forebrain, midbrain and cerebellum were visualized as heat map (a). Markers considered for re-screening are given in (b). Level of co-expression of a given markers on GLAST and ACSA-2 positive astrocytes is indicated by color key: Green (0-40%), black (41-60%) and red (61-100%). Hierarchical clustering using distance matrix of Pearson's correlation was performed using MeV software.

In the re-screening approach some markers could not be validated. These markers were removed from the marker list. In total, 10 markers were identified, which were further validated by individual re-screening approaches. The data from the rescreen on the flow cytometer (n=3) was also visualized by a heat map (Fig. 3.2 a). Hierarchical clustering grouped ACSA-2 and GLAST positive astrocytes of forebrain (F), midbrain (M) and cerebellum (C). This illustrated that GLAST positive astrocytes of a given brain region are closer related to ACSA-2 positive astrocytes in this brain region than to GLAST positive astrocytes of another brain region (Fig. 3.2 a). In addition, the relative expression of each marker on $GLAST^+$ (1) and $ACSA\text{-}2^+$ (2) astrocytes was compared, as calculated in 2.2.7. The relative expression frequencies of each marker were comparable between ACSA-2 and GLAST positive astrocytes (Fig. 3.2 b). Marker expression on astrocytes in forebrain (F), midbrain (M) and cerebellum (C) were additionally visualized as bar diagrams (Supplementary Fig. 1). As seen in heat map and bar diagrams (Fig. 3.2 and Supplementary Fig. 1), the integrin beta-1 (CD29), the integrin associated Protein (CD47), and the a membrane glycoprotein (CD200), were co-expressed on 85 to 100% of GLAST and ACSA-2 positive astrocytes. In addition, CD29, CD47 and CD200 were detected on neurons (data not shown) indicating that these markers are commonly expressed by neural cells. Part of the T cell receptor named as CD3e and the dipeptidyl peptidase-4 ((DPP4) CD26), presented very low frequencies on astrocytes (arround 5% or less). It is likely that this expression is background staining caused by unspecific binding of the antibody or an inappropriate titer. Basigin (CD147) and vascular cell adhesion protein 1 ((VCAM-1) CD106) presented a similar expression patter. Both markers showed highest expression in forebrain, lower expression in midbrain and weak expression in cerebellum (Fig. 3.2 a, Supplementary Fig. 1). CD147 expression on astrocytes is not well characterized whereas CD106 is described e.g. to be expressed on astrocyte endfeet in the SVZ [203]. Interferon gamma receptor (CD119) and integrin α5 (CD49e) presented comparable frequencies in fore- and midbrain and were weaker expressed in the cerebellum. In contrast, the heat stable antigen (CD24) was expressed on 60% of cerebellar astrocytes and on 30-50% astrocytes from fore- and midbrain. In a further approach all 10 markers were tested on neuronal cells of the retina derived from P6 mice (Fig. 3.2 c). As in brain, the relative expression of each marker on GLAST and ACSA-2 positive astrocytes was calculated (2.2.7). In comparison to the tested brain samples CD49e (<5%), CD106 (<10%) and CD119 (<5%) showed a weak expression in the retina. Only CD24 (80-100%) and $ACSA\text{-}2^+/CD147^+$ cells (90%) showed a higher expression in the retina compared to brain samples.

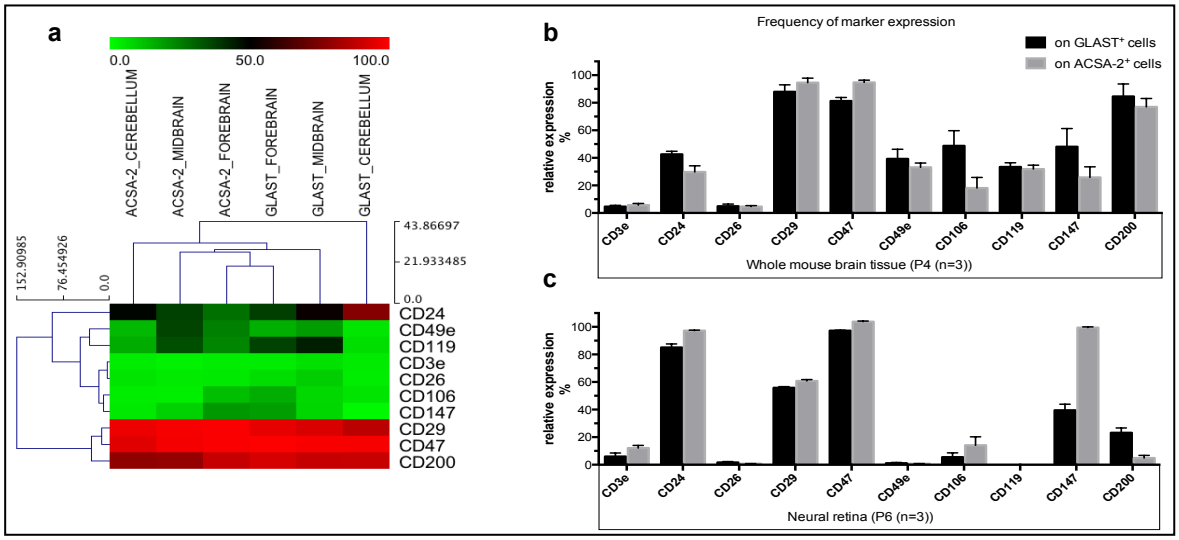

Figure 3.2: Re-screening of potential astrocyte subpopulation markers.
A surface marker screen was conducted to identify novel astrocyte subpopulation markers. Brain tissue derived from forebrain, midbrain and cerebellum was dissociated and co-labeled with the marker of interest and Anti-ACSA-2 and Anti-GLAST to discriminate marker co-expression on astrocytes. 10 markers were identified using re-screenings. The level of co-expression is indicated by color key: Green (0-40%), black (41-60%) and red (61-100%). Hierarchical clustering using distance matrix of Pearson's correlation was performed using MeV software (a). Relative expression frequency of the marker was calculated for brain tissue derived from P4 mice (b) and retina samples derived from P6 mice (c). Historgams show relative marker expression ± SD (n=3).

In the next step, pure or PE coupled antibodies directed against the identified markers were used for immunohistochemistry (IHC) or Multidimensional *in situ* Cytometry Survey (MICS) analyses. Unfortunately, only antibodies against CD24 (clone: 194-4.3) and CD119 could be used for IHC approaches. All other tested antibodies (2.2.7 Table 2) did not result in any staining. In addition, all PE coupled antibodies were tested by MICS on cultivated mixed mouse brain cells derived from P1 dissociated mouse brain. In the immunocytochemical (ICC) analysis most of the antibodies labeled different kind of neuronal cells, including astrocytes and neurons. Marker expression on astrocytes was validated by co-stainings with Anti-GLAST, Anti-GFAP and Anti-ACSA-2 specific antibodies. In the ICC, the antibody did either not result in any staining (CD49d, CD2) or the antibody recognized all astrocytes as indicated by co-labeling with the astrocyte specific antibody Anti-GLAST, as demonstrated for CD26 (Supplementary Fig. 2 a-c) and CD119 (Supplementary Fig. 2 d-f). According to these results, significant differences seen in marker expression on the flow cytometer are considered being caused by enzymatic treatment in the dissociation step. Since the epitope is able to recover during cultivation, this could explain why tested markers were expressed by all GLAST expressing astrocytes when analyzed by ICC.

3.2 Generation of astrocyte subpopulation specific antibodies by immunization

Astrocytes fulfill various tasks in different parts of the brain. Because of their ambiguous heterogeneity it is suggested that the astrocyte cell compartment is composed of different subpopulations [204,205]. Some specific subpopulation markers such as Aquaporin-4 and Kir4.1 were already identified [95,96]. For the identification and characterization of astrocyte subpopulations novel monoclonal antibodies directed against cell surface molecules would be of great benefit. To address this, one approach of this study aimed at the generation of novel antibodies directed against astrocyte subpopulations. In contrast to a 'defined-target immunization', which is conducted using transfectants and usually based on an optimized sequence of one single target gene, an 'undefined-target immunization' approach was performed using dissociated primary mouse brain tissue. The advantage to use primary cells is that the whole cell serves as immunogen. Thus, this strategy favors the generation of highly diverse antibodies. In this study, the production of monoclonal antibodies was induced by contralateral footpad immunization in rats (2.2.8) [206]. Primary GLAST positive astrocytes obtained from postnatal mice by MACS (2.2.6) served as immunogen. Cells were enriched to high purity (Fig. 3.3 a) and coated with adjuvants (2.2.8) to increase the immunological potential. The immunogen was injected subcutaneously into the left hind footpad. Unspecific immune response of the target lymph node was prevented by administration of a decoy, a neuronal cell cocktail consisting of non-astrocytes, obtained by astrocyte depletion (Fig. 3.3 b). After fusion to Sp2/0 hybridoma cells, antibody-containing supernatant of each clone was screened on dissociated primary brain tissue derived from neonatal mouse brains. Within the screening approach, the specificity of the generated monoclonal antibodies towards astrocyte cell surface epitopes was tested using co-stainings with astrocyte markers (GLAST, ACSA-2). The majority of monoclonal antibody clones obtained in these approaches recognized either all astrocytes (Fig. 3.3 c) or did not reveal specific staining (Fig. 3.3 d). In total, the generation of subpopulation specific antibodies was performed four times. Unfortunately, no subpopulation specific antibody clones were obtained by immunization.

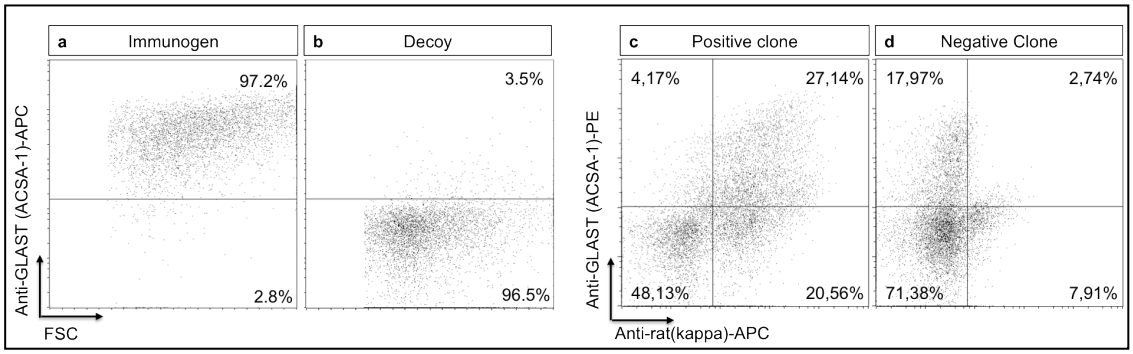

Figure 3.3: Generation of subpopulation specific antibodies by immunization.
Lewis rats were immunized by contralateral footpad immunization over a time period of 18 days. Pure astrocytes (> 95%) enriched by MACS (Anti-GLAST Biotin + Anti-Biotin MicroBeads) served as immunogen (a). For the decoy fraction, astrocytes were depleted to high purity (>95%) (b). Purities were determined on a flow cytometer. 0.5- 2 x 10^6 cells per fraction were coated with adjuvants and injected subcutaneously. Clones did either recognize all GLAST expressing astrocytes (27%) (c) or did not reveal specific staining (d).

3.3 ACSA-2 - An astrocyte specific cell surface marker

3.3.1 General expression profile of the ACSA-2 antigen

ACSA-2 antigen expression was partially investigated in collaboration with the group of Dr. Harold Cremer at the Institut de Biologie du Développement de Marseille (IBDM). The Anti-ACSA-2 antibody was titrated on adult mouse brain coronal sections of the cerebellum to determine the optimal titer. Bright specific staining in the Gcl of the cerebellum was observed at a concentration of 0.4 µg/mL. This concentration was used for all subsequent IHC experiments of adult mouse brain sections. Thereafter, the expression profile of the ACSA-2 antigen was analyzed by single stainings of the Anti-ACSA-2 antibody on sagittal and coronal adult mouse brain sections. Brightest expression of ACSA-2 was observed in brainstem (Fig. 3.4 a), the glomeruli of the olfactory bulb (Fig. 3.4 b), the globus pallidus in the telencephalon (Fig. 3.4 c) and the Gcl of cerebellum (Fig. 3.4 d). Corpus callosum, cortex and SVZ presented weaker ACSA-2 expression. Very low ACSA-2 expression was detected in the white matter of the cerebellum and the dentate gyrus of the hippocampus (Table 3, Fig. 3.4 a).

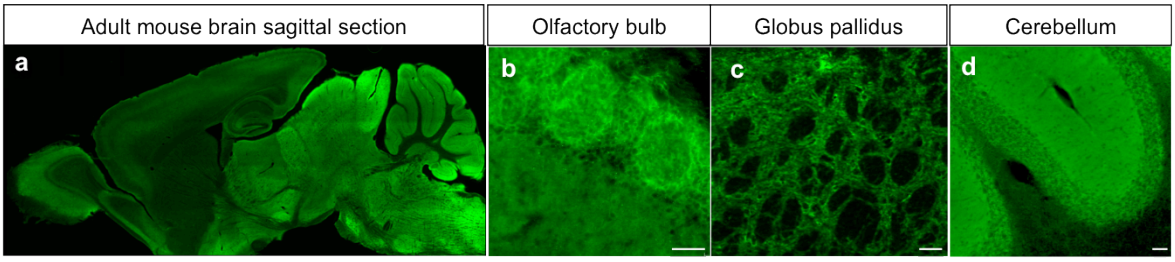

Figure 3.4: Expression profile of ACSA-2 in adult mouse brain sections.
Expression of ACSA-2 was investigated on coronal and sagittal sections. Intensity of ACSA-2 expression varies between brain regions, as illustrated in the sagittal mouse brain section (a). Highest intensities of ACSA-2 expression were detected in the glomeruli of the olfactory bulb (b), the globus pallidus (c) and the Gcl of the cerebellum (d). Scale bar represents 50 µm (b-d).

Table 3: Expression profile of ACSA-2 in adult mouse brain

Brain area	Expression level
Glomeruli (OB)	++
Mitral cell layer (OB)	+
Inner plexiform layer (OB)	+
Olfactory nerve layer (OB)	+
RMS	-
Cerebral hemispheres	+
Hippocampus (DG)	-
Hippocampus CA1/CA3	+
Corpus callosum	+
Lateral wall of the SVZ	+

Brain area	Expression level
Dorsal wall of the SVZ	+
Striatum	+
Globus pallidus	++
Thalamus	+
Granule cell layer (Cerebellum)	++
Molecular cell layer (Cerebellum)	-
White Matter (Cerebellum)	-
Pons	++
Medulla	++

Legend: Staining intensities: - very low, + low to moderate, ++ moderate to strong

3.3.2 ACSA-2 expression on different neuronal cell populations

The Anti-ACSA-2 antibody resulted from a previous immunization of rats immunized with astrocytes isolated from GFAP-eGFP mice[100]. Anti-ACSA-2 recognizes a currently uncharacterized cell surface antigen. In the following approaches, the target of the antibody, the antigen expression profile and its specificity were investigated. The expression profile of ACSA-2 was validated by different approaches: IHC analysis of adult mouse brain sections (in co-operation with the IBDM in Marseille), ICC analysis of primary mouse brain cells, including MICS of cultivated and flow cytometry analysis of dissociated neonatal mouse brain samples. Using these techniques, the co-expression of ACSA-2 with common astrocyte markers (S100β, GFAP, GLAST), oligodendrocyte markers (NG2, MBP, CD140a, O4) and neuronal markers (MAP-2, calretinin, GAD67, PSA-NCAM) was investigated. In the first step, co-expression of ACSA-2 with astrocyte specific markers such as GFAP, the calcium binding protein S100β and the astrocyte cell surface marker GLAST was tested by IHC. Therefore, the co-expression with astrocyte specific markers was investigated in the corpus callosum of adult mouse brain coronal sections. The corpus callosum is a myelin rich area that is involved in interhemispheric communication. Although the corpus callosum harbors a high frequency of glia cells, it comprises a low frequency of astrocytes [207]. This allows studying marker expression on single astrocytes. In the corpus callosum co-expression of ACSA-2 (Fig. 3.5 b,e,h) with all three tested astrocyte markers (GFAP (Fig. 3.5 a), S100β (Fig. 3.5 d) and GLAST (Fig. 3.5 g)) could be demonstrated (Fig. 3.5 c,f,i). Co-expression of ACSA-2 (Fig. 3.5 k) with GFAP (Fig. 3.5 j) was further confirmed by ICC on cultivated whole mouse brain tissue cell cultures using live cell staining (2.3.5) (Fig. 3.5 j-l). In a flow cytometric approach, co-expression of GLAST and ACSA-2 was investigated and revealed approximately 12% co-expressing cells derived from P3 mouse brain (Fig. 3.5 m). ICC analysis performed by MICS

showed that all GFAP^{+} cells expressed ACSA-2. In addition, ACSA-2^{+}/GFAP^{-} negative cells were detected (Fig. 3.5 p). Furthermore, all GLAST^{+} cells depicted ACSA-2 expression. However, GLAST^{bright}/ACSA–2^{dim} and ACSA-2^{bright}/GLAST^{dim} cells were also identified (Fig. 3.5 s).

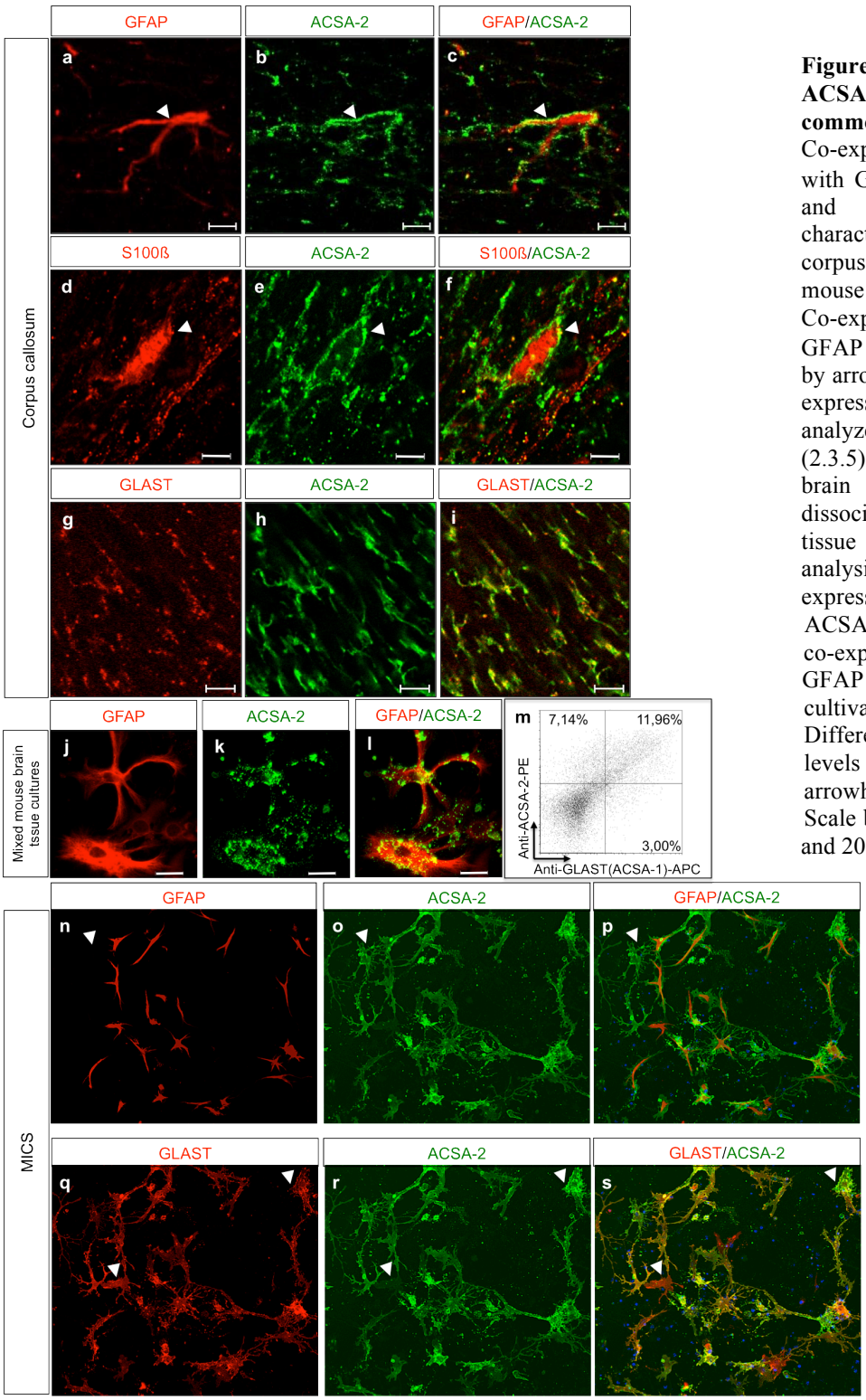

Figure 3.5:
ACSA-2 is co-expressed with common astrocyte markers.
Co-expression of ACSA-2 with GFAP (a-c), S100β (d-f) and GLAST (g-i) was characterized by IHC in the corpus callosum of adult mouse brain coronal sections. Co-expressed of ACSA-2 with GFAP and S100β is indicated by arrowheads. In addition, co-expression with GFAP was analyzed using live staining (2.3.5) on cultivated primary brain cells derived from dissociated P1 mouse brain tissue (j-l). Flow cytometric analysis showed co-expression of GLAST and ACSA-2 (m). MICS revealed co-expression of ACSA-2 with GFAP and GLAST on cultivated brain cells. Differences in the expression levels are indicated by arrowheads (n-s).
Scale bars represent 5 µm (a-i) and 20 µm (j-l).

Next, the expression of ACSA-2 on oligodendrocyte precursors and mature oligodendrocytes was investigated. Oligodendrocyte progenitors were identified by the expression of proteoglycan NG2 [208]. The corpus callosum was tested, which is mainly composed of mature oligodendrocytes but also harbors some oligodendrocyte precursors. In general, the cell surface marker NG2 showed a weak expression in the adult mouse brain. But, some NG2 positive cells were detected in the corpus callosum. These cells were not labeled by the ACSA-2 antibody (Fig. 3.6 a-c). In addition, co-expression of ACSA-2 with the myelin basic protein (MBP), a protein expressed by mature oligodendrocytes [209], was investigated in the olfactory bulb. Here, MBP was predominantly expressed in the internal plexiform layer (ipl), in the Gcl and weakly expressed in the mitral cell layer (mi). None of these layers presented co-expression of MBP and ACSA-2 (Fig. 3.6 d-f). The same result was obtained by co-stainings of MBP and ACSA-2 on mixed mouse brain tissue cultures using live staining (Fig. 3.6 g-i). In an additional approach, the co-expression of O4 (Fig. 3.6 j) and ACSA-2 was tested by MICS (Fig. 3.6 j-l). The cultivated cells did not show any co-expression of O4 and ACSA-2. These results were further supported by flow cytometric data. Therefore, mouse brain tissue cells derived from P4 mice were co-labeled with Anti-ACSA-2 and oligodendrocyte specific cell surface markers (O4, CD140a). As shown in Figure 3.6 m,n, the oligodendrocyte precursor marker CD140a and the mature oligodendrocyte marker O4 were not co-expressed with ACSA2.

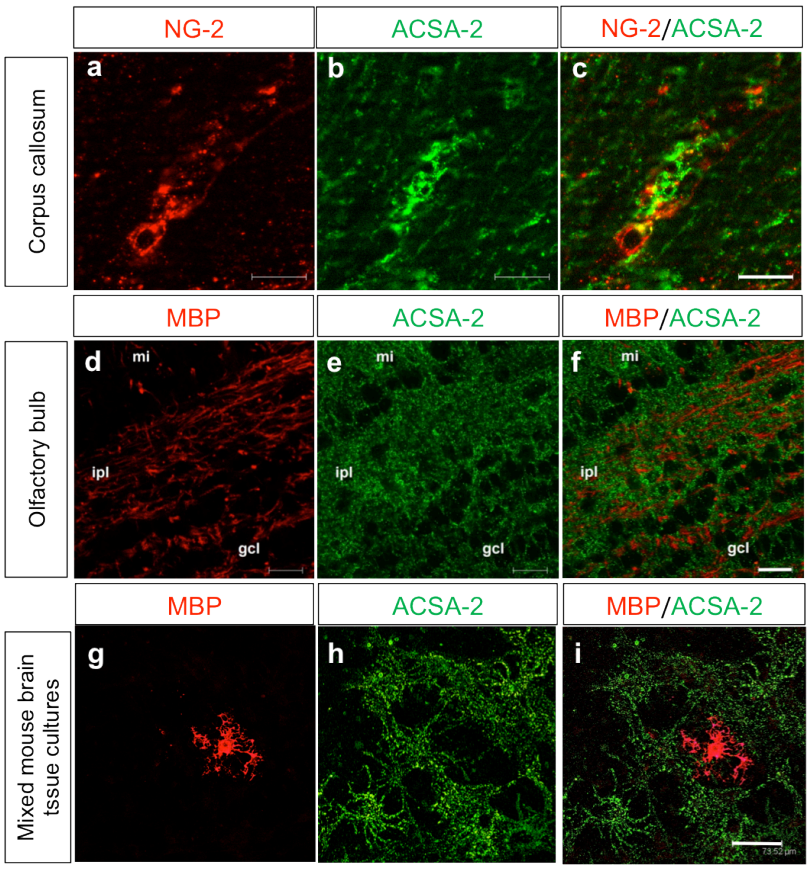

Figure 3.6:
ACSA-2 is not co-expressed with oligo-dendrocyte markers. Co-expression of ACSA-2 with oligodendrocyte specific markers was tested by IHC on adult mouse brain sections, by ICC on mixed brain tissue cells derived from P1 mice using live cell staining and MICS. Flow cytometry was performed with dissociated brain samples from P4 mice. ACSA-2 was not co-localized with NG2 in the corpus callosum (a-c). ACSA-2 was neither expressed on MBP positive oligo-dendrocytes in the corpus callosum (d-f) nor on MBP expressing cells in miced mouse brain tissue cultures derived from P3 mice (g-i). Scale bars represent 10 µm (a-c), 20 µm (d-f), 73 µm (g-i).

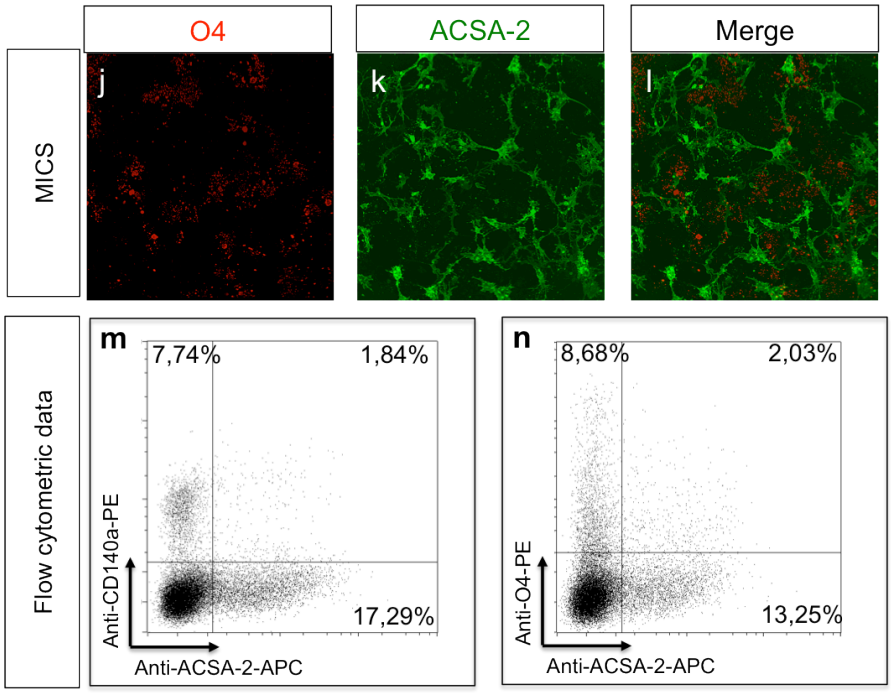

Figure 3.6: ACSA-2 is not co-expressed with oligodendrocyte markers. ACSA-2 expression was further not identified on O4 positive cells in cultivated mixed brain tissue samples derived from P1 brain tissue, as tested by MICS (2.6.4). Co-expression of ACSA-2 on CD140a and O4 positive oligodendrocytes (j,k) was further excluded by flow cytomtric analysis. Abbreviations: internal plexiform layer (ipl) mitral cell layer (mi)

In a further experiment the co-expression of ACSA-2 with neuronal markers was tested. To determine if ACSA-2 is expressed by interneurons of the olfactory bulb, calretinin, a calcium binding protein was chosen, which is expressed by interneurons in the periglomerular olfactory bulb [210]. As depicted in Fig. 3.7 a-c, calretinin was not co-expressed with ACSA-2. Additionally, expression of microtubule-associated protein MAP-2, which is a neuronal marker expressed in the dendrites of postmitotic neurons, was tested [211]. The co-expression of MAP-2 (Fig. 3.7 d,g) with ACSA-2 (Fig. 3.7 e,h) was investigated in the glomeruli of the olfactory bulb by IHC on adult mouse brain sections and by ICC on cultivated mixed neuronal brain samples using live cell staining (2.3.5) (Fig. 3.7 g-i). Both methods did not reveal ACSA-2 expression on MAP-2 positive neurons. Co-expression of ACSA-2 with the neuronal precursor marker PSA-NCAM was further tested by MICS. As shown in Figure 3.7 j-l, PSA-NCAM positive cells did not show ACSA-2 co-expression. On the single cell level, expression of ACSA-2 on GABAergic neurons and neuronal precursor cells was investigated by flow cytometry. Neuronal precursors were again discriminated by PSA-NCAM expression, as described before. Single cell suspensions were derived from P3 wt and P4 GAD67-eGFP transgenic mice. Both neuronal populations marked by GAD67-eGFP or PSA-NCAM did not present co-expression with ACSA-2 (Fig. 3.7 m,n). Thus, ACSA-2 is not expressed by neurons, neuronal subpopulations or neuronal precursors (Fig. 3.7). In addition, expression of ACSA-2 on hematopoietic cells and microglia was investigated by flow cytometry and MICS (Supplementary Fig. 3). Co-expression of ACSA-2 with CD45, a marker of hematopoietic

cells and CD11b, a marker for microglia was below 1.5% and can be considered as background staining. Besides, MICS analysis did not show co-expression of ACSA-2 and CD11b (Supplementary Fig. 3). In summary, this data shows that ACSA-2 is exclusively expressed by astrocytes and not by neurons, oligodendrocytes and microglia.

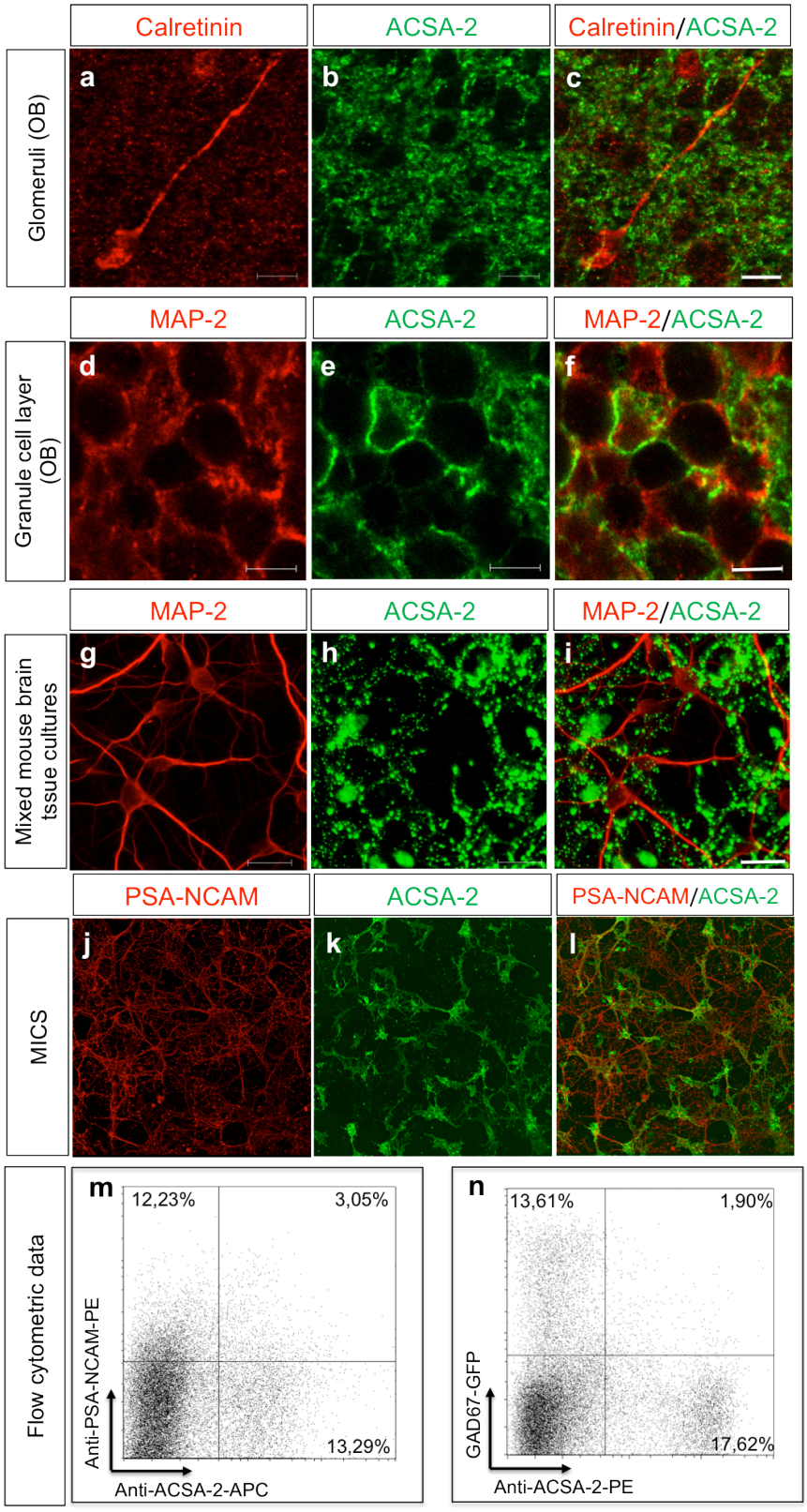

Figure 3.7:
ACSA-2 is not expressed by neurons.
Co-expression studies of Anti-ACSA-2 with different neuronal markers were performed using IHC, ICC and flow cytometry. Co-staining with the neuronal marker calretinin (a-c) and MAP-2 (d-i) did not reveal ACSA-2 expression on neurons. The expression of ACSA-2/MAP-2 was tested on cultivated brain cells by live cell staining (2.6.4). MICS experiments of ACSA-2 and PSA-NCAM were performed on cultivated mouse brain samples derived from P1 brain tissue samples (j-l). Flow cytometric data of neonatal mouse brain tissue labeled with the Anti-ACSA-2 antibody, the neuronal progenitor marker PSA-NCAM and the GABAergic marker GAD67 (m,n) did not show ACSA-2 co-expression on neuronal cells. Scale bar: 10 µm (a-c), 5 µm (d-f), 20 µm (g-i)

3.3.3 Identification of the ACSA-2 antigen

Different approaches were followed to identify the antigen which is detected by the Anti-ACSA-2 antibody. The first goal was to identify ACSA-2 expression on a cell line, which could be expanded and used for the discovery of the epitope. However, none of the cell lines showed reproducible ACSA-2 expression (tested cell lines see 2.1.8). Therefore, the following approaches had to be conducted using mouse brain tissue cells as primary cell source.

3.3.3.1 Identification of ACSA-2 antigen candidates by ligand receptor capturing

In one approach, the identification of the ACSA-2 antigen was performed by ligand receptor capturing **(**LRC) in co-operation with the group of Prof. Dr. Bernd Wollscheid at the ETH Zurich. The LRC is a mass-spectrometric approach for ligand-based identification of antigens [197]. As no suitable cell line was identified, nitrogen frozen mouse brain sections obtained from P1 mice were used. Sections were cut on the vibratome, shock frozen in liquid nitrogen and analyzed in Zurich. The LRC revealed two different candidates for the ACSA-2 antigen: GABA transporter-3 (GAT-3), with a molecular mass of around 70 kDa and Neural cell adhesion molecule (NrCAM), with a molecular mass of 131 kDa (Supplementary Fig. 4). Both markers were described being expressed by astrocytes. GAT-3 is expressed by astrocytes [231] and NrCAM is expressed by astroglioma [212]. The expression profile of ACSA-2 (3.3.1) was compared with the *in situ* hybridization pattern of both candidates (ALLEN BRAIN ALTAS [213]). Based on these findings and literature, GAT-3 was the more promising candidate [214,215].

3.3.3.2 Identification of the ACSA-2 epitope by Western Blot analyses and immunoprecipitation

Western blot analyses and immunoprecipitation were performed to verify the candidates obtained by LRC. In the first step, different cell lysis techniques were tested and validated by their signal intensity in Western Blot analysis. Western Blot analyses were performed with brain tissue lysates from early postnatal and adult brains. Mechanical cell disruption by ultra turrax and by gentleMACS was tested. Furthermore, different lysis buffers, with different ion concentrations and pH were tested (Table 4). Samples treated with the ultra turrax and RIPA buffer presented the strongest signal (a band around 40 kDa (Supplementary Fig. 5)). In the next step, reducing, non-reducing, denaturing and non-denaturing conditions were tested. Minor differences between the reducing and non-reducing, the denaturing and non-denaturing conditions were detected by Western Blotting. Afterwards, incubation time and temperature of the heating block were tested. Optimal condition were an incubation at 75°C for

8 min. For further analyses of the 40 kDa band an SDS Page was performed, the gel was stained with Coommassie and the 40 kDa band was cut out and analyzed by mass spectroscopy. The peptide identified by mass spectroscopy was α-Actin, an intermediate filament ubiquitously expressed in all cells. Accordingly, the Western Blot analysis could not address the epitope detected by the Anti-ACSA-2 antibody. To exclude technical problems, the same lysate sample was tested under the same conditions with an Anti-GAT-3 specific antibody. This positive control presented band at 70 kDa, which corresponds to the described mass of GAT-3. Therefore, technical problems could be excluded.

The next step was the establishment of an immunoprecipitation protocol, as this technique is more stringent than a Western Blot experiment. Distinct immunoprecipitation protocols were tested (Table 4). First experiments were performed using a Protein G MicroBead Kit, as described in 2.4.3. In addition, lysing isolated ACSA-2 positive cells directly on a μ column was tested. Using these methods, peptides of 40 kDa, 55 kDa and 70 kDa were identified and analyzed by mass spectroscopy. However, only ubiquitiously expressed intracellular proteins (ATPases, intermediate filaments and heat shock proteins) were identified in the mass spectroscopy approach. In co-operation with Tobias Haas from the University of Rome, a protocol for the immunoprecipitation upon surface biotinylation was established for neural tissue samples. In this method, single suspension cells are biotinylated prior to cell lysis. This protocol enables the discrimination of surface molecules including sugars from intracellular molecules. The analysis was conducted by an Anti-Streptavidin HPR labeling step, which specifically detects biotinylated molecules. The protocol was tested with different chaotropic and bionic detergents (Triton-X-100, NP-40, Brij35, Tween20). In addition, different cell numbers were tested ($0.5 \times 10^6 - 1 \times 10^8$). Unfortunately, it was not possible to address the epitope of the ACSA-2 antibody by immunoprecipitation upon biotinylation. In summary, it was not possible to address the ACSA-2 antigen by Western Blot or immunprecipitation.

Table 4: Tested conditions for Western Blot analysis and immunoprecipitation

Western Blot analysis		Neonatal tissue	Adult tissue
Lysis buffer based on:	Tris-HCl, TritonX100	x	x
	Igepal, EDTA	x	x
	RIPA	x	x
Tissue preparation methods:	Ultra turrax	x	x
	Gentle MACS	x	x
SDS-PAGE conditions	Denaturing	x	x
	Non-denaturing	x	x
	Reducing	x	x
	Non-reducing	x	x

Secondary antibodies:	Anti-rat HRP (stemgent) Anti-rat HRP (dianova) Anti-rat Fab HRP

Immunoprecipitation 0.5 x 10^6 - 1 x 10^8 cells	
Dissociated tissue	Whole brain tissue Sorted astrocytes
Cell treatment	Biotinylation
IP	Upon surface biotinylation With sorted astrocytes Protein G Sepharose Protein G Microbeads
Detergents	TritonX100 Brij-35 Tween20 Np-40

3.3.3.3 Transfection of Slc6a11 in HEK cells

Western Blot analysis and immunoprecipitation were not able to identify the ACSA-2 antigen. Expression analyses of the ACSA-2 antigen (3.3.1) demonstrated a low expression of ACSA-2 in hippocampus and high expression in cerebellum and globus pallidus (Fig. 3.4 c). In addition, immunohistochemical stainings of ACSA-2 and GAT-3 revealed a high level on co-expression as depicted by sagittal sections (Supplementary Fig. 6). Moreover, ICC on isolated astrocytes revealed co-expression of GAT-3 and ACSA-2 on astrocytes (Supplementary Fig. 7). To reveal if GAT-3 is the target of the Anti-ACSA-2 antibody, a DNA-plasmid encoding GAT-3 coupled to a GFP reporter was used (Slc6a11-GFP (Vector map see Supplementary Fig. 8)). This DNA-plasmid was amplified in *E-coli* using standard protocols (2.8.1-2.8.3). The plasmid was transfected into 1881, CHO and HEK cells using a cationic lipopolyamine transfection reagent (MACSfectin) (2.5.2-2.5.4). None of the cell lines expressed ACSA-2 prior to transfection. Best transfection efficiency was obtained in HEK cells with around 35% transfection efficiency (Supplementary Fig. 9). HEK cells were seeded at 60% confluence one day before transfection and transfected as described before (2.8.4). 50,000 cells were treated with 2 µg DNA-plasmid. For positive control, transfected HEK cells were fixed with 4% PFA 24 h after transfection, permeabilized, stained against the intracellular domaine of GAT-3 using an Anti-GAT-3 specific antibody and analyzed by microscopy. The transfected cells showed co-expression of reporter gene and Anti-GAT-3 antibody labeling (Fig. 3.8 a-d).

Samples stained with the Anti-ACSA-2 antibody did not present any co-staining on the transfected cells (Fig. 3.8 e-h). For flow cytometry, samples were harvested using Trypsin/EDTA. Cells were fixed, permeabilized for intracellular staining using fix and perm and stained with Anti-GAT-3 and Anti-ACSA-2. The flow cytometry data did neither show any ACSA-2 expression on transfected cells (Fig. 3.9 a) nor co-expression of ACSA-2 and GAT-3 (Fig. 3.9 c) was detected. In contrast, the transgene was recognized by the Anti-GAT-3 antibody as demonstrated by intracellular staining (Fig. 3.9 b). From this data it can be concluded that Anti-ACSA-2 does not recognize GAT-3.

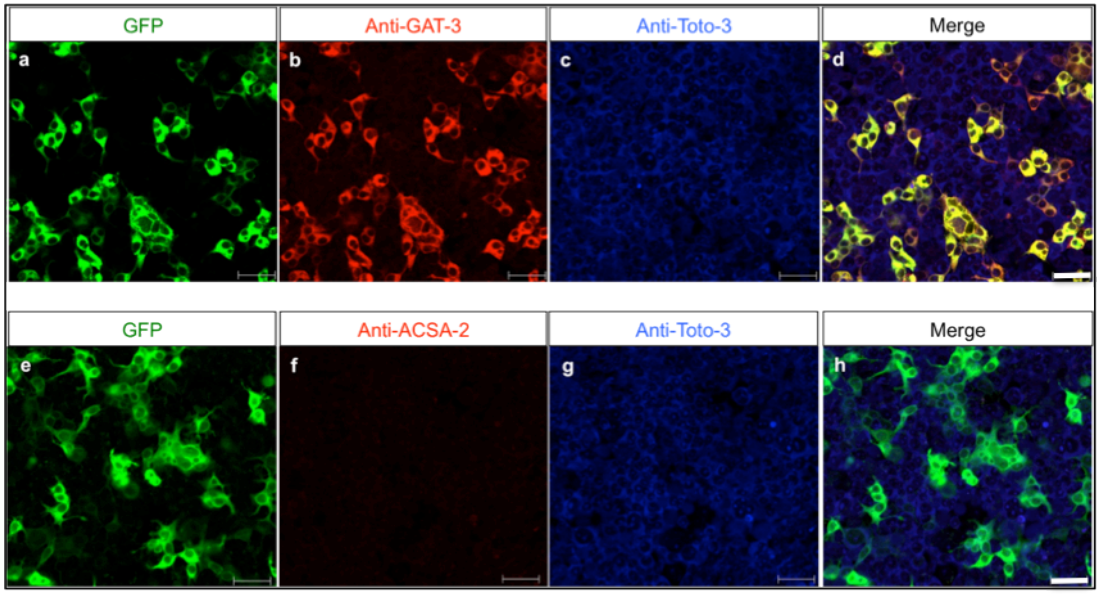

Figure 3.8: Transfection of HEK cells with the Slc6a11 plasmid.
HEK cells were seeded at 60% confluence one day before transfection. Cells were fixed with 4% PFA 24 h post transfection. The plasmid harbors a GFP reporter. Cells were stained with Anti-ACSA-2 (1 µg/mL), Anti-GAT-3 (0.4 µg/mL) and Anti-Toto-3 for nuclei staining. Analysis revealed co-expression of GFP with Anti-GAT-3 (a-d) but no co-expression of GFP with Anti-ACSA-2 (e-h). Scale bar represents 50 µm.

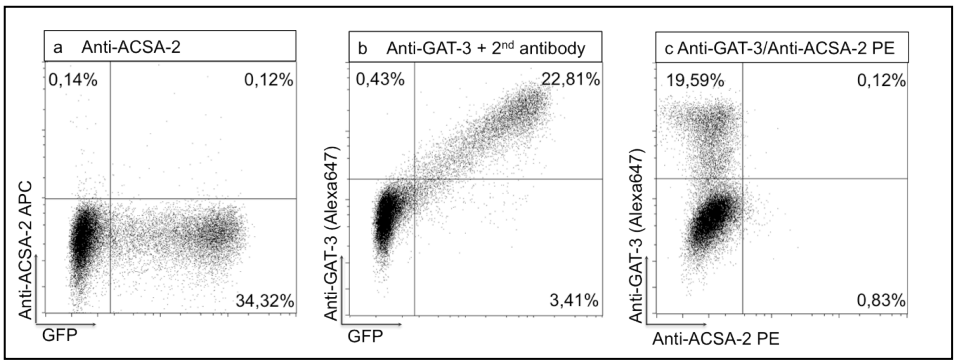

Figure 3.9: Transfection of HEK cells with the Slc6a11 plasmid.
HEK cells were seeded at 60% confluence and transfected with the DNA-Plasmid (Slc6a11) 24h later. Cells were fixed 24 h after transfection and stained against ACSA-2 (a), GAT-3 (b) and a combination of both markers (c). Cells were analyzed by flow cytometry. The expression of the reporter (GFP) was detected in the FITC channel.

3.3.3.4 Deglycolsylation assay

A deglycosylation assay was established to address whether the Anti-ACSA-2 antibody recognizes a glycosylation pattern on astrocytes. In the first test, whole mouse brain single cell suspension cells were used. Cells were incubated with a deglycosylation mix for 2, 4 and 6 h at 37°C (2.5.5). Thereafter, cells were stained with the Anti-ACSA-2 antibody and the deglycosylation efficiency was measured by flow cytometry. No effect was seen after 2 h. After 6 h cells were dead as indicated by PI labeling. In correspondence to the protocol, the optimal incubation time to obtain a deglycosylation effect on astrocytes was 4 h. The mean fluorescence intensity (MFI) and also the cell number of viable ACSA-2 positive cells was moderately decreased after the deglycosylation treatment, whereas control samples presented a higher MFI (data not shown). For validation, the experiment was repeated by ICC on plated cells after 3 days *in vitro*. This treatment was performed under equal conditions, cells were treated with the enzyme mix for 4 h at 37°C. In this experiment, the deglycosylation reaction revealed a decrease in the signal intensity of the Anti-ACSA-2 labeling, which was measured by the decrease of the mean signal intensity as calculated using ImageJ (Fig. 3.10 a). In addition, immunocytochemical stainings revealed a strong decrease in the signal intensity of the Anti-ACSA-2 labeling in the presence of the deglycosylation enzyme (Fig. 3.10 c). As control, equal cell amouts were treated under buffer only conditions (Fig. 3.10 b). As positive control, wheat germ agglutinin (WGA) was chosen, which is an ubiquitiously expressed lectin [216]. It selectively binds to N-acetylglucosamine and N-acetylneuraminic acid (sialic acid) residues [217]. The WGA specific antibody revealed co-expression with the Anti-ACSA-2 specific antibody (not shown). Upon deglycosylation, the signal intensity of the WGA labeling was decreased (Fig. 3.10 d,e). As negative controls, GFAP and CD81 were chosen. GFAP served as survival control of treated astrocytes and was not affected by the deglcyosylation treatment (Fig. 3.10 f,g). CD81 is a not post-transcripionally glycosylated and was therefore chosen as negative control [218]. In this assay, the signal of the labeling of the CD81 antibody did not show an alteration in the signal intensity after deglycoslyation (Fig. 3.10 h,i). In conclusion, this data presents that the Anti-ACSA-2 antibody most likely recognizes a sugar moiety or a glycosylation related pattern on the astrocyte cell surface.

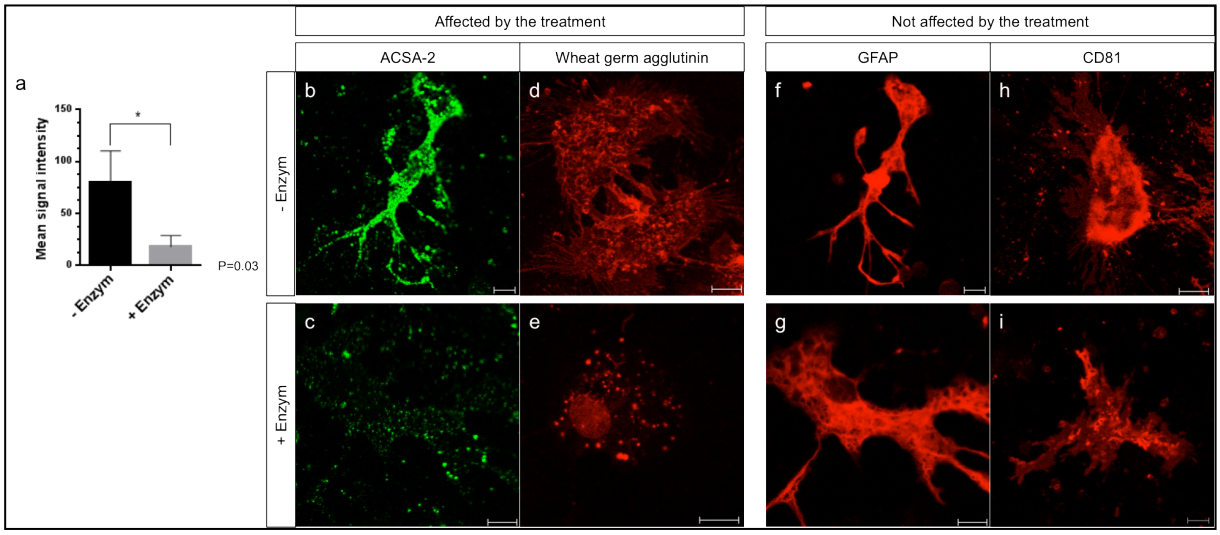

Figure 3.10: Addressing the ACSA-2 antigen by deglycosylation assay.
The deglycosylation assay was conducted on isolated ACSA-2 positive cells derived from P2 mice after 4 days *in vitro*. Deglycosylation has a significant effect on the signal intensity of the Anti-ACSA-2 labeling, as measured by the decrease of the mean signal intensity (Calculated in ImageJ) (a). ICC revealed a decreased in the signal intensity of the Anti-ACSA-2 and the WGA labeling upon declycosylation (b-e). Labeling of Anti-GFAP and the CD81 specific antibody were not affected by the treatment (f-i). Scale bar represents 10 µm.

3.4 Comparison of GLAST and ACSA-2 expression

3.4.1 Expression of GLAST and ACSA-2 in the embryonic mouse brain

Approaches to generate and identify novel astrocyte subpopulation specific antibodies were performed to enlarge the antibody panel for the isolation and subsequent analyses of astrocyte subpopulations. Unfortunately, both approaches were not successful. Therefore, ACSA-2 and GLAST were used in a comprehensive analysis to analyse whether ACSA-2 and GLAST allow for the discrimination of astrocyte subpopulations. Distinct regions of central nervous tissue were tested at several developmental stages using different methods. In the first step, the expression of ACSA-2 and GLAST was analyzed on embryonic whole mouse brain tissue by flow cytometry. This study addressed whether ACSA-2 and GLAST reveal differences in the expression at embryonal age and allow for the disctimination of astrocyte subpopulations at this stage. As reported in literature, in mice, precursors differentiate into astrocytes around E14 [219]. To address this, the ACSA-2 and GLAST expression was analyzed on dissociated embryonic brain tissue samples derived from E12, E14, E16 and E18 mouse brains by flow cytometry (2.2.5.1). To address glial precursors, a co-staining with the cell surface ganglioside A2B5 was performed. Expression of A2B5 is upregulated during embryonic development [220,221]. In this analysis, A2B5 was detected on E12 mouse brain tissue (Fig. 3.11 a,e) [222]. In contrast, the frequencies of GLAST and ACSA-2 positive astrocytes detected between E12 and E16 were less than 5% (Fig. 3.11 b,c,e,f). Frequencies of GLAST$^+$ and ACSA-2$^+$ astrocytes increased rapidly around E18 (Fig. 3.11 d,h). In parallel, the co-

expression of A2B5 with GLAST and ACSA-2 increased to 10% (Fig. 3.11 d,h). At late embryonic stage (E18) arround 10% GLAST$^+$/A2B5$^+$, ACSA-2$^+$/A2B5$^+$ double positive and approximately 5% GLAST$^+$/A2B5$^-$, ACSA-2$^+$/A2B5$^-$ cells negative for A2B5 expression were detected (Fig. 3.11 d,h).

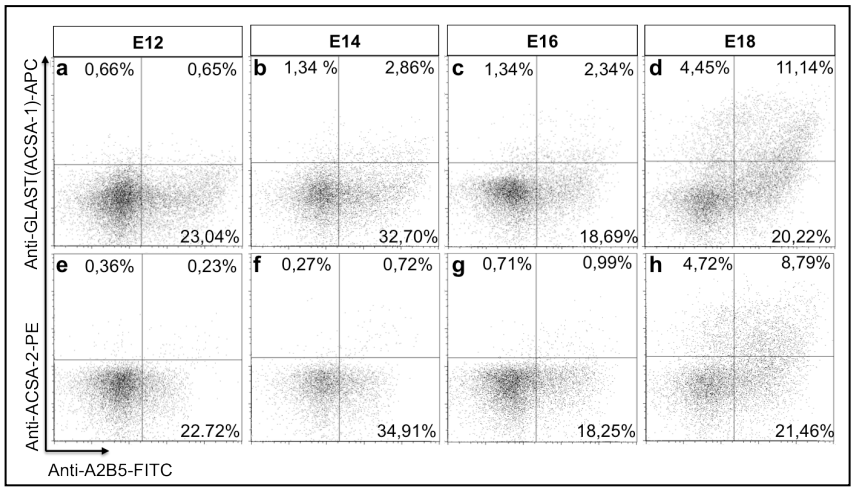

Figure 3.11: Expression profile of GLAST, ACSA-2 and A2B5 in embryonic mouse brain.
Dissociated embryonic mouse brain tissue samples derived from different developmental stages (E12/E14/E16/E18) were dissociated and analyzed by flow cytometry for GLAST, ACSA-2 and A2B5 expression.

In the next step, frequencies of GLAST$^{+/-}$/ACSA-2$^{+/-}$ cells were investigated at embryonic age. As seen in Figure 3.12, between E12 and E16 GLAST or ACSA-2 positive cells were not detected (< 5%). A population of around 10% GLAST$^+$/ACSA-2$^+$ cells was first detected at E18 (Fig. 3.12 d). Furthermore, approximately 6% ACSA-2$^+$/GLAST$^-$ and 4% ACSA-2$^-$/GLAST$^+$ cells were identified at E18 (Fig. 3.12 d). In summary, this approach shows that ACSA-2 and GLAST expression on embryonic mouse brain tissue was seen as early as E18. ACSA-2 and GLAST are co-expressed but minor frequencies of ACSA-2$^+$/GLAST$^-$ and ACSA-2$^-$/GLAST$^+$ are detectable in the embryonic brain.

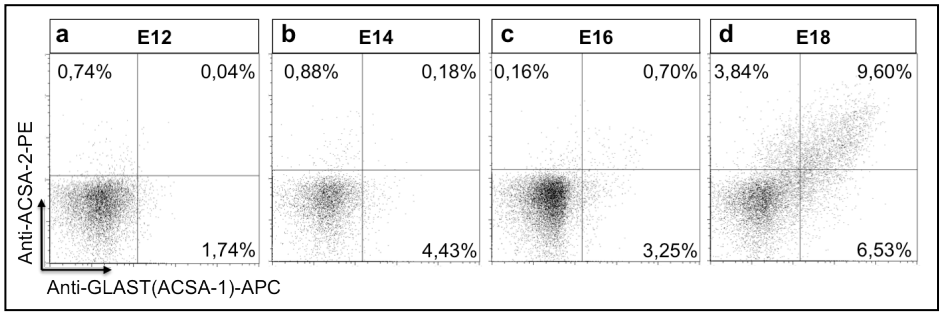

Figure 3.12: Expression profile of GLAST and ACSA-2 in embryonic mouse brain.
Embryonic mouse brain tissue samples (E12/E14/E16/E18) were further investigated for their co-expression profile of GLAST and ACSA-2.

3.4.2 Expression of GLAST and ACSA-2 in neonatal mouse brain tissue

In comparison to embryonic mouse brain, the percentage of astrocytes in postnatal (also referred as neonatal brain) and adult brain increased substantially. Therefore, the expression profile of GLAST and ACSA-2 was investigated at neonatal age. As depicted in Figure 3.13, a total frequency of 15% GLAST$^+$ astrocytes was detected in postnatal mouse brain (P3). ACSA-2$^+$ astrocytes revealed total frequencies of approximately 20% in P3 mouse brain samples. Although GLAST and ACSA-2 are co-expressed by the majority of astrocytes (11.94%) a low frequency of ACSA-2$^-$/GLAST$^+$ cells (3%) and a higher frequency of ACSA-2$^+$/GLAST$^-$ cells (7,14%) was detectable.

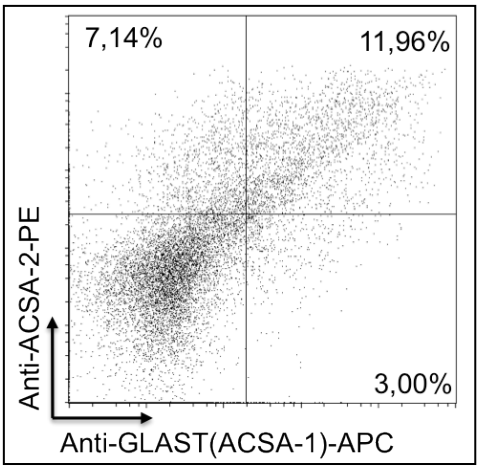

Figure 3.13:
Expression of GLAST and ACSA-2 in early postnatal mouse brain
Expression of GLAST and ACSA-2 was investigated by flow cytometry using P3 mouse brain tissue. Minor frequencies of single positive populations were seen although in the major fraction both markers are co-expressed.

Frequencies of ACSA-2$^-$/GLAST$^+$, ACSA-2$^+$/GLAST$^+$ and ACSA-2$^+$/GLAST$^-$ were further addressed in an age-dependent manner. Therefore, whole brain tissue at developmental stages (between P1 and P7) was chosen. In biological replicates (n=3), frequencies of ACSA-2$^-$/GLAST$^+$ (Fig. 3.14 a), ACSA-2$^+$/GLAST$^+$ (Fig. 3.14 b) and ACSA-2$^+$/GLAST$^-$ (Fig. 3.14 c) were analyzed. This analyses revealed differences between the three populations (Fig. 3.14). Thus, subsequent investigations aimed at the prospective characterization of the ACSA-2$^-$/GLAST$^+$ and the ACSA-2$^+$/GLAST$^-$ cell subset, as differences in marker expression were considered to display astrocyte subpopulations.

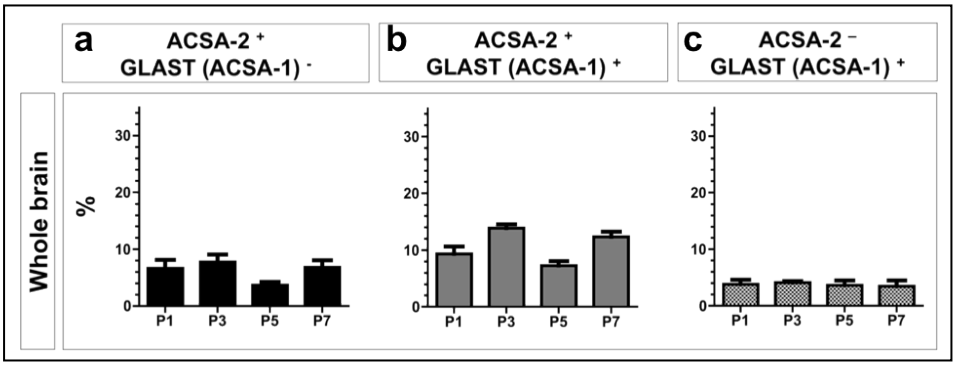

Figure 3.14: Comparison of GLAST and ACSA-2 expression on whole mouse dissociated brain tissue. Whole mouse brain tissue of P1, P3, P5 and P7 mice was dissociated and stained against GLAST and ACSA-2. Frequencies of ACSA-2$^+$/GLAST$^-$ (a), ACSA-2$^+$/GLAST$^+$ (b) and GLAST$^+$/ACSA-2$^-$ cells (c) were identified using flow cytometry (n=3). Shown are frequencies ± SD.

To address the cellular origin of the single positive populations the expression profile of ACSA-2 and GLAST was investigated in different areas of the brain by flow cytometry and IHC. At first, the expression of GLAST and ACSA-2 in postnatal mouse brain tissue was analyzed between P1 and P7 on the single cell level by flow cytometry. Single cell suspensions of olfactory bulb, midbrain and diencephalon, cerebral hemispheres, hippocampus and cerebellum were analyzed. These regional expression profiles revealed characteristic expression patterns of GLAST and ACSA-2 for each brain region (Fig. 3.15 and Supplementary Fig. 10). Besides, the area specific analyses enabled for the identification of minor cell populations that are under-represented in the whole mouse brain (compare Fig. 3.14, Fig. 3.15). In the olfactory bulb a high percentage of ACSA-2$^+$/GLAST$^-$ (20%) and a low percentage of ACSA-2$^-$/GLAST$^+$ (<5%) and ACSA-2$^+$/GLAST$^+$ cells (<8%) was identified (Fig. 3.15 Supplementary Fig. 10). For further analysis, ACSA-2$^+$/GLAST$^-$ cells of the olfactory bulb were isolated, plated and stained against GLAST and ACSA-2. However, after isolation the plated cells were immunopositive for GLAST as analyzed by ICC (data not shown). This effect can be caused either by an application dependent sensitivity of the GLAST antibody, which is more sensitive in ICC and IHC than in flow cytometry, or by a slight trypsin sensitivity of the GLAST epitope. In comparison to the olfactory bulb, the frequency of GLAST$^+$/ACSA-2$^+$ cells was higher in the other tested brain regions between P1 and P7: In cerebral hemispheres the majority of astrocytes co-expressed both markers (11-25%). ACSA-2$^-$/GLAST$^+$ or ACSA-2$^+$/GLAST$^-$ astrocytes were detected with frequencies less than 7% at P7 (on average). In midbrain and hippocampus high frequencies of ACSA-2$^+$/GLAST$^-$ (8-25%) and ACSA-2$^+$/GLAST$^+$ cells (7-18%) were detected. Frequencies of ACSA-2$^-$/GLAST$^+$ cells in midbrain and hippocampus were lower than 5%. In summary, ACSA-2$^-$/GLAST$^+$ presented low percentages (<5%) in cortical hemispheres, midbrain and hippocampus. In contrast, in cerebellum, a high frequency of ACSA-2$^-$/GLAST$^+$ cells was detected (2-8%). Based on these analyses the highest expression was detected at P1 (8%).

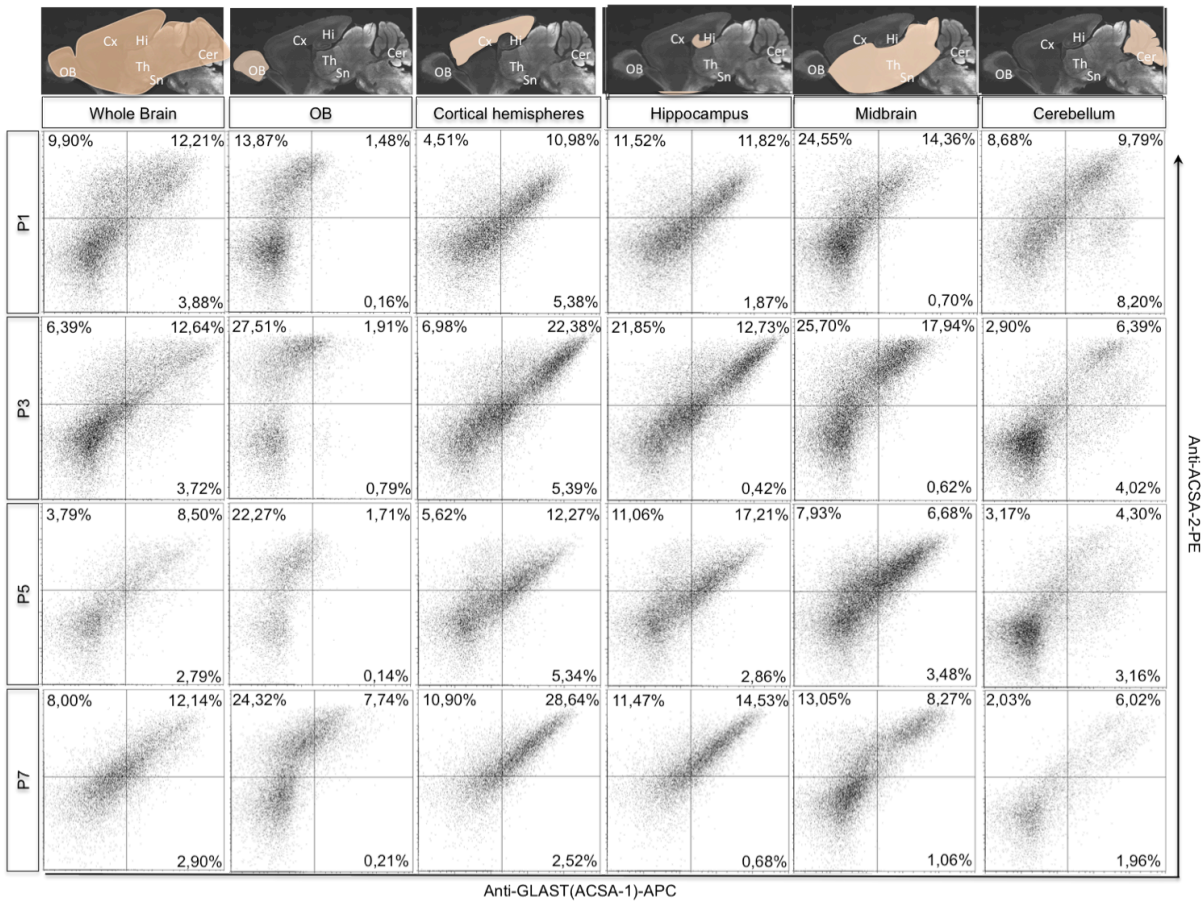

Figure 3.15: Expression of GLAST and ACSA-2 in distinct regions of neonatal mouse brain (P1-P7). Tissue samples were dissociated, stained with GLAST and ACSA-2 specific antibodies and analyzed by flow cytometry. Whole brain tissue and brain areas olfactory bulb, cortex, hippocampus, midbrain/diencephalon and cerebellum were investigated at P1, P3, P5 and P7. Frequencies of ACSA-2$^+$/GLAST$^-$, ACSA-2$^+$/GLAST$^+$ cells ACSA-2$^+$/GLAST$^-$ cells were analyzed by flow cytometry. Shown is one representative dot plot per age and region.

3.4.3 Comparison of GLAST and ACSA-2 expression in olfactory bulb, RMS and cortical hemispheres

Aim of this approach was to address the differences between GLAST and ACSA-2 expression in the adult mouse brain by IHC, similar to those observed in neonatal brain. However, it was not possible to obtain a specific staining of the ACSA-2 antibody on neonatal brain tissue. Different treatments, increasing antibody concentration and decreasing PFA concentration could finally reveal a weak labeling of the ACSA-2 antibody in brain reagions, which show a high ACSA-2 expression (e.g. the cerebellum). Therefore, following analysis of GLAST and ACSA-2 expression were performed on adult mouse brain coronal sections. Immunohistochemical analysis of adult mouse brain sections revealed co-expression of GLAST and ACSA-2 in most areas of the adult brain. Co-expression of GLAST and ACSA-2 in the corpus callosum was described earlier in chapter 3.3.2 (Fig. 3.5 g-i). As demonstrated in

Figure 3.16, co-expression between ACSA-2 and GLAST was detected in different cortical layers. GLAST expression was restricted to defined layers in the cortex, whereas ACSA-2 presented a homogenous expression pattern in the cortex.

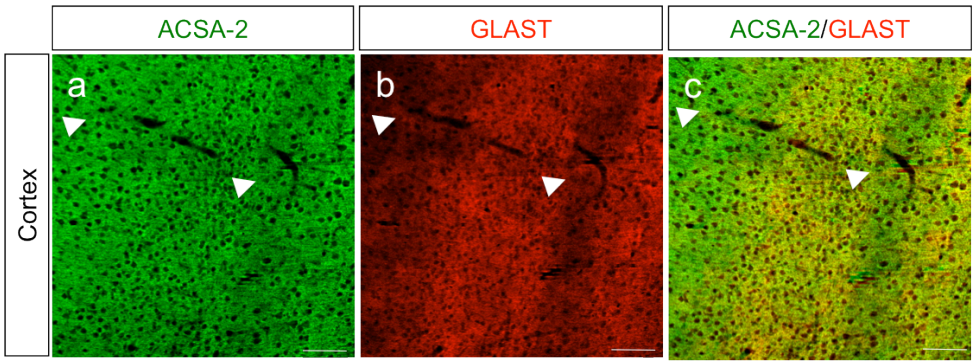

Figure 3.16: Expression of GLAST and ACSA-2 in the cortex of adult mice brains.
Expression of GLAST and ACSA-2 in the cortex of adult mouse brain coronal sections. Floating sections (40 µm) were stained with Anti-ACSA-2 (a) and Anti-GLAST (b). Not all layers present ACSA-2/GLAST co-expression as shown by overlay and arrowheads (c).

A difference in the expression pattern between GLAST and ACSA-2 was seen at lower magnification in the olfactory bulb (Fig. 3.17 a-c). As depicted, GLAST presented homogenous expression profile in all layers of the olfactory bulb (Fig. 3.17 b). Expression of ACSA-2 was predominant in the glomeruli of the olfactory bulb and weaker in the inner layers of the olfactory bulb (Fig. 3.17 a). Higher magnification images of the olfactory bulb revealed co-expression of both markers in the glomeruli of the olfactory bulb (Fig. 3.17 d-f). Differences in the expression pattern of GLAST and ACSA-2 were seen for the 'tunneling astrocytes' in the RMS (Fig. 3.17 g-i). As reported by Jungblut *et al.* GLAST is expressed on astrocytes in the RMS. In contrast to GLAST, ACSA-2 was weakly expressed on 'tunneling astrocytes' (Fig. 3.17 g (arrowheads)). In the olfactory bulb at the level of the rostral margin of the accessory olfactory bulb in the area of the anterior olfactory nucleus high expression of ACSA-2 and low expression of GLAST was detected (Fig. 3.17 g-i (*)).

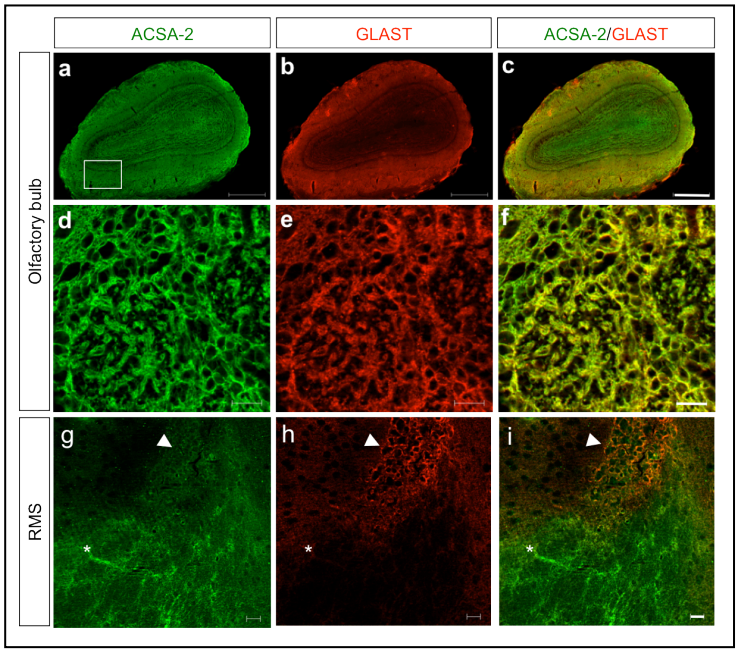

Figure 3.17: Area specific expression pattern of ACSA-2 and GLAST.
Adult mouse brain coronal sections (40 µm) were stained as floating sections. Brain sections revealed differences in the expression pattern between ACSA-2 and GLAST in the olfactory bulb (a-c, d-f) and RMS (g-i). Arrowheads indicate strong GLAST expression in the RMS. (*) indicates ACSA-2 expression in the anterior olfactory nucleus.
Scale bars: 500 µm, (a-c), 20 µm (d-i).

Tunneling astrocytes are a specialized subtype of astrocytes, which serves as scaffold for migrating neuroblasts in the RMS. The interaction between astrocytes and neurons of the RMS is mediated by soluble molecules and by cell-cell contacts, mainly through interaction of receptors and ligands. Apart from their interaction with migrating neuroblasts and their migration supporting function, little is known about the properties of this specialized subset of astrocytes. The following experiment aimed at the characterization of ACSA-2 and GLAST expressing 'tunneling astrocytes' by flow cytometry. Therefore, RMS tissue was dissected from adult mice (10 weeks (n=3)) and analyzed on the single cell level using a flow cytometer (Fig. 3.18 a). For regional control striatal tissue was dissociated and stained in parallel (Fig. 3.18 d). Migrating neuroblasts were detected by the expression of PSA-NCAM. As demonstrated in Figure 3.18 b, the frequency of migrating neuroblasts in the RMS tissue was 13.10%. In contrast, PSA-NCAM positive cells were not detected in striatum (1% (Fig. 3.18 e)). Frequencies of astrocytes in striatum and RMS were measured based on equal cell amounts. A high frequency of astrocytes was detected in the striatum with approx. 40% (Fig. 3.18 f). 14% of the cells were $GLAST^+/ACSA\text{-}2^-$ and 27% $GLAST^-/ACSA\text{-}2^+$. Low percentages of astrocytes were detected in the area around the RMS (<5%) (Fig. 3.18 c). In contrast to the IHC data $GLAST^+/ACSA\text{-}2^+$ and also $GLAST^-/ACSA\text{-}2^+$ cells were detected by flow cytometry. According to the flow cytometric data the identification of $GLAST^+/ACSA\text{-}2^-$ cells in the RMS could not be validated.

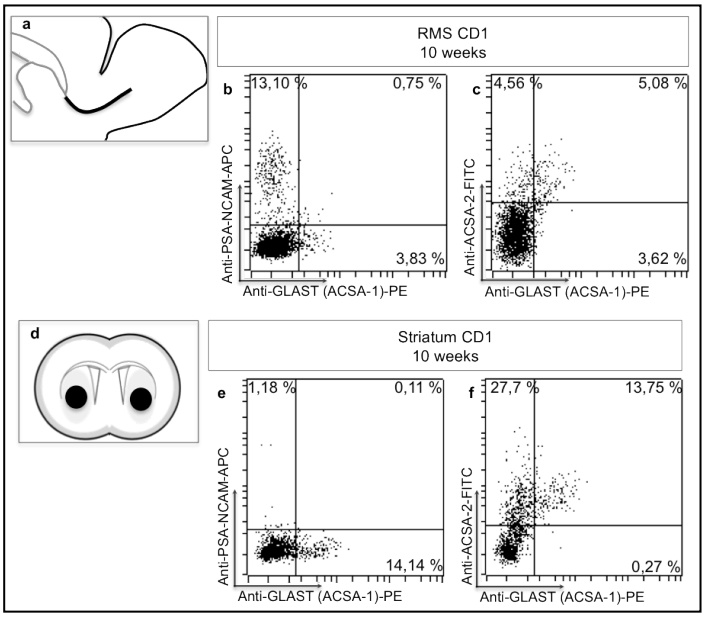

Figure 3.18: Flow cytometric analyses of astrocytes in the RMS and striatum.
RMS and Striatum were dissected from adult mouse brain, dissociated, stained and analyzed by flow cytometry. Tissue samples from RMS (a) and striatum (b) were stained against GLAST and ACSA-2. Migrating neuroblasts were discriminated by PSA-NCAM labeling (b,e).

3.4.4 Comparison of GLAST and ACSA-2 expression in neurogenic regions of adult and neonatal mice

A further question addressed in this work was whether GLAST and ACSA-2 allow for the identification and prospective isolation of neural stem cells. The dentate gyrus of the hippocampus is one neurogenic niche, which was already investigated in the neonatal mouse brain by flow cytometry. In the neonatal hippocampus high frequencies of $GLAST^+/ACSA\text{-}2^+$ cells was detected (3.4.2). In this study, the expression of GLAST and ACSA-2 in the hippocampus of the adult mouse brain was investigated by IHC. As known from literature, the dentate gyrus of the hippocampus is a glutamate rich area and reveals a high expression of the glutamate transporter GLAST [104]. Interestingly, a very weak expression of ACSA-2 was detected in the hippocampus of adult mouse brain (Fig. 3.19 a). To further address these differences, the adult hippocampus was dissected and analyzed. Therefore, the dissociation protocol was optimized to obtain viable cells. However, it was not possible to obtain enough vital cells from this brain region to perform further analyses.

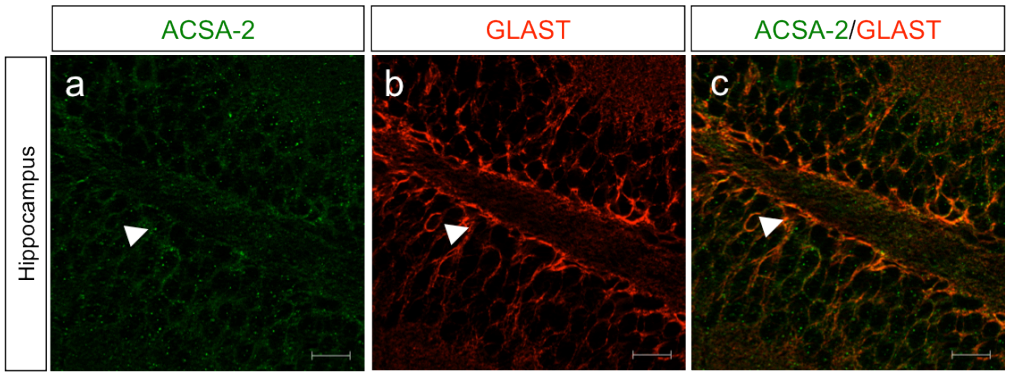

Figure 3.19: Expression of GLAST and ACSA-2 in adult hippocampus.
Coronal sections of adult mouse brain (40 µm) were stained as floating sections against ACSA-2 (a) and GLAST (b). Very weak staining of ACSA-2 was detected in the hippocampus. In contrast a high expression of GLAST was detected. Scale bar represents 20 µm.

One aim of current stem cell research is the identification of a cell surface marker that allows for the isolation of adult SVZ stem cells. However, the major problem is the identification of a marker, which is neither expressed by ependymal cells nor by surrounding astrocytes in the SVZ. For GLAST it was already shown that it is expressed by stem cells of the SVZ using *in vivo* electroporation and IHC [104]. However, GLAST is further expressed by surrounding astrocytes in the lateral ventricle. Therefore, GLAST alone is not sufficient for the enrichment of SVZ derived stem cells. This approach addressed whether ACSA-2 is expressed by SVZ stem cells or by surrounding astrocytes in the SVZ. If ACSA-2 is not expressed by SVZ derived stem cells a combination of ACSA-2 and GLAST could be used to isolate SVZ stem cells. Therefore, the expression profile of ACSA-2 and GLAST was investigated in the dorsal and lateral wall and the dorsal horn of the SVZ on adult mouse brain coronal sections. The dorsal part of the SVZ adjoins the corpus callosum and the lateral wall adjoins the striatum (Fig. 3.20 a). The dorsal horn (Fig. 3.20 a-c) forms ventrally and dorsally and connects dorsal and lateral wall (Fig. 3.20 g-i). All stem cell areas presented a bright expression of GLAST (Fig. 3.20 b,e,h) and a comparatively weak expression of ACSA-2 (Fig. 3.20 a,d,g). The expression of ACSA-2 was weakest in the dorsal wall (Fig. 3.20 d) and brighter in the dorsal horn and the lateral wall (Fig. 3.20 a,g). In all stem cell regions of the SVZ the expression of ACSA-2 was brighter than in the surrounding tissue of striatum and corpus callosum (Fig. 3.20 a). In summary, the IHC analyses showed GLAST and ACSA-2 co-expression in all three compartments of the SVZ (Fig. 3.20 c,f,i).

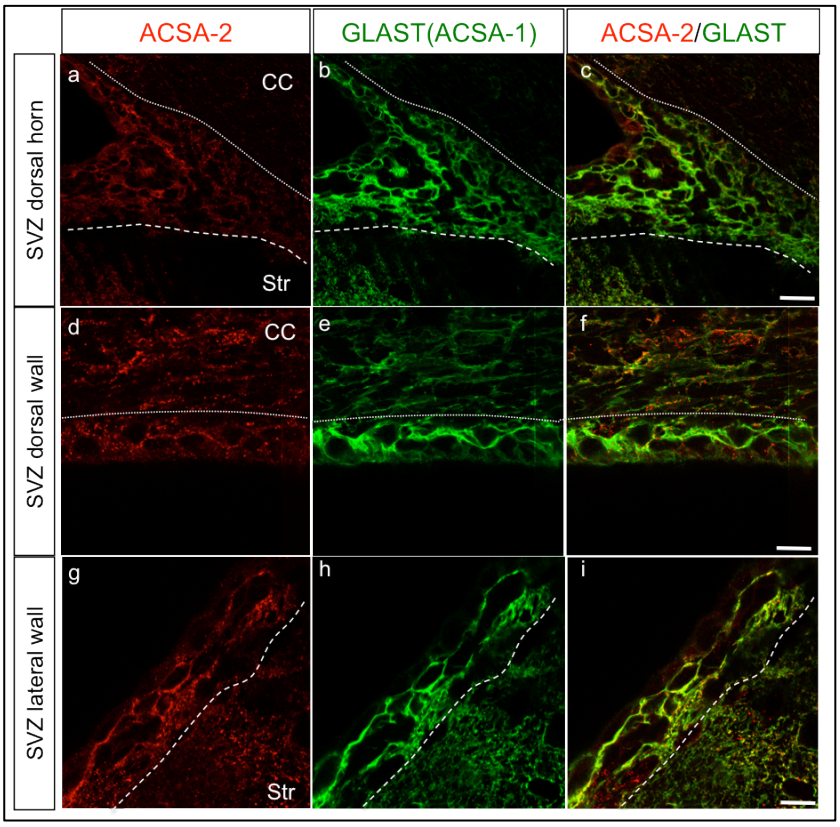

Figure 3.20: ACSA-2/GLAST (ACSA-1) co-staining in the SVZ. Coronal sections of the adult mouse brain were stained as floating sections (40 µm). The SVZ was co-stained with ACSA-2 and GLAST (ACSA-1) specific antibodies. Marker expression was investigated on the dorsal horn (a-c), the dorsal wall (d-f) and the lateral wall (g-i) of the SVZ. Scale bar represents 10 µm. Abbreviations: CC: Corpus callosum, Str: Striatum.

In a further step, the expression of ACSA-2 on electroporated neonatal tissue was investigated in collaboration with the IBDM in Marseille. *In vivo* electroporation of the dorsal and a lateral wall of the SVZ was performed with a GFP plasmid to efficiently target neural precursor (NPCs) in the SVZ [212]. The animals were perfused on day one post electroporation (1dpe). At this time, the GFP-encoding plasmid is detectable in radial glia, the neural stem cells of the postnatal SVZ [195,223] (Fig. 3.21 b). The better staining of the ACSA-2 antibody was observed in the dorsally electroporated mice (Fig. 3.21 a). As described previously, ACSA-2 presents a weak labeling in the neonatal tissue. Nevertheless, a weak co-expression of ACSA-2 on the cell membrane and GFP staining in the cytoplasm could be detected in the dorsal horn at 1dpe (Fig. 3.21 c). This result supports that ACSA-2 is expressed by stem cells of the SVZ.

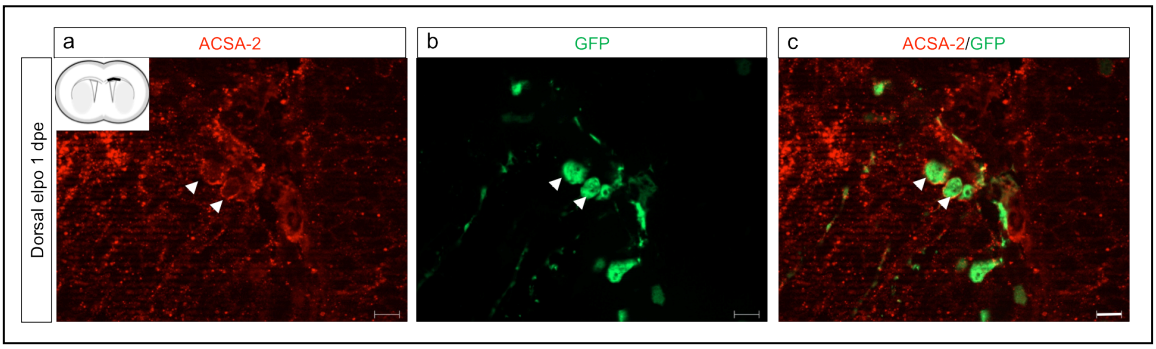

Figure 3.21: ACSA-2 expression on NPCs using *in vivo* electroporation.
P1 pups were electroporated dorsally using a GFP plasmid [195]. The animals were perfused and dissected one day after electroporation and cut as floating sections at 50 µm. The dorsal part of the SVZ was investigated using coronal sections. Sections were stained with the astrocyte specific antibody Anti-ACSA-2 and Anti-GFP. Scale bar represents 5 µm.

In a subsequent experiment, expression of GLAST and ACSA-2 in the lateral wall of the SVZ was analyzed by flow cytometry. Therefore, the lateral wall of the SVZ was dissected from coronal sections of early neonatal (P4,P5) and adult mice (6 weeks) (Fig. 3.22 a). SVZ tissue was dissociated and stained against GLAST, ACSA-2 and CD24. CD24 is reported to be strongly expressed by ependymal cells [68,75]. However, lower expression of CD24 was also seen on neuroblasts [224]. Considering that CD24 allows for the discrimination of ependymal cells, the antibody against CD24 was used in the following experiment to discriminate ependymal cells and astrocytes, including stem cells, by flow cytometry. In adult SVZ tissue (Fig. 3.22 b), CD24 was expressed on 50% of all viable cells. The flow cytometric data showed a low percentage of $CD24^+/GLAST^+$ (4%) and $CD24^+/ACSA\text{-}2^+$ cells (5%) (Fig. 3.22 b). A higher percentage of $ACSA\text{-}2^+$ and $GLAST^+$ did not show CD24 expression (15-23%). Therefore, CD24 can be used to discriminate $ACSA\text{-}2^+$ and $GLAST^+$ astrocytes from ependymal cells or neuroblasts. In a co-staining with the GLAST and the ACSA-2 specific antibodies it was addressed if the marker combination of GLAST and ACSA-2 can be used to discriminate subpopulations of SVZ astrocytes. The majority of adult SVZ astrocytes co-expressed ACSA-2 and GLAST, as seen by co-stainings, Figure 3.22 e. The expression profile was further investigated on different mouse strains: BALB/c, C57BL/6 and CD1 (Fig. 3.22 c-e). This analyses revealed only minor differences in the expression profile between the selected mouse strains. Further analyses of SVZ derived astrocytes were performed using neonatal mice. At P5, the ependymal cell layer and the periventricular zone (PVZ) are tightly connected to each other. A distinct ependymal cell layer is not given, yet. Therefore, $CD24^+/ GLAST^+$ cells and $CD24^+/ACSA\text{-}2^+$ cells present higher co-expression compared to adult tissue (11-16%) (Fig. 3.22 f). Moreover, in correspondence to the architecture of the PVZ the frequency of CD24 positive cells was higher at P5 compared to adult tissue samples. Nevertheless, at P5, GLAST

and ACSA-2 were co-expressed on the majority of PVZ derived astrocytes (11.6%) (Fig. 3.22 f).

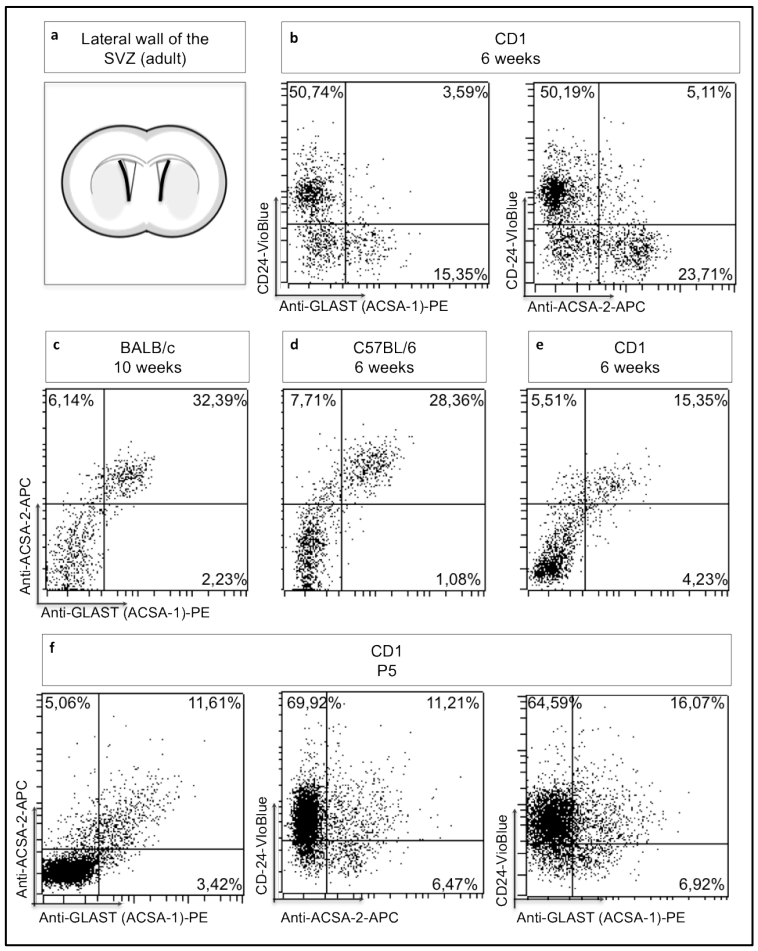

Figure 3.22:
Expression of GLAST and ACSA-2 on neonatal and adult SVZ tissue. The lateral wall of the SVZ (a) was dissociated and stained against ACSA-2, GLAST and CD24 on adult mice (b) and neonatal mice (P5) (f). The staining pattern of GLAST and ACSA-2 on adult mice was further investigated on BALB/c and C57BL/6 mice (c-e).

In summary, the astrocyte markers GLAST and ACSA-2 were co-expressed by SVZ derived astrocytes. Therefore, it is not possible to discriminate stem cells of the SVZ by the expression of the cell surface markers ACSA-2 and GLAST neither in the neonatal nor in the adult SVZ. In addition to these analyses, several antibodies directed against ependymal cells and surrounding astrocytes of the SVZ were tested: S100β, Notch-1 and CD24 (Table 5). Furthermore, markers that were considered to discriminate stem cells, such as EGF receptor, CD106 and LGR5 (Table 5) were tested by IHC or flow cytometry. However, in this study, no suitable marker combination could be identified that allows for the prosective isolation of SVZ stem cells.

Table 5: Markers tested on SVZ tissue

Marker	Expressed by	Reference
CD24	Ependymal cells	CV Pfenninger *et al.* (2011)
Notch-1	Ependymal cells	G Stump *et al.* (2002)
S100ß	Ependymal cells, SVZ astrocytes	M Carlén *et al.* (2009)

α-tubulin	Ependymal cells	Vukojevic *et al.* 2014
EGFR	Stem cells of the SVZ	Y Suh *et al.* 2009 and others
CD106	Stem cells - Endfeed NSC	Kokovay *et al.* 2012
LGR5	Stem cells	Barker *et al.* 2007

3.4.5 Comparison of GLAST and ACSA-2 expression in neural retina and spinal cord

The expression profile of the astrocyte cell surface markers GLAST and ACSA-2, which was carefully analyzed on different brain regions, was further analyzed in retina and spinal cord. Spinal cord was harvested from P6 mice. The retina is the inner layer of the eye, as demonstrated in Figure 3.23. It was harvested from P2 and P6 mice. All samples were dissociated (2.2.2.5/2.2.2.6) and labeled with the astrocyte specific antibodies Anti-GLAST and Anti-ACSA-2. Single cell suspensions were analyzed by flow cytometry (n=3). Expression of GLAST on retinal cells was demonstrated in previous studies [225,226]. Expression of ACSA-2 was not tested on neural retina before. In brain, frequencies of ACSA-2 expression varied between 5% and 30% depending on age and brain region. Expression of GLAST spaned from 5% to 20%, also depending on the aforementioned parameters. In the retina of P2 and P6 mice ACSA-2 presented a frequency of 25-35% and GLAST expression accounted for 20-25% (n=6). Very interestingly, a high percentage of ACSA-2$^-$/GLAST$^+$ single positive cells was detected in P2 and P6 retina (Fig. 3.23 b,c). This expression pattern was comparable to ACSA-2$^-$/GLAST$^+$ detected in neonatal cerebelli (11-14% (Fig. 3.15)). This can be explained as Müller glia of the retina and Bergmann glia of the cerebellum have been reported to be similar in morphology and phenotype [227]. Results of this study indicate that neural cells of the retina and the cerebellum share similar marker expression of GLAST and ACSA-2 during development.

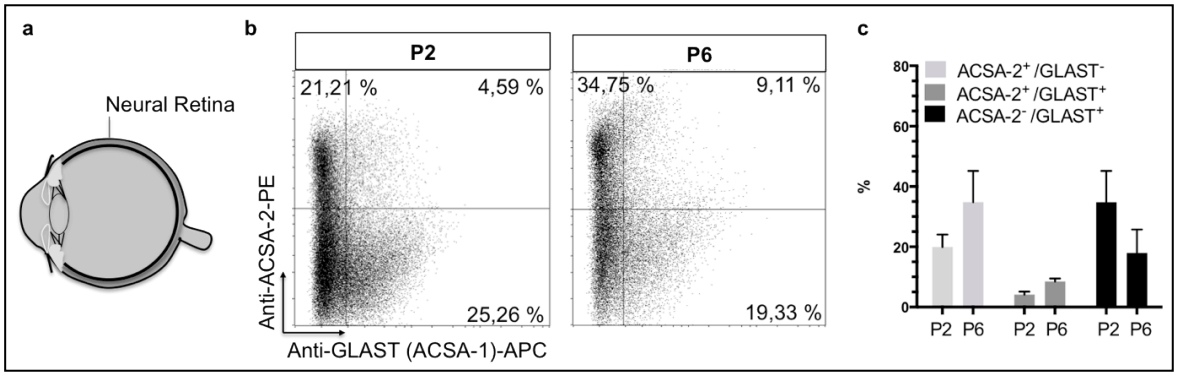

Figure 3.23: Expression of GLAST and ACSA-2 in the retina.
Retinal tissue was harvested from the eyes (a) of P2 and P6 mice. A single cell suspension was obtained by dissociation, cells were stained against GLAST and ACSA-2 (b). The frequencies of ACSA-2$^-$/GLAST$^+$, ACSA-2$^+$/GLAST$^-$, ACSA-2$^+$/GLAST$^+$ (n=3) were measured and visualized as bar diagrams (c). ACSA-2$^+$/GLAST$^-$ and ACSA-2$^-$/GLAST$^+$ show a higher frequency than ACSA-2$^+$/GLAST$^+$ cells.

Next, spinal cord tissue derived from P6 mice was analyzed for the expression of ACSA-2 and GLAST. In comparison to neural retina and mouse brain regions the staining pattern of dissociated spinal cord did not present ACSA-2$^-$/GLAST$^+$ cells (< 1% (n=3) Fig. 3.24). Spinal cord tissue samples contained 5% ACSA-2$^+$/GLAST$^+$ cells. The majority (15%) was ACSA-2$^+$/GLAST$^-$. Like other brain regions tested before (compare Figure 3.15) and retina (Fig. 3.23) spinal cord tissue samples (Fig. 3.24) demonstrated a region dependent expression pattern of ACSA-2 and GLAST.

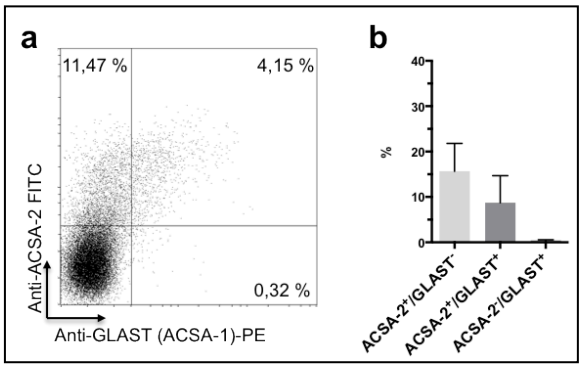

Figure 3.24:
Expression of GLAST and ACSA-2 on dissociated spinal cord tissue.
Dissociated spinal cord samples derived from P6 mice were analyzed by flow cytometry (a). Bar diagrams illustrate the frequencies of ACSA-2$^+$/GLAST$^-$, ACSA-2$^+$/GLAST$^+$ and ACSA-2$^-$/GLAST$^+$ cells (b) (n=3).

3.5 Analysis of GLAST and ACSA-2 expression on reactive astrocytes

In this study genetic mouse models with a deficiency in the *m*-AAA protease of mitochondria were used to study GLAST and ACSA-2 expression on reactive astrocytes. Mitochondria's major function is to support oxidative respiration. Point mutations in mitochondrial DNA lead to protein misfolding. These misfolded proteins cause defects in respiratory chain and lead to a variety of ageing related diseases, as for example neuromuscular or neurodegenerative diseases [228]. Sections of *Afg3l2*$^{PC–KO}$ mice[228] and Afg3l1 d/d Afg3l2 fl/fl GFAP cre$^+$ as well as control animals were kindly provided by Eva Almajan (former PhD student in the group of Professor Rugarli at the university of cologne). Sections were stained against ACSA-2, GLAST and GFAP, which is highly expressed by reactive astrocytes. In section of wt animals low GFAP expression was detected in the Mcl and moderate expression was seen in the Gcl (Fig. 3.24 a). As demonstrated by MIP, GFAP was co-expressed with ACSA-2 in the Gcl of wt mice (Fig. 3.24 c). The *Afg3l2*$^{PC–KO}$ mice is a Cre inducible system under the L7 promotor that affects Purkinje cells. As reported by Almajan *et al.,* in this mouse model secondary inflammation can be monitored by infiltration of microglia and astrocyte activation. In *Afg3l2*$^{PC–KO}$ mice the activation of reactive astrocytes was monitored by the upregulation of GFAP (Fig. 3.24 e). The expression of ACSA-2 was not altered in *Afg3l2*$^{PC–KO}$ mice (Fig. 3.24 d) and ACSA-2 was further not co-expressed with GFAP (Fig. 3.24 f). The Afg3l1 d/d Afg3l2 fl/fl GFAP cre$^+$ system is an inducible cell line

under the human GFAP promoter. Therefore, the deletion directly addresses astrocytes and results in a strong activation of reactive astrocytes (unpublished observation of Eva Almajan). Upon tamoxifen application cre recombination is induced and leads to the deletion of Afg3l2 in GFAP positive cells.

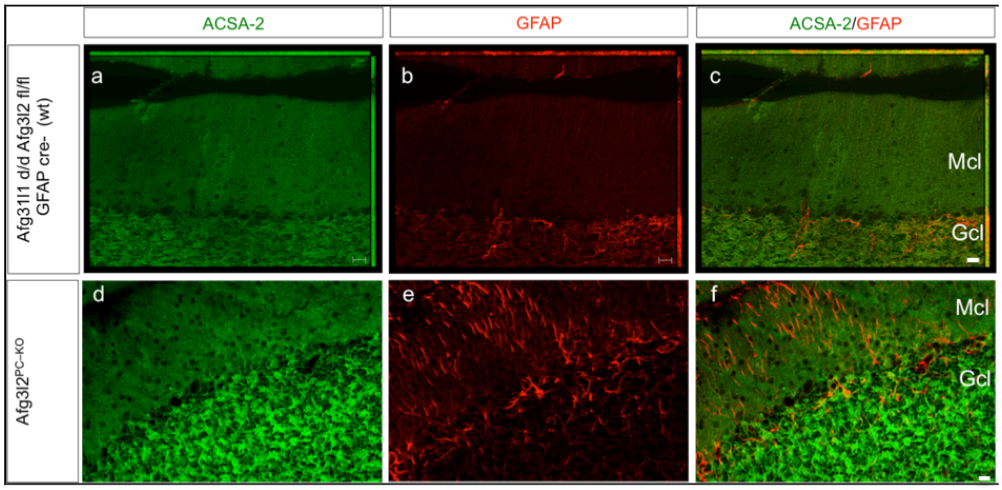

Figure 3.24: Staining of GLAST and ACSA-2 on wt and Afg3l2^{PC-KO} mice.
Afg3l1 d/d Afg3l2 fl/fl GFAP cre- sections (wt) and Afg3l2^{PC-KO} sections were kindly provided by Prof. Rugarli. Sections were cut at 40 µm sagittal floating sections. Sections of Afg3l1 d/d Afg3l2 fl/fl GFAP cre- mice (wt) serve as control for Afg3l1 d/d Afg3l2 fl/fl GFAP cre+ (Fig. 3.25) and depict a bright expresssion of ACSA-2 in the Gcl (a) and a moderate expression of GFAP (b). The Afg3l2^{PC-KO} model harbors an inducible form of the Cre recombinase under the L7 promoter. This system specifically addresses Purkinje cells. Upon cre recombination this model reveals a loss of Purkinje cells and in parallel leads to secondary inflammation indicated by the activation of astrocytes. This was monitored by GFAP staining (e). In wt mice, the astrocyte cell surface markers ACSA-2 (d) and GLAST (not shown) were not affected. Scale bar represents 20 µm. Abbreviations: granule cell layer (Gcl), molecular cell layer (Mcl).

Sections of the Afg3l1 d/d Afg3l2 fl/fl GFAP cre^{+} mice revealed stronger astrocyte activation (Fig. 3.25 d) in comparison to wt controls (Fig. 3.24 b) and Afg3l2^{PC-KO} mice (Fig. 3.24 e). Besides, strong signal decrease of GLAST expression was detected in the Mcl. This is most likely caused by cell death of GLAST expressing astrocytes (Fig. 3.25 a,b). In comparison to wt mice, ACSA-2 expression was also decreased in mutant mice as seen for the cells in the Gcl (Fig. 3.25 c compared to Fig. 3.24 d). This study reveals that ACSA-2 and GFAP expression are not correlated on reactive astrocytes (Fig. 3.24 e). Therefore, ACSA-2 might be a versatile for the discrimination and sorting of non-reactive astrocytes in a reactive or diseased mouse model.

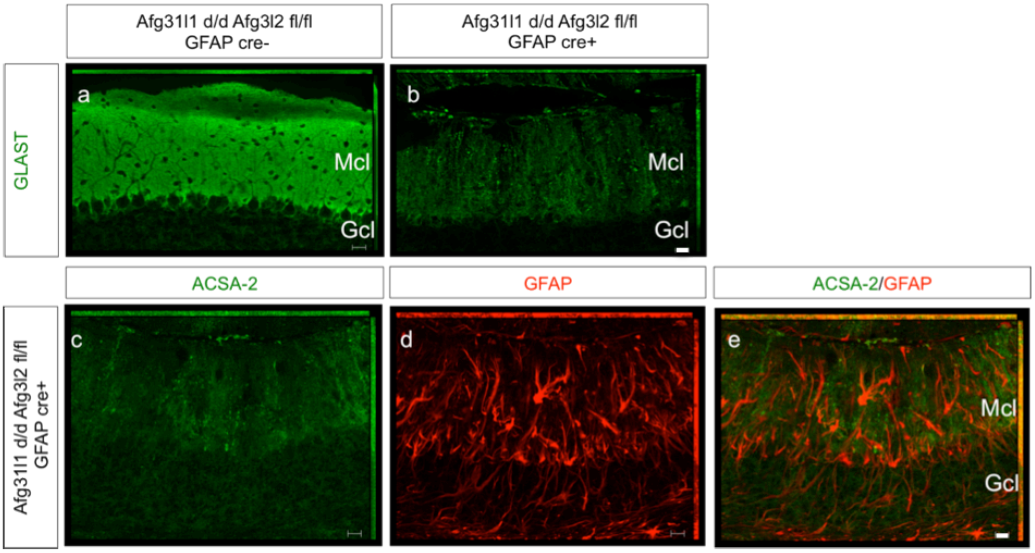

Figure 3.25: Staining of GLAST and ACSA-2 on Afg31l1 d/d Afg3l2 fl/fl GFAP cre mice.
Sagittal floating sections (40 µm) of Afg31l1 d/d Afg3l2 fl/fl GFAP cre mice were kindly provided by the Rugarli lab. This conditional model harbors an inducible form of the Cre recombinase under the human GFAP promoter. This system specifically addresses astrocytes. Upon cre recombination this model reveals a strong activation of astrocytes as monitored by GFAP staining (d,e). In contrast to wt mice, GLAST (a,b) and ACSA-2 expression (c) were rapidly decreased in the conditional knock-out. ACSA-2 was not co-expressed by GFAP positive reactive astrocytes (e) which allow the usage of ACSA-2 for the discrimination of non-reactive astrocytes. Scale bar represents 20 µm. Abbreviations: granule cell layer (Gcl), molecular cell layer (Mcl).

3.6 Analyses of GLAST and ACSA-2 in cerebellum

3.6.1 Immunohistochemical analyses of GLAST and ACSA-2 in adult cerebellum

In the next approach, differences seen in cerebellum of neonatal mice were further addressed in the adult brain. Therefore, the expression of ACSA-2 and GLAST was investigated in the cerebellum using adult mouse brain sections. After maturation, the adult cerebellum comprises a distinct layer structure. The innermost layer is rich in myelin and called white matter (WM). GLAST and ACSA-2 were weakly expressed in this part of the cerebellum (data not shown). The white matter follows the Gcl, an area with a very high cell density composed of granule neurons and Gcl glia [229]. The subsequent layer is composed of Purkinje cells and named Purkinje cell layer (Pcl). The Pcl separates the Gcl from the Mcl [104]. Numerous dendrite arbors reside in this layer. GLAST is predominantly expressed in the Mcl and weaker in the Gcl (Fig. 3.26 a) [104]. This results from distribution and local concentration of glutamate in the different cerebellar layers [230]. The co-expression studies of GLAST and ACSA-2 demonstrated a different expression pattern for ACSA-2 in adult cerebellum (Fig. 3.26 b). ACSA-2 presented a bright expression in the Gcl but in contrast to GLAST, ACSA-2 shows a weak expression in the Mcl. Nevertheless, co-expression of GLAST and ACSA-2 was detected in both layers (Fig. 3.26 c).

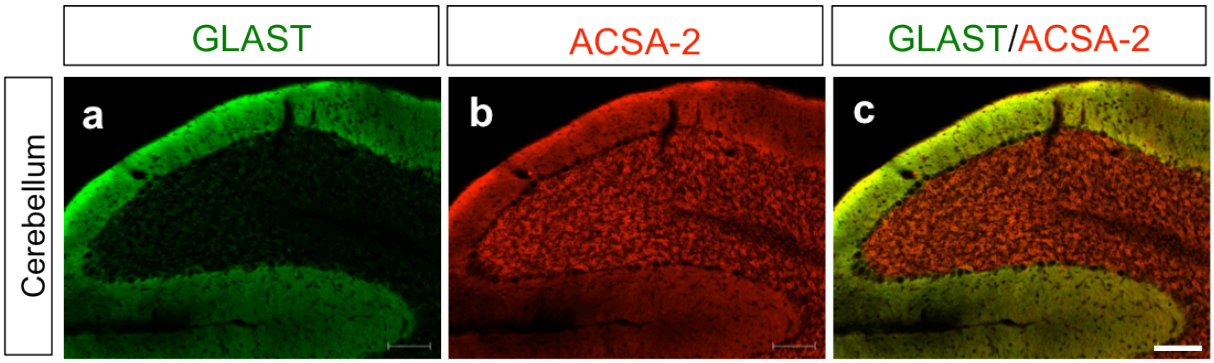

Figure 3.26: ACSA-2 and GLAST expression in the adult cerebellum
Expression of ACSA-2 and GLAST was investigated on adult mouse brain coronal sections using IHC. Analysis revealed different expression pattern between ACSA-2 and GLAST in the Mcl and the Gcl of the cerebellum. Scale bar: 100 µm.

At higher magnification, the expression of GLAST and ACSA-2 in Mcl, Gcl and on Bergmann glia cells was investigated (Fig. 3.27 a-c). Thereby, co-staining of GLAST and ACSA-2 in the Gcl was demonstrated (Fig. 3.27 d-f). However, ACSA-2 was expressed on a broader population than GLAST (Fig. 3.27 d-f (indicated by arrowheads)). A high expression of GLAST was detected on Bergmann glia cells in the Mcl (Fig. 3.27 g). Purkinje cell nuclei were labeled using DRAQ5 antibody (Fig. 3.27 h). Bergmann glia cells project through the Mcl towards the pial surface. Their somata are located in the Pcl [231]. Expression of ACSA-2 was weak on Bergmann glia cell bodies, which are located around the Purkinje cells (Fig. 3.27 h). Bergmann glia processes, which express GLAST, did not or weakly express ACSA-2 (Fig. 3.27 h,i). This data supports that GLAST and expression level of ACSA-2 mark different populations of astrocytes in the cerebellum.

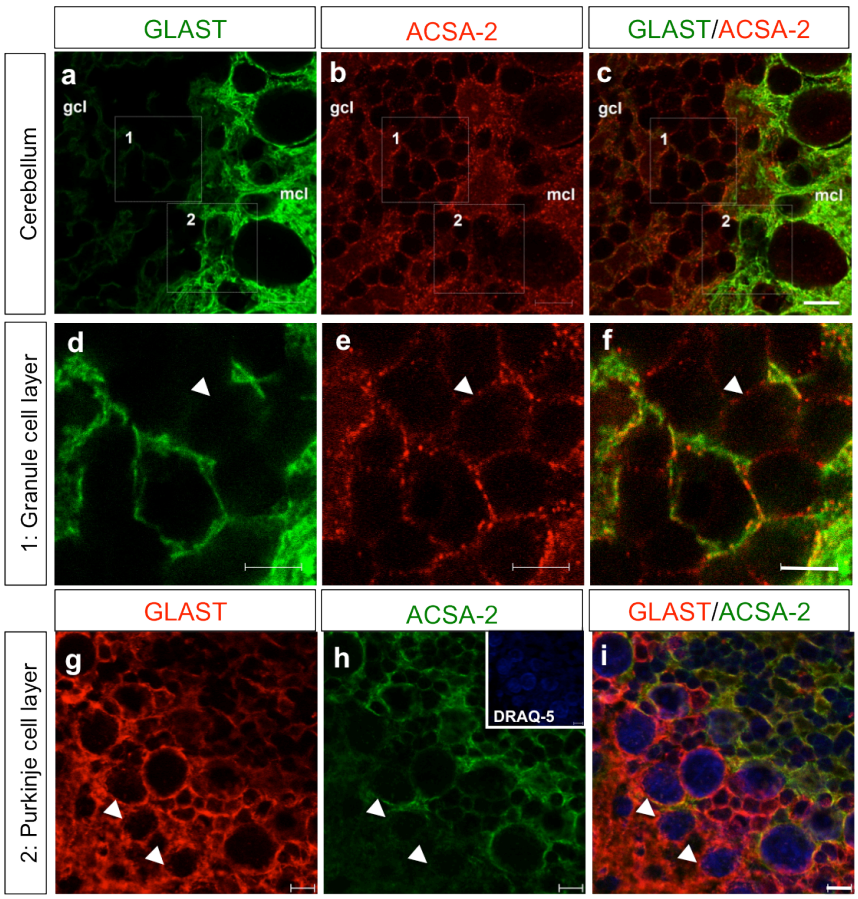

Figure 3.27: Expression of ACSA-2 and GLAST in adult cerebellum. Expression of ACSA-2 and GLAST on Bergmann glia cells were investigated in the Gcl (1) and Pcl of the adult cerebellum (2) using coronal floating sections at 40 µm. The expression of GLAST is very bright in the molecular cell layer (Mcl). Therefore, in this picture the bright signal of GLAST in the Mcl was decreased. Accordingly, GLAST expression in the Gcl appears very weak in this picture (a-c). ACSA-2 was expressed on a broader cell population in the Gcl than GLAST (d-f (indicated by arrowheads)). GLAST presents a bright expression on Bergmann glia cells. Purkinje cell nuclei were labeled by DRAQ5. ACSA-2 was not expressed on Bergmann glia processes (g-i (arrowheads). Scale bar represents 5 µm (d-i). Abbreviations: granule cell layer (gcl), molecular cell layer (Mcl).

3.6.2 Immunohistochemical analyses of GLAST and ACSA-2 in the neonatal cerebellum

Flow cytometric analysis of GLAST and ACSA-2 in neonatal mice identified an ACSA-2$^-$/GLAST$^+$ population in the neonatal cerebellum (compare 3.4.2). The expression of ACSA-2$^-$/GLAST$^+$ was most prominent at P1 and decreased around P7 (compare Fig. 3.15). It is known that GLAST is expressed by radial glia during development and further expressed by radial glia in the developing cerebellum [48]. This was demonstrated by co-stainings of Anti-GLAST with the radial glia marker RC2 [52,53] (Fig. 3.28). As the GLAST antibody detects a surface antigen and radial glia marker RC2 addresses an intracellular epitope the picture does not show a 100% overlap of the two markers (Fig. 3.28 c,f).

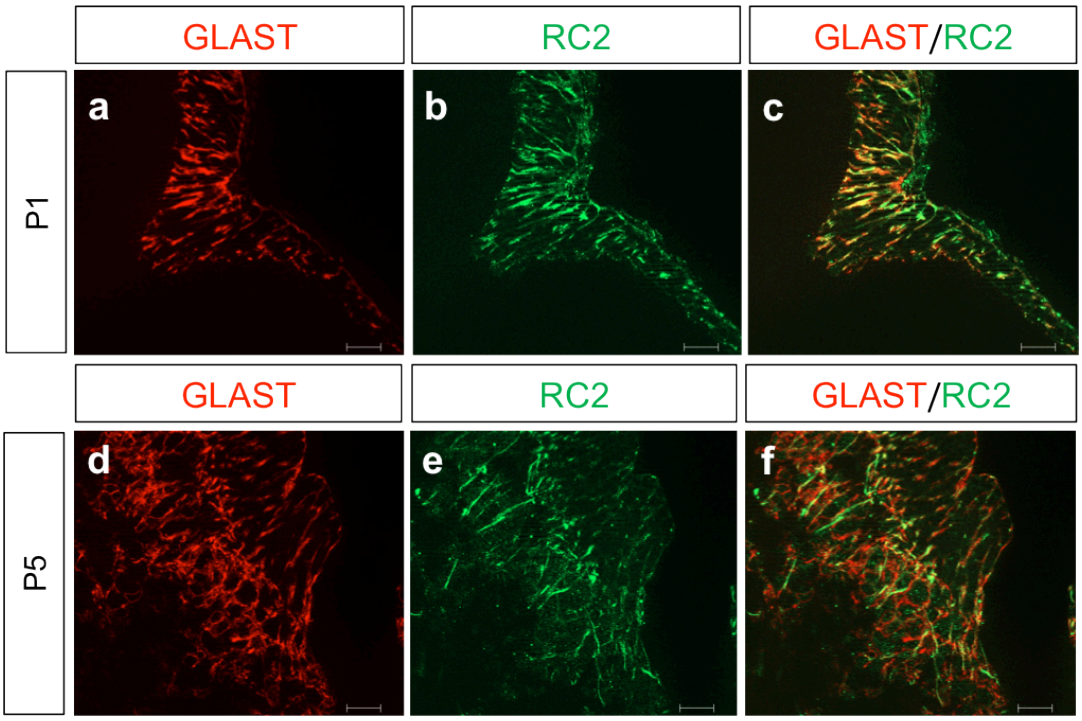

Figure 3.28: Expression profile of RC2 and GLAST in developing cerebellum.
Coronal floating sections (50 µm) derived from neonatal mouse brain cerebellum (P1, P5) were analyzed for the expression of the cell surface marker GLAST and the intracellular marker RC2. Radial processes co-express GLAST and ACSA-2. Scale bar represents 20 µm (a-f).

Little is known about the origin of cerebellar glia and their precursors [169]. Based on the expression profile (3.4.2) and differences in marker expression on Bermann glia (Fig. 3.27) the expression profile of ACSA-2 and GLAST was investigated in the developing cerebellum. The aim was to address whether GLAST and ACSA-2 mark different progenitors of the developing cerebellum. First, the expression pattern of GLAST and ACSA-2 was investigated in the cerebellum on coronal sections derived from early postnatal developmental stages P1 and P3 (Fig. 3.29). At this age, foliation of the cerebellum, which lasts until adult stage, is still in progress. As mentioned previously, staining of the ACSA-2 antibody was in general weakly and revealed high background staining. On radial glia ACSA-2 was rather weakly expressed as compared to GLAST (Fig. 3.29). Nevertheless, co-expression of GLAST and ACSA-2 was seen at P1 and at P3 (Fig. 3.29 c,f).

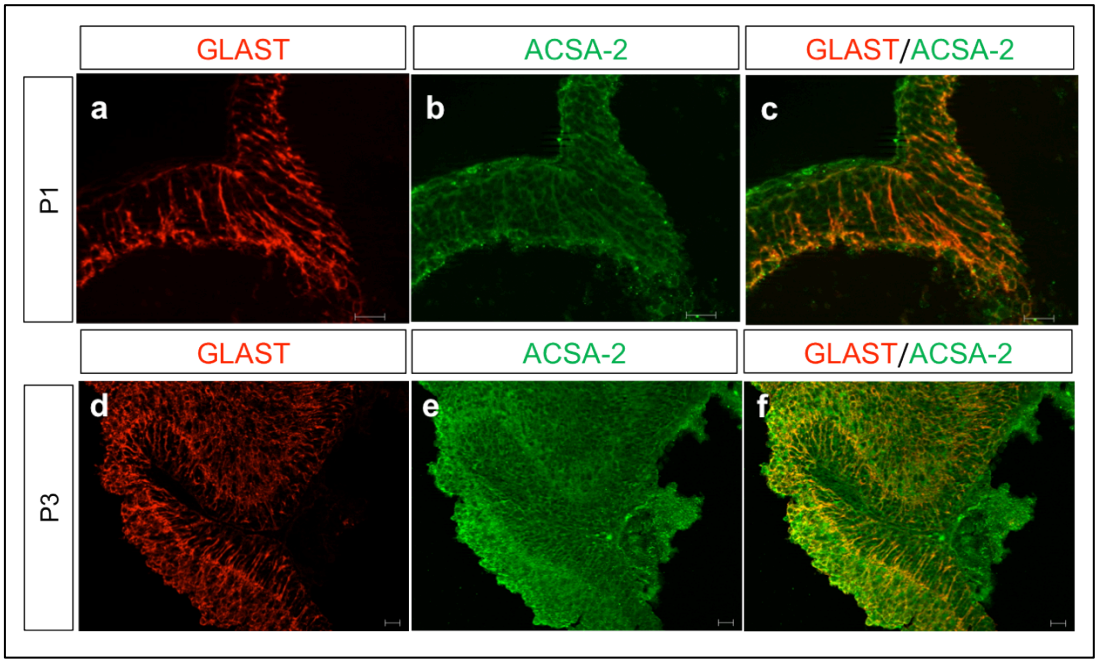

Figure 3.29: Expression profile of ACSA-2 and GLAST in developing cerebellum.
Coronal brain sections derived from neonatal mouse brain cerebellum (P1, P3) were analyzed for co-expression of ACSA-2 and GLAST. GLAST is very prominent on radial glia. Staining of the ACSA-2 antibody was rather weak on neonatal tissue. Scale bars: 20 µm (a-c) 10 µm (d-f).

3.6.3 Analyses of GLAST and ACSA-2 in embryonic and neonatal cerebellum by flow cytometry

GLAST and ACSA-2 expression on cerebellar precursors was further characterized during cerebellar development. For investigation, cerebellar samples from E12-P12 mice were collected and analyzed using flow cytometry (Fig. 3.30). At embryonic stage (E13, E15, E17) the cerebellar anlage, the lateral cerebellar primordium [144] the main cell source of the developing cerebellum [232], was dissected. As early as E19 the developing cerebellum spreads medially and is detectable as monolayer. Analyses at embryonic age revealed that ACSA-2 and GLAST expression are hardly detectable at E13 (Fig. 3.30 a). ACSA-2$^-$/GLAST$^+$ and ACSA-2$^+$/GLAST$^+$ cells were first detected around E15 (Fig. 3.30 b). Highest frequencies of ACSA-2$^+$/GLAST$^-$ cells were detected at E17 (Fig. 3.30 c), whereas highest frequencies of GLAST$^+$/ACSA-2$^-$ cells was visible around birth between E19 and P1 (Fig. 3.30 d,e). Postnatally the frequency of GLAST$^+$/ACSA-2$^-$ cells decreased with the onset of development and was not detectable after P12 (Fig. 3.30 i). In samples of P12 and adult cerebellum (not shown) ACSA-2$^-$/GLAST$^+$ cells were not detected.

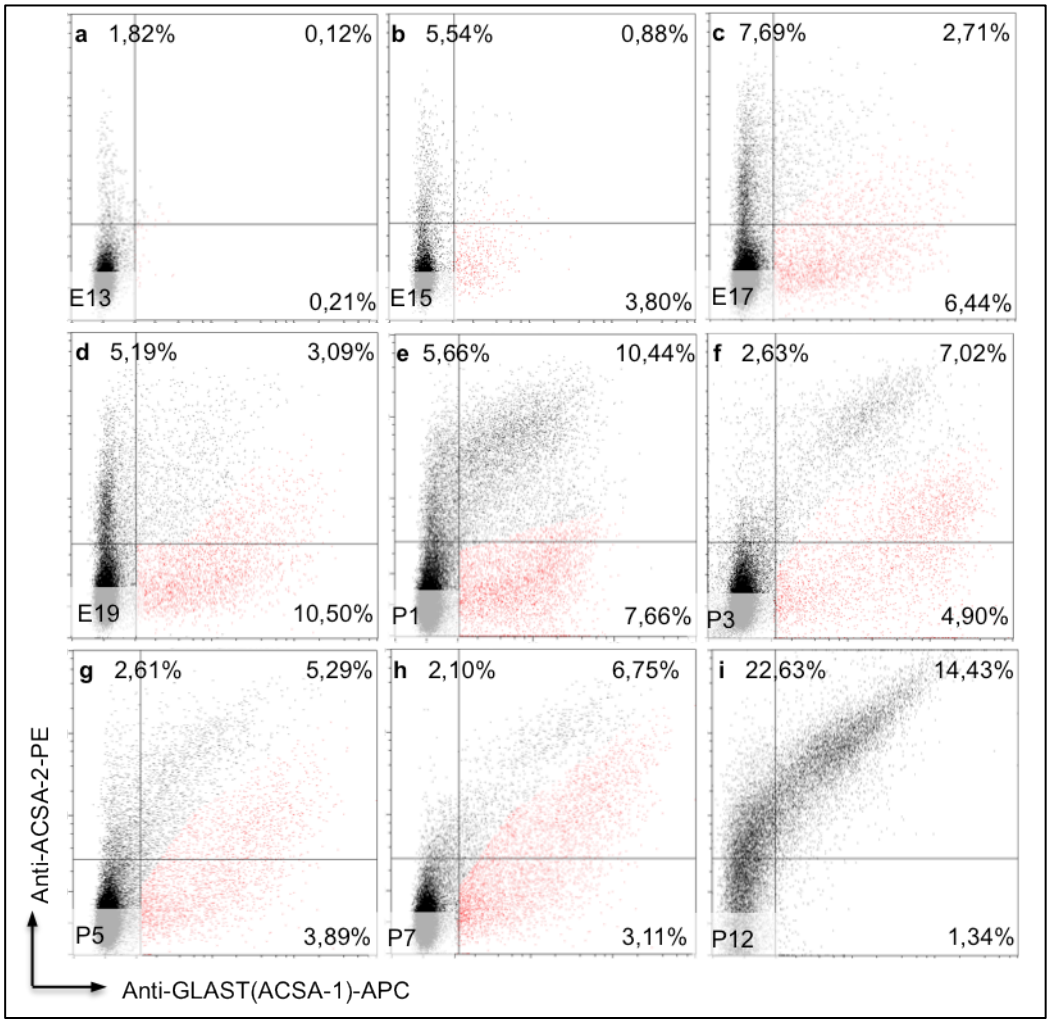

Figure 3.30: Expression of GLAST and ACSA-2 in embryonal and neonatal cerebellum
Tissue of E12-P12 cerebellum was dissociated, stained and analyzed by flow cytometry. ACSA-2 and GLAST staining were assigned against each other and visualized as a dot plot. The ACSA-2$^-$ /GLAST$^+$ population is marked in red for better visualization. 50,000 cells are depicted.

In the following step, frequencies of A2B5, Prominin-1 and CD15 on ACSA-2$^+$/GLAST$^-$, ACSA-2$^+$/GLAST$^+$ and ACSA-2$^-$/GLAST$^+$ cells were determined using samples of P1/P2 and P6/P7 cerebelli (Fig. 3.31). A2B5 is a glial precursor marker expressed during development, as already described previously (Fig. 3.11). Prominin-1 is described as a stem cell marker for different regions of the murine brain including the cerebellum [179]. CD15 was recently described as an indicator for gliogenenic fate by Fleming *et al.* in 2013. A2B5 expression was investigated on ACSA-2$^+$/GLAST$^-$, ACSA-2$^+$/GLAST$^+$ and ACSA-2$^-$/GLAST$^+$ cells using flow cytometry (Fig. 3.31). The expression of A2B5 in P1 cerebellar samples was significantly higher ($p<0.05$) in the ACSA-2$^+$/GLAST$^+$ compartment than in ACSA-2$^-$/GLAST$^+$ and ACSA-2$^+$/GLAST$^-$ samples (Fig. 3.31 a). At P7 the frequency of A2B5 positive astrocytes was reduced and differences between subsets were not significant. In addition, CD15 expression was analyzed. CD15 was significantly higher expressed ($p<0.001$) by ACSA-2$^+$/GLAST$^+$ cells of the P2 cerebellum than by ACSA-2$^-$/GLAST$^+$ and

ACSA-2$^+$/GLAST$^-$ cells at the same age. The differences in CD15 expression were maintained until P6 (Fig. 3.3.1 b). However, Prominin-1 expression did not reveal significant differences between the sample sets (data not shown). These analyses indicate that ACSA-2$^+$/GLAST$^-$, ACSA-2$^+$/GLAST$^+$ and ACSA-2$^-$/GLAST$^+$ astrocyte potentially have different phenotypes. Taken from this anlysis, ACSA-2$^+$/GLAST$^+$ cells marker expression correlated with a glial cell fate.

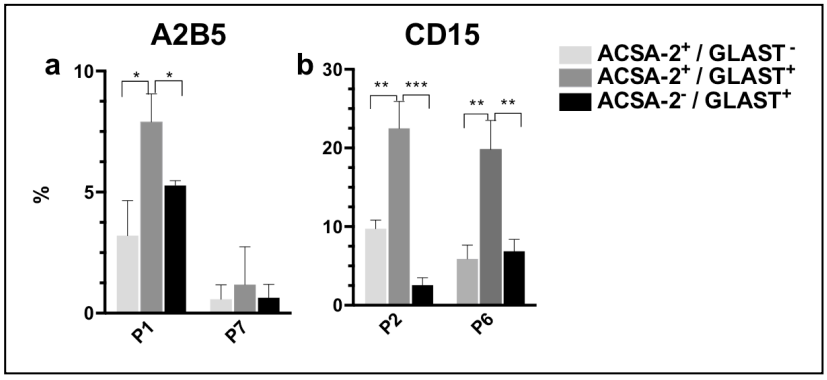

Figure 3.31: Co-expression of A2B5 and CD15 on ACSA-2$^+$ and GLAST$^+$ cerebellar astrocytes.
Cerebelli of P1/P2 and P6/7 mice were dissociated and stained against ACSA-2 and GLAST in combination with A2B5 (a) and CD15 (b). Frequencies of ACSA-2$^+$/GLAST$^-$, ACSA-2$^+$/GLAST$^+$ and ACSA-2$^-$/GLAST$^+$ cells are shown as bar diagrams. Significance levels were determined by Student's t test (*** $p<0.001$)(** $p<0.01$) (* $p<0.05$).

3.6.4 Analyses of ACSA-2$^+$/GLAST$^{+/-}$ and ACSA-2$^-$/GLAST$^+$ cells by neurosphere assay and cell transplantation

To address multipotent characteristics of ACSA-2$^+$/GLAST$^{+/-}$ and ACSA-2$^-$/GLAST$^+$ cells a magnetic isolation protocol was developed. This step was needed to conduct single cell analyses such as gene expression profiling and Neurosphere assay. ACSA-2$^+$/GLAST$^-$ cells were obtained through depletion of GLAST$^+$ astrocytes, PSA-NCAM$^+$ and L1CAM$^+$ neurons, CD45$^+$ and Ter119$^+$ hematopoietic cells and subsequent ACSA-2 enrichment. Cells were obtained at purities of around 60% (n=5). Unfortunately, very low cell counts were obtained using this strategy. For this reason, further analyses were performed with ACSA-2$^+$/GLAST$^{+/-}$ cells, which were directly isolated using Anti-ACSA-2 MicroBeads. This population is composed of ACSA-2$^+$/GLAST$^-$ and ACSA-2$^+$/GLAST$^+$ cells and could be enriched to high purities (85%- 95% (n=15)). Additionally, higher cell numbers could be obtained using this ACSA-2 enrichment protocol. Isolation of ACSA-2$^-$/GLAST$^+$ was performed by depletion of ACSA-2$^+$ astrocytes, PSA-NCAM$^+$ and L1CAM$^+$ neurons, CD45$^+$ and Ter119$^+$ hematopoietic cells and a subsequent enrichment step of GLAST positive cells. A purity of 70-85% was obtained when P0-P2 cerebelli were used (Isolation of ACSA-2$^+$/GLAST$^-$, ACSA-2$^+$/GLAST$^{+/-}$, ACSA-2$^-$/GLAST$^+$: Supplementary Fig. 11). In general it was possible to isolate

ACSA-2$^+$/GLAST$^-$ from P0 to P9 cerebelli. Starting frequencies of ACSA-2$^+$/GLAST$^-$ decreased from 10% (P0) to 3% (P7 (Fig. 3.30). However, at P9 very low cell numbers were obtained and the purity decreased to 50%. Nevertheless, it was possible to plate and analyse these cells by ICC. Cells of original (before separation), negative (non-target cells) and positive (target cells) fraction were plated at equal cell numbers and analyzed for BLBP and GLAST co-expression (Supplementary Fig. 12). Despite low purities in the target fraction it was possible to obtain a 3-fold enrichment for ACSA-2$^-$/GLAST$^+$ cells from P9 cerebelli (Supplementary Fig. 12). Furthermore, ACSA-2$^-$/GLAST$^+$ isolated cells presented RC2 expression as analyzed by ICC (Fig. 3.32).

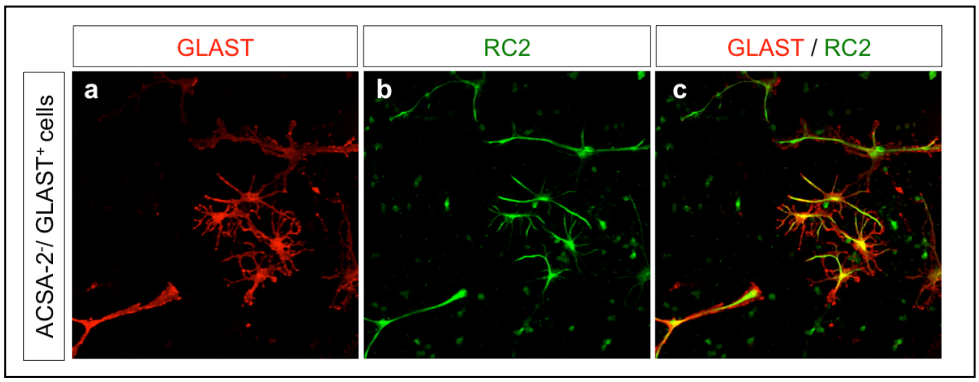

Figure 3.32: Immunocytochemistry of isolated ACSA-2$^-$/GLAST$^+$ cells from P9 cerebelli.
Cerebelli of P9 mice were dissociated and plated on poly-L-lysine coated cover slips. After 5 days in complete medium cells were fixed and permeabilized for intracellular stainings. Co-labeling of GLAST and RCs was seen on the isolated cells as monitored by confocal microscopy.

Co-expression of GLAST and RC2 suggested that it is possible to enrich ACSA-2$^-$/GLAST$^+$ progenitor cells with a radial glia phenotype using the above mentioned isolation protocol. A neurosphere assay was established to address the multipotency of ACSA-2$^-$/GLAST$^+$ and ACSA-2$^+$/GLAST$^-$ cells. At a cell denity of 1,000 cells per µL isolated ACSA-2$^-$/GLAST$^+$ cells and ACSA-2$^+$/GLAST$^{+/-}$ cells were treated as described in 2.2.3.3. The principle of the neuroshere assay is to obtain multipotent self-replicating stem cells in culture and lose non-replicating cells through several passaging steps. It was possible to obtain secondary neurospheres from ACSA-2$^-$/GLAST$^+$ cells and ACSA-2$^+$/GLAST$^{+/-}$ cells. Tertiary neurospheres could not be obtained although tested several times (n=5). Based on the sphere diameter ACSA-2$^-$/GLAST$^+$ cells formed larger neurospheres than ACSA-2$^+$/GLAST$^{+/-}$ (Supplementary Fig. 13 a,b). However, upon plating and differentiation, neurospheres of both cell populations were able to differentiate into astrocyte and neurons (Supplementary Fig. 13 c). In addition, few oligodendrocytes were obtained after a 6 day differentiation step (data not shown). As the differentiation potentials of the cell populations could not be addressed by neurosphere assay a transplantation experiment was performed. Thereby, the differentiation

potential of ACSA-2^{+}/GLAST$^{+/-}$ and ACSA-2^{-}/GLAST^{+} cells was compared and analyzed in an *in vivo* setting. This experiment was conducted at the Neuroscienze Institute Cavalieri Ottolenghi in Turin in collaboration with the group of Dr. Annalisa Buffo. Target cells were isolated from β-actin GFP positive mice and the cerebelli of P0 to P3 donors were dissected (2.2.10). 50,000 cells per fraction of each fraction were injected into the lateral part of the vermis of recipient mice, as depicted in Figure 3.35 a. Grafted mice were dissected after 30 days. The brains were cut into sagittal sections at 40 µm. The integration capacity, the localization and the differentiation potential of the grafted populations were analyzed. Integrated cells were discriminated as neurons or glia based on morphology and marker expression. Parvalbumin was used as marker for GABAergic interneurons (Fig. 3.33 c,d,g,h). Astrocytes were discriminated by S100β or GFAP (Fig. 3.33 b,f, 3.34 b,g,k). For discrimination of oligodendrocytes O4 and transcription factor Olig2 were used (Fig. 3.34 f,j). For each host a representative amount of tissue sections (15-25) was analyzed and integrated cells were counted. ACSA-2^{-}/GLAST^{+} transplants were able to differentiate into neuronal cells (45%) and glia cells (55%) (Fig. 3.35 b). Grafts presented integration of different GABAergic interneurons: stellate cells and basket cells. In addition, Bergmann glia, glia cells of the Gcl, the Mcl and the white matter were identified (Fig. 3.35 c). In ACSA-2^{+}/GLAST$^{+/-}$ grafts less than 2.5% neuronal cells were found (Fig. 3.35 b). This compartment differentiated preferentially into glia (Fig. 3.35 b).

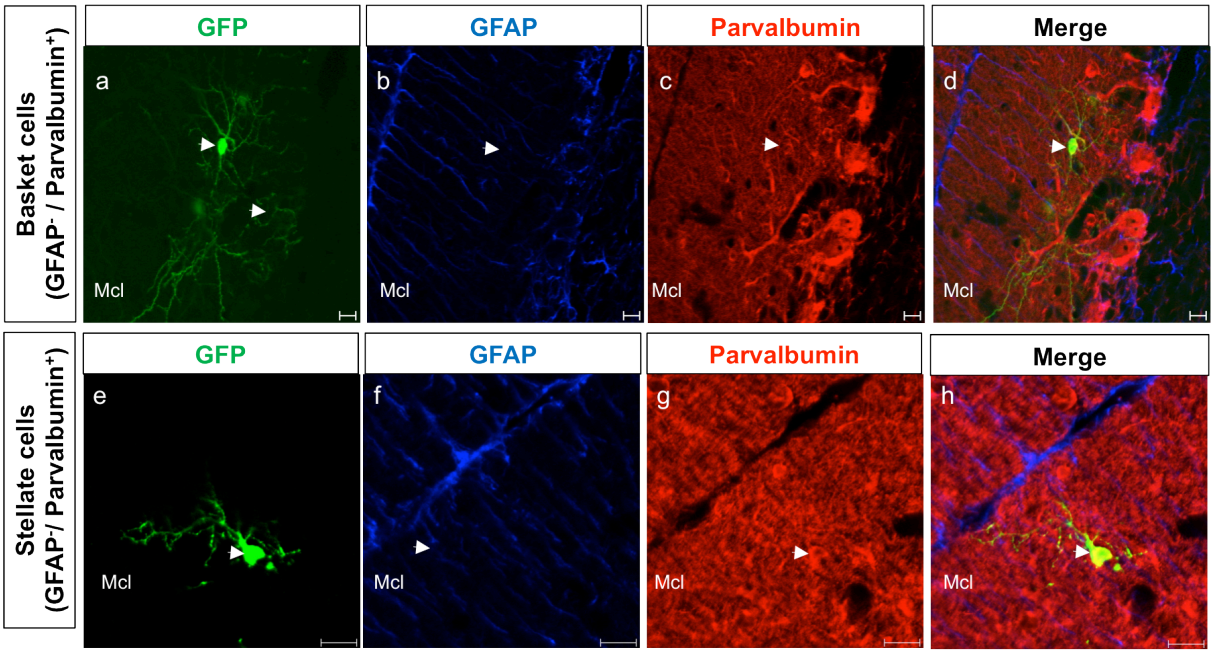

Figure 3.33: Cell types identified in the transplants.
Host animals were perfused after 30 days, brains were cut as sagittal cryo sections at 40 µm and analyzed by IHC. Integrated cells were analyzed by cell morphology and marker co-expression. Transplanted cells were GFP positive. Co-expression of parvalbumin and the absence of GFAP) identified interneurons (Basket or Stellate cells). Scale bar represents 10 µm. Abbreviations: Mcl: Molecular cell layer.

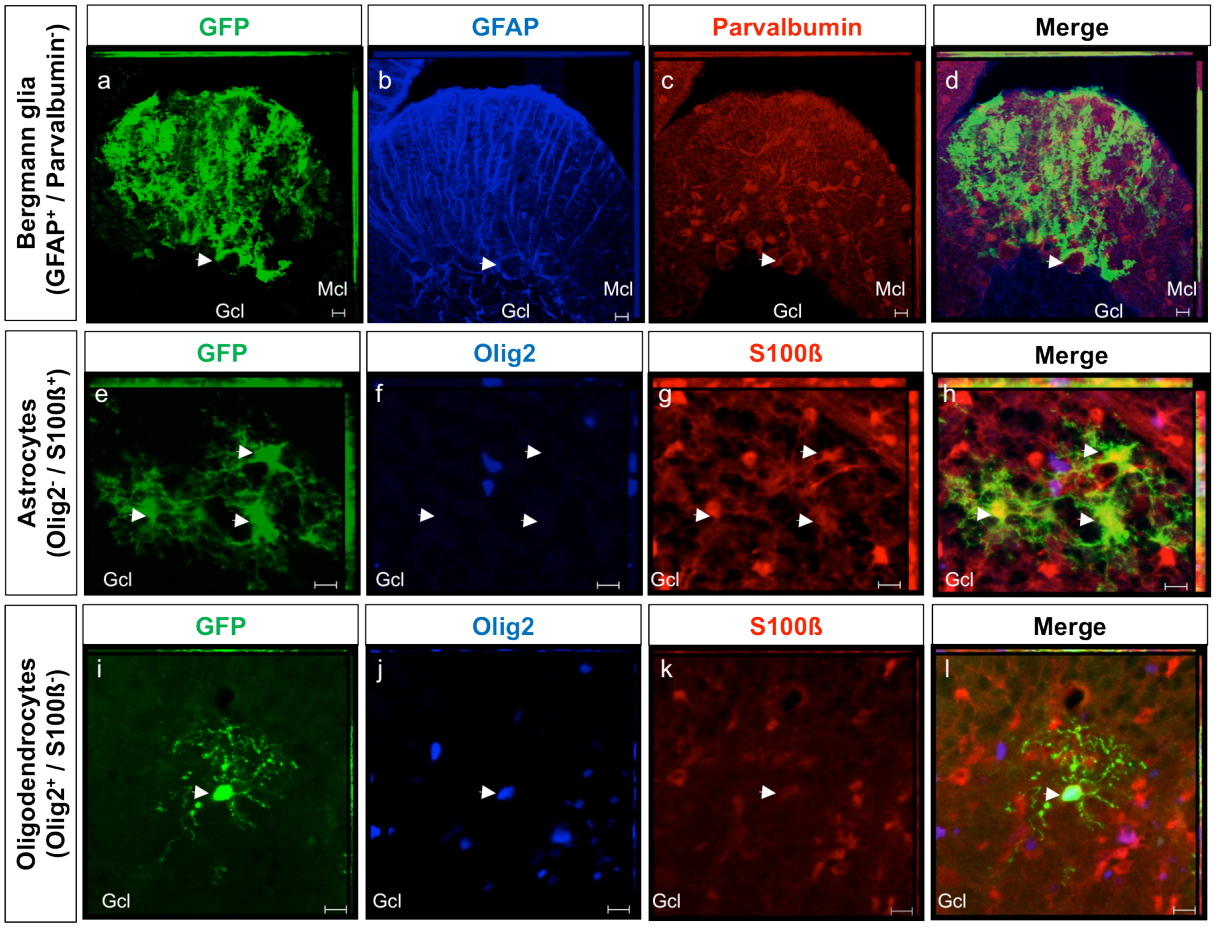

Figure 3.34: Cell types identified in the transplanted animals.
Host animals were perfused after 30 days, brains were cut as sagittal cryo sections at 40 µm and analyzed by IHC. Integrated cells were analyzed by cell morphology and marker co-expression. Transplanted cells were GFP positive. The co-expression of GFAP and S100ß identified astrocytes (a-h). Bergmann glia cells were further classified by cell morphology (a-d) and oligodendrocytes by the expression of transcription factor Olig2 (i-l). Scale bar: 10 µm. Abbreviations: Gcl: Granule cell layer, Mcl: Molecular cell layer.

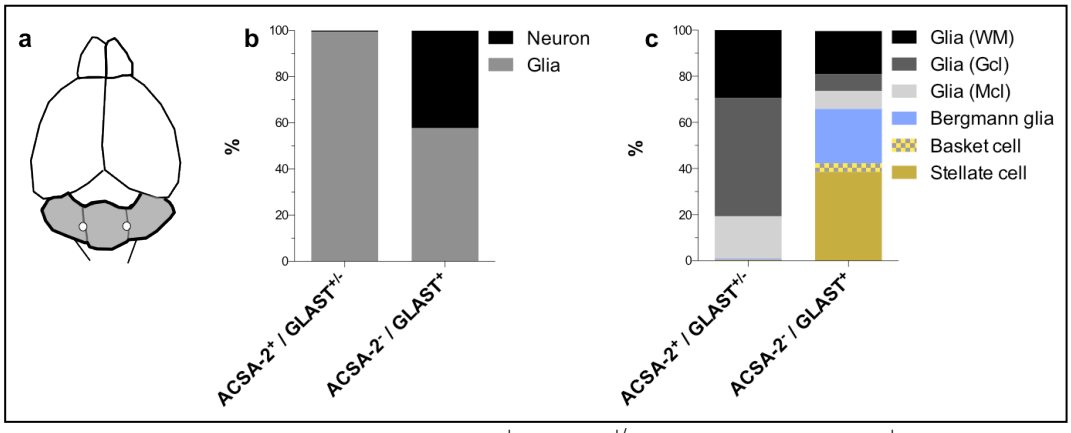

Figure 3.35: Cell transplantation of ACSA-2$^+$/GLAST$^{+/-}$ and ACSA-2$^-$/GLAST$^+$ cells.
ACSA-2$^+$/GLAST$^{+/-}$ and ACSA-2$^-$/GLAST$^+$ cells of P0 to P3 were isolated from β-actin GFP positive cerebelli. 50,000 cells were injected into P1 and P3 hosts. Injection was performed into both sides of the lateral part of the vermis (a). Cells were classified as neurons or glia by morphology and marker expression as depicted as stacked bar plots (b). Transplanted cells were able to differentiate into stellate and basket cells, Bergmann glia and glia cells of the Gcl, Mcl and WM.

ACSA-2$^-$/GLAST$^+$ transplants presented a significantly higher frequency of stellate cells and basket cells (Fig. 3.36 a,b). Additionally, it was shown that stellate cells and basket cells integrated significantly better in a P1 hosts than in a P3 hosts (Supplementary Fig. 15). Furthermore, Bergmann glia were exclusively identified in the ACSA-2$^-$/GLAST$^+$ grafts (Fig. 3.36 c). On the other side, Gcl glia cells were significantly higher in ACSA-2$^+$/GLAST$^{+/-}$ grafts compared to ACSA-2$^-$/GLAST$^+$ transplants. For ACSA-2$^+$/GLAST$^{+/-}$ cells a slightly higher integration potential was observed in P3 hosts (Supplementary Fig. 14).

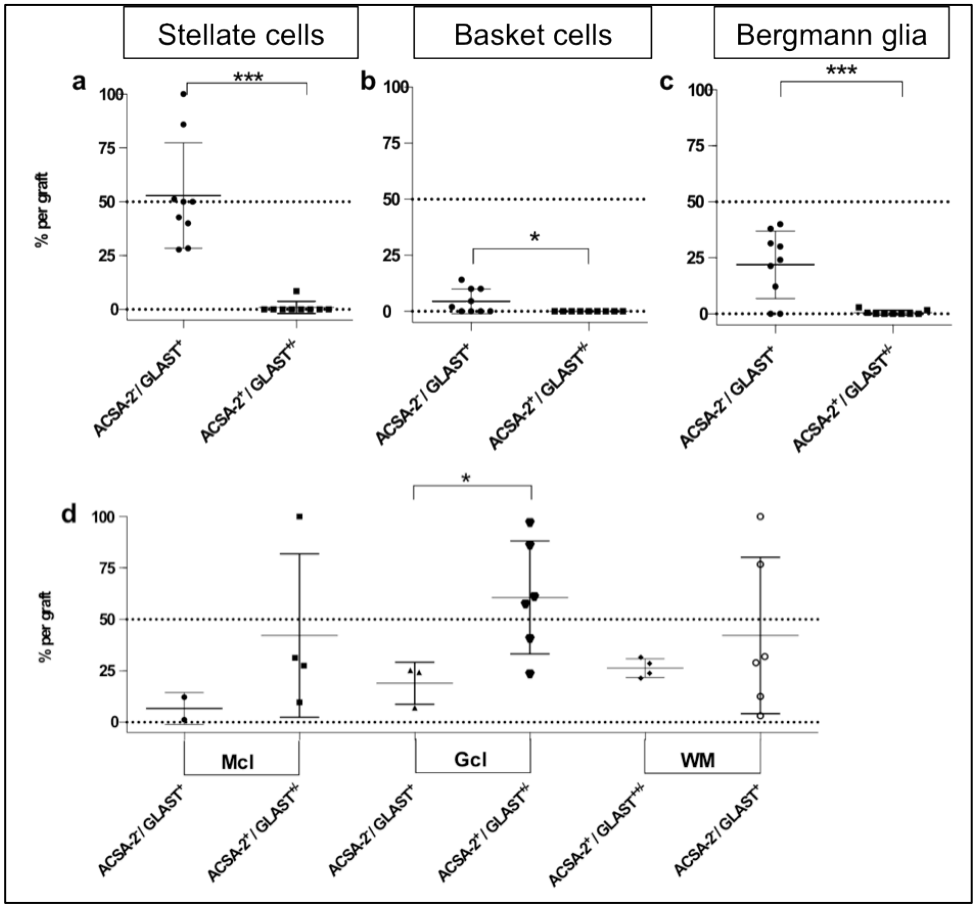

Figure 3.36: Differentiation potential of transplanted cells.
ACSA-2$^+$/GLAST$^{+/-}$ and ACSA-2$^-$/GLAST$^+$ cells of P0 to P3 were isolated from β-actin GFP positive cerebelli. Integration as determined on a representative amount of tissue sections (15-25) of each host. Integrated cells of each group were classified according to cell morphology and marker expression as stellate cells (a), basket cells (b), Bergmann glia (c), Glia of the Gcl, Mcl and WM. Significance levels were determined by Student's t test (*** $p<0.001$) (** $p<0.01$) (* $p<0.05$).

In a further validation step, frequencies of oligodendrocytes and astrocytes in Gcl, Mcl and WM were determined. For ACSA-2$^+$/GLAST$^{+/-}$ and ACSA-2$^-$/GLAST$^+$ grafts the majority of the integrated glia cells were astrocytes as analyzed by GFAP and Olig2 staining (Supplementary Fig. 15).

3.6.5 Analyses of GLAST and ACSA-2 astrocytes of the neonatal cerebellum by gene expression profiling

Gene expression profiling of ACSA-2 and GLAST positive astrocytes of the neonatal cerebellum was performed to investigate the transcriptome of the identified subpopulations. Therefore, ACSA-2$^+$/GLAST$^-$, ACSA-2$^+$/GLAST$^{+/-}$ and ACSA-2$^-$/GLAST$^+$ cells were isolated based on the established protocols by magnetic cell separation (Supplementary Fig. 11). The purities between the biological triplicates were comparable as analyzed by marker co-stainings. ACSA-2$^+$/GLAST$^-$ cells were enriched to 70% (± 5%), ACSA-2$^+$/GLAST$^{+/-}$ to 87% (± 7%) and ACSA-2$^-$/GLAST$^+$ cells to 75% (± 5%). The cDNA microarray was processed as described in chapter 2.5.5. In the first step, the gene expression profile over all genes was investigated for all sample groups. In an unsupervised hierarchical clustering the gene expression of each group was compared with the gene expression of another group using correlation matrix (Fig. 3.37). This analysis was chosen to quantify the similarity between the three populations of the cerebellum. In the correlation matrix, low gene expression levels are indicated by black color and high gene expression levels is indicated by red color. As seen in Figure 3.37 gene expression levels were similar between sample groups. In addition, the pairwise distance analysis revealed that ACSA-2$^+$/GLAST$^+$ samples presented an intermediate group between ACSA-2$^+$/GLAST$^-$ and ACSA-2$^-$/GLAST$^+$ samples. However, ACSA-2$^+$/GLAST$^+$ samples were closer related to ACSA-2$^+$/GLAST$^-$ samples than to ACSA-2$^-$/GLAST$^+$ as shown in Figure 3.37.

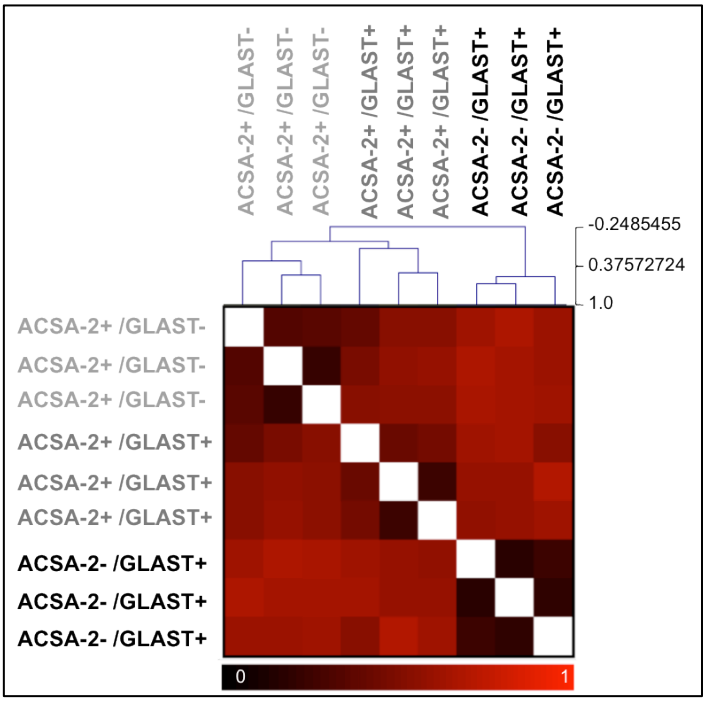

Figure 3.37:
Sample clustering.
In the first step, the unprocessed data set was clustered according to the samples groups. This clustering was visualized using MeV. Correlation coefficients are indicated by their color from black (0) to red (1.0). Replicates for each sample group clustered together, indicating a specific expression profile within one group. Sample labeling according to Supplementary Fig. 12.

As mentioned before, ACSA-2^{+}/GLAST^{-} cells contribute to the ACSA-2^{+}/GLAST$^{+/-}$ sample set. Therefore, in subsequent analysis the ACSA-2^{+}/GLAST^{-} sample set and the ACSA-2^{+}/GLAST^{-} sample set were compaired against each other to identify the highest discriminatory regulated genes. The total number of genes addressed by the microarray were 55681. As visualized by a Volcano plot the data set was reduced to 91 candidates overexpressed in the ACSA-2^{-}/GLAST^{+} group and 380 candidates overexpressed in the ACSA-2^{+}/GLAST^{-} using stringent filtering ((Fig. 3.38 a) Gene lists are given in AppendixII).

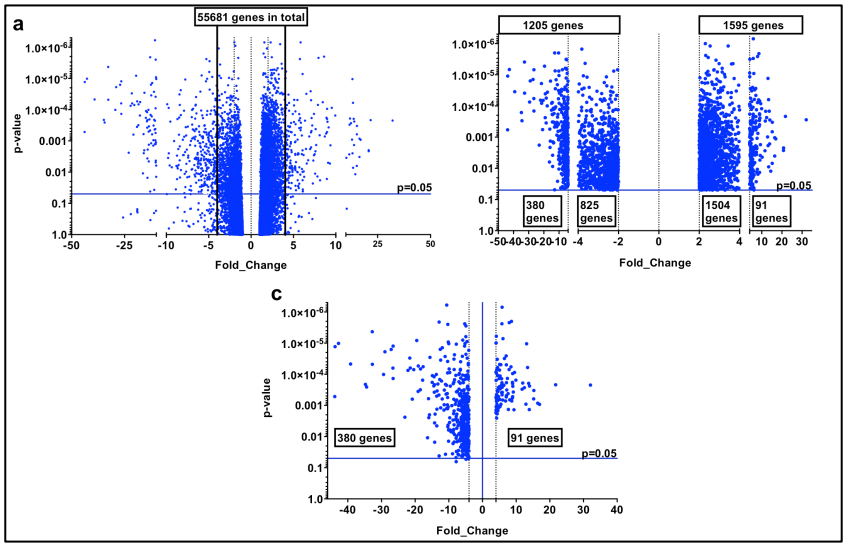

Figure 3.38: Volcano plot of preselected genes.
The Volcano plot is a tool to visualize fold change and p-values of genes as scatter plot. In total 5581 genes were addressed by the array (a). Normalized gene samples with a p-value less than 0.05 (Tukey's range test) and less than one outlier per sample group are shown in b. By furtherprocessing the data set was grouped into genes with a fold change of 2/-2 and 4/-4 corresponding to a log_2 ratio of 2/-2 (b,c). Genes with log_2 ratios of 2/-2 were considered in subsequent analysis All Volcano plots were generated in Prism.

In subsequent steps both gene lists were used to identify bias towards biological processes and pathways (Table 6). Genes were categorized to gene ontology families by their gene identifier. However, gene ontology listing is not redundant and genes can therefore be categorized into different gene ontology families. Functional classes such as 'receptor signaling', 'cellular import and export' as well as 'intracellular trafficking' and 'proliferation' were significantly upregulated in the ACSA-2^{+}/GLAST^{-} sample sets and were not identified in the ACSA-2^{-}/GLAST^{+} samples (Table 6). The 'receptor signaling' cluster comprised several solute carrier transporter which are important for the uptake of biologically active compounds and metabolites [233]. This suggests that ACSA-2^{+}/GLAST^{-} cells already acquired a certain function and show less plasticity. Families such as 'development', 'cell differentiation/migration' or 'extracellular matrix proteins' were found in both gene groups. However, single genes were never identified in both sample groups as shown by Venn diagrams.

Table 6: Pathway families

Higher on ACSA-2^{+}/GLAST$^{+/-}$

Biological process	Gene Hits	p Value
Receptor signaling	98	7.64E-04
Cellular Import/Export	96	7.25E-06
Development	88	7.11E-03
Cell differentiation	85	9.24E-06
Response to toxins	73	4.27E-02
Cell proliferation	55	2.06E-06
Intracellular trafficking	55	2.45E-03
Innate Immunity	41	7.25E-06
Kinase/Phosphatase signaling	37	1.17E-02
Cell migration	35	1.84E-04
Lipid metabolism	34	4.20E-04
Extracellular matrix	26	7.25E-06
Angiogenesis	26	1.26E-05
Cell adhesion	26	2.46E-02
Inflammation	21	1.84E-04
Carbohydrate metabolism	18	4.53E-02
B-cell Immunity	17	4.20E-04
Lipid signaling	6	2.47E-02

Repressed by TGF-beta Receptor Pathway	20	1.39E-05
Induced by FSH	12	6.24E-05
Induced by IL1 Pathway	6	1.12E-02

Higher on ACSA-2^{-}/GLAST^{+}

Biological process	Gene Hits	p Value
Development	32	1.22E-03
Cell differentiation	25	3.60E-03
Cell migration	13	3.60E-03
Extracellular matrix	7	3.42E-02

Hedgehog Pathway	3	1.20E-03

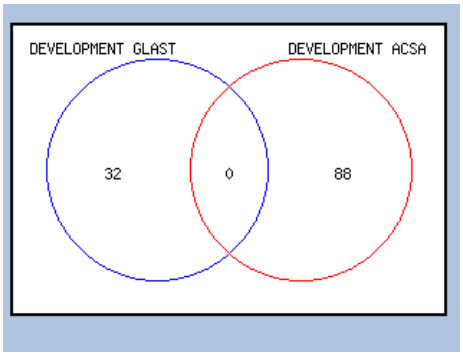

In the ACSA-2^{-}/GLAST^{+} sample set CXCR4, which was shown to control migration of the cerebellar development at embryonic stage was identified [233]. Besides, different genes of the Wnt pathway such as *Frizzled-1* or *Wif1* but also *fgf8* were identified (Fig. 3.39). Fgf8 is important for the development of the cerebellum [234]. The members of the Wnt family are also important for development but furthermore for the regulation of cell fate and proliferation as well as for migration [235]. In addition, members of the sonic hedgehog family including *Gli1* the hedgehog interacting protein (hhip) and patched homologue 2 (*Ptch2*) were significantly upregulated. Also *Hes5*, reflecting Notch signaling activity in the progenitor pool was identified [236]. However, Hes5 was rather weak expressed in 2 from 3 samples of the ACSA-2^{-}/GLAST^{+} sample set. All three pathways, SHH, Wnt and Notch are described to influence cell fate specification [237]. The enrichment of these genes suggests that ACSA-2^{-}/GLAST^{+} are at an early developmental state. To address this further, stem cell factors such as Nestin (*Nes*) [70] were investigated and revealed to be significantly upregulated in the ACSA-2^{-}/GLAST^{+} sample set. In addition, upregulation of the *Lgr5* gene was detected. The Lgr5 protein is reported to be expressed by distinct stem or progenitor cells in various tissues [238,239]. Common stem cell factors known to be expressed by embryonic stem cells (*Klf-4, Nanog, Sox-2* [240]) were suppressed in the ACSA-2^{-}/GLAST^{+} samples. This indicates that ACSA-2^{-}/GLAST^{+} are restricted stem cells.

The sample set was further investigated for the expression of Parvalbumin, a marker for interneurons, [241] which was seen to be expressed by the ACSA-2^{-}/GLAST^{+} transplants, as shown in chapter 3.6.4. In correlation to the transplantation experiment the expression of *Pvlb*

was significantly upregulated in the ACSA-2$^-$/GLAST$^+$ sample set. In addition, pancreas transcription factor 1 subunit alpha (*Ptf1a*), which is specifically expressed on VZ derived cells and important for the generation of interneurons was upregulated on ACSA-2$^-$/GLAST$^+$ cells [242]. Furthermore, *Ascl1 (Mash1)*, which is predominat expressed by cells of the prospective white matter cells was upregulated in the ACSA-2$^-$/GLAST$^+$ sample set [243] (Fig. 3.39 b). As reported by Leto *et al*. prospective white matter cells compose a defined neurogenic niche in the cerebellum [244]. In contrast, the ACSA-2$^-$/GLAST$^+$ sample set did not show an enrichment for serotonergic or domaminergic neurons marked by *Nk2-2, PTEN,* or *OTX-2, Lmx1a* [240,245] (Fig. 3.39 c). Furthermore, the *GAD1* gene encoding the GAD67 transporter and doublecortin (*Dcx*) a microtubule-associated protein expressed by interneurons of the SVZ/RMS were suppressed in the ACSA-2$^-$/GLAST$^+$ sample set. This indicates that ACSA-2$^-$/GLAST$^+$ cells are primed to differentiate into GABAergic interneurons. The oligodendrocyte specific gene *Mbp* was further identified and differentiation into oligodendrocytes was seen in the transplantation experiment (Supplementary Fig. 15). In addition, the glial marker Tenascin C, which is reported to be expressed by radial glia and Bergmann glia of the cerebellum was enriched in the ACSA-2$^-$/GLAST$^+$ sample set [246]. GFAP was weak expressed in the ACSA-2$^-$/GLAST$^+$ sample set. In summary, this analysis indicates that a specification of t he ACSA-2$^-$/GLAST$^+$ cells towards a GABAergic cell type as well as to a glia cell type is favoured. Based on the transplantation experiment and the gene expression profiling it is likely that prospectic white matter cells can be characterized by the absence of ACSA-2 expression and the prescence of GLAST expression.

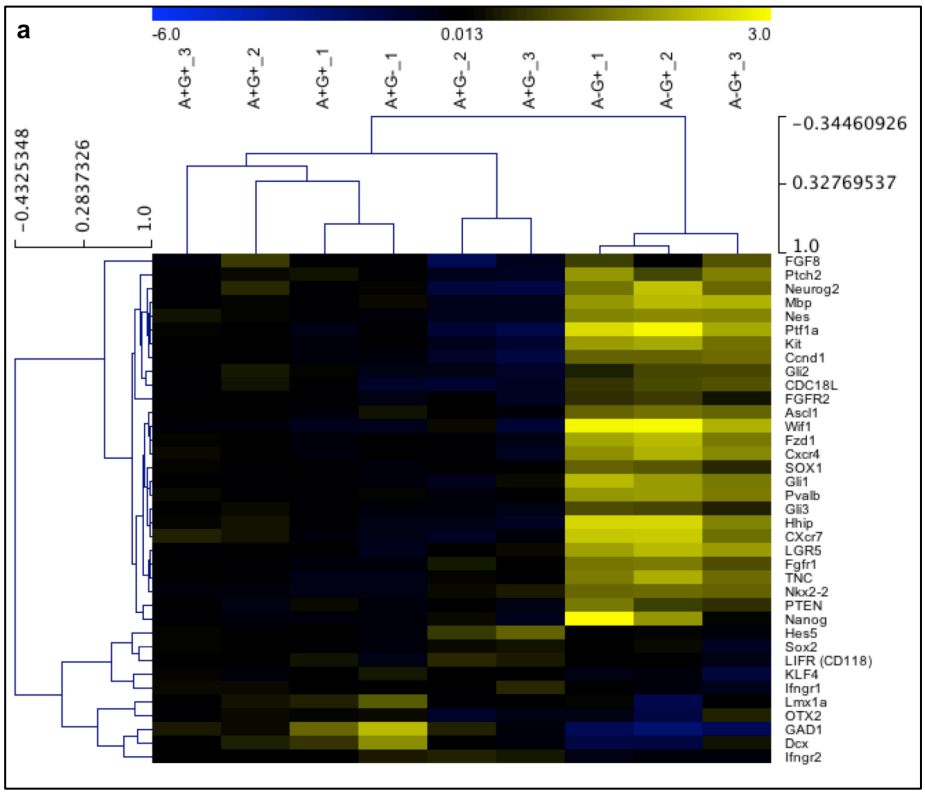

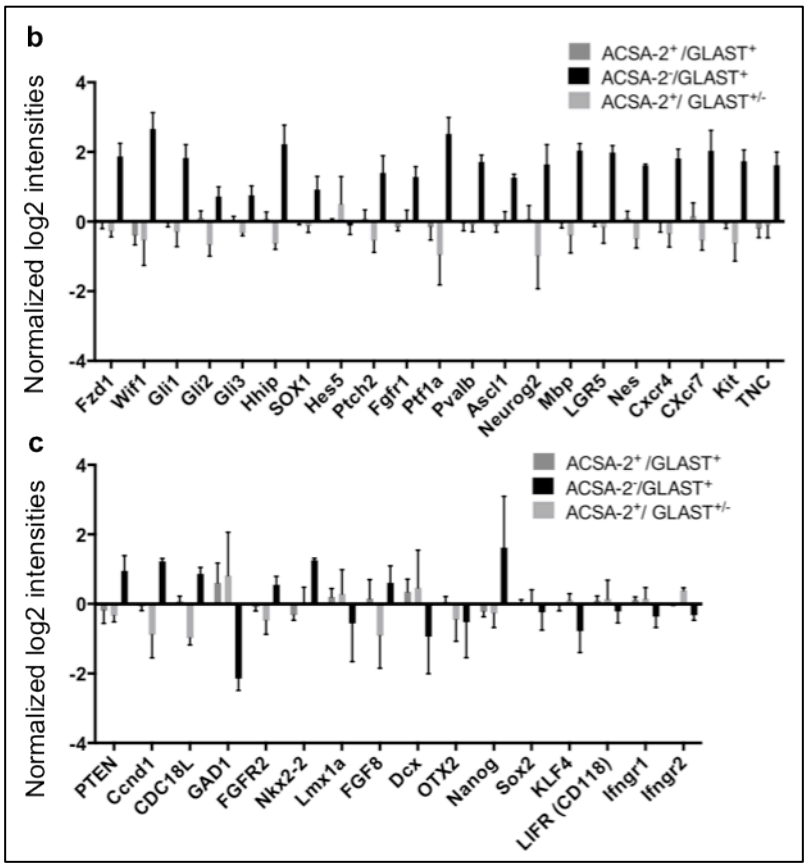

Figure 3.39: **Clustering of genes upregulated in the ACSA-2$^-$/GLAST$^+$ sample set.**
Data set was preprocessed using quantil normalization. Samples were compared using ANOVA. Samples with a p-value less than 0.05 (Tukey's range test), less than one outlier per sample group, a log_2 ratio of (2/-2) were considered for this analyses. Samples of ACSA-2$^+$/GLAST$^-$ (A$^+$/G$^-$), ACSA-2$^+$ /GLAST$^+$ (A$^+$/G$^+$), ACSA-2$^-$/GLAST$^+$ (A$^-$/G$^+$) were visualized using MeV. Correlation co-efficients are indicated by their color from blue (-6) to yellow (+3) (a). Data was further illustrated as bar diagrams. Triplicates of normalized log_2 intensities are indicated as Mean ± SD (b).

In the ACSA-2$^+$/GLAST$^-$ sample set several genes of extracellular matrix epitopes such as *Gjb2*, *Gjb6*, *Gja1* encoding connexin 26, 30 and 43 were found. All of these hemichannels are reported to be only expressed by astrocytes [247]. Besides, tetraspanin (CD82) and vitronectin (VTN) that promote cell adhesion were identified in the ACSA-2$^+$/GLAST$^-$ sample set (Fig. 3.40). Furthermore, genes of the slit family, which interact with ligands expressed by neurons, were upregulated in the ACSA-2$^+$/GLAST$^-$ samples. These genes were *Slit1* and *Slitrk1*. Besides, the gene of the astrocyte specific markers glial fibrillary acidic protein (*GFAP*) (Supplementary Figure 16) and *VCAM-1* (CD106) as well as the oligodendrocyte specific basic-loop-helix transcription factors *Olig1* and *Olig2* were upregulated in the ACSA-2$^+$/GLAST$^-$ samples (Fig. 3.40). In contrast, the neuronal gene *Ptf1a* was not expressed and *Nestin* was suppressed in the ACSA-2$^+$/GLAST$^-$ sample set (compare Fig. 3.39). As shown in Table 6, genes coding for different receptors were enriched in the ACSA-2$^+$/GLAST$^-$ data set. Out of these genes five genes of the solute carrier transporter family (Slc family) were

enriched in the ACSA-2$^+$/GLAST$^-$ samples: *Slc32a1* a vesicular inhibitory amino acid transporter, *Slc6a11* encoding GAT-3, and the *Slc6a12* a neurotransmitter transporter *Slc6a12* and *Slc6a13*, which correspond to solute carriers and indicate members of receptor signaling pathway family.

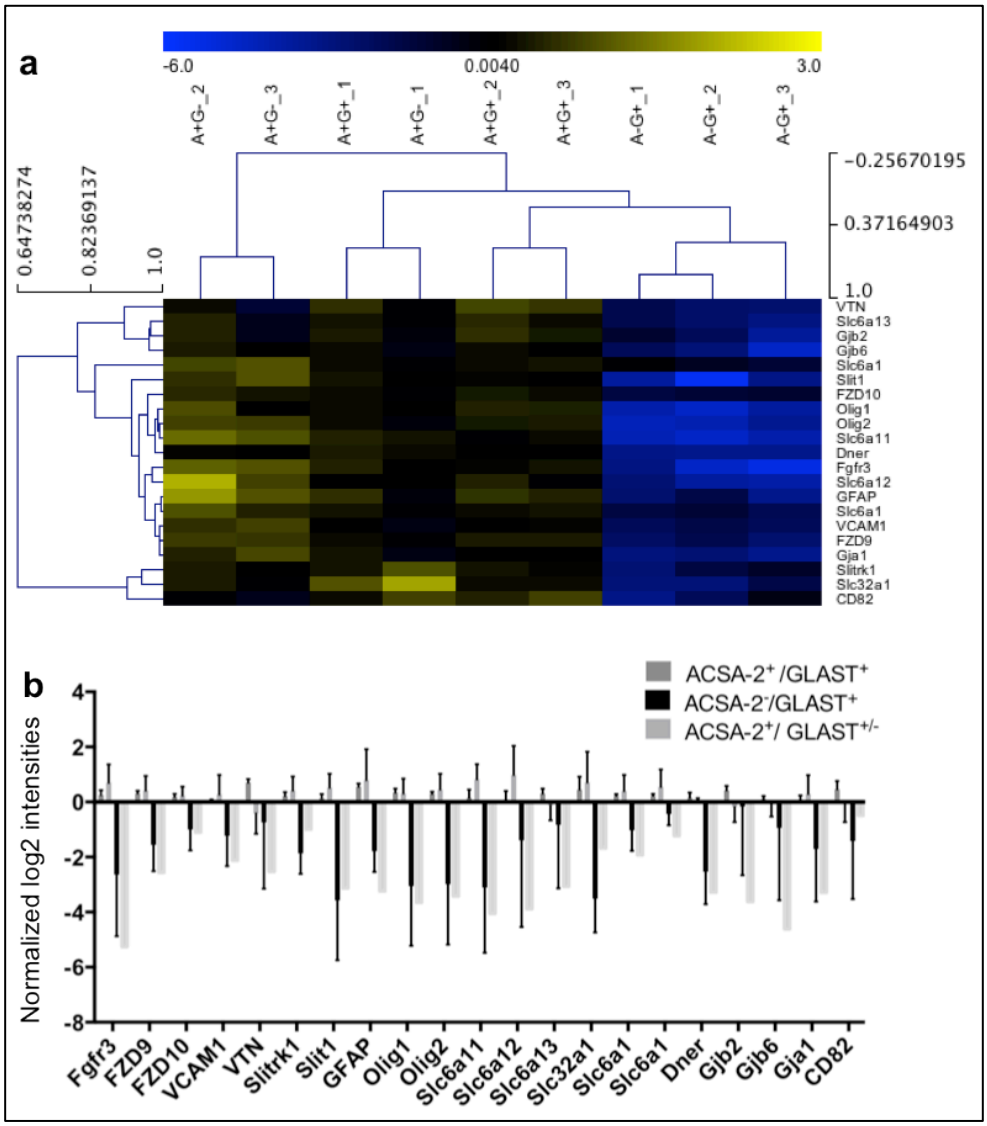

Figure 3.40: Clustering of genes upregulated in the ACSA-2$^+$/GLAST$^-$ sample set.
Data set was preprocessed using quantil normalization. Samples were compared using ANOVA. Normalized gene samples with a p-value less than 0.05 (Tukey's range test), less than one outlier per sample group, a log_2 ratio of (2/-2) were considered for this analyses. Pathways were identified using MetaCore. Samples of ACSA-2$^+$/GLAST$^-$ (A$^+$/G$^-$), ACSA-2$^+$/GLAST$^+$ (A$^+$/G$^+$), ACSA-2$^-$/GLAST$^+$ (A$^-$/G$^+$) were visualized using MeV. Correlation coefficients are indicated by color from blue (-6) to yellow (3) (a). Data further illustrated using bar diagrams. Triplicates of normalized log_2 intensities are indicated as Mean ± SD (b).

Genes such as Sox-2 and or PDGFR did not reveal significant differences between the tested samples (Supplementary Figure 17). Furthermore, *ATOH1 (Math-1), Zic1*, *Tbr2* [248,249], specific markers for granule cells of the cerebellum, showed low levels of gene expression in the tested samples. This indicates a low percentage of granule cell contaminations in ACSA-2^+/GLAST$^-$, ACSA-2^+/GLAST$^+$ and ACSA-2^-/GLAST$^+$ samples of the cerebellum. In summary, this transcriptome analysis supports the differences between ACSA-2^+/GLAST$^-$ cells and ACSA-2^+/GLAST$^-$ cells seen in the transplantation experiment. The gene expression profiling showed a close lineage relationship between ACSA-2^+/GLAST$^-$ and ACSA-2^+/GLAST$^+$ cells. ACSA-2^-/GLAST$^+$ were enriched for stem cell factors and genes of GABAergic phenotype indicating higher plasticity. In contrast, ACSA-2^+/GLAST$^-$ showed an enrichment of cell adhesion and cell matrix proteins indicating a lower plasticity and more tissue integrated phenotype.

4. Discussion

4.1 Mapping astrocyte heterogeneity by cell surface marker expression

At the time of their discovery in the 1800s, astrocytes have been considered as passive cells that support neuronal activity. In the last 50 years, the functional variety of astrocytes was investigated in more detail. It was demonstrated that astrocytes are active elements of the neural network and different astrocyte subclasses with different molecular identities and specialized functions [250] were identified. Beside their housekeeping functions, astrocytes are an essential element of the blood-brain barrier and present neural stem cell characteristics as demonstrated by Doetsch *et al.* in 1999 [68]. However, addressing different astrocyte subgroups within the astrocyte cell compartment still is a major challenge. Moreover, there is an ongoing discussion whether astrocyte subsets exist or whether astrocytes adjust to the local microenvironment and thereby become a specified subset. First astrocyte subclassification studies were performed in 1987 by Miller and Raff. They identified protoplasmic and fibrous astrocytes based on morphological differences [32] and the expression levels of GFAP. In 2007, Cai *et al.* showed that protoplasmic and fibrous astrocytes differ in respect to their transcriptional regulation [251]. However, there is currently no cell surface marker combination described that allows for the isolation of protoplasmic and fibrous astrocytes from wt mice. Besides, the cell bodies of protoplasmic and fibrous astrocytes can be located close to each other in the same brain region. This is based on the fact that astrocytes arise from different lineages or cell sources during development and that transcription factors and gene regulation promote the generation of different astrocyte subtypes at radial glia state [252]. Therefore, it is rather difficult to discriminate protoplasmic and fibrous astrocytes in tissue sections by antibody staining. Protoplasmic and fibrous astrocytes are one example showing that morphological classification alone is not sufficient to class astrocyte subpopulations. The general aim is to subclassify astrocytes by functional properties based on the expression of one or two cell surface markers. The classical tool to study astrocytes is immunostaining. However, IHC and ICC results are sometimes difficult to interpret as markers only reveal a punctuated staining, like GLT-1 or ACSA-2, are less sensitive for the given application or are restricted to cellular compartments like Aquaporin-4 that is expressed on astrocyte endfeet [97]. In the last two decades, novel methods such as the generation of different transgenic mice lines, patch clamp recordings, single cell electroporation approaches as well as flow cytometric analysis were introduced. Many of these efforts, including the transcriptome study performed by Cahoy *et al.* in 2008 [88], the microarray analysis performed by Bachoo *et al.* in 2004 [96] or the identification of different guidance molecules expressed by different astrocyte subtypes [253] lead to the identification of novel astrocyte markers. However, these studies also demonstrated that classical astrocyte markers, such as GS [254] or glutamate transporter (GLT-1) [255] are not

restricted to the astrocyte subset as these markers were demonstrated to be expressed by other neural cell types. In addition, these studies identified some novel astrocyte subpopulation specific markers like Kir4.1 [93,256]. Besides, they revealed some information about the marker expression pattern of astrocytes. Studies presented e.g. that calcium-binding protein S100β is predominantly expressed by mature astrocytes that surround blood vessels [92]. All these studies emphasize that our knowledge about the marker expression on astrocyte subpopulations is still limited. As a consequence this illustrates that novel markers and novel tools are needed to address and analyse the functional divergence of astrocytes. Transgenic mice, which are often used for comprehensive analyses [88], are a powerful tool but also have several limitations. On the one hand, the transgene can be expressed by non-astrocytes, as shown for the GLAST-GFP mice [102]. On the other hand, as reported for the GFAP-LacZ mice [257], it can occur that not all target cells express the transgene. These problems were overcome by the generation of the astrocyte specific antibody Anti-GLAST (ACSA-1) that allows for direct isolation of GLAST expressing primary astrocytes [104]. An antibody based isolation strategy enables for the characterization of astrocytes on the single cell level. In addition, subsequent analyses such as gene expression profiling, molecular or cell-based assays can be performed. Therefore, this work aimed at the identification of novel astrocyte cell surface markers for the prospective characterization of astrocyte subpopulations. As shown by Jungblut *et al*. GLAST is expressed by common astrocytes in the CNS [104]. Therefore, it was chosen as basis for the identification and characterization of astrocyte subpopulations. Within this study, the novel astrocyte marker ACSA-2 was characterized as an astrocyte specific cell surface marker. The Anti-ACSA-2 antibody was generated by contralateral footpad immunization in rats using GFAP-eGFP sorted astrocytes. Differences between GLAST and ACSA-2 expression were seen in the neonatal and adult brain. Further analyses were performed to investigate astrocyte subpopulations based on the expression of this two cell surface markers in combination. These analyses revealed that GLAST and ACSA-2 are co-expressed by the majority of astrocytes including protoplasmic and fibrous astrocytes in the cortex (Fig. 3.16). Brain regions displaying discriminative ACSA-2 and GLAST expression were thereafter investigated in more detail. However, marker expression often correlates with the specification or the localization of a cell. This explains why different expression dynamics were seen between the tested areas of the CNS.

4.2 Generation of novel astrocyte subpopulation specific antibodies and identification of novel astrocyte cell surface markers

Monoclonal antibodies are a valuable tool for research and clinics, as they bind to specific targets. Therefore, one approach of this study aimed at the generation of novel monoclonal astrocyte cell surface specific antibodies by immunization. Immunization strategies based on primary material were used previously for the generation of the ACSA-2 antibody and the oligodendrocyte specific antibody MBP [258]. In this approach, astrocytes served as immunogen and were isolated using the Anti-GLAST MicroBead Kit. An isolation strategy based on GLAST was chosen as this marker is expressed by common astrocytes of the CNS [104]. Furthermore, the Anti-GLAST (ACSA-1) antibody allows for the enrichment and depletion of astrocytes to high purities. For the immunization approach high purities of the target cell group were mandatory to prevent antibody generation against impurities. Therefore, depleted astrocytes were applied as decoy to decrease unspecific immune response against non-target cells. The use of primary cells as immunogen further supported the generation of various antibody-producing clones within the immunization approach. However, the immunization strategy used in this study did not result in the generation of astrocyte subpopulation specific antibody clones. As shown in Figure 3.3, antibodies did either recognize all GLAST positive astrocytes or none. Further studies on the astrocyte proteome would help to understand which astrocyte cell surface molecules can classify astrocyte subclasses. The identified candidates could than be used for an immunization approach against 'defined-targets'.

A further approach of this study was the identification of novel subpopulation specific markers by cell surface marker screening by flow cytometry. The screen was used to identify novel surface epitopes expressed by subpopulations of GLAST and/or ACSA-2 positive astrocytes. Flow cytometry allows for the screening of markers in a high throughput setup in a short time range. In addition, a flow cytometry based assay can be performed with rather low cell numbers (down to 1000 cells per sample). General limitation for the investigation of neural samples on the flow cytometer is the requirement of single cell suspensions, which are commonly obtained by tissue dissociation. The enzymes used for dissociation can potentially harm cell surface epitopes and thereby cause false negative results, as described for other cell sources before [259]. One further disadvantage is that the information about the localization of a cell in a solid tissue is lost once single cell suspensions are generated. To address the localization of the identified markers in brain tissue, the markers were tested by IHC. However, 13 of 15 markers were not suitable for IHC approaches. Therefore, it was decided to

investigate the 15 markers also on whole brain tissue cultures after 3 days *in vitro* by ICC and by MICS (Multidimensional *in situ* Cytometry Survey technology) [196]. In comparison to classic immunochemical approaches, which enable for the investigation of two or three markers on one tissue section at a time, the MICS experiment enables for the investigation of up to 100 different markers using one tissue section [196]. For this reason, this technique can also be used to study rare cells. Using this technology it was possible to investigate the expression profile, the distribution and the expression intensity of the identified marker panel on astrocytes and other neural cells. Different markers, such as VCAM-1 (CD106) revealed an inhomogenous distribution on the cell surface of the cultivated astrocytes. In the MICS analyses VCAM-1 was not restricted to the astrocyte endfeet, as discussed for astrocytes in the SVZ [260]. Besides VCAM-1, interferon-gamma receptor (CD119) was identified in this surface marker screening approach. The expression of CD119 was also investigated by MICS and IHC. In wt mice CD119 was expressed by all GLAST$^+$ astrocytes. Therefore, CD119 was not considered as a suitable candidate to discriminate astrocyte subpopulations. However, Beurel *et al.* reported about a decreased expression of the CD119 membrane protein upon interferon-gamma treatment. Therefore, CD119 is considered to be a versatile astrocyte marker to study astrocytes in the context of neuroinflammatory diseases such as Alzheimer's or multiple sclerosis [261]. Moreover, CD119 might characterize a subpopulation of astrocytes in the diseased brain.

4.3 Identification of the ACSA-2 antigen

The identification of the ACSA-2 antigen was addressed in several ways. One way was a ligand receptor capturing (LRC) approach[198] that lead to the identification of two glycoproteins: GAT-3 and NrCAM. According to the expression profile described in the ALLEN BRAIN ATLAS and the IHC data of this study GAT-3 was the more promising candidate. In addition, a significant enrichment of the gene encoding GAT-3 (*Slc6a11*) was seen in the transcriptome analysis of the ACSA-2$^+$/GLAST$^-$ samples. However, Western Blot analysis, immunoprecipitation and the overexpression of GAT-3-GFP in HEK cells did not confirm GAT-3 as target of the Anti-ACSA-2 antibody. In this work, Western Blot analysis and immunoprecipitation were used to prove or disprove the hits of the LRC approach. Immunoprecipitation is a complex process; it consists of different steps and for this reason it is error-prone. As all tested cell lines did not reveal any ACSA-2 antigen expression the only suitable cell source was primary material. In comparison to an adherent growing cell line, dissociated tissue is heterogeneous considering cell composition. In addition, the dissociation of primary material results in a high level of cell debris that is remained in the lysate after cell

lysis and often causes high background signals or false positive signals. In the experimental setup, the major problem was the unspecific binding of the catching antibody to intracellular components such as α-Actin, heat shock proteins or intermediate filaments. These proteins are ubiquitously expressed by all cells and are therefore present in the lysate at high concentrations. Thus, it is likely that the capture antibody binds preferably to unspecific binding partners than to its specific binding site.

In addition, transmembrane proteins are integrated into the lipid bilayer and detergents are needed to solubilize these proteins [262]. Membrane proteins can further be established as dimers, heteromers or oligomers. This bears the risk, that subunits are separated from each other during the solubilization or precipitation process. In addition, antibodies that recognize a conformational structure cannot bind their specific targets. If the target protein had been a known G protein-coupled receptor it would have been possible to co-immunoprecipitate the epitope using GPCRs [263]. As the biochemical composition of the epitope was not known, the immoprecipitation was tested in different experimental setups to identify the optimal protocol. In one setup, sepharose, a classical matrix used for immunprecipitation, was tested. Sepharose is characterized by a high binding affinity and binding capacity. However, this leads to high background signals [264]. To saturate unspecific binding sides several pre-clearing steps were performed. The other setup tested in this study was the immunoprecipitation based on Protein G MicroBeads [265]. MircoBeads have lower binding capacity and lower avidity than Sepharose. Therefore, MicroBeads cause less background signals. The principle of the immunoprecipitation upon surface biotinylation was the use of a biotin linker for the discrimination of surface membrane and intracellular molecules. For detection, a Streptavidin HRP conjugate was used which binds to biotin at a very high affinity and therefore causes low background signals. The major problem of the biotinylation protocol was to obtain the recommended cell number of 1×10^8 sorted cells per approach. As 1×10^6 astrocytes can be obtained from one mouse brain using the Anti-ACSA-2 MicroBeads, 100 brains were needed for one biotinylation approach. In summary, the targets of the LRC could not be validated by Western Blot analysis neither by immunoprecipitation nor by the over-expression of the GAT-3 protein. In a further approach a deglycosylation assay was established to address whether the ACSA-2 antibody recognizes a glycosylation pattern on astrocytes. The assay revealed a decreased signal of the ACSA-2 antibody staining upon deglycosylation. Glycosylation is the most complex posttranslational modification [266]. Based on the glycoside hydrolases used in this work the ACSA-2 antibody can either recognize an O- or N-glycosylated glycoprotein, a glycolipid, a post-glycosylation modification of branches, unbranched side-chains or a sugar moiety involved in conformational stabilization N-glycans, O-glycans and glycolidips are products of the biosynthesis pathway. Besides, N-linked glycosylation patterns are more

frequent than O-linked glycosylation patterns. However, some glycoproteins reveal O- and N-glycosylation, e.g. CD24 [267]. In addition, N-acetylglucosamine (GlcNAc) and N-acetylneuraminic acid but also mannose, fructose and galactose can be added. These residues are often characteristic for tissues or developmental stages [268]. In an ongoing approach it will be validated which glycosylation structure is recognized by the ACSA-2 antibody.

4.4 Investigations of SVZ stem cells by surface marker expression

The investigation of self-renewing and multipotent stem cells in the adult brain is of emerging interest, as these cells are considered to serve as targets against neurodegenerative diseases. However, since the identification of transit-amplifying stem cells in 1999 by Doetsch *et al*. researchers try to identify a defined marker combination to address and isolate stem cells from the SVZ. Stem cells of the SVZ derive from radial glia. They have astrocyte characteristics such as marker expression. Moreover, these cells are able to give rise to neuronal progenitors during embryonic development [47,53,269]. SVZ stem cells retain radial glia marker expression but also express markers shared by neuronal precursors such as β-III tubulin, PSA-NCAM and doublecortin. The first problem, when it comes to the identification of specific stem cell markers is the architecture of the murine SVZ. In comparison to human, where a gap separates the ependymal cell layer from the stem cell layer, the layers in the murine SVZ are tightly connected with each other. The stem cells of the SVZ, also named as B1 astrocytes, contact ependymal cells via gap junctions [81]. Due to the tight architecture of the SVZ, it was difficult to evaluate if ependymal cells express ACSA-2 in this study. Besides the architecture, the major problem is to identify novel markers that allow for the classification of cellular identities in the SVZ, as summarized by Mamber *et al* in 2013. As discussed by Beckervordersandforth *et al*. marker expression is not static and markers can be shared by different identities within the SVZ [72]. Several research groups try to address the generic profile of different astrocyte subpopulations in the SVZ. A panel of potential novel markers was identified by microarray analyses. Common markers discussed to classify stem cells are cell surface molecules including (Prominin-1), transporters (GLAST, GLT-1 and GAT-3), receptors (EGFR) [271,272] and cell adhesion molecules such as SSEA-1 and VCAM-1. Furthermore, different cytoskeletal components are described to be expressed by SVZ stem cells. This are intermediate filaments such as vimentin, GFAP and Nestin, which is not present in mature astrocytes [270]. Additionally, transcription factors such as Sox-2 are potential SVZ stem cell markers. However, most of these markers were tested in previous studies and were reported to be shared by ependymal cells or surrounding astrocytes. Moreover, GFAP or Prominin-1 alone are not sufficient for the identification and isolation of SVZ stem cells. As

shown in independent studies, two or more markers in combination are needed to address SVZ stem cells [75]. In addition, intracellular markers such as Sox-2 are not appropriate for the prospective isolation of NSCs as they require an intracellular labeling step. Thus, this study aimed at the isolation of SVZ stem cells by cell surface marker expression. In this study, the SVZ tissue was analyzed on the single cell level on a flow cytometer. The dissociation process of SVZ tissue from adult mice resulted in high frequencies of dead cells and high amount of cell debris. This was due to high cell connectivity in the adult brain tissue, as described before. In this study, GLAST and ACSA-2 were stained in combination with CD24 to discriminate ependymal cells from stem cells and surrounding astrocytes. This strategy was chosen, as CD24 is a published marker characterized to discriminate ependymal cells and SVZ stem cells in combination with Prominin-1 [271]. In this study, CD24 was shown to be versatile for the discrimination of ependymal cells from GLAST expressing astrocytes –including stem cells- in the SVZ on the flow cytometer. In parallel, the expression of ACSA-2 in the SVZ was investigated by flow cytometry. The expression study of GLAST and ACSA-2 revealed that these markers are co-expressed in the SVZ tissue, which was validated using different mouse strains. Thereafter, different markers found in literature were chosen to address the stem cell compartment in more detail. The stem cell marker Lgr5 was tested, as this marker is reported being expressed by distinct stem cell populations in various tissues [238]. Markers used to discriminate ependymal cells such as Notch-1 and α-tubulin were also tested [272,273]. However, all tested markers in this study were either co-expressed by ependymal cells or by surrounding astrocytes. In summary this work did not find a marker combination for the isolation of SVZ stem cells.

4.5 GLAST and ACSA-2: A versatile tool to discriminate astrocyte precursors of the neonatal cerebellum

The development of the cerebellum continues after birth. It has been shown that germinal niches of the prospective white matter give rise to interneurons, astrocytes and oligodendrocytes. Therefore the prospective white matter was named as the neurogenic niche of the cerebellum. The prospective white matter disappears when the cerebellum maturates [241,274]. Although the cerebellum is one of the best studied brain region origin and lineage relationships of cerebellar glia are less investigated [169]. This study provides a novel approach to address stem cells and glial precursors of the neonatal cerebellar by the use of the astrocyte cell surface markers GLAST and ACSA-2. To address this, the cell differentiation capacities and the transcriptome of the ACSA-2^{+}/GLAST$^{+/-}$, ACSA-2^{-}/GLAST^{+} and ACSA-2^{+}/GLAST^{-} cells

were investigated. GLAST is not a novel marker for the identification of multipotent precursors and stem cells of the murine brain. It was already shown that GLAST positive radial glia [47] of the cortex are neurogenic. GLAST is also described as a stem cell marker for SVZ stem cells. For the identification of cerebellar glia surface markers such as CD44 [275,276], Prominin-1[179,249] and CD15 [249] were used in different studies. CD44 is a classical astrocyte marker. However, CD44 is not restricted to the astrocyte subset. In the cerebellum, CD44 is also expressed by neurons [275,276]. In contrast, GLAST and ACSA-2 are restricted to the astrocyte lineage. Interestingly, the transplants revealed a high amount of granule cells in both groups. All samples used for the transplantion had purities between 75% and 95%. However, granule cell undergo clonal expansion. Therefore, low impurities of granule cells in the grafted fraction can lead to a high number of granule cells found in the graft after 30 days [277]. Naruse *et al*. reported about a strong decrease of Nestin and Sox-2 expression on $CD44^+$ isolated stem/progenitor cells at P10. The developmental analysis of this study revealed that frequencies of $ACSA\text{-}2^-/GLAST^+$ multipotent cells decrease with the onset of development and are not detectable later than P12. A2B5 defines developing glia and becomes down-regulated when glia maturate. Therefore, the expression of A2B5 was addressed in this study. Analysis of A2B5 expression at P1 and P7 showed a significant decrease in A2B5 expression on $ACSA\text{-}2^-/GLAST^+$ cells at P7 compared to P1. As reported by Fleming *et al.* intermediate astrocyte precursors can be characterised by high expression levels of CD15 and low expression levels of Tenascin C (Tnc^{low} $CD15^+$ cells). To address a potential correlation between $ACSA\text{-}2^-/GLAST^+$ cells and Tnc^{low} $CD15^+$ cells, the expression of CD15 was monitored on $ACSA\text{-}2^+/GLAST^-$, $ACSA\text{-}2^-/GLAST^+$ and $ACSA\text{-}2^+/GLAST^{+/-}$ cells. In fact, highest CD15 expression was detected on the $ACSA\text{-}2^-/GLAST^+$ subset (Fig. 3.31).

Lee *et al*. studied cerebellar stem cells based on the expression of Prominin-1. They transplanted multipotent cells derived from cultivation as neurospheres. In this study, all sample groups were transplanted directly after cell sorting without any cultivation step to prevent any selection. The cells were further transplanted in the absence of any growth factors in order to prevent any specification due to extrinsic factors. To further prevent preselection in the dissociation step a gentle dissociation protocol was followed. However, the loss of certain subtypes within the dissociation process cannot be excluded. This work is the first study that describes an efficient enrichment of cerebellar precursor populations from wt mice based on the expression of two astrocyte cell surface markers. Lee *et al*. had a starting frequency of 0.2% $Prominin\text{-}1^+$ and lin^- cells. Lee *et al*. characterized lin^- cells as cells lacking neuronal and glial lineage markers [179]. However, Prominin-1 has distinct splice variants and the isolation efficiency is dependent on the antibody clone [278]. Fleming *et al*. reported about a frequency of less than 0.5% Tenascin $C^+/Prominin\text{-}1^+$ cells in their multipotent cell population.

Both approaches were based on transgenic mice. The system based on the expression of GLAST and ACSA-2 presented a population of 10% ACSA-2$^-$/GLAST$^+$ cells at P1. However, the frequency of stem cells within the ACSA-2$^-$/GLAST$^+$ needs to be addressed.

This study showed that a novel multipotent precursor cell type of the early neonatal cerebellum can be characterized by the expression of GLAST and the absence of ACSA-2. Cells characterized by the expression of GLAST and ACSA-2 revealed a limited differentiation potential and were restricted to a glial cell fate, as seen by transplantation. The molecular and cellular interactions that regulate cell fate and control the differentiation of the glia lineage in the developing cerebellum are currently unknown. Based on the transplantation experiments of this study ACSA-2$^-$/GLAST$^+$ cells show higher plasticity. This further suggests that ACSA-2$^-$/GLAST$^+$ cells are able to adapt to a given phenotype in respect to local conditions. In contrast, ACSA-2$^+$/GLAST$^{+/-}$ were shown to have a lower plasticity. Therefore, this study suggests that this cell population is already 'primed' and cannot acquire to a local environment.

4.5.1 Gene expression profiling of ACSA-2$^+$/GLAST$^-$, ACSA-2$^+$/GLAST$^{+/-}$ and ACSA-2$^-$/GLAST$^+$ sorted cells from neonatal cerebellum

The gene expression profile of ACSA-2$^+$/GLAST$^-$, ACSA-2$^-$/GLAST$^+$ and ACSA-2$^+$/GLAST$^{+/-}$ cells was investigated by microarray analysis. For better comparison between the transplantation experiment and the gene expression profiling samples were isolated using the same protocols. The isolated cells showed impurities between 7 to 25%. However, impurities within one sample group were comparable. The hybridisation of the ACSA-2$^+$/GLAST$^{+/-}$ sample group revealed weak signals. However, this was normalized in the subsequent step by quantil normalization. ACSA-2$^+$/GLAST$^{+/-}$ samples displayed an intermediate group between ACSA-2$^+$/GLAST$^-$ and ACSA-2$^-$/GLAST$^+$ cells, which was already monitored in the flow cytometric analyses. In a correlation matrix the relationship between the ACSA-2$^-$/GLAST$^+$, ACSA-2$^+$/GLAST$^-$ and ACSA-2$^+$/GLAST$^{+/-}$ samples was illustrated. This illustration depicted a closer relationship between the ACSA-2$^+$/GLAST$^-$ and the ACSA-2$^+$/GLAST$^{+/-}$ sample sets. This data supports the idea that presence and abscence of ACSA-2 allow for the discrimination of astrocyte subpopulations in the cerebellum. The data set did not reveal a significant increase of genes described for the granule cell lineage (*ATOH1 (Math-1), Zic1*, *Tbr2* [248,249]). This supports that granule cells detected in the transplants are likely to be derived from clonal expansion. However, it has to be considered that the gene expression level does not correlate with the protein expression level. Stem cell factors described for embryonic stem cells *(Nanog, Klf-4, Sox-2* [240]) were further not identified in the ACSA-2$^-$/GLAST$^+$ samples. This illustrated that ACSA-2$^-$/GLAST$^+$ cells are more restricted stem cells. Factors involved in dopaminergic or serotonergic differentiation were slightly

upregulated in the ACSA-2$^-$/GLAST$^+$ samples (*Nkx2-.2, Lmx1a, Otx2* [240,245]). In contrast, a gene correlated with a GABAergic phenotype (*Ptf1a*) was upregulated in the ACSA-2$^-$/GLAST$^+$ samples. This illustrated a specification of ACSA-2$^-$/GLAST$^+$ cells towards a GABAergic cell type. Besides, Nestin a common stem cell marker and Sox1, a gene described to be enriched in Bergmann glia precursors and neurosphere forming cells of the cerebellum were upregulated in the ACSA-2$^-$/GLAST$^+$ samples [279]. One further gene expressed by Bergmann glia was Tenascin C, which was identified in the ACSA-2$^-$/GLAST$^+$ samples [280]. The upregulation of Bergmann glia specific genes is supported by the transplantation experiment showing that ACSA-2$^-$/GLAST$^+$ differentiated into Bergmann glia whereas ACSA-2$^+$/GLAST$^{+/-}$ were not able to acquire this cell type. In addition, Achaete-scute homolog-1-Ascl1 (*Mash1*) was upregulated. It was shown, that mice lacking Ascl-1 prefentially differentiated into astrocytes [281]. Leto *et al*. described Ascl-1 expressing cells as a precursor population of Ascl-1/Sox-2 expressing cells. The data of *ex vivo* sorted cells did not present Sox-2 expression [274] in any group. Therefore, ACSA-2$^-$/GLAST$^+$ cells are considered to be progenitors of an earlier developmental stage and though do not yet express Sox-2. The ACSA-2$^-$/GLAST$^+$ data set revealed the enrichment of the gene encoding Parvalbumin, a marker for interneurons. In addition, it showed the upregulation of a very important gene required for the differentiation of cerebellar cells into interneurons. This was pancreas transcription factor 1 subunit alpha (*Ptf1a*) [242]. Moreover, *Ptf1a* is described as a marker for neurogenic cells of the prospective white matter. Thus, this study is considered to provide a novel transgen-free tool for the isolation of prospective white matter cells. Fleming *et al.* described that prospective white matter cells respond to SHH and differentiate into GABAergic interneurons and glia, as also shown for ACSA-2$^-$/GLAST$^+$ cells by transplantation. Fleming *et al*. studied the SHH pathway activity using a *Gli1*^{nlacZ} mouse model [249]. In this study the activation of the Wnt and the SHH signaling pathways were addressed by gene expression profiling. In contrast to their observation that *Gli1* is higher expressed in CD15$^+$ glial precursors, the gene expression data of this study pointed to a higher expression of *Gli1* in the neural stem cell compartment (ACSA-2$^-$/GLAST$^+$ cells). Besides, *Gli1*, *Gli2* and *Gli3* as well as the hedgehog interacting protein (*hhip*) and patched homologue 2 (*Ptch2*) were significantly enriched in the ACSA-2$^-$/GLAST$^+$ samples. Patched homologue 2 (*Ptch2*) is a direct target of *Gli* [282,283]. The ACSA-2$^+$/GLAST$^{+/-}$ sample set revealed an enrichment of genes encoding connexin 26 (*Gjb2*), connexin 30 (*Gjb6*) , connexin 43 (*Gja1*) and CD82 the extracellular matrix protein vitronectin. All hemichannels are exclusively expressed by astrocytes. Especially connexin 30 is broadly expressed on astrocytes and important for ion exchange [284]. A further gene group related to cellular function and predominantly expressed by the ACSA-2$^+$/GLAST$^{+/-}$ sample set were the members of the solute carrier transporter (Scl)

family. Solute carrier transporters are important for the transport of ions and organic molecules. Besides, the guidance molecules Slit1 and Slitrk1 were identified. In contrast to the SVZ/RMS/olfactory bulb system little is known about the role of guidance molecules in the cerebellum. Slitrk1 is reported to be important for neurite outgrowth. However, this was not specified for the cerebellum [285]. In the ACSA-2^{+}/$GLAST^{+/-}$ sample set neuronal genes were not identified. In contrast, an enrichment for genes such as *VCAM, GFAP*, *Olig1* and *Olig2* was seen in the ACSA-2^{+}/$GLAST^{+/-}$ sample set. In summary, the transplantation assay and the gene expression profiling demonstrated ACSA-2^{+}/$GLAST^{+/-}$ cells as glial precursors and ACSA-2^{-}/$GLAST^{+}$ cells as multipotent cells of the cerebellum.

5. Outlook

In this study combining the astrocyte specific cell surface markers ACSA-2 and GLAST successfully identified astrocyte subpopulations. Comprehensive analysis of GLAST and ACSA-2 expression in distinct brain areas revealed very significant differences in the cerebellum of neonatal mice. These subpopulations were described as ACSA-2$^-$/GLAST$^+$ and ACSA-2$^+$/GLAST$^+$ cells. The ACSA-2$^-$/GLAST$^+$ population will be further characterized for its cell integration capacity, stem cell potential and plasticity. In a further transplantation assay ACSA-2$^-$/GLAST$^+$ cells will be isolated from the cerebellum of β-actin GFP mice at neonatal age and transplanted into the cerebellum of adult mice. As a negative control, ACSA-2$^+$/GLAST$^+$ cells will be isolated and transplanted into a second group in parallel, as these cells did not reveal multipotent differentiation capacities in this study.

Major focus of this work was to map the divergence of astrocyte subpopulations by cell surface markers. In one approach, the expression profile of the novel ACSA-2 antibody in the murine brain and its target were investigated. The glycopattern recognized by the ACSA-2 antibody will be further characterized for N- or O-glycosylation using specific glycoside hydrolases.

ACSA-2 shows a broad expression in the mouse brain, spinal cord and retina. Analysis of retina and spinal cord were performed and revealed specific ACSA-2 staining in both areas. Therefore, the ACSA-2 antibody can be used in future studies to investigate and isolate astrocytes of spinal cord and retina.

Moreover, similar expression patterns between GLAST and ACSA-2 expressing astrocytes of the neural retina and the cerebellum were seen. Further approaches, including gene expression profiling or patch clamp recordings, could address lineage relationships between ACSA-2$^-$/GLAST$^+$ cells of the cerebellum and the retina. In addition, the differentiation potential and the plasticity of ACSA-2$^-$/GLAST$^+$ cells of the retina or the cerebellum could be addressed by cell transplantation experiments. Therefore, ACSA-2$^-$/GLAST$^+$ cells of retina isolated and transplanted into the cerebellum or vice versa.

In this study one approach aimed at the identification of astrocyte cell surface markers by antibody screening. Apart from published markers such as the heat stable antigen (CD24) or the vascular cell adhesion protein 1 (VCAM (CD106)) the interferon-gamma receptor (CD119) was identified. However, as tested by MICS, CD119 was co-expressed on all $GLAST^+$ astrocytes in wt mice and could not be validated as a subpopulation marker. Therefore, it would be interesting to study interferon-gamma receptor expression on astrocytes in the context of neuroinflammatory diseases e.g. in experimental autoimmune encephalomyelitis mice.

In a side project, the expression profile of ACSA-2 on reactive astrocytes was investigated. GFAP is a marker for reactive astrocytes and is strongly induced upon reactive gliosis, e.g. in the Afg3l1 d/d Afg3l2 fl/fl GFAP cre mouse model. In the tested mouse model ACSA-2 and GFAP expression were not correlated. Therefore, ACSA-2 is considered being expressed by non-activated astrocytes and ACSA-2 could be used to study non-activated vs. activated astrocytes in a reactive gliosis model. Stab-wound-lesions in the cortex could be introduced to study this subset in further detail.

I Supplementary data:

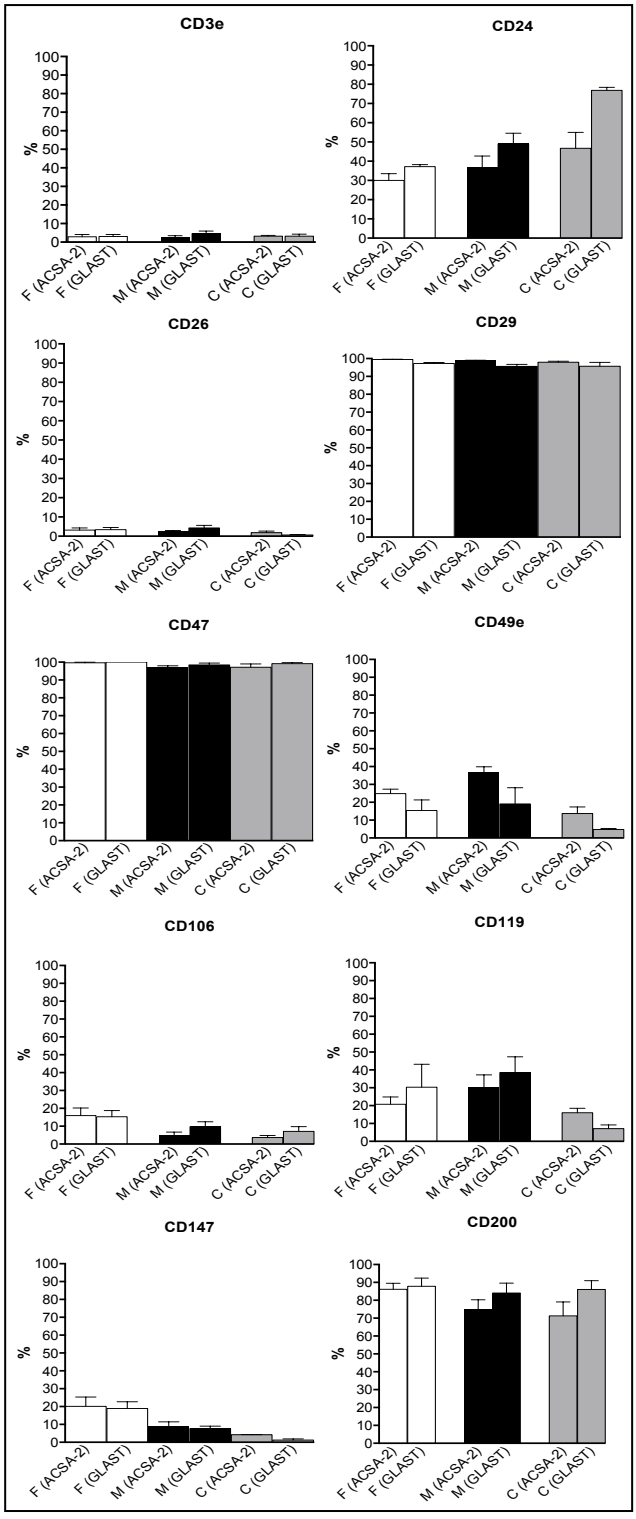

Supplementary Figure 1: Frequencies of marker expression in different brain regions.
The identification of novel astrocyte subpopulation markers was performed by cell surface marker screening. 10 markers were identified and investigated in a subsequent re-screening approach on forebrain, midbrain and cerebellar samples in a co-staining with the GLAST and the ACSA-2 antibody. Except from CD24, markers presented a comparable frequency on the ACSA-2 positive and the GLAST positive astrocytes.

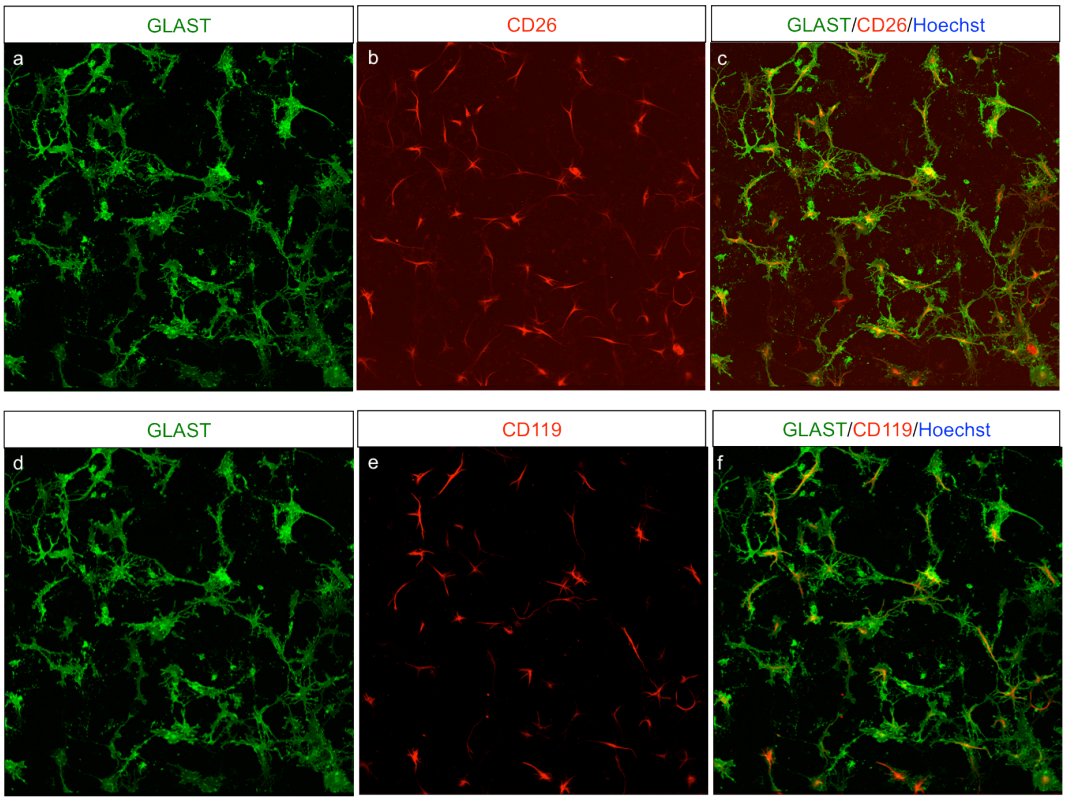

Supplementary Figure 2: Marker validation using MICS.
Expression of different markers identified by surface marker screening was validated by MICS. The MICS experiment was performed on mixed mouse brain cells derived from P1 mice. For MICS cells were cultivated for 7 days. Exemplified for all positive tested markers are CD26 (b) and CD119 (e). Both revealed co-expression (c,f) on all GLAST positive cells (a,d).

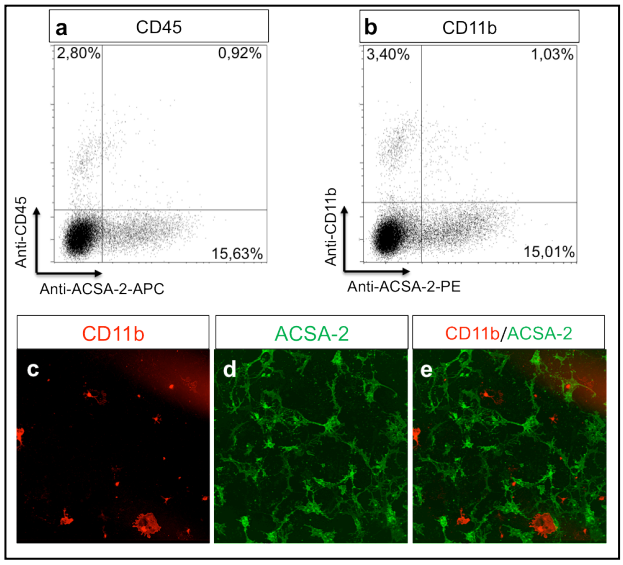

Supplementary Figure 3: Co-staining of ACSA-2 with CD45 and CD11b by MICS.
Dissociated neonatal mouse brain samples of P3 mice were used to discriminate ACSA-2 staining on CD45 positive hematopoietic cells (a) and CD11b positive microglia (b) by flow cytometry. CD45 positive and CD11b positive cells presented co-expression with ACSA-2 to less than 2%, which is considered as background staining. Dissociated neonatal mouse brain samples of P1 mice were used for MICS. ACSA-2 did not present co-expression with CD11b (c-e).

F	G	H	L
Highest mean condition	Lowest mean condition	Description	log 2 ratio (ACSA-2/Insulin)
ACSA-2	Insulin	S6A11_MOUSE Sodium- and chloride-dependent GABA transporter 3 GN=Slc6a11	5.26
ACSA-2	Insulin	NRCAM_MOUSE Neuronal cell adhesion molecule GN=Nrcam	3.34
Insulin	ACSA-2	IGF1R_MOUSE Insulin-like growth factor 1 receptor GN=Igf1r	-2.65
Insulin	ACSA-2	INSR_MOUSE Insulin receptor GN=Insr	-4.91

Supplementary Figure 4: Candidates obtained by LRC approach.
The LRC was performed to identify the target of the ACSA-2 antibody. This approach was conducted at the ETH Zurich using nitrogen frozen brain sections derived from P1 mice. The capturing is based on a TRICEPS linker followed by a mass spec. analysis step [198]. The LRC pointed to two candidates: GABA transporter 3 (GAT-3) and Neuronal cell adhesion molecule (NrCAM).

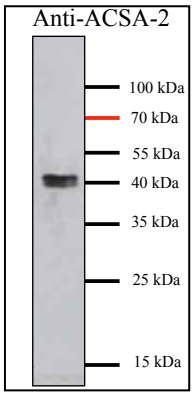

Supplementary Figure 5: Identification of the ACSA-2 antigen by Western Blot analysis.
Western Blot analysis against ACSA-2 was performed on lysates derived from adult mouse brains. A band of 40 kDa was identified. Analysis of this band by mass spectroscopy did not identify the antigen of ACSA-2 and pointed to α-Actin, which was considered as an unspecific hit.

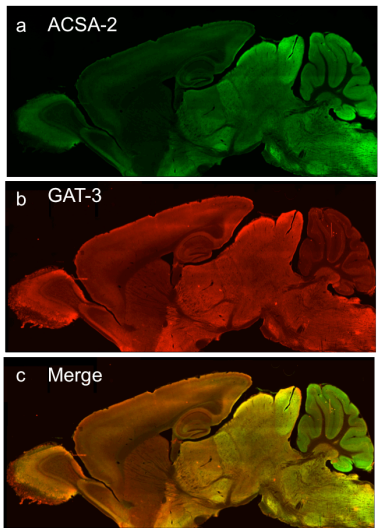

Supplementary Figure 6: Immunohistochemical analysis of ACSA-2 and GAT-3 expression.
The expression profile of ACSA-2 and GAT-3 was investigated on adult mouse brain sagittal sections stained as floating sections (40 µm). GAT-3 and ACSA-2 show a high level of co-expression in parts of the olfactory bulb, midbrain, cerebellum and brain stem.

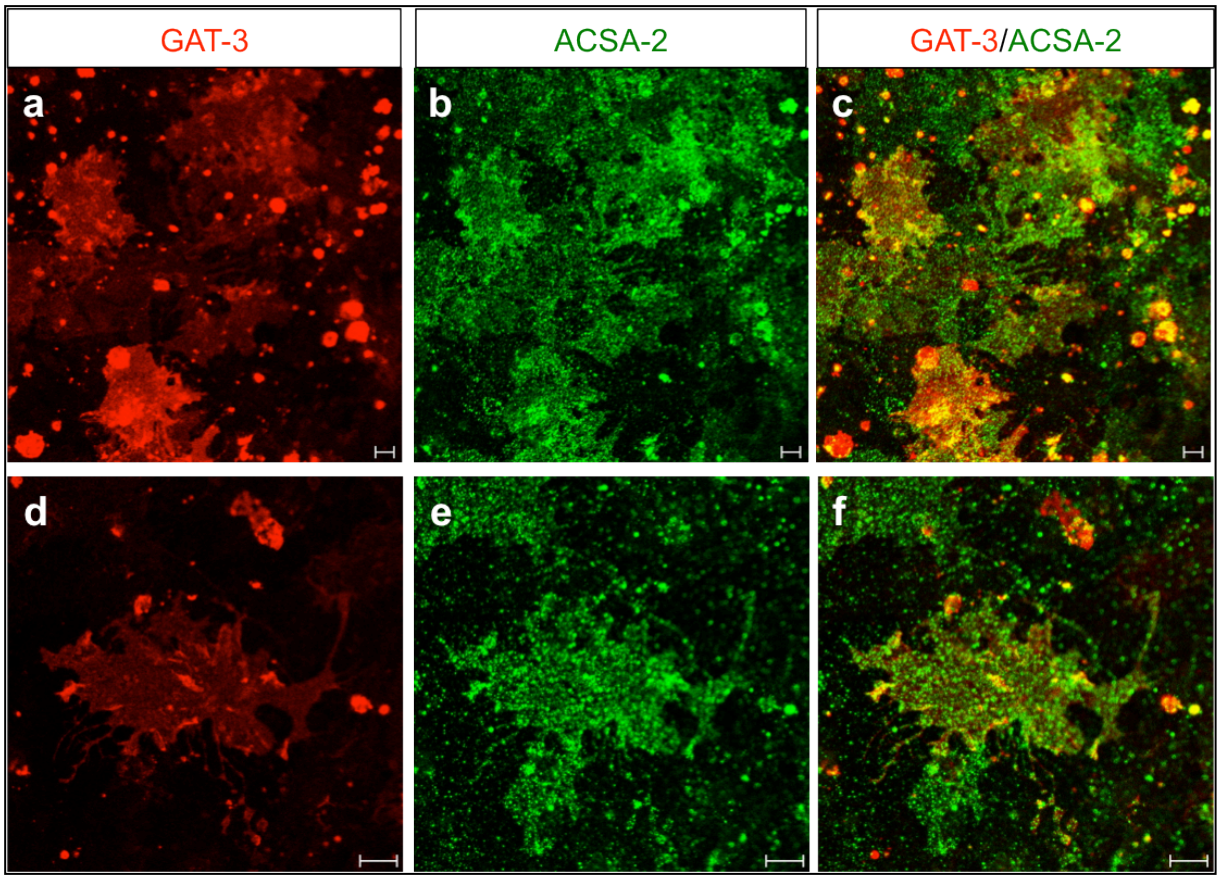

Supplementary Figure 7: Immunocytochemical analysis of ACSA-2 and GAT-3 expression on astrocytes.
ACSA-2 positive astrocytes were isolated using Anti-ACSA-2 MicroBeads. Cells were plated on Poly-L lysin coated cover slips and cultivated for 3 days in complete medium. Cells were fixed with 2% PFA and stained against ACSA-2 (b,e) in the absence of Triton-X-100. Thereafter cells were permeabilized and stained against GAT-3 (a,d). Merged picture (c,f) show co-expression of ACSA-2 and GAT-3. Scale bar represents 10 µm.

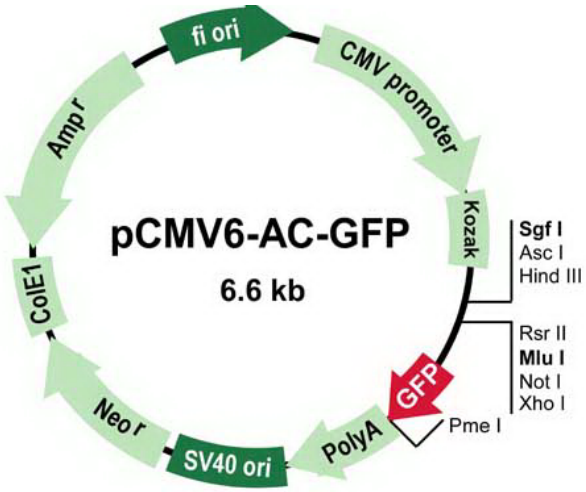

Supplementary Figure 8: Vector map of pCMV6-AC-GFP (Order no: MG222134).
The vector is a cDNA clone containing the sequence of the mouse solute carrier family 6 member 11 (Slc6a11). Encoding GAT-3. The insert is tagged by a GFP. The plasmid was amplified using common protocols (2.8.1-2.8.3).

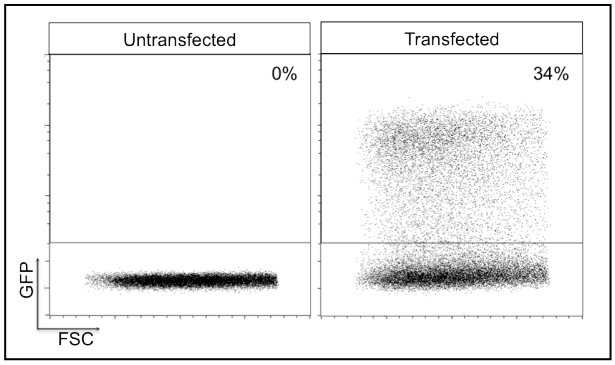

Supplementary Figure 9: Transfection efficiency.
Cells were transfected with the Slc6a11 plasmid (Supplementary Figure 8). Cells were harvested 24 h after transfection, fixed and analyzed on the flow cytometer. The Slc6a11 construct incorporats a GFP sequence. The fluorescence signal of GFP was measured in the FITC channel. Untransfected cells did not show a signal in the FITC channel (a). In this experiment 34% of the cells were tranfected cells (b).

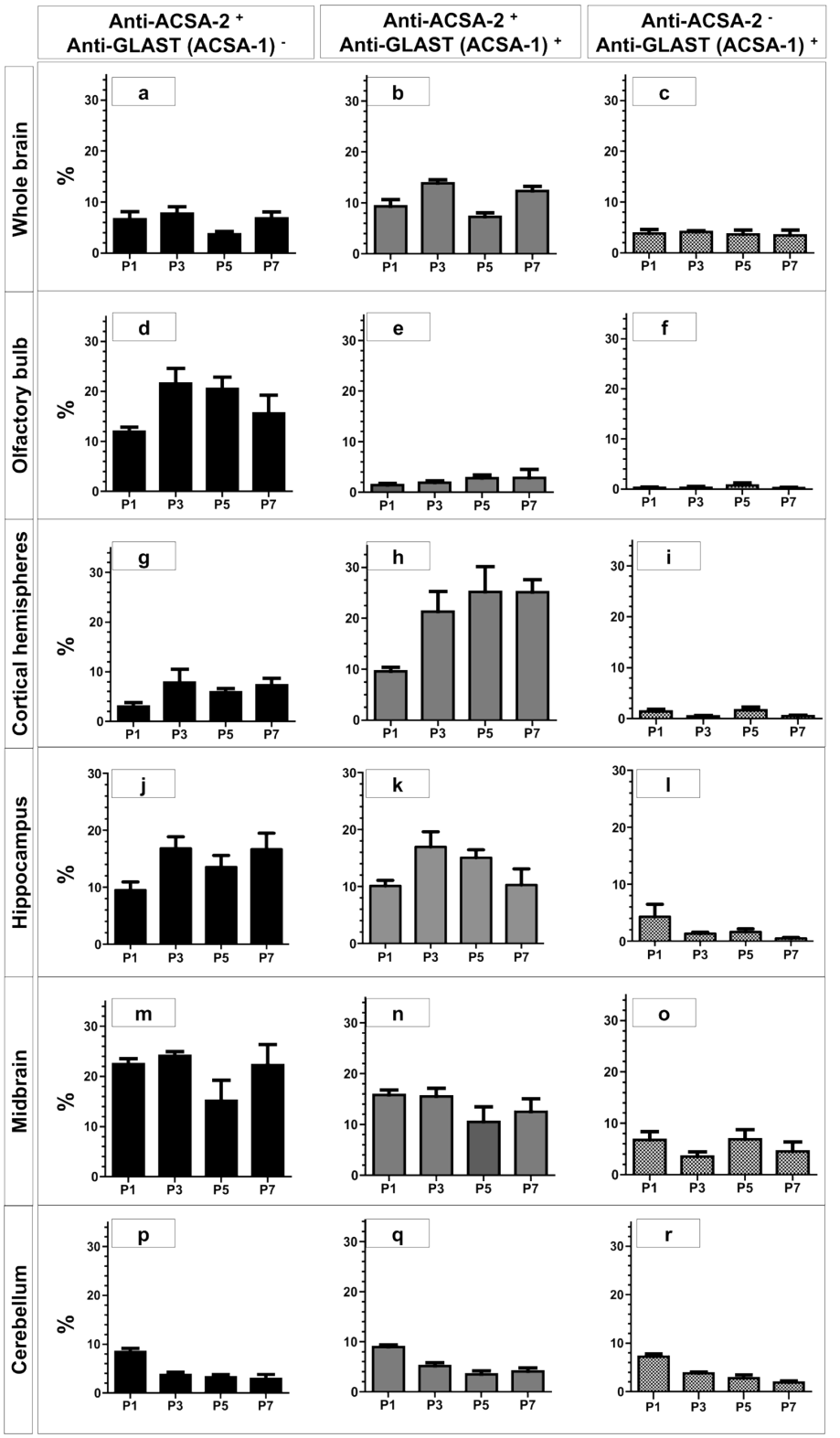

Supplementary Figure 10: Expression of GLAST and ACSA-2 in neonatal mouse brain areas.

Brain tissue samples were dissociated from whole brain tissue, brain areas of the olfactory bulb, cortical hemispheres, hippocampus, midbrain/diencephalon and cerebellum at P1/P3/P5 and P7 (n=3). Cells were stained with the GLAST and the ACSA-2 antibodies and measured on the flow cytometer. Frequencies of ACSA-2^+/GLAST$^-$, ACSA-2^+/GLAST$^+$ cells ACSA-2^+/GLAST$^-$ cells were analyzed and illustrated as bar diagram (± SD).

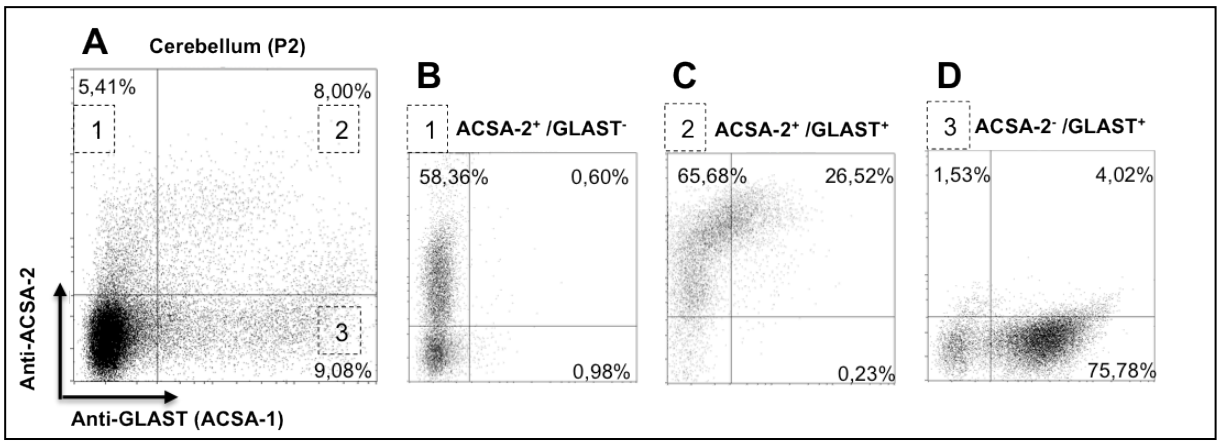

Supplementary Figure 11: Isolation of ACSA-2$^{+/-}$/GLAST$^{+/-}$ cells from neonatal cerebellum.
The neonatal cerebellum (P0 to P2) (A) was dissociated and ACSA-2^{+}/GLAST^{-} (B), ACSA-2^{+}/GLAST$^{+/-}$ (C) and ACSA-2^{-}/GLAST^{+} cells (D) were isolated. Cells were depleted (B, D) prior to isolation or enriched directly (C) using MicroBead conjugates. Purities were determined on the MACSQuant by co-labeling of Anti-ACSA-2 and Anti-GLAST (ACSA-1).

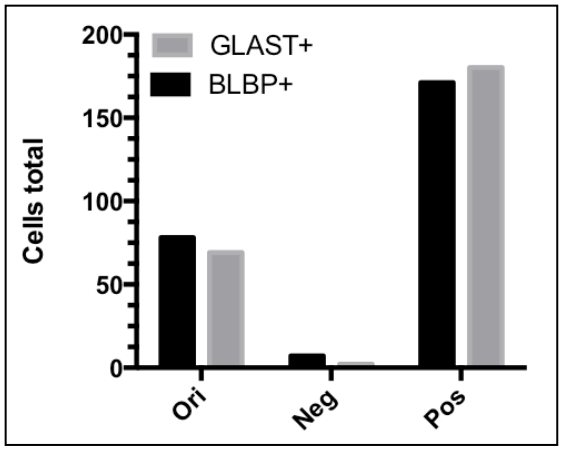

Supplementary Figure 12: Isolation of ACSA-2^{-}/GLAST^{+} cells from P9 cerebellum.
Dissociated cerebelli of P9 mice were used for the enrichment of ACSA-2^{-}/GLAST^{+} cells. Fractions were plated, stained against BLBP and GLAST and the total number of cells per cover slip was counted and depicted as bar diagrams. The isolation protocol was suitable. ACSA-2^{-}/GLAST^{+} were enriched to 3-fold in the positive cell fraction (Pos) compared to the original cell fraction (Ori). The recovery was moderate low frequencies of BLBP/GLAST^{+} cells were identified in the negative cell fraction (Neg).

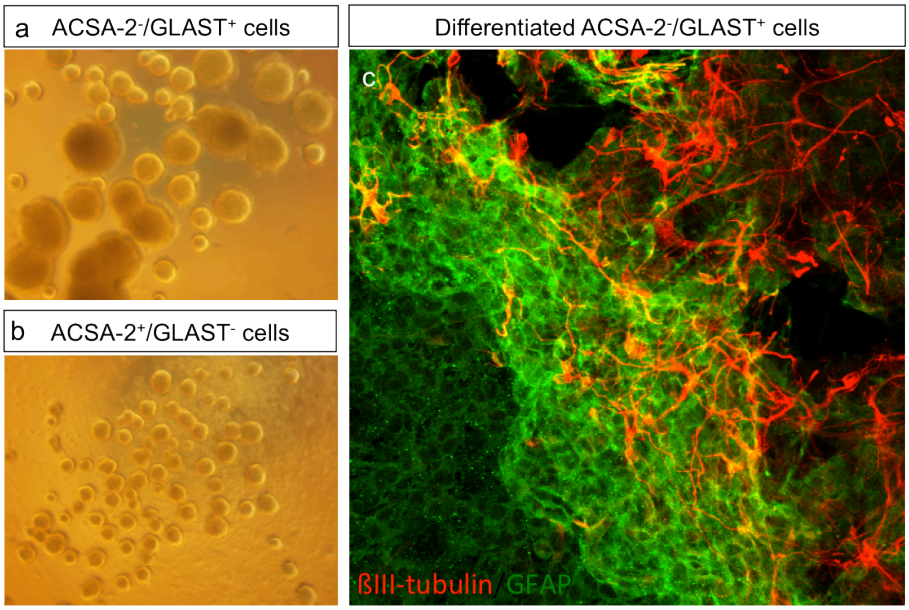

Supplementary Figure 13: Neurosphere assay.

The differentiation potential of ACSA-2^{+}/GLAST$^{+/-}$ and ACSA-2^{-}/GLAST^{+} cells was investigated *in vitro* by neurosphere assay. 50,000 cells were seeded in a 24 well plate in the presence of 20 ng/mL EGF and FGF (Fig. 2.1). Although ACSA-2^{-}/GLAST^{+} were able to form larger spheres (a) than ACSA-2^{+}/GLAST$^{+/-}$ cells (b) as monitored at magnification on the light microscopy. Both fractions were able to differentiate into βIII tubulin positive neurons and GFAP positive astrocytes in the absence of EGF and FGF on poly-L-lysine coated cover slips (c). In addition, very few oligodendrocytes were detected after differentiation (not shown).

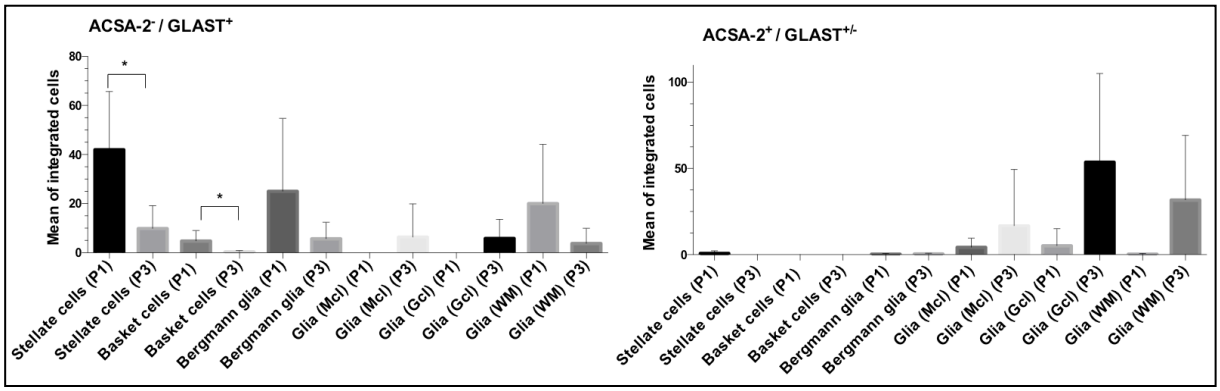

Supplementary Figure 14: Integration capacity of transplants into hosts at P1 and P3.

Sorted ACSA-2^{-}/GLAST^{+} and ACSA-2^{+}/GLAST$^{+/-}$ cells from P0-P3 cerebelli were transplanted into P1 and P3 hosts. Cell types were classified by morphology and immunostaining. For each group of ACSA-2^{-}/GLAST^{+} and ACSA-2^{+}/GLAST$^{+/-}$ hosts the mean of integrated cells in P3 and P1 was determined and is shown as bar diagram (± SD).

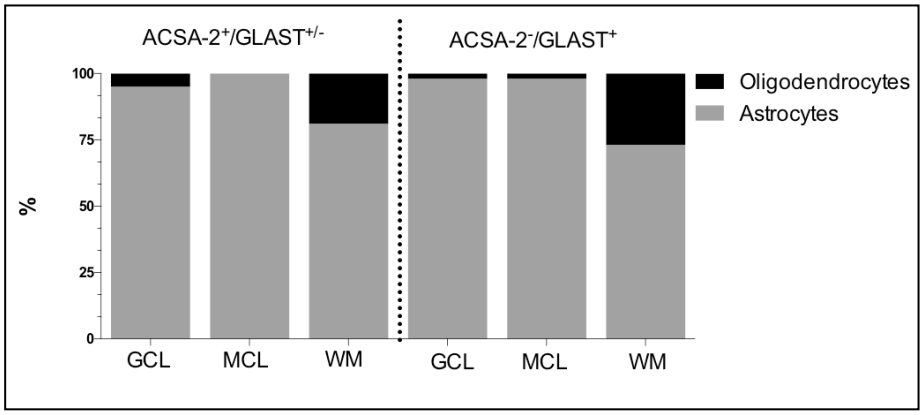

Supplementary Figure 15: Discrimination of astrocytes and oligodendrocytes in the transplants.
Isolated ACSA-2$^-$/GLAST$^+$ and ACSA-2$^+$/GLAST$^{+/-}$ cells were transplanted into same-aged donors. The differentiation into astrocytes and oligodendrocytes was investigated by GFAP and Olig2 staining. For each group 3 animals with a high cell integration (> 50 cells/section) were chosen. Percentages of astrocytes and oligodendrocytes were calculated and illustrated as stacked bar plots.

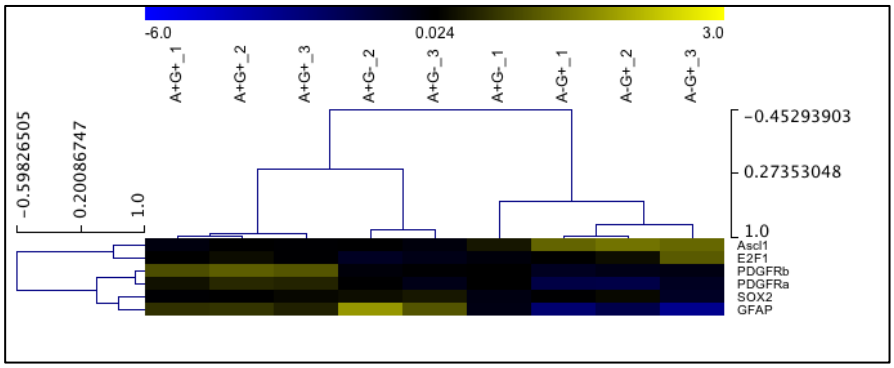

Supplementary Figure 16: Clustering of genes identified by gen expression profiling.
The data set was preprocessed using quantil normalization. Samples were compared by ANOVA. Normalized gene samples presented a p-value higher than 0.05 (Tukey's range test). Pathways were identified using MetaCore. Samples of ACSA-2$^+$/GLAST$^-$ (A+/G-), ACSA-2$^+$/GLAST$^+$ (A+/G+), ACSA-2-/GLAST+ (A-/G+) were visualized using MeV. Correlation coefficients are indicated by color key: Blue (-6) to yellow (3.0).

II Appendix I: Cell surface marker screen – Antibody list

	Marker	Dye	Clone	Lot	Concentration
1	CD1d	PE	1B1		
2	CD2	PE	RM2-5	E00979-1630	10 µg/mL
	CD2	APC	RM2-5	BD Lyoplate	0.5 µg/mL
3	CD3	PE	17A2	B126693	10 µg/mL
4	CD3e	PE	145-2C11		
5	CD4	APC	GK1.5	BD Lyoplate	0.5 µg/mL
	CD4	PE	GK1.5		
6	CD5	APC	53-7.3	BD Lyoplate	0.5 µg/mL
	CD5	APC	53-7.3	E07049-1630	10 µg/mL
	CD5	Biotin	53-7.3	B128879	10 µg/mL
7	CD8a	PE	53-67		
	CD8a	APC	53-67	BD Lyoplate	0.5 µg/mL
8	CD9	PE	MZ3	B137401	10 µg/mL
	CD9	APC	KMC8	BD Lyoplate	0.5 µg/mL

9	CD11a	APC	M17/4	BD Lyoplate	0.5 µg/mL
10	CD11b	APC	M1/70	BD Lyoplate	0.5 µg/mL
	CD11b	PE	M1/70.15.11.5		
11	CD11c	PE	N418		
12	CD13	PE	RE-242	8533	10 µg/mL
	CD13	APC	RE-242	BD Lyoplate	0.5 µg/mL
13	CD14	APC	rmC5-3	BD Lyoplate	0.5 µg/mL
	CD14	PE	rmC5-3	53274	10 µg/mL
14	CD15	PE	VIMV6		
15	CD16/32	PE	93		
	CD16/32	APC	2.G2	BD Lyoplate	0.5 µg/mL
16	CD18	APC	C71/16	BD Lyoplate	0.5 µg/mL
	CD18	Biotin	C71/16	27781	10 µg/mL
17	CD19	APC	1 D3	BD Lyoplate	0.5 µg/mL
	CD19	PE	6 D 5		
18	CD21/35	APC	7G6	BD Lyoplate	0.5 µg/mL
	CD21/35	PE	7 E 9		
19	CD22	FITC	Ox97	3116485	10 µg/mL
	CD22	PE	C2	CO52	10 µg/mL
20	CD22.2	FITC	Cy34.1	82707	10 µg/mL
	CD23	APC	B3B4	BD Lyoplate	0.5 µg/mL
21	CD23	Biotin	B3B4	B101603	10 µg/mL
	CD23	FITC	B3B4	96786	10 µg/mL
	CD23	PE	B3B4	57969	2.5 µg/mL
22	CD24	APC	M1/69	BD Lyoplate	0.5 µg/mL
	CD24	Biotin	M1/69	42453	10 µg/mL
	CD24	FITC	M1/69	E015148	10 µg/mL
	CD24	PE	30-F1	E019757	10 µg/mL
	CD24	PE	30-F1	E019757	10 µg/mL
	CD24	PE	30-F1	E019757	10 µg/mL
23	CD25	APC	PC61	BD Lyoplate	0.5 µg/mL
	CD25	PE	7 D 4		
24	CD26	APC	H194-112	BD Lyoplate	0.5 µg/mL
	CD26	FITC	H194-112	40143	10 µg/mL
25	CD27	PE	LG3A10		10 µg/mL
26	CD28	APC	37.51	BD Lyoplate	0.5 µg/mL
	CD28	PE	37.51		
27	CD29	APC	9EG7	BD Lyoplate	0.5 µg/mL
	CD29	PE	HMß1-1		
28	CD30	Biotin	MEC13.3	45230	10 µg/mL
29	CD31	APC	MEC13.3	BD Lyoplate	0.5 µg/mL
	CD31	PE	MEC13.3	14611	10 µg/mL
	CD31	PE	MEC13.3	14611	10 µg/mL
	CD31	Biotin	MEC13.3		10 µg/mL
30	CD34	PE	RAM34	73417	10 µg/mL
	CD34	APC	RAM34	BD Lyoplate	0.5 µg/mL
31	CD35	APC	8C12	BD Lyoplate	0.5 µg/mL
32	CD36	PE	No72.1		10 µg/mL
33	CD38	APC	90	BD Lyoplate	0.5 µg/mL
	CD38	Pur	HIT2	B101603	10 µg/mL
	CD38	PE	90/CD38	70421	10 µg/mL
	CD38	Biotin	90	B106207	10 µg/mL
34	CD40	PE	FGK45.5		
35	CD41	APC	MWREG30	BD Lyoplate	0.5 µg/mL

	CD41	FITC	MWReg30	56305	10 µg/mL
	CD41	APC	MWReg30	E10380-1631	4 µg/mL
	CD41	FITC	MWReg30	56305	20 µg/mL
36	CD43	APC	S7	BD Lyoplate	0.5 µg/mL
	CD43	PE	L11		
37	CD44	APC	IM7	BD Lyoplate	0.5 µg/mL
	CD44	PE	IM7.8.1		
	CD44	PE	IM7	E01239-366	2 µg/mL
38	CD45	APC	30-F11	BD Lyoplate	0.5 µg/mL
	CD45	PE	30F11		
39	CD45.1	PE	A20		
40	CD45.2	PE	104-2		
41	CD45R	APC	RA3-6B2	BD Lyoplate	0.5 µg/mL
42	CD45R	PE	RA3-6B2		
43	CD45RA	APC	14 8	BD Lyoplate	0.5 µg/mL
44	CD45RB	PE		D809-Q524Y	n.calculated
45	CD45RC	APC	DNL-1.9	BD Lyoplate	0.5 µg/mL
46	CD47	APC	MIAP301	BD Lyoplate	0.5 µg/mL
47	CD48	PE	HM48-1		10 µg/mL
48	CD49b	APC	DXS	BD Lyoplate	0.5 µg/mL
	CD49b	PE	DX5		
49	CD49D	APC	9C10(MRF4.B)	BD Lyoplate	0.5 µg/mL
50	CD49e	APC	5H10-27	BD Lyoplate	0.5 µg/mL
	CD49e	PE	5H10-27 (MFR5)	82702	10 µg/mL
	CD49e	PE	5H10-27 (MFR5)	82702	2 µg/mL
51	CD49f	PE	R1-2		
52	CD51	APC	RMV-7	BD Lyoplate	0.5 µg/mL
	CD51	Biotin	RMV-7	42371	10 µg/mL
53	CD53	APC	OX-79	BD Lyoplate	0.5 µg/mL
54	CD54	Biotin	3 E 2	40251	10 µg/mL
55	CD55	PE	Rico-5	45695	10 µg/mL
56	CD61	Biotin	2C9.G2	66973	10 µg/mL
57	CD61	FITC	2C9.G2	15763	10 µg/mL
58	CD62E	APC	10E9.6	BD Lyoplate	0.5 µg/mL
59	CD62P	Biotin	RB40.43	50110	10 µg/mL
60	CD62L	APC	mEL-14	BD Lyoplate	0.5 µg/mL
	CD62 L	PE	mEL-14		
61	CD69	PE	L78	8905	1 zu 10
62	CD70	APC	FR70	BD Lyoplate	0.5 µg/mL
	CD70	PE	FR70		
63	CD71	APC	C2	BD Lyoplate	0.5 µg/mL
	CD71	Biotin	C2		
64	CD72	FITC	K10.6	9892	10 µg/mL
65	CD72 b/c	APC	JY/93	BD Lyoplate	0.5 µg/mL
66	CD73	PE	TY/23	69498	10 µg/mL
	CD73	APC	TY/23	BD Lyoplate	0.5 µg/mL
	CD73	PE	TY/23	14174	
67	CD74	Pur	LN2	36068	10 µg/mL
68	CD79b	Pur	HM79B	63464	
69	CD80	APC	1G10/b7	BD Lyoplate	0.5 µg/mL
	CD80	FITC	16-10A1	9530	10 µg/mL
	CD80	PE	16-10A1	34045	10 µg/mL
70	CD81	PE	Eaat2	21109	10 µg/mL

	CD81	Biotin	Eaat2	30599	10 µg/mL
71	CD83	PE	Michel-19	B122661	10 µg/mL
	CD83	APC	Michel-19	BD Lyoplate	0.5 µg/mL
72	CD86	APC	PO3	BD Lyoplate	0.5 µg/mL
	CD86	PE	24 F		10 µg/mL
	CD86	PE	PO3.3		
	CD86	FITC	GL1	7110	10 µg/mL
73	CD90.1	PE	His51		
74	CD90.2	APC	30-H12	BD Lyoplate	0.5 µg/mL
75	CD90.2	PE	30-H12		
76	CD93	FITC	AA4.1	E00719-196	10 µg/mL
	CD93	APC	AA4.1	E029489	
	CD93	Biotin	AA4.1	E008623	
77	CD94	APC	18D3	BD Lyoplate	0.5 µg/mL
	CD94	Biotin	18d3	12702	
78	CD95	PE	15A7	E01394-204	
79	CD98	APC	H202-141	BD Lyoplate	0.5 µg/mL
80	CD100	Biotin	BMA12	E02654-1-1630	
81	CD102	APC	3C4(MIC2/4)	BD Lyoplate	0.5 µg/mL
	CD102	Biotin	3C4	61794	10 µg/mL
82	CD103	APC	M290	BD Lyoplate	0.5 µg/mL
	CD103	FITC	2 E 7		10 µg/mL
83	CD104	APC	346-11A	BD Lyoplate	0.5 µg/mL
84	CD105	PE	MJ7/18		
85	CD106	FITC	429	E000558	10 µg/mL
	CD106	APC	429	BD Lyoplate	0.5 µg/mL
	CD106	Alexa 647	429	6825	
	CD106	PE	429	142218	
86	CD107b	APC	ABL-93	24095	
87	CD115	PE	AFS98		10 µg/mL
88	CD117	APC	2B8	BD Lyoplate	0.5 µg/mL
	CD117	PE	3C1		
89	CD118	PE		980779	
90	CD119	Biotin	2 E 2	66391	10 µg/mL
91	CD121a	APC	35F5	BD Lyoplate	0.5 µg/mL
92	CD121b	APC	4.00E+02	BD Lyoplate	0.5 µg/mL
93	CD122	PE	5H4		10 µg/mL
	CD122	APC	TM-BETA1	BD Lyoplate	0.5 µg/mL
94	CD123	APC	5B11	BD Lyoplate	0.5 µg/mL
	CD123	Biotin	5B11	E000228	10 µg/mL
95	CD124	APC	mIL4R-M1	BD Lyoplate	0.5 µg/mL
	CD124	Biotin	mIL4R-M1	30599	10 µg/mL
96	CD125	APC	T21	BD Lyoplate	0.5 µg/mL
97	CD126	PE	D7715A7	70421	10 µg/mL
98	CD127	APC	B12-1	BD Lyoplate	0.5 µg/mL
	CD127	PE	3C1		
99	CD131	APC	JORO50	BD Lyoplate	0.5 µg/mL
	CD131	PE	JORO50	63983	10 µg/mL
100	CD132	APC	TUGm2	BD Lyoplate	0.5 µg/mL
	CD132	Biotin	TUGm2	53852	10 µg/mL
101	CD134	APC	Ox-86	BD Lyoplate	0.5 µg/mL
	CD134	PE	Ox-86	B129281	10 µg/mL
102	CD135	APC	A2F10.1	BD Lyoplate	0.5 µg/mL
	CD135	PE	A2F10.1	60614	10 µg/mL

103	CD137	APC	1AH2	BD Lyoplate	0.5 µg/mL
	CD137	PE	17B5	12-1371-83	10 µg/mL
104	CD138	APC	281-2	BD Lyoplate	0.5 µg/mL
	CD138	FITC	281-2	10611	10 µg/mL
105	CD140a	APC	APA5	BD Lyoplate	0.5 µg/mL
	CD140a	PE	APA5		
	CD140a	PE	APA5		
106	CD140b	PE	APB5		
107	CD144	APC	11D4.1	BD Lyoplate	0.5 µg/mL
	CD144	PUR		59054	
108	CD146	PE	ME-9F1		
109	CD147	APC	RL73	BD Lyoplate	0.5 µg/mL
110	CD152	PE	UC10-4F10-11	68895	10 µg/mL
	CD152	PE	UC10-4F10-11	68895	
111	CD153	APC	RM153	BD Lyoplate	0.5 µg/mL
	CD153	PE	RM153	E01274-1631	
112	CD154	PE	MR1		
113	CD162	APC	2PH1	BD Lyoplate	0.5 µg/mL
	CD162	PE	2PH1	63676	10 µg/mL
114	CD166	PE	eBioALC48	E015555-1373	
115	CD172A	APC	P84	BD Lyoplate	0.5 µg/mL
116	CD172A	APC	P84	E14163-102	
117	CD178	Biotin	MFL3	45020	10 µg/mL
118	CD178.1	Biotin	KAY-10	63818	10 µg/mL
119	CD179a	APC	R3/VPREB	BD Lyoplate	0.5 µg/mL
120	CD179b	APC	LM34	BD Lyoplate	0.5 µg/mL
	CD179b	Biotin	LM34	46674	10 µg/mL
121	CD180	APC	RP/14	BD Lyoplate	0.5 µg/mL
	CD180	Biotin	RP/14	44142	10 µg/mL
122	CD184	PE	2B11/CXCR4	26361	10 µg/mL
	CD184	Biotin	2B11/CXCR4	37846	10 µg/mL
	CD184	APC	2B11/CXCR4	BD Lyoplate	0.5 µg/mL
123	CD185	APC	2G8	BD Lyoplate	0.5 µg/mL
124	CD195	APC	C43-3448	BD Lyoplate	0.5 µg/mL
125	CD197	APC	4B12	BD Lyoplate	0.5 µg/mL
126	CD200	APC	OX-90	BD Lyoplate	0.5 µg/mL
	CD200	Biotin	OX-90	B116104	
127	CD205	PE	NLDC145		
128	CD209a	APC	Ox-90	BD Lyoplate	0.5 µg/mL
129	CD210	APC	5H10	BD Lyoplate	0.5 µg/mL
	CD210	PE	1B1.3a	43380	10 µg/mL
130	CD223	PE	C9B7W	30101	10 µg/mL
	CD223	APC	C9B7W	BD Lyoplate	0.5 µg/mL
	CD223	PE	C9B7W		
131	CD224.2	Biotin	2B4	44892	10 µg/mL
132	CD229.1	Biotin	30C7	7002	10 µg/mL
134	CD244.1	APC	C9.1	BD Lyoplate	0.5 µg/mL
135	CD252	APC	RM134L	BD Lyoplate	0.5 µg/mL
136	CD253	APC	N2B2	BD Lyoplate	0.5 µg/mL
	CD253	PE	N2B5		
137	CD254	APC	IK22-5	BD Lyoplate	0.5 µg/mL
138	CD262	PE	MD5-1	B127799	
139	CD267	APC	8F10	BD Lyoplate	0.5 µg/mL
140	CD268	PE	7H22-E16		

141	CD271	PE			
142	CD273	APC	TY25	BD Lyoplate	0.5 µg/mL
	CD273	PE	TY25	69347	10 µg/mL
143	CD274	APC	MIH5	BD Lyoplate	0.5 µg/mL
144	CD278	APC	7E.17G9	BD Lyoplate	0.5 µg/mL
	CD278	PE	E7.17G9		
145	CD279	PE	J43	64077	10 µg/mL
	CD279	PE	HA2-7B1		
146	CD284	APC	MTS5510	BD Lyoplate	0.5 µg/mL
	CD284	PE	MTS510		
	CD284	PE	MTS510	66992	
	CD284	PE	MTS510	66992	
147	CD309	APC	AVas12	BD Lyoplate	0.5 µg/mL
	CD309	PE	AVas12		
148	CD314	APC	CX5	BD Lyoplate	0.5 µg/mL
	CD314	PE	CX5	1748	
149	CD326	PE	caa7-9G8		
	CD326	APC	G8.8	BD Lyoplate	0.5 µg/mL
150	CD335	APC	29A1.4	BD Lyoplate	0.5 µg/mL
151	A2B5	PE	105H29		
152	BP-1	FITC	6C3	E023756	10 µg/mL
	BP-1	PE	FG35.4	E02013-260	
153	BCL-2				
154	CCR2	PE	454301		
155	Clec12A	PE	inhouse		
156	Crry/p65	APC	1F2	BD Lyoplate	0.5 µg/mL
157	DCs	APC	33D1	BD Lyoplate	0.5 µg/mL
158	DCAR1	PE	SKa5-3D5		
159	DCIR2	PE	33D1		
160	DDR-2	PUR	N-20	A0810	
161	Dectin-2	FITC	KVa7-6E7		
162	Delta like 1	PE			1 zu 50
163	Do11.10	PE	KJ1-26		
164	Early B cell	APC	493	BD Lyoplate	0.5 µg/mL
165	EOMES	Pur	21Mags8	E034391	
166	E-Cadherin	Pur			
167	EGF-receptor	Pur			
168	Erythroid cells	APC	Terr-119	BD Lyoplate	0.5 µg/mL
169	FceRI alpha	PE	MAR-1	E01907-1460	10 µg/mL
	FceRI alpha	PE	MAR-1		
170	Feeder	PE	mEF-SK4		
171	FET 4	Biotin			
172	FR4	PE	TH6		
173	F4/80	APC	6F12	BD Lyoplate	0.5 µg/mL
	F4/80	PE	BM8		10 µg/mL
174	Fgfr3 CD333				
175	FLK-1	PE			
176	gamma d. TcR	PE	UC7 13D5	97702	
177	Galectin-9	PE	10A82	B131154	10 µg/mL
178	GITR	APC	DTA-1	BD Lyoplate	0.5 µg/mL
	GITR	PE	RB6-8C5		
179	GR-1				

180	GL-7	Biotin	GL7	E027851	10 µg/mL
181	H2kk	PE	H100-27.R55		
182	I-A/I-E	APC	2G9	BD Lyoplate	0.5 µg/mL
183	Integrin beta 7	PE	FIB27	B126977	
184	Int 7ß chain	APC	FIB27	BD Lyoplate	0.5 µg/mL
185	IL12R	Biotin			
186	IL21R	APC	4A9	BD Lyoplate	0.5 µg/mL
187	ICOS				
188	Jagged 1 CD339	PE	HMJ1-29	E11619-1630	10 µg/mL
189	Jagged 2	PE	HMJ2-1	B136766	10 µg/mL
190	Jagged 2	PE	HMJ2-1	B134201	
191	KLRG1	PE	2F1		
	KLRG1	APC	2F1	BD Lyoplate	0.5 µg/mL
192	LPAM-1	APC	DATK32	BD Lyoplate	0.5 µg/mL
193	Ly-6A/E	APC	E13-161.7	BD Lyoplate	0.5 µg/mL
194	Ly-6C	PE	1G7.G10		
195	Ly-6D	APC	49-H4	BD Lyoplate	0.5 µg/mL
196	Ly-6G	APC	1A8	BD Lyoplate	0.5 µg/mL
	Ly-6G	PE	1AB		
197	Ly-6G/ly-6C	APC	RB6-BC5	BD Lyoplate	0.5 µg/mL
198	Ly 49D	PE	4 E 5	B136428	10 µg/mL
199	MHC class II	PE	M5/114.15.2		
200	Mac-3	APC	M3/84	BD Lyoplate	0.5 µg/mL
201	MAdCAM-1	APC	MECA-89	BD Lyoplate	0.5 µg/mL
202	MD-1	APC	20D5	BD Lyoplate	0.5 µg/mL
203	mPDCA-1	PE	JF05-1C2.4.1		
204	NK1.1	PE	PK136		
205	NKG2A/C/E	APC	20D5	BD Lyoplate	0.5 µg/mL
206	NTK/NK Cell Antigen	APC	U5A2-13	BD Lyoplate	0.5 µg/mL
207	NKp46	PE	29A1.4		
208	Notch1	PE	22 E 5		
209	Notch1	PE			0.5
210	Notch2	PE			0.5
	Notch2	PE	HMN2-35	B124873	10 µg/mL
211	Notch3	PE	HMN3-133		
212	Notch4	PE	HMN-14	B118926	
213	OX-90	PE			10 µg/mL
214	O4	PE			
215	Panendothelial cell AG	APC	MECA_32	BD Lyoplate	0.5 µg/mL
216	PDCA-1	PE	JF05-1C2.4.1		
217	PIRA/B	APC	6C1	BD Lyoplate	0.5 µg/mL
218	PSA-NCAM	PE	2-2B		
219	Pre-BCR	APC			
220	Prominin	PE	MB9-3G8		
221	Sca-1	PE	D/7		
222	SiglecH	PE	551.3D3		
223	SiglecF	APC	E50-2440	BD Lyoplate	0.5 µg/mL
	SiglecF	PE	E50-2440		2,5 µg/mL
224	Syndecan	APC	KY/8.2	BD Lyoplate	0.5 µg/mL
225	SSEA 3	Pur			
225	T/B cell activation	APC	U5A2-13	BD Lyoplate	0.5 µg/mL
227	TcR	PE			10 µg/mL
	TcR	FITC			10 µg/mL
228	Trail	Biotin	N2B2		

229	Tim-3	PE	RMT3-23		10 µg/mL
	Tim-3				
230	Vegfr3	Biotin	BAF743	DDN0207101	
231	Vgamma3TCR	APC	536	BD Lyoplate	0.5 µg/mL
232	4-1BB	APC	TKS_1	BD Lyoplate	0.5 µg/mL

III Appendix II: Gene list gen expression profiling

		A-G+ vs A+G-		
GeneName	**ProbeName**	**Tukey.p-value**	**Fold_Change**	**log_2 ratio**
Nphs1	A_55_P1996479	2.23E-04	32.078	5.004
Mybpc1	A_55_P2165299	2.17E-04	21.736	4.442
Kirrel2	A_51_P512306	9.23E-04	16.965	4.085
Ptf1a	A_51_P226711	8.48E-04	16.421	4.038
A_30_P01019652	A_30_P01019652	3.32E-04	15.263	3.932
ENSMUST00000112841	A_66_P110542	6.14E-04	15.216	3.928
Gdf10	A_51_P185247	2.39E-04	13.987	3.806
Myh8	A_51_P143296	1.35E-03	13.905	3.798
Slco4a1	A_55_P1989653	1.96E-04	13.704	3.777
Ccbe1	A_52_P39083	6.05E-05	13.408	3.745
Greb1l	A_52_P60353	1.05E-05	13.118	3.714
LOC552873	A_55_P2237142	9.08E-04	12.924	3.692
Npy	A_51_P454873	2.69E-04	12.454	3.639
Ass1	A_55_P2143070	1.92E-04	11.967	3.581
Msx2	A_55_P2043486	3.02E-04	11.774	3.558
0610040J01Rik	A_51_P483617	1.54E-04	9.935	3.313
Scube2	A_55_P2060429	8.71E-05	9.533	3.253
Prdm13	A_55_P2044897	1.38E-03	9.370	3.228
A_30_P01030328	A_30_P01030328	3.70E-04	9.151	3.194
Hmga2	A_52_P300730	2.44E-04	9.013	3.172
Wipf3	A_51_P316951	1.99E-04	8.972	3.166
Col25a1	A_55_P2160750	9.46E-05	8.969	3.165
Tbc1d4	A_52_P381430	5.23E-04	8.960	3.164
Gm5089	A_55_P2030496	1.81E-04	8.907	3.155
Ass1	A_55_P2004781	5.80E-04	8.861	3.148
Wif1	A_51_P484526	7.20E-04	8.700	3.121
Col2a1	A_55_P2004179	2.05E-06	8.616	3.107
Hhip	A_55_P1969276	5.77E-05	8.465	3.082
Cdh4	A_55_P2150831	6.59E-04	8.095	3.017
Gas2l3	A_55_P2120189	2.22E-06	7.959	2.993
Tbc1d4	A_55_P2024953	7.06E-05	7.890	2.980
LOC100048332	A_55_P1970715	1.35E-03	7.687	2.943
Cdh4	A_52_P402897	4.19E-04	7.613	2.929
LOC674761	A_55_P2093231	1.36E-04	7.423	2.892
LOC552901	A_55_P2243828	3.20E-04	7.220	2.852

Cxcr4	A_52_P585124	1.86E-04	7.140	2.836
Atp1b1	A_51_P151484	4.84E-04	7.133	2.835
Myh7	A_55_P2093232	4.96E-05	7.089	2.826
Scube2	A_55_P2232988	5.32E-04	7.067	2.821
Lrba	A_55_P2100305	2.57E-05	7.030	2.814
Irx4	A_51_P412508	7.22E-04	6.866	2.780
Mbp	A_55_P1992160	3.12E-05	6.523	2.706
Mybpc1	A_55_P2008443	2.25E-04	6.366	2.671
Gas2l3	A_55_P2100475	7.16E-06	6.086	2.606
Fam118a	A_55_P2147886	6.72E-04	5.996	2.584
Lmcd1	A_51_P405912	3.78E-04	5.881	2.556
Dach1	A_65_P07627	2.62E-04	5.879	2.556
Dach1	A_55_P1959763	4.56E-04	5.848	2.548
Lmcd1	A_55_P1985273	7.24E-07	5.846	2.548
Auts2	A_55_P2015807	1.86E-04	5.786	2.533
Gas2l3	A_55_P2064676	2.36E-06	5.770	2.529
A_30_P01025154	A_30_P01025154	2.21E-04	5.712	2.514
Stk10	A_51_P192130	1.39E-04	5.690	2.509
A_30_P01018665	A_30_P01018665	3.87E-04	5.686	2.508
Gucy1a3	A_55_P1992049	2.22E-04	5.665	2.502
Pla2g5	A_55_P1962693	9.12E-04	5.496	2.459
LOC100048353	A_55_P2098603	4.91E-05	5.470	2.452
Gria4	A_52_P349182	2.92E-04	5.251	2.393
A_30_P01029151	A_30_P01029151	1.05E-03	5.238	2.389
Gli1	A_55_P2183587	1.14E-04	5.227	2.386
Vcan	A_55_P1960208	1.10E-03	5.184	2.374
Gpr126	A_66_P114451	6.47E-04	5.160	2.368
Emid1	A_55_P1954276	4.83E-05	5.095	2.349
Rad51	A_55_P2008126	7.32E-05	5.068	2.342
A_30_P01031644	A_30_P01031644	2.49E-04	5.061	2.340
A_30_P01027548	A_30_P01027548	1.37E-04	4.928	2.301
Magi2	A_66_P106750	5.31E-04	4.790	2.260
Vwa5b1	A_55_P2081990	2.67E-04	4.719	2.239
Kit	A_66_P128434	1.08E-03	4.691	2.230
Fam60a	A_55_P2180551	1.23E-03	4.690	2.230
ENSMUST00000054333	A_55_P2057051	5.15E-04	4.683	2.228
D6Ertd131e	A_55_P2360501	3.47E-04	4.606	2.204
1700084M14Rik	A_51_P428297	1.48E-03	4.571	2.193
A_30_P01024922	A_30_P01024922	3.60E-04	4.546	2.185
Nav2	A_55_P2071961	1.08E-04	4.491	2.167
Pion	A_66_P129710	6.06E-05	4.482	2.164
A_30_P01024586	A_30_P01024586	7.04E-04	4.465	2.159
XM_888730	A_55_P2022870	4.87E-04	4.415	2.143
Fzd1	A_52_P597634	3.30E-05	4.409	2.141
Gm9631	A_55_P2013029	1.86E-03	4.385	2.133
AU024581	A_55_P2417212	3.36E-04	4.383	2.132

A_30_P01017899	A_30_P01017899	9.25E-04	4.281	2.098
A_30_P01029325	A_30_P01029325	1.33E-03	4.269	2.094
Cep55	A_55_P2187918	7.08E-05	4.237	2.083
Kif15	A_52_P227391	1.83E-03	4.235	2.083
A_30_P01028127	A_30_P01028127	2.55E-03	4.215	2.076
Hells	A_51_P351970	6.45E-04	4.200	2.071
Ptch2	A_55_P1999408	4.56E-04	4.179	2.063
Baz1a	A_66_P139196	7.39E-04	4.176	2.062
A_30_P01031709	A_30_P01031709	1.16E-03	4.158	2.056
Arid3b	A_51_P161554	6.03E-06	4.132	2.047
A_30_P01029269	A_30_P01029269	9.03E-05	4.130	2.046
Ttll2	A_55_P1962756	1.10E-03	4.078	2.028
2900072G11Rik	A_55_P2422243	1.56E-04	4.057	2.021
Nes	A_55_P1953728	9.83E-06	4.054	2.020
Cdc6	A_52_P219473	1.43E-03	4.032	2.012
A_30_P01033354	A_30_P01033354	9.99E-06	4.025	2.009
Pvalb	A_55_P2114437	5.52E-04	4.011	2.004
A_30_P01023742	A_30_P01023742	8.52E-05	4.011	2.004
Med12l	A_55_P2134616	1.72E-03	4.001	2.001

		A-G+ vs A+G-		
GeneName	**ProbeName**	**Tukey.p-value**	**Fold_Change**	**log_2 ratio**
Mag	A_55_P2062757	2.89E-02	-4.004	-2.002
Slc25a18	A_55_P2103225	1.39E-02	-4.004	-2.002
Ccdc19	A_55_P2015485	8.02E-03	-4.007	-2.003
Higd1b	A_55_P2111523	1.58E-01	-4.017	-2.006
Bcl6	A_52_P161495	3.02E-04	-4.018	-2.007
Slc14a1	A_51_P312336	6.34E-03	-4.018	-2.007
3110082D06Rik	A_51_P161257	5.53E-03	-4.024	-2.009
Aqp11	A_55_P1995507	1.45E-03	-4.024	-2.009
Tmem117	A_51_P207940	5.45E-04	-4.028	-2.010
Scd1	A_52_P682382	1.70E-02	-4.029	-2.011
Nrsn2	A_55_P2009427	4.55E-02	-4.038	-2.014
Rora	A_55_P2078123	2.73E-03	-4.047	-2.017
A_30_P01022407	A_30_P01022407	1.93E-03	-4.049	-2.018
Frat1	A_52_P584188	7.63E-03	-4.061	-2.022
Pld2	A_55_P2049567	1.43E-02	-4.069	-2.025
Slc22a8	A_55_P1995407	4.52E-03	-4.069	-2.025
Padi2	A_55_P2074656	4.38E-02	-4.073	-2.026
Hebp1	A_51_P376347	1.70E-05	-4.074	-2.027
Il34	A_51_P268234	1.50E-02	-4.076	-2.027
S100a6	A_51_P281089	1.39E-03	-4.076	-2.027
Tle2	A_55_P2185543	6.56E-04	-4.084	-2.030
Foxc1	A_55_P1967761	9.00E-03	-4.097	-2.035

4933407E14Rik	A_55_P2253284	6.13E-04	-4.098	-2.035
Slc25a34	A_55_P2073248	2.59E-03	-4.104	-2.037
Trnp1	A_55_P2123673	1.33E-02	-4.104	-2.037
Cfh	A_55_P2017418	2.04E-02	-4.120	-2.043
Ddit4	A_51_P245796	5.15E-03	-4.128	-2.046
Qprt	A_51_P394014	1.76E-02	-4.128	-2.046
Acot5	A_55_P2038362	3.14E-04	-4.148	-2.053
Slc6a9	A_55_P1973838	4.91E-03	-4.148	-2.053
Igfbp2	A_66_P135391	2.22E-03	-4.161	-2.057
Srpx	A_55_P2207255	5.08E-02	-4.170	-2.060
Fhl2	A_51_P140237	7.14E-03	-4.174	-2.062
1110017D15Rik	A_55_P2133365	1.91E-02	-4.176	-2.062
A_30_P01026000	A_30_P01026000	4.99E-05	-4.181	-2.064
Metrnl	A_52_P355084	1.22E-04	-4.186	-2.066
Neat1	A_51_P234692	2.26E-02	-4.187	-2.066
Chst10	A_51_P445562	1.43E-04	-4.196	-2.069
Retsat	A_51_P319070	3.51E-03	-4.197	-2.070
Dnahc2	A_55_P2106180	7.45E-04	-4.197	-2.070
A_30_P01021613	A_30_P01021613	4.45E-05	-4.202	-2.071
Nr2f2	A_55_P2128283	1.18E-04	-4.209	-2.074
Lepr	A_55_P2177911	4.01E-02	-4.219	-2.077
Arhgdig	A_55_P2096762	2.14E-02	-4.221	-2.078
A_30_P01029720	A_30_P01029720	2.36E-02	-4.230	-2.081
Clu	A_55_P2017929	5.78E-03	-4.262	-2.092
Lrrc46	A_52_P375546	4.43E-03	-4.262	-2.092
Tmco4	A_55_P2180944	2.20E-03	-4.269	-2.094
S100a16	A_66_P114627	2.15E-03	-4.274	-2.096
Ppp1r3d	A_51_P169516	9.84E-03	-4.277	-2.097
Plcg2	A_51_P279163	2.04E-03	-4.293	-2.102
Pear1	A_52_P278295	2.15E-02	-4.298	-2.104
Emid2	A_55_P1954271	6.77E-03	-4.317	-2.110
Csdc2	A_51_P183561	8.68E-03	-4.318	-2.111
Slc38a3	A_51_P139030	7.94E-05	-4.324	-2.113
Gjb2	A_52_P382886	4.24E-02	-4.329	-2.114
Ednra	A_52_P156190	1.04E-04	-4.330	-2.115
Cdhr4	A_55_P2141782	3.41E-03	-4.341	-2.118
Col16a1	A_55_P2124751	2.44E-04	-4.342	-2.119
A2m	A_55_P2459897	4.92E-03	-4.351	-2.122
Prkcz	A_55_P1987761	7.37E-03	-4.370	-2.128
Cyp4v3	A_52_P302345	1.76E-03	-4.370	-2.128
Epas1	A_51_P250058	1.38E-02	-4.374	-2.129
Sod3	A_55_P2077558	1.37E-03	-4.376	-2.130
ENSMUST00000051089	A_51_P361620	5.89E-03	-4.377	-2.130
Aldh1a2	A_52_P58145	1.15E-02	-4.377	-2.130
Adcy2	A_51_P337523	1.28E-03	-4.400	-2.138
Zdhhc2	A_51_P117226	8.20E-03	-4.411	-2.141

Slc24a3	A_55_P2099650	2.42E-04	-4.418	-2.144
A_30_P01026656	A_30_P01026656	3.87E-03	-4.452	-2.155
Gatm	A_51_P461319	4.09E-04	-4.460	-2.157
Amy1	A_55_P1983418	1.02E-03	-4.477	-2.163
C1s	A_55_P2042612	9.40E-03	-4.480	-2.164
Cml5	A_52_P2710	3.93E-02	-4.489	-2.167
Rgs9	A_55_P2032232	1.22E-02	-4.502	-2.171
A_30_P01023417	A_30_P01023417	2.81E-03	-4.517	-2.176
Cebpb	A_55_P2165869	3.04E-05	-4.519	-2.176
Zfp503	A_55_P2001998	2.79E-04	-4.522	-2.177
ENSMUST00000000102	A_55_P2185362	2.16E-02	-4.552	-2.187
A_30_P01023251	A_30_P01023251	1.63E-02	-4.558	-2.189
1110006E14Rik	A_55_P2419296	3.19E-02	-4.565	-2.191
Acp5	A_55_P2037608	3.11E-02	-4.579	-2.195
Lrrc51	A_55_P2099627	3.87E-02	-4.580	-2.196
Parm1	A_51_P114693	8.07E-04	-4.582	-2.196
Ank2	A_55_P2131288	8.92E-06	-4.585	-2.197
Spon2	A_52_P381484	2.39E-02	-4.592	-2.199
Rapgef5	A_55_P1968568	4.04E-02	-4.598	-2.201
A_30_P01027987	A_30_P01027987	1.34E-03	-4.611	-2.205
Rnf128	A_55_P2007088	4.84E-03	-4.636	-2.213
Pdk4	A_51_P350453	1.49E-03	-4.648	-2.217
Nr1d1	A_51_P223776	7.04E-04	-4.672	-2.224
Sdsl	A_55_P2055557	1.07E-04	-4.695	-2.231
Wdr16	A_51_P288558	5.92E-03	-4.704	-2.234
Sfrp5	A_55_P2020203	1.10E-02	-4.714	-2.237
Gm5151	A_55_P2087061	2.74E-02	-4.719	-2.239
Osr1	A_55_P1962901	1.10E-02	-4.731	-2.242
Klhdc9	A_51_P479352	4.86E-04	-4.737	-2.244
Gm2a	A_52_P353417	1.18E-03	-4.767	-2.253
Hbegf	A_51_P181565	1.38E-04	-4.798	-2.263
Isg15	A_55_P2103698	4.04E-03	-4.803	-2.264
Kcnd3	A_66_P122219	1.35E-03	-4.810	-2.266
Lnx1	A_55_P2076462	2.82E-03	-4.832	-2.273
Osmr	A_51_P319460	5.08E-03	-4.867	-2.283
Ccdc67	A_55_P2002642	5.35E-02	-4.869	-2.284
Olfm1	A_55_P2160296	1.63E-02	-4.877	-2.286
Foxj1	A_51_P456870	2.71E-03	-4.885	-2.289
Sema4a	A_55_P2014229	1.40E-02	-4.889	-2.290
H2-Bl	A_55_P1981494	2.28E-05	-4.894	-2.291
Susd4	A_55_P1954393	2.79E-06	-4.897	-2.292
Rgs9	A_55_P1969032	4.92E-03	-4.908	-2.295
Vpreb3	A_55_P2136906	1.71E-02	-4.916	-2.298
A2ld1	A_51_P262230	6.71E-04	-4.923	-2.300
Rarres1	A_51_P401184	4.46E-03	-4.923	-2.300
LOC100046471	A_55_P2028382	6.20E-06	-4.938	-2.304

Lgals3	A_55_P2171116	1.05E-03	-4.940	-2.305
4933430H15Rik	A_51_P485472	5.41E-04	-4.952	-2.308
Gm10134	A_55_P2277171	1.17E-02	-4.988	-2.319
Lor	A_51_P495269	2.21E-03	-4.988	-2.319
Sphk1	A_55_P2186005	1.67E-03	-5.000	-2.322
Cxcl1	A_51_P363187	7.24E-03	-5.009	-2.325
VCAM-1	A_51_P210956	6.09E-04	-5.012	-2.326
Adm	A_51_P265571	8.47E-04	-5.016	-2.327
Meg3	A_51_P455997	9.52E-04	-5.019	-2.328
Dync1i1	A_55_P2090429	1.40E-02	-5.039	-2.333
Tmem229a	A_66_P139666	3.97E-03	-5.040	-2.334
Vstm2a	A_55_P1973377	1.68E-02	-5.040	-2.334
Aif1	A_51_P400543	2.97E-02	-5.051	-2.337
Itgb3	A_52_P553890	7.69E-04	-5.060	-2.339
Cd82	A_55_P2137927	3.80E-02	-5.081	-2.345
Apod	A_55_P2093286	4.39E-03	-5.118	-2.356
Cgref1	A_51_P372550	2.02E-03	-5.125	-2.358
Crlf1	A_55_P2052240	7.15E-03	-5.127	-2.358
Klf2	A_51_P144264	1.10E-04	-5.159	-2.367
Lst1	A_55_P2052834	1.51E-02	-5.160	-2.368
Erbb4	A_55_P2119892	7.81E-03	-5.173	-2.371
Lhfp	A_51_P505868	1.03E-05	-5.182	-2.374
C1qtnf2	A_52_P601021	1.74E-02	-5.187	-2.375
Rsph1	A_51_P373901	7.28E-03	-5.191	-2.376
Gnal	A_55_P2119633	2.63E-02	-5.198	-2.378
Socs3	A_51_P474459	1.46E-04	-5.214	-2.383
Mirg	A_66_P121059	6.34E-04	-5.220	-2.384
H19	A_55_P1961127	3.95E-03	-5.258	-2.395
Entpd2	A_55_P1974645	1.53E-03	-5.263	-2.396
Alcam	A_51_P359272	2.59E-03	-5.265	-2.397
A_30_P01028827	A_30_P01028827	9.32E-03	-5.274	-2.399
Tm4sf1	A_51_P240614	5.33E-04	-5.274	-2.399
Hist1h1c	A_51_P516133	2.44E-06	-5.274	-2.399
Lrtm2	A_55_P1954231	5.82E-03	-5.285	-2.402
Tmem100	A_52_P368306	1.26E-03	-5.291	-2.404
Slc22a6	A_51_P360655	8.96E-03	-5.291	-2.404
Rnase4	A_51_P237383	3.84E-03	-5.300	-2.406
Sepp1	A_51_P470328	1.24E-05	-5.317	-2.411
A_30_P01028007	A_30_P01028007	6.14E-03	-5.341	-2.417
BC026782	A_52_P796840	1.27E-02	-5.346	-2.419
A_30_P01021588	A_30_P01021588	5.07E-03	-5.385	-2.429
Mfsd2a	A_51_P279437	4.13E-04	-5.391	-2.431
Mtus2	A_55_P2083252	2.56E-02	-5.396	-2.432
Crlf1	A_52_P304720	2.41E-02	-5.413	-2.437
Rsph1	A_55_P2044684	1.49E-03	-5.462	-2.450
Cadm2	A_55_P2142928	5.31E-04	-5.466	-2.451

Parp10	A_55_P2130970	2.34E-03	-5.466	-2.451
Ranbp3l	A_55_P1969306	2.03E-02	-5.472	-2.452
Rapgef3	A_51_P116906	3.16E-04	-5.481	-2.455
1520402A15Rik	A_52_P547491	1.59E-02	-5.493	-2.458
Rtp4	A_51_P304170	3.28E-04	-5.514	-2.463
Vtn	A_51_P109840	2.39E-02	-5.533	-2.468
Cadm2	A_51_P442642	5.12E-04	-5.548	-2.472
A_30_P01026972	A_30_P01026972	3.88E-03	-5.548	-2.472
Eml2	A_55_P1989921	3.23E-03	-5.550	-2.473
Chst11	A_51_P275101	4.13E-03	-5.562	-2.476
Olfml3	A_55_P2102540	2.78E-02	-5.606	-2.487
Acsl6	A_51_P380699	9.02E-03	-5.649	-2.498
Gpr146	A_55_P2027392	7.71E-04	-5.661	-2.501
Negr1	A_55_P2012572	1.09E-03	-5.667	-2.503
Hist2h3c2-ps	A_55_P2142251	1.86E-04	-5.675	-2.505
Sall1	A_55_P1977850	1.92E-03	-5.676	-2.505
Gm3088	A_55_P2163897	7.13E-04	-5.692	-2.509
Epha5	A_55_P2100425	9.08E-03	-5.694	-2.510
Tap2	A_55_P2017645	8.32E-04	-5.698	-2.511
Ccdc113	A_55_P1981704	9.05E-03	-5.706	-2.513
Samd9l	A_55_P2151601	1.24E-02	-5.714	-2.515
A_30_P01033149	A_30_P01033149	2.88E-03	-5.756	-2.525
A_30_P01032682	A_30_P01032682	1.52E-04	-5.764	-2.527
LOC100045638	A_55_P1974984	7.50E-03	-5.790	-2.534
B3gat2	A_55_P2079679	3.73E-02	-5.810	-2.539
1190002A17Rik	A_51_P101006	2.61E-02	-5.812	-2.539
A_30_P01032789	A_30_P01032789	2.76E-03	-5.830	-2.544
Aspa	A_51_P259975	7.24E-04	-5.834	-2.545
Ccdc85a	A_55_P1980521	7.97E-06	-5.838	-2.546
Gpr17	A_51_P170463	2.90E-02	-5.842	-2.547
Hspa1a	A_55_P2068459	1.80E-02	-5.862	-2.552
Ephx2	A_55_P2002572	3.66E-03	-5.877	-2.555
Rgs16	A_51_P249286	1.06E-04	-5.889	-2.558
A_30_P01032469	A_30_P01032469	7.68E-03	-5.893	-2.559
Synm	A_55_P2052696	1.36E-02	-5.897	-2.560
Tctex1d1	A_55_P2051270	1.07E-02	-5.899	-2.561
Ifi27l2a	A_52_P90363	4.23E-02	-5.901	-2.561
Cdh13	A_51_P114826	2.18E-03	-5.915	-2.565
Slc7a10	A_51_P268193	1.62E-03	-5.934	-2.569
A_30_P01025068	A_30_P01025068	4.18E-03	-5.938	-2.570
Mbp	A_52_P329451	5.77E-03	-5.940	-2.571
Tcp11	A_55_P1986421	5.60E-03	-5.942	-2.571
Lgi3	A_51_P356967	5.47E-03	-5.971	-2.578
Plxdc2	A_55_P2022211	2.64E-05	-5.975	-2.579
Crip3	A_51_P325501	1.19E-03	-5.977	-2.580
Papss2	A_55_P2080021	1.49E-03	-6.002	-2.586

Serp2	A_52_P539310	2.95E-02	-6.013	-2.588
1700016K19Rik	A_55_P2068356	5.32E-03	-6.017	-2.589
Fzd9	A_51_P511015	6.42E-04	-6.048	-2.597
Tmem132b	A_52_P38908	1.15E-02	-6.069	-2.602
Rbp4	A_55_P2006118	1.18E-03	-6.080	-2.604
Meg3	A_55_P2033407	5.11E-04	-6.124	-2.615
Car2	A_51_P455647	3.38E-04	-6.145	-2.620
Plp1	A_55_P2069850	4.21E-03	-6.165	-2.624
Crispld2	A_55_P2052016	1.82E-02	-6.167	-2.625
Meg3	A_52_P196568	4.24E-02	-6.169	-2.625
Ccno	A_51_P291501	6.68E-03	-6.199	-2.632
ENSMUST00000097840	A_66_P139703	7.34E-03	-6.223	-2.638
A_30_P01026518	A_30_P01026518	4.69E-03	-6.235	-2.641
Hspb8	A_51_P464387	3.50E-03	-6.240	-2.642
Mrgprf	A_55_P2116180	1.13E-02	-6.259	-2.646
A_30_P01020627	A_30_P01020627	3.86E-03	-6.264	-2.647
Slc6a13	A_51_P438083	5.43E-03	-6.272	-2.649
Nrxn3	A_55_P2054643	9.99E-04	-6.272	-2.649
Morn5	A_51_P201785	2.42E-03	-6.303	-2.656
Dapl1	A_51_P391955	6.71E-03	-6.312	-2.658
A_30_P01026799	A_30_P01026799	2.73E-03	-6.327	-2.662
A_30_P01033229	A_30_P01033229	3.81E-03	-6.366	-2.671
Slc7a11	A_52_P368057	3.95E-03	-6.429	-2.685
C1qtnf4	A_52_P633489	1.09E-02	-6.444	-2.688
Stk33	A_51_P511511	1.32E-04	-6.446	-2.689
Zfp503	A_51_P126626	4.24E-04	-6.449	-2.689
Kcna6	A_52_P130787	4.10E-04	-6.476	-2.695
Srgn	A_55_P2094925	2.18E-02	-6.480	-2.696
Crabp2	A_55_P2059432	3.40E-03	-6.489	-2.698
Pid1	A_52_P269158	3.95E-05	-6.491	-2.699
Cpe	A_55_P2024704	6.94E-05	-6.530	-2.707
Pdzk1ip1	A_55_P2011678	8.82E-03	-6.555	-2.713
Gabbr1	A_55_P2082135	7.29E-04	-6.561	-2.714
Rcan2	A_55_P1961736	7.35E-05	-6.564	-2.715
Nek5	A_51_P347529	1.38E-02	-6.582	-2.719
Apoc1	A_55_P1975370	1.94E-04	-6.589	-2.720
Sult1a1	A_51_P321341	1.44E-03	-6.596	-2.722
Wnt4	A_51_P130475	3.78E-03	-6.632	-2.730
A_30_P01018420	A_30_P01018420	3.65E-03	-6.635	-2.730
Sult1a1	A_55_P2005475	8.84E-04	-6.641	-2.732
S100a1	A_55_P1979645	4.88E-04	-6.653	-2.734
A_30_P01018307	A_30_P01018307	1.21E-02	-6.665	-2.737
Sidt1	A_51_P393305	5.93E-03	-6.699	-2.744
Tekt4	A_51_P387868	4.44E-04	-6.765	-2.758
Gabbr1	A_52_P16232	7.77E-04	-6.790	-2.764
Hif3a	A_55_P2015541	9.40E-05	-6.847	-2.776

Wnt5b	A_55_P1984976	4.30E-04	-6.878	-2.782
Ncan	A_55_P2453279	8.42E-04	-6.950	-2.797
Aebp1	A_55_P2035662	3.00E-04	-6.952	-2.798
1700045I19Rik	A_51_P408703	7.96E-03	-6.952	-2.798
Cdc42ep2	A_52_P155554	1.01E-04	-6.964	-2.800
Hist2h2aa1	A_55_P1962084	1.74E-04	-6.996	-2.807
Fam189a2	A_52_P369123	8.30E-03	-7.010	-2.810
Zdhhc2	A_52_P651248	3.89E-02	-7.059	-2.820
Wnt7a	A_52_P79782	1.01E-03	-7.096	-2.827
Arhgdig	A_51_P172085	2.80E-02	-7.116	-2.831
Creg2	A_55_P2140651	1.36E-03	-7.193	-2.847
Aldh1a1	A_51_P334942	4.44E-03	-7.263	-2.861
4930506M07Rik	A_51_P200561	3.68E-02	-7.268	-2.862
Gfap	A_52_P52303	1.40E-02	-7.295	-2.867
Dynlrb2	A_51_P227962	2.93E-03	-7.413	-2.890
Asrgl1	A_55_P2056310	3.43E-03	-7.426	-2.893
S100a1	A_55_P1979650	3.50E-04	-7.469	-2.901
Nrxn3	A_66_P127136	1.46E-02	-7.532	-2.913
Gm7676	A_55_P2087265	1.91E-03	-7.589	-2.924
Gjb6	A_52_P482251	5.40E-03	-7.626	-2.931
Atp13a5	A_52_P607195	6.69E-04	-7.648	-2.935
Foxc2	A_51_P196444	9.64E-03	-7.666	-2.939
Ctgf	A_51_P157042	3.65E-04	-7.706	-2.946
6430519N07Rik	A_55_P2205226	3.01E-02	-7.754	-2.955
Maob	A_51_P302566	1.08E-05	-7.768	-2.958
Oprl1	A_55_P2066593	6.40E-02	-7.789	-2.962
Fam166b	A_66_P137660	2.28E-03	-7.789	-2.962
Gbp2	A_51_P203955	1.13E-02	-7.830	-2.969
Epha8	A_55_P2100485	4.73E-02	-7.868	-2.976
Rap1gap	A_55_P2039225	7.35E-04	-7.893	-2.981
Irgm1	A_51_P262171	1.08E-04	-7.915	-2.985
ENSMUST00000110985	A_55_P2096602	2.83E-03	-7.953	-2.992
Wnt6	A_52_P415155	2.85E-03	-8.019	-3.004
Car10	A_55_P2397904	9.19E-04	-8.053	-3.010
Cbr2	A_55_P2122605	8.62E-03	-8.279	-3.050
Tmem51	A_51_P125842	1.49E-04	-8.294	-3.052
Sulf2	A_52_P193925	2.37E-05	-8.305	-3.054
Lims2	A_55_P2174203	1.49E-02	-8.389	-3.069
Nrxn1	A_52_P121342	7.06E-05	-8.409	-3.072
Ifitm1	A_55_P2146254	1.50E-03	-8.415	-3.073
Mt1	A_52_P423810	4.20E-03	-8.427	-3.075
Sphk1	A_51_P501248	3.26E-05	-8.453	-3.080
Cybrd1	A_55_P1956472	1.79E-04	-8.483	-3.085
Plin5	A_55_P2104259	6.33E-04	-8.503	-3.088
Fam134b	A_51_P428578	5.91E-03	-8.547	-3.096
Thy1	A_55_P2072035	1.83E-03	-8.586	-3.102

Wdr63	A_55_P1975989	7.60E-03	-8.655	-3.114
Cpe	A_55_P2025038	2.01E-04	-8.688	-3.119
Fam92b	A_52_P26626	6.59E-03	-8.721	-3.125
Hdc	A_51_P254656	1.68E-02	-8.733	-3.127
4930579J09Rik	A_51_P358462	2.96E-03	-8.745	-3.129
Mal	A_55_P2113160	6.31E-03	-8.815	-3.140
Lyl1	A_51_P143190	3.55E-02	-8.877	-3.150
Rgs4	A_55_P2026738	1.01E-03	-9.088	-3.184
Crispld2	A_55_P2004016	6.97E-03	-9.363	-3.227
Nrxn1	A_55_P2054628	2.41E-04	-9.533	-3.253
Mpzl2	A_52_P322421	6.10E-03	-9.603	-3.264
Slc6a20a	A_55_P2032916	2.49E-03	-9.707	-3.279
Dner	A_52_P671132	8.76E-05	-9.727	-3.282
Gfap	A_55_P2157250	3.51E-03	-9.788	-3.291
Cpne7	A_55_P2150962	6.73E-05	-9.887	-3.306
Trim47	A_55_P2066697	1.04E-05	-10.004	-3.323
Rspo1	A_51_P142421	6.17E-03	-10.060	-3.331
Dok7	A_51_P155458	1.41E-02	-10.070	-3.332
1190002H23Rik	A_51_P226269	9.19E-06	-10.161	-3.345
Gabbr1	A_51_P464900	1.12E-03	-10.175	-3.347
Cmbl	A_51_P272283	4.27E-03	-10.235	-3.356
Fam176a	A_51_P140641	4.88E-03	-10.285	-3.363
Dcdc2a	A_52_P640922	2.48E-06	-10.285	-3.363
Csgalnact1	A_55_P2077618	9.03E-05	-10.335	-3.370
Gpr182	A_51_P436068	1.27E-03	-10.339	-3.370
Gja1	A_52_P174915	3.86E-05	-10.339	-3.370
Rap1gap	A_55_P2068096	5.57E-04	-10.350	-3.372
Itih2	A_51_P196726	9.58E-04	-10.418	-3.381
Ntsr2	A_52_P266686	4.15E-04	-10.461	-3.387
Pygl	A_51_P452779	5.95E-07	-10.615	-3.408
Itpka	A_51_P273609	1.26E-03	-10.633	-3.411
Adora2b	A_55_P1993503	2.25E-04	-10.677	-3.417
Cxcl14	A_51_P209183	4.35E-04	-10.808	-3.434
Dbc1	A_55_P2124941	3.70E-02	-10.970	-3.456
Htra1	A_51_P225224	2.10E-04	-10.985	-3.458
Dbx2	A_51_P352452	2.69E-05	-11.096	-3.472
Cldn10a	A_51_P456465	3.21E-04	-11.318	-3.501
Igsf1	A_55_P2059864	9.50E-04	-11.373	-3.508
1700001C02Rik	A_55_P2111825	1.41E-03	-11.444	-3.517
Trim47	A_55_P2105256	1.40E-05	-11.917	-3.575
C2cd4b	A_55_P2054261	6.18E-04	-11.963	-3.581
Gbx2	A_51_P179578	1.65E-04	-12.143	-3.602
Paqr7	A_51_P430973	3.49E-05	-12.406	-3.633
Fam183b	A_55_P2137527	1.19E-03	-12.424	-3.635
AU021034	A_55_P1973526	1.58E-05	-12.523	-3.647
Plcd4	A_52_P327588	1.46E-04	-12.707	-3.668

3110035E14Rik	A_52_P400355	4.17E-02	-12.871	-3.686
Cebpd	A_51_P444447	2.14E-06	-12.879	-3.687
Pla2g3	A_55_P2043033	4.63E-04	-12.938	-3.694
Cpe	A_55_P2152248	2.05E-04	-13.246	-3.728
Ntsr2	A_55_P1974527	3.42E-04	-13.473	-3.752
Gstt3	A_51_P377856	1.32E-03	-13.534	-3.759
Odf3b	A_51_P422369	4.54E-03	-13.553	-3.761
Meig1	A_55_P2093705	5.03E-04	-13.595	-3.765
C2	A_51_P497985	1.01E-04	-13.713	-3.778
Cidea	A_51_P199168	1.90E-03	-14.065	-3.814
Ccdc153	A_52_P352735	1.52E-02	-14.182	-3.826
Pla2g3	A_55_P2043039	3.64E-03	-14.221	-3.830
Adora2b	A_66_P118906	2.16E-04	-14.231	-3.831
Trim9	A_55_P2073059	3.77E-04	-14.296	-3.838
Cybrd1	A_52_P124734	1.20E-04	-14.360	-3.844
Plcd4	A_55_P2090359	2.36E-04	-14.445	-3.853
Adra2a	A_55_P2021505	1.10E-04	-14.861	-3.894
Slc39a12	A_55_P2036392	1.82E-04	-14.944	-3.902
Olig1	A_52_P603038	2.87E-05	-15.600	-3.964
Slit1	A_55_P1958379	2.00E-03	-15.720	-3.975
Chst1	A_55_P2061620	2.47E-03	-15.923	-3.993
Lrfn2	A_51_P229498	6.06E-04	-16.033	-4.003
Odz2	A_55_P2011290	1.09E-02	-16.302	-4.027
Ppp1r3c	A_52_P30451	5.71E-05	-17.630	-4.140
Foxb1	A_55_P2026405	1.54E-04	-17.772	-4.152
Mgll	A_55_P2063316	6.76E-05	-18.405	-4.202
C4b	A_55_P2078633	3.14E-04	-18.469	-4.207
Slc39a12	A_55_P2036394	5.41E-05	-19.047	-4.252
Kcnd2	A_52_P124472	3.56E-04	-19.113	-4.257
Kcnj16	A_55_P2156304	8.21E-06	-19.522	-4.287
Fndc5	A_52_P213696	7.11E-05	-20.407	-4.351
Fmod	A_51_P207622	6.30E-04	-20.821	-4.380
Slc16a11	A_55_P2061338	6.27E-05	-21.422	-4.421
Olig2	A_52_P223626	3.01E-05	-21.578	-4.432
Dclk3	A_51_P419637	7.51E-05	-22.131	-4.468
Ptpn5	A_55_P1955726	2.38E-03	-23.047	-4.527
Slc14a2	A_55_P1964028	1.24E-05	-26.529	-4.730
Agt	A_66_P112356	1.36E-04	-26.538	-4.730
Mgll	A_55_P2114863	6.30E-05	-26.584	-4.733
Mgll	A_55_P2063312	1.60E-05	-27.096	-4.760
Slc6a11	A_51_P271311	1.90E-05	-28.960	-4.856
Fgfr3	A_65_P06147	1.01E-04	-29.375	-4.877
Slc13a3	A_55_P2067518	4.79E-05	-32.684	-5.031
Ptgds	A_55_P2100928	4.30E-06	-32.729	-5.033
Slc6a12	A_51_P323812	2.56E-04	-34.416	-5.105
Fgfr3	A_55_P1996578	2.11E-04	-34.763	-5.120

Trim9	A_52_P625640	4.70E-05	-39.165	-5.292
Grm5	A_55_P2033425	1.02E-05	-42.754	-5.418
Hsd11b1	A_51_P127297	1.30E-05	-43.789	-5.453
Baalc	A_55_P2075469	5.18E-04	-43.880	-5.456

IV Literature:

1 De Robertis, E. M. Spemann's organizer and self-regulation in amphibian embryos. *Nature reviews. Molecular cell biology* **7**, 296-302, doi:10.1038/nrm1855 (2006).

2 Liu, A. & Niswander, L. A. Bone morphogenetic protein signalling and vertebrate nervous system development. *Nature reviews. Neuroscience* **6**, 945-954, doi:10.1038/nrn1805 (2005).

3 Kimelberg, H. K. & Norenberg, M. D. Astrocytes. *Scientific American* **260**, 66-72, 74, 76 (1989).

4 O'Kusky, J. & Colonnier, M. A laminar analysis of the number of neurons, glia, and synapses in the adult cortex (area 17) of adult macaque monkeys. *The Journal of comparative neurology* **210**, 278-290, doi:10.1002/cne.902100307 (1982).

5 Rose, C. R. & Ransom, B. R. Gap junctions equalize intracellular Na+ concentration in astrocytes. *Glia* **20**, 299-307 (1997).

6 Wang, X. *et al.* Astrocytic Ca2+ signaling evoked by sensory stimulation in vivo. *Nature neuroscience* **9**, 816-823, doi:10.1038/nn1703 (2006).

7 Wang, X., Takano, T. & Nedergaard, M. Astrocytic calcium signaling: mechanism and implications for functional brain imaging. *Methods in molecular biology* **489**, 93-109, doi:10.1007/978-1-59745-543-5_5 (2009).

8 Ransom, B. R. *Gap junctions*. Vol. 299-318 (Oxford University press, 1995).

9 Charles, A. Intercellular calcium waves in glia. *Glia* **24**, 39-49 (1998).

10 Scemes, E., Dermietzel, R. & Spray, D. C. Calcium waves between astrocytes from Cx43 knockout mice. *Glia* **24**, 65-73 (1998).

11 Bushong, E. A., Martone, M. E., Jones, Y. Z. & Ellisman, M. H. Protoplasmic astrocytes in CA1 stratum radiatum occupy separate anatomical domains. *J Neurosci* **22**, 183-192 (2002).

12 Ventura, R. & Harris, K. M. Three-dimensional relationships between hippocampal synapses and astrocytes. *J Neurosci* **19**, 6897-6906 (1999).

13 Halassa, M. M., Fellin, T., Takano, H., Dong, J. H. & Haydon, P. G. Synaptic islands defined by the territory of a single astrocyte. *J Neurosci* **27**, 6473-6477, doi:10.1523/JNEUROSCI.1419-07.2007 (2007).

14 Barres, B. A. The mystery and magic of glia: a perspective on their roles in health and disease. *Neuron* **60**, 430-440, doi:10.1016/j.neuron.2008.10.013 (2008).

15 Christopherson, K. S. *et al.* Thrombospondins are astrocyte-secreted proteins that promote CNS synaptogenesis. *Cell* **120**, 421-433, doi:10.1016/j.cell.2004.12.020 (2005).

16 Schousboe, A. Transport and metabolism of glutamate and GABA in neurons are glial cells. *International review of neurobiology* **22**, 1-45 (1981).

17 Volterra, A. & Meldolesi, J. Astrocytes, from brain glue to communication elements: the revolution continues. *Nat Rev Neurosci* **6**, 626-640, doi:10.1038/nrn1722 (2005).

18 Haydon, P. G. & Carmignoto, G. Astrocyte control of synaptic transmission and neurovascular coupling. *Physiol Rev* **86**, 1009-1031, doi:10.1152/physrev.00049.2005 (2006).

19 Halassa, M. M., Fellin, T. & Haydon, P. G. The tripartite synapse: roles for gliotransmission in health and disease. *Trends in molecular medicine* **13**, 54-63, doi:10.1016/j.molmed.2006.12.005 (2007).

20 Pfrieger, F. W. & Ungerer, N. Cholesterol metabolism in neurons and astrocytes. *Progress in lipid research* **50**, 357-371, doi:10.1016/j.plipres.2011.06.002 (2011).
21 Rudge, J. S. *et al.* Expression of Ciliary Neurotrophic Factor and the Neurotrophins-Nerve Growth Factor, Brain-Derived Neurotrophic Factor and Neurotrophin 3-in Cultured Rat Hippocampal Astrocytes. *The European journal of neuroscience* **4**, 459-471 (1992).
22 Anderson, C. M. & Swanson, R. A. Astrocyte glutamate transport: review of properties, regulation, and physiological functions. *Glia* **32**, 1-14 (2000).
23 Danbolt, N. C. Glutamate uptake. *Prog Neurobiol* **65**, 1-105 (2001).
24 Wen, H. *et al.* Ontogeny of water transport in rat brain: postnatal expression of the aquaporin-4 water channel. *The European journal of neuroscience* **11**, 935-945 (1999).
25 Kofuji, P. & Newman, E. A. Potassium buffering in the central nervous system. *Neuroscience* **129**, 1045-1056, doi:10.1016/j.neuroscience.2004.06.008 (2004).
26 Deitmer, J. W. & Schlue, W. R. The regulation of intracellular pH by identified glial cells and neurones in the central nervous system of the leech. *The Journal of physiology* **388**, 261-283 (1987).
27 Sontheimer, H. Astrocytes, as well as neurons, express a diversity of ion channels. *Canadian journal of physiology and pharmacology* **70 Suppl**, S223-238 (1992).
28 Sontheimer, H., Black, J. A. & Waxman, S. G. Voltage-gated Na+ channels in glia: properties and possible functions. *Trends in neurosciences* **19**, 325-331 (1996).
29 Wiese, S., Karus, M. & Faissner, A. Astrocytes as a source for extracellular matrix molecules and cytokines. *Frontiers in pharmacology* **3**, 120, doi:10.3389/fphar.2012.00120 (2012).
30 Wells, G. M. *et al.* Quantitation of matrix metalloproteinases in cultured rat astrocytes using the polymerase chain reaction with a multi-competitor cDNA standard. *Glia* **18**, 332-340 (1996).
31 Oberheim, N. A., Goldman, S. A. & Nedergaard, M. Heterogeneity of astrocytic form and function. *Methods Mol Biol* **814**, 23-45, doi:10.1007/978-1-61779-452-0_3 (2012).
32 Miller, R. H. & Raff, M. C. Fibrous and protoplasmic astrocytes are biochemically and developmentally distinct. *J Neurosci* **4**, 585-592 (1984).
33 Rakic, P. Mode of cell migration to the superficial layers of fetal monkey neocortex. *The Journal of comparative neurology* **145**, 61-83, doi:10.1002/cne.901450105 (1972).
34 Hatten, M. E. New directions in neuronal migration. *Science* **297**, 1660-1663, doi:10.1126/science.1074572 (2002).
35 Nedergaard, M., Ransom, B. & Goldman, S. A. New roles for astrocytes: redefining the functional architecture of the brain. *Trends Neurosci* **26**, 523-530, doi:10.1016/j.tins.2003.08.008 (2003).
36 Shu, T. & Richards, L. J. Cortical axon guidance by the glial wedge during the development of the corpus callosum. *J Neurosci* **21**, 2749-2758 (2001).
37 Kaneko, N. *et al.* New neurons clear the path of astrocytic processes for their rapid migration in the adult brain. *Neuron* **67**, 213-223, doi:10.1016/j.neuron.2010.06.018 (2010).

38 Abbott, N. J., Patabendige, A. A., Dolman, D. E., Yusof, S. R. & Begley, D. J. Structure and function of the blood-brain barrier. *Neurobiology of disease* **37**, 13-25, doi:10.1016/j.nbd.2009.07.030 (2010).

39 Fu, L., Zhu, X., Yi, F., Liu, G. H. & Izpisua Belmonte, J. C. Regenerative medicine: transdifferentiation in vivo. *Cell Res* **24**, 141-142, doi:10.1038/cr.2013.165 (2014).

40 Kornblum, H. I. Introduction to neural stem cells. *Stroke* **38**, 810-816, doi:10.1161/01.STR.0000255757.12198.0f (2007).

41 Ulloa, F. & Marti, E. Wnt won the war: antagonistic role of Wnt over Shh controls dorso-ventral patterning of the vertebrate neural tube. *Dev Dyn* **239**, 69-76, doi:10.1002/dvdy.22058 (2010).

42 Mori, T., Buffo, A. & Gotz, M. The novel roles of glial cells revisited: the contribution of radial glia and astrocytes to neurogenesis. *Current topics in developmental biology* **69**, 67-99, doi:10.1016/S0070-2153(05)69004-7 (2005).

43 Gotz, M. & Huttner, W. B. The cell biology of neurogenesis. *Nature reviews. Molecular cell biology* **6**, 777-788, doi:10.1038/nrm1739 (2005).

44 Kriegstein, A. & Alvarez-Buylla, A. The glial nature of embryonic and adult neural stem cells. *Annual review of neuroscience* **32**, 149-184, doi:10.1146/annurev.neuro.051508.135600 (2009).

45 Alvarez-Buylla, A., Garcia-Verdugo, J. M. & Tramontin, A. D. A unified hypothesis on the lineage of neural stem cells. *Nature reviews. Neuroscience* **2**, 287-293, doi:10.1038/35067582 (2001).

46 Bentivoglio, M. & Mazzarello, P. The history of radial glia. *Brain research bulletin* **49**, 305-315 (1999).

47 Malatesta, P., Hartfuss, E. & Gotz, M. Isolation of radial glial cells by fluorescent-activated cell sorting reveals a neuronal lineage. *Development* **127**, 5253-5263 (2000).

48 Shibata, T. *et al.* Glutamate transporter GLAST is expressed in the radial glia-astrocyte lineage of developing mouse spinal cord. *The Journal of neuroscience : the official journal of the Society for Neuroscience* **17**, 9212-9219 (1997).

49 Choi, B. H. Radial glia of developing human fetal spinal cord: Golgi, immunohistochemical and electron microscopic study. *Brain Res* **227**, 249-267 (1981).

50 Kurtz, A. *et al.* The expression pattern of a novel gene encoding brain-fatty acid binding protein correlates with neuronal and glial cell development. *Development* **120**, 2637-2649 (1994).

51 Hartfuss, E., Galli, R., Heins, N. & Gotz, M. Characterization of CNS precursor subtypes and radial glia. *Developmental biology* **229**, 15-30, doi:10.1006/dbio.2000.9962 (2001).

52 Misson, J. P., Edwards, M. A., Yamamoto, M. & Caviness, V. S., Jr. Identification of radial glial cells within the developing murine central nervous system: studies based upon a new immunohistochemical marker. *Brain research. Developmental brain research* **44**, 95-108 (1988).

53 Campbell, K. & Gotz, M. Radial glia: multi-purpose cells for vertebrate brain development. *Trends in neurosciences* **25**, 235-238 (2002).

54 Rakic, P. Neuron-glia relationship during granule cell migration in developing cerebellar cortex. A Golgi and electronmicroscopic study in Macacus Rhesus.

The Journal of comparative neurology **141**, 283-312, doi:10.1002/cne.901410303 (1971).

55 Noctor, S. C., Martinez-Cerdeno, V., Ivic, L. & Kriegstein, A. R. Cortical neurons arise in symmetric and asymmetric division zones and migrate through specific phases. *Nat Neurosci* **7**, 136-144, doi:10.1038/nn1172 (2004).

56 Voigt, T. Development of glial cells in the cerebral wall of ferrets: direct tracing of their transformation from radial glia into astrocytes. *The Journal of comparative neurology* **289**, 74-88, doi:10.1002/cne.902890106 (1989).

57 Levitt, P., Cooper, M. L. & Rakic, P. Coexistence of neuronal and glial precursor cells in the cerebral ventricular zone of the fetal monkey: an ultrastructural immunoperoxidase analysis. *J Neurosci* **1**, 27-39 (1981).

58 Guo, Z. *et al.* Early postnatal GFAP-expressing cells produce multilineage progeny in cerebrum and astrocytes in cerebellum of adult mice. *Brain Res* **1532**, 14-20, doi:10.1016/j.brainres.2013.08.003 (2013).

59 Surzenko, N., Crowl, T., Bachleda, A., Langer, L. & Pevny, L. SOX2 maintains the quiescent progenitor cell state of postnatal retinal Muller glia. *Development* **140**, 1445-1456, doi:10.1242/dev.071878 (2013).

60 Kriegstein, A. & Parnavelas, J. G. Changing concepts of cortical development. *Cereb Cortex* **13**, 541 (2003).

61 Kriegstein, A. R. & Gotz, M. Radial glia diversity: a matter of cell fate. *Glia* **43**, 37-43, doi:10.1002/glia.10250 (2003).

62 Fishell, G. & Kriegstein, A. R. Neurons from radial glia: the consequences of asymmetric inheritance. *Curr Opin Neurobiol* **13**, 34-41 (2003).

63 Reynolds, B. A. & Weiss, S. Generation of neurons and astrocytes from isolated cells of the adult mammalian central nervous system. *Science* **255**, 1707-1710 (1992).

64 Kaplan, M. S. & Hinds, J. W. Neurogenesis in the adult rat: electron microscopic analysis of light radioautographs. *Science* **197**, 1092-1094 (1977).

65 Ernst, A. *et al.* Neurogenesis in the striatum of the adult human brain. *Cell* **156**, 1072-1083, doi:10.1016/j.cell.2014.01.044 (2014).

66 Davis, A. A. & Temple, S. A self-renewing multipotential stem cell in embryonic rat cerebral cortex. *Nature* **372**, 263-266, doi:10.1038/372263a0 (1994).

67 Richards, L. J., Kilpatrick, T. J. & Bartlett, P. F. De novo generation of neuronal cells from the adult mouse brain. *Proc Natl Acad Sci U S A* **89**, 8591-8595 (1992).

68 Doetsch, F., Caille, I., Lim, D. A., Garcia-Verdugo, J. M. & Alvarez-Buylla, A. Subventricular zone astrocytes are neural stem cells in the adult mammalian brain. *Cell* **97**, 703-716 (1999).

69 Spassky, N. *et al.* Adult ependymal cells are postmitotic and are derived from radial glial cells during embryogenesis. *J Neurosci* **25**, 10-18, doi:10.1523/JNEUROSCI.1108-04.2005 (2005).

70 Park, D. *et al.* Nestin is required for the proper self-renewal of neural stem cells. *Stem cells* **28**, 2162-2171, doi:10.1002/stem.541 (2010).

71 Doetsch, F., Garcia-Verdugo, J. M. & Alvarez-Buylla, A. Cellular composition and three-dimensional organization of the subventricular germinal zone in the adult mammalian brain. *J Neurosci* **17**, 5046-5061 (1997).

72 Beckervordersandforth, R. *et al.* In vivo fate mapping and expression analysis reveals molecular hallmarks of prospectively isolated adult neural stem cells. *Cell stem cell* **7**, 744-758, doi:10.1016/j.stem.2010.11.017 (2010).

73 Coskun, V. *et al.* CD133+ neural stem cells in the ependyma of mammalian postnatal forebrain. *Proceedings of the National Academy of Sciences of the United States of America* **105**, 1026-1031, doi:10.1073/pnas.0710000105 (2008).

74 Walker, T. L. *et al.* Prominin-1 allows prospective isolation of neural stem cells from the adult murine hippocampus. *J Neurosci* **33**, 3010-3024, doi:10.1523/JNEUROSCI.3363-12.2013 (2013).

75 Mich, J. K. *et al.* Prospective identification of functionally distinct stem cells and neurosphere-initiating cells in adult mouse forebrain. *Elife* **3**, e02669, doi:10.7554/eLife.02669 (2014).

76 Kiss, J. Z. & Rougon, G. Cell biology of polysialic acid. *Curr Opin Neurobiol* **7**, 640-646 (1997).

77 Chazal, G., Durbec, P., Jankovski, A., Rougon, G. & Cremer, H. Consequences of neural cell adhesion molecule deficiency on cell migration in the rostral migratory stream of the mouse. *J Neurosci* **20**, 1446-1457 (2000).

78 Jankovski, A. & Sotelo, C. Subventricular zone-olfactory bulb migratory pathway in the adult mouse: cellular composition and specificity as determined by heterochronic and heterotopic transplantation. *The Journal of comparative neurology* **371**, 376-396, doi:10.1002/(SICI)1096-9861(19960729)371:3<376::AID-CNE3>3.0.CO;2-# (1996).

79 Menezes, J. R., Marins, M., Alves, J. A., Froes, M. M. & Hedin-Pereira, C. Cell migration in the postnatal subventricular zone. *Brazilian journal of medical and biological research = Revista brasileira de pesquisas medicas e biologicas / Sociedade Brasileira de Biofisica ... [et al.]* **35**, 1411-1421 (2002).

80 Alvarez-Buylla, A., Seri, B. & Doetsch, F. Identification of neural stem cells in the adult vertebrate brain. *Brain research bulletin* **57**, 751-758 (2002).

81 Mirzadeh, Z., Merkle, F. T., Soriano-Navarro, M., Garcia-Verdugo, J. M. & Alvarez-Buylla, A. Neural stem cells confer unique pinwheel architecture to the ventricular surface in neurogenic regions of the adult brain. *Cell stem cell* **3**, 265-278, doi:10.1016/j.stem.2008.07.004 (2008).

82 Raff, M. C., Abney, E. R., Cohen, J., Lindsay, R. & Noble, M. Two types of astrocytes in cultures of developing rat white matter: differences in morphology, surface gangliosides, and growth characteristics. *J Neurosci* **3**, 1289-1300 (1983).

83 Eng, L. F. Glial fibrillary acidic protein (GFAP): the major protein of glial intermediate filaments in differentiated astrocytes. *Journal of neuroimmunology* **8**, 203-214 (1985).

84 Bignami, A., Eng, L. F., Dahl, D. & Uyeda, C. T. Localization of the glial fibrillary acidic protein in astrocytes by immunofluorescence. *Brain research* **43**, 429-435 (1972).

85 Rothstein, J. D. *et al.* Knockout of glutamate transporters reveals a major role for astroglial transport in excitotoxicity and clearance of glutamate. *Neuron* **16**, 675-686 (1996).

86 Martinez-Hernandez, A., Bell, K. P. & Norenberg, M. D. Glutamine synthetase: glial localization in brain. *Science* **195**, 1356-1358 (1977).

87 Wender, R. *et al.* Astrocytic glycogen influences axon function and survival during glucose deprivation in central white matter. *The Journal of neuroscience : the official journal of the Society for Neuroscience* **20**, 6804-6810 (2000).

88 Cahoy, J. D. *et al.* A transcriptome database for astrocytes, neurons, and oligodendrocytes: a new resource for understanding brain development and function. *The Journal of neuroscience : the official journal of the Society for Neuroscience* **28**, 264-278, doi:10.1523/JNEUROSCI.4178-07.2008 (2008).
89 Sofroniew, M. V. & Vinters, H. V. Astrocytes: biology and pathology. *Acta Neuropathol* **119**, 7-35, doi:10.1007/s00401-009-0619-8 (2010).
90 Allaman, I., Belanger, M. & Magistretti, P. J. Astrocyte-neuron metabolic relationships: for better and for worse. *Trends in neurosciences* **34**, 76-87, doi:10.1016/j.tins.2010.12.001 (2011).
91 Benesova, J. *et al.* Distinct expression/function of potassium and chloride channels contributes to the diverse volume regulation in cortical astrocytes of GFAP/EGFP mice. *PloS one* **7**, e29725, doi:10.1371/journal.pone.0029725 (2012).
92 Deloulme, J. C. *et al.* Nuclear expression of S100B in oligodendrocyte progenitor cells correlates with differentiation toward the oligodendroglial lineage and modulates oligodendrocytes maturation. *Molecular and cellular neurosciences* **27**, 453-465, doi:10.1016/j.mcn.2004.07.008 (2004).
93 Higashi, K. *et al.* An inwardly rectifying K(+) channel, Kir4.1, expressed in astrocytes surrounds synapses and blood vessels in brain. *American journal of physiology. Cell physiology* **281**, C922-931 (2001).
94 Stahlberg, A. *et al.* Defining cell populations with single-cell gene expression profiling: correlations and identification of astrocyte subpopulations. *Nucleic acids research* **39**, e24, doi:10.1093/nar/gkq1182 (2011).
95 Benesova, J. *et al.* Quantification of astrocyte volume changes during ischemia in situ reveals two populations of astrocytes in the cortex of GFAP/EGFP mice. *Journal of neuroscience research* **87**, 96-111, doi:10.1002/jnr.21828 (2009).
96 Bachoo, R. M. *et al.* Molecular diversity of astrocytes with implications for neurological disorders. *Proceedings of the National Academy of Sciences of the United States of America* **101**, 8384-8389, doi:10.1073/pnas.0402140101 (2004).
97 Nielsen, S. *et al.* Specialized membrane domains for water transport in glial cells: high-resolution immunogold cytochemistry of aquaporin-4 in rat brain. *J Neurosci* **17**, 171-180 (1997).
98 Vives, V., Alonso, G., Solal, A. C., Joubert, D. & Legraverend, C. Visualization of S100B-positive neurons and glia in the central nervous system of EGFP transgenic mice. *The Journal of comparative neurology* **457**, 404-419, doi:10.1002/cne.10552 (2003).
99 Yang, Y. *et al.* Molecular comparison of GLT1+ and ALDH1L1+ astrocytes in vivo in astroglial reporter mice. *Glia* **59**, 200-207, doi:10.1002/glia.21089 (2011).
100 Nolte, C. *et al.* GFAP promoter-controlled EGFP-expressing transgenic mice: a tool to visualize astrocytes and astrogliosis in living brain tissue. *Glia* **33**, 72-86 (2001).
101 Zhuo, L. *et al.* Live astrocytes visualized by green fluorescent protein in transgenic mice. *Developmental biology* **187**, 36-42, doi:10.1006/dbio.1997.8601 (1997).
102 Regan, M. R. *et al.* Variations in promoter activity reveal a differential expression and physiology of glutamate transporters by glia in the developing and mature CNS. *The Journal of neuroscience : the official journal of the Society*

for Neuroscience **27**, 6607-6619, doi:10.1523/JNEUROSCI.0790-07.2007 (2007).
103 Schmid, R. S., Yokota, Y. & Anton, E. S. Generation and characterization of brain lipid-binding protein promoter-based transgenic mouse models for the study of radial glia. *Glia* **53**, 345-351, doi:10.1002/glia.20274 (2006).
104 Jungblut, M. *et al.* Isolation and characterization of living primary astroglial cells using the new GLAST-specific monoclonal antibody ACSA-1. *Glia* **60**, 894-907, doi:10.1002/glia.22322 (2012).
105 Pekny, M., Wilhelmsson, U. & Pekna, M. The dual role of astrocyte activation and reactive gliosis. *Neuroscience letters* **565**, 30-38, doi:10.1016/j.neulet.2013.12.071 (2014).
106 Pekny, M. & Nilsson, M. Astrocyte activation and reactive gliosis. *Glia* **50**, 427-434, doi:10.1002/glia.20207 (2005).
107 Miller, D. W., Cookson, M. R. & Dickson, D. W. Glial cell inclusions and the pathogenesis of neurodegenerative diseases. *Neuron glia biology* **1**, 13-21, doi:10.1017/s1740925x04000043 (2004).
108 Salmina, A. B. Neuron-glia interactions as therapeutic targets in neurodegeneration. *Journal of Alzheimer's disease : JAD* **16**, 485-502, doi:10.3233/JAD-2009-0988 (2009).
109 Hanisch, U. K. & Kettenmann, H. Microglia: active sensor and versatile effector cells in the normal and pathologic brain. *Nature neuroscience* **10**, 1387-1394, doi:10.1038/nn1997 (2007).
110 Landreth, G. E. Microglia in central nervous system diseases. *Journal of neuroimmune pharmacology : the official journal of the Society on NeuroImmune Pharmacology* **4**, 369-370, doi:10.1007/s11481-009-9173-3 (2009).
111 Mariani, M. M. & Kielian, T. Microglia in infectious diseases of the central nervous system. *Journal of neuroimmune pharmacology : the official journal of the Society on NeuroImmune Pharmacology* **4**, 448-461, doi:10.1007/s11481-009-9170-6 (2009).
112 Nelson, P. T., Soma, L. A. & Lavi, E. Microglia in diseases of the central nervous system. *Annals of medicine* **34**, 491-500 (2002).
113 Sheng, W. S., Hu, S., Feng, A. & Rock, R. B. Reactive oxygen species from human astrocytes induced functional impairment and oxidative damage. *Neurochemical research* **38**, 2148-2159, doi:10.1007/s11064-013-1123-z (2013).
114 Lenaz, G. Role of mitochondria in oxidative stress and ageing. *Biochimica et biophysica acta* **1366**, 53-67 (1998).
115 Snyder, C. M., Shroff, E. H., Liu, J. & Chandel, N. S. Nitric oxide induces cell death by regulating anti-apoptotic BCL-2 family members. *PloS one* **4**, e7059, doi:10.1371/journal.pone.0007059 (2009).
116 Park, S. J. *et al.* Astrocytes, but not microglia, rapidly sense H(2)O(2)via STAT6 phosphorylation, resulting in cyclooxygenase-2 expression and prostaglandin release. *Journal of immunology* **188**, 5132-5141, doi:10.4049/jimmunol.1101600 (2012).
117 Chen, Y. *et al.* Astrocytes protect neurons from nitric oxide toxicity by a glutathione-dependent mechanism. *Journal of neurochemistry* **77**, 1601-1610 (2001).

118 Blom, M. A. *et al.* NSAIDS inhibit the IL-1 beta-induced IL-6 release from human post-mortem astrocytes: the involvement of prostaglandin E2. *Brain Res* **777**, 210-218 (1997).

119 Eng, L. F. & Ghirnikar, R. S. GFAP and astrogliosis. *Brain pathology* **4**, 229-237 (1994).

120 Landis, D. M. The early reactions of non-neuronal cells to brain injury. *Annual review of neuroscience* **17**, 133-151, doi:10.1146/annurev.ne.17.030194.001025 (1994).

121 Pekny, M. & Pekna, M. Astrocyte intermediate filaments in CNS pathologies and regeneration. *The Journal of pathology* **204**, 428-437, doi:10.1002/path.1645 (2004).

122 Robel, S., Berninger, B. & Gotz, M. The stem cell potential of glia: lessons from reactive gliosis. *Nature reviews. Neuroscience* **12**, 88-104, doi:10.1038/nrn2978 (2011).

123 Faulkner, J. R. *et al.* Reactive astrocytes protect tissue and preserve function after spinal cord injury. *J Neurosci* **24**, 2143-2155, doi:10.1523/JNEUROSCI.3547-03.2004 (2004).

124 Yang, H. Y., Lieska, N., Shao, D., Kriho, V. & Pappas, G. D. Proteins of the intermediate filament cytoskeleton as markers for astrocytes and human astrocytomas. *Molecular and chemical neuropathology / sponsored by the International Society for Neurochemistry and the World Federation of Neurology and research groups on neurochemistry and cerebrospinal fluid* **21**, 155-176, doi:10.1007/BF02815349 (1994).

125 Fine, E. J., Ionita, C. C. & Lohr, L. The history of the development of the cerebellar examination. *Seminars in neurology* **22**, 375-384, doi:10.1055/s-2002-36759 (2002).

126 Rapoport, M., van Reekum, R. & Mayberg, H. The role of the cerebellum in cognition and behavior: a selective review. *The Journal of neuropsychiatry and clinical neurosciences* **12**, 193-198 (2000).

127 Gowen, E. & Miall, R. C. The cerebellum and motor dysfunction in neuropsychiatric disorders. *Cerebellum* **6**, 268-279, doi:10.1080/14734220601184821 (2007).

128 Kim, J. Y. *et al.* Medulloblastoma tumorigenesis diverges from cerebellar granule cell differentiation in patched heterozygous mice. *Developmental biology* **263**, 50-66 (2003).

129 Wang, V. Y. & Zoghbi, H. Y. Genetic regulation of cerebellar development. *Nature reviews. Neuroscience* **2**, 484-491, doi:10.1038/35081558 (2001).

130 Llinas, R., Hillman, D. E. & Precht, W. Neuronal circuit reorganization in mammalian agranular cerebellar cortex. *Journal of neurobiology* **4**, 69-94, doi:10.1002/neu.480040106 (1973).

131 Brodal, A. Anatomical studies of cerebellar fibre connections with special reference to problems of functional localization. *Progress in brain research* **25**, 135-173, doi:10.1016/S0079-6123(08)60964-4 (1967).

132 Hallonet, M. E., Teillet, M. A. & Le Douarin, N. M. A new approach to the development of the cerebellum provided by the quail-chick marker system. *Development* **108**, 19-31 (1990).

133 Wingate, R. J. & Hatten, M. E. The role of the rhombic lip in avian cerebellum development. *Development* **126**, 4395-4404 (1999).

134 Sgaier, S. K. *et al.* Morphogenetic and cellular movements that shape the mouse cerebellum; insights from genetic fate mapping. *Neuron* **45**, 27-40, doi:10.1016/j.neuron.2004.12.021 (2005).
135 Larsell, O. [The corpus cerebelli in birds & mammals]. *Archivio di scienze biologiche* **42**, 90-104 (1958).
136 Larsell, O. The morphogenesis and adult pattern of the lobules and fissures of the cerebellum of the white rat. *The Journal of comparative neurology* **97**, 281-356 (1952).
137 Sudarov, A. & Joyner, A. L. Cerebellum morphogenesis: the foliation pattern is orchestrated by multi-cellular anchoring centers. *Neural development* **2**, 26, doi:10.1186/1749-8104-2-26 (2007).
138 Sillitoe, R. V. & Joyner, A. L. Morphology, molecular codes, and circuitry produce the three-dimensional complexity of the cerebellum. *Annual review of cell and developmental biology* **23**, 549-577, doi:10.1146/annurev.cellbio.23.090506.123237 (2007).
139 Martinez, S. & Alvarado-Mallart, R. M. Rostral Cerebellum Originates from the Caudal Portion of the So-Called 'Mesencephalic' Vesicle: A Study Using Chick/Quail Chimeras. *The European journal of neuroscience* **1**, 549-560 (1989).
140 Zhang, L. & Goldman, J. E. Developmental fates and migratory pathways of dividing progenitors in the postnatal rat cerebellum. *The Journal of comparative neurology* **370**, 536-550, doi:10.1002/(SICI)1096-9861(19960708)370:4<536::AID-CNE9>3.0.CO;2-5 (1996).
141 Hoshino, M. *et al.* Ptf1a, a bHLH transcriptional gene, defines GABAergic neuronal fates in cerebellum. *Neuron* **47**, 201-213, doi:10.1016/j.neuron.2005.06.007 (2005).
142 Cheng, L. *et al.* Tlx3 and Tlx1 are post-mitotic selector genes determining glutamatergic over GABAergic cell fates. *Nature neuroscience* **7**, 510-517, doi:10.1038/nn1221 (2004).
143 Morales, D. & Hatten, M. E. Molecular markers of neuronal progenitors in the embryonic cerebellar anlage. *J Neurosci* **26**, 12226-12236, doi:10.1523/JNEUROSCI.3493-06.2006 (2006).
144 Altman, J. & Bayer, S. A. Embryonic development of the rat cerebellum. I. Delineation of the cerebellar primordium and early cell movements. *The Journal of comparative neurology* **231**, 1-26, doi:10.1002/cne.902310103 (1985).
145 Pierce, E. T. Histogenesis of the deep cerebellar nuclei in the mouse: an autoradiographic study. *Brain research* **95**, 503-518 (1975).
146 Hatten, M. E. & Heintz, N. Mechanisms of neural patterning and specification in the developing cerebellum. *Annual review of neuroscience* **18**, 385-408, doi:10.1146/annurev.ne.18.030195.002125 (1995).
147 Sidman, R. L. & Rakic, P. Neuronal migration, with special reference to developing human brain: a review. *Brain research* **62**, 1-35 (1973).
148 Altman, J. Postnatal development of the cerebellar cortex in the rat. I. The external germinal layer and the transitional molecular layer. *The Journal of comparative neurology* **145**, 353-397, doi:10.1002/cne.901450305 (1972).
149 Silbereis, J., Cheng, E., Ganat, Y. M., Ment, L. R. & Vaccarino, F. M. Precursors with glial fibrillary acidic protein promoter activity transiently generate GABA interneurons in the postnatal cerebellum. *Stem cells* **27**, 1152-1163, doi:10.1002/stem.18 (2009).

150 Alder, J., Cho, N. K. & Hatten, M. E. Embryonic precursor cells from the rhombic lip are specified to a cerebellar granule neuron identity. *Neuron* **17**, 389-399 (1996).
151 Gao, W. Q. & Hatten, M. E. Immortalizing oncogenes subvert the establishment of granule cell identity in developing cerebellum. *Development* **120**, 1059-1070 (1994).
152 Wechsler-Reya, R. J. & Scott, M. P. Control of neuronal precursor proliferation in the cerebellum by Sonic Hedgehog. *Neuron* **22**, 103-114 (1999).
153 Miller, T. E. *et al.* Lgr5 Marks Post-Mitotic, Lineage Restricted Cerebellar Granule Neurons during Postnatal Development. *PLoS One* **9**, e114433, doi:10.1371/journal.pone.0114433 (2014).
154 Akazawa, C., Ishibashi, M., Shimizu, C., Nakanishi, S. & Kageyama, R. A mammalian helix-loop-helix factor structurally related to the product of Drosophila proneural gene atonal is a positive transcriptional regulator expressed in the developing nervous system. *The Journal of biological chemistry* **270**, 8730-8738 (1995).
155 Wingate, R. J. The rhombic lip and early cerebellar development. *Current opinion in neurobiology* **11**, 82-88 (2001).
156 Edmondson, J. C. & Hatten, M. E. Glial-guided granule neuron migration in vitro: a high-resolution time-lapse video microscopic study. *J Neurosci* **7**, 1928-1934 (1987).
157 Hatten, M. E. Neuronal regulation of astroglial morphology and proliferation in vitro. *The Journal of cell biology* **100**, 384-396 (1985).
158 Gasser, U. E. & Hatten, M. E. Central nervous system neurons migrate on astroglial fibers from heterotypic brain regions in vitro. *Proceedings of the National Academy of Sciences of the United States of America* **87**, 4543-4547 (1990).
159 Hatten, M. E. Central nervous system neuronal migration. *Annual review of neuroscience* **22**, 511-539, doi:10.1146/annurev.neuro.22.1.511 (1999).
160 Edmondson, J. C., Liem, R. K., Kuster, J. E. & Hatten, M. E. Astrotactin: a novel neuronal cell surface antigen that mediates neuron-astroglial interactions in cerebellar microcultures. *The Journal of cell biology* **106**, 505-517 (1988).
161 Borghesani, P. R. *et al.* BDNF stimulates migration of cerebellar granule cells. *Development* **129**, 1435-1442 (2002).
162 Mori, T. *et al.* Inducible gene deletion in astroglia and radial glia--a valuable tool for functional and lineage analysis. *Glia* **54**, 21-34, doi:10.1002/glia.20350 (2006).
163 Carletti, B. & Rossi, F. Neurogenesis in the cerebellum. *The Neuroscientist : a review journal bringing neurobiology, neurology and psychiatry* **14**, 91-100, doi:10.1177/1073858407304629 (2008).
164 van der Lugt, N. M. *et al.* Posterior transformation, neurological abnormalities, and severe hematopoietic defects in mice with a targeted deletion of the bmi-1 proto-oncogene. *Genes & development* **8**, 757-769 (1994).
165 Englund, C. *et al.* Unipolar brush cells of the cerebellum are produced in the rhombic lip and migrate through developing white matter. *J Neurosci* **26**, 9184-9195, doi:10.1523/JNEUROSCI.1610-06.2006 (2006).
166 Jensen, P., Smeyne, R. & Goldowitz, D. Analysis of cerebellar development in math1 null embryos and chimeras. *J Neurosci* **24**, 2202-2211, doi:10.1523/JNEUROSCI.3427-03.2004 (2004).

167 Silbereis, J. *et al.* Astroglial cells in the external granular layer are precursors of cerebellar granule neurons in neonates. *Molecular and cellular neurosciences* **44**, 362-373, doi:10.1016/j.mcn.2010.05.001 (2010).

168 Okano-Uchida, T., Himi, T., Komiya, Y. & Ishizaki, Y. Cerebellar granule cell precursors can differentiate into astroglial cells. *Proceedings of the National Academy of Sciences of the United States of America* **101**, 1211-1216, doi:10.1073/pnas.0307972100 (2004).

169 Buffo, A. & Rossi, F. Origin, lineage and function of cerebellar glia. *Prog Neurobiol* **109**, 42-63, doi:10.1016/j.pneurobio.2013.08.001 (2013).

170 Bower, J. M. The organization of cerebellar cortical circuitry revisited: implications for function. *Annals of the New York Academy of Sciences* **978**, 135-155 (2002).

171 Voogd, J. & Glickstein, M. The anatomy of the cerebellum. *Trends in cognitive sciences* **2**, 307-313 (1998).

172 Alcantara, S., Ruiz, M., De Castro, F., Soriano, E. & Sotelo, C. Netrin 1 acts as an attractive or as a repulsive cue for distinct migrating neurons during the development of the cerebellar system. *Development* **127**, 1359-1372 (2000).

173 Ashwell, K. W. & Zhang, L. L. Ontogeny of afferents to the fetal rat cerebellum. *Acta anatomica* **145**, 17-23 (1992).

174 Komine, O. *et al.* The monolayer formation of Bergmann glial cells is regulated by Notch/RBP-J signaling. *Developmental biology* **311**, 238-250, doi:10.1016/j.ydbio.2007.08.042 (2007).

175 Xu, H. *et al.* Bergmann glia function in granule cell migration during cerebellum development. *Molecular neurobiology* **47**, 833-844, doi:10.1007/s12035-013-8405-y (2013).

176 Seil, F. J. Interactions between cerebellar Purkinje cells and their associated astrocytes. *Histology and histopathology* **16**, 955-968 (2001).

177 Hatten, M. E., Liem, R. K. & Mason, C. A. Two forms of cerebellar glial cells interact differently with neurons in vitro. *The Journal of cell biology* **98**, 193-204 (1984).

178 Kenney, A. M. & Segal, R. A. Subtracting the Math: prominin-positive cerebellar stem cells in white matter. *Nature neuroscience* **8**, 699-701, doi:10.1038/nn0605-699 (2005).

179 Lee, A. *et al.* Isolation of neural stem cells from the postnatal cerebellum. *Nature neuroscience* **8**, 723-729, doi:10.1038/nn1473 (2005).

180 Kobielak, A. & Fuchs, E. Alpha-catenin: at the junction of intercellular adhesion and actin dynamics. *Nature reviews. Molecular cell biology* **5**, 614-625, doi:10.1038/nrm1433 (2004).

181 Tanaka, M. *et al.* Connexin43 and bergmann glial gap junctions in cerebellar function. *Frontiers in neuroscience* **2**, 225-233, doi:10.3389/neuro.01.038.2008 (2008).

182 Polgar, L. The catalytic triad of serine peptidases. *Cellular and molecular life sciences : CMLS* **62**, 2161-2172, doi:10.1007/s00018-005-5160-x (2005).

183 Hedin, S. G. Observations on the action of trypsin. *The Journal of physiology* **32**, 468-485 (1905).

184 Milstein, C. The hybridoma revolution: an offshoot of basic research. *BioEssays : news and reviews in molecular, cellular and developmental biology* **21**, 966-973, doi:10.1002/(SICI)1521-1878(199911)21:11<966::AID-BIES9>3.0.CO;2-Z (1999).

185 Kohler, G. & Milstein, C. Continuous cultures of fused cells secreting antibody of predefined specificity. *Nature* **256**, 495-497 (1975).
186 Tjio, J. H. & Puck, T. T. Genetics of somatic mammalian cells. II. Chromosomal constitution of cells in tissue culture. *The Journal of experimental medicine* **108**, 259-268 (1958).
187 Wurm, F. M. Production of recombinant protein therapeutics in cultivated mammalian cells. *Nature biotechnology* **22**, 1393-1398, doi:10.1038/nbt1026 (2004).
188 Graham, F. L., Smiley, J., Russell, W. C. & Nairn, R. Characteristics of a human cell line transformed by DNA from human adenovirus type 5. *The Journal of general virology* **36**, 59-74 (1977).
189 Siden, E. J., Baltimore, D., Clark, D. & Rosenberg, N. E. Immunoglobulin synthesis by lymphoid cells transformed in vitro by Abelson murine leukemia virus. *Cell* **16**, 389-396 (1979).
190 Jacques, T. S. *et al.* Neural precursor cell chain migration and division are regulated through different beta1 integrins. *Development* **125**, 3167-3177 (1998).
191 Neumann, E., Schaefer-Ridder, M., Wang, Y. & Hofschneider, P. H. Gene transfer into mouse lyoma cells by electroporation in high electric fields. *The EMBO journal* **1**, 841-845 (1982).
192 Aihara, H. & Miyazaki, J. Gene transfer into muscle by electroporation in vivo. *Nature biotechnology* **16**, 867-870, doi:10.1038/nbt0998-867 (1998).
193 de Melo, J. & Blackshaw, S. In vivo electroporation of developing mouse retina. *Journal of visualized experiments : JoVE*, doi:10.3791/2847 (2011).
194 Saito, T. & Nakatsuji, N. Efficient gene transfer into the embryonic mouse brain using in vivo electroporation. *Developmental biology* **240**, 237-246, doi:10.1006/dbio.2001.0439 (2001).
195 Boutin, C., Diestel, S., Desoeuvre, A., Tiveron, M. C. & Cremer, H. Efficient in vivo electroporation of the postnatal rodent forebrain. *PloS one* **3**, e1883, doi:10.1371/journal.pone.0001883 (2008).
196 Schubert, W. *et al.* Analyzing proteome topology and function by automated multidimensional fluorescence microscopy. *Nature biotechnology* **24**, 1270-1278, doi:10.1038/nbt1250 (2006).
197 Frei, A. P. *et al.* Direct identification of ligand-receptor interactions on living cells and tissues. *Nature biotechnology* **30**, 997-1001, doi:10.1038/nbt.2354 (2012).
198 Frei, A. P., Moest, H., Novy, K. & Wollscheid, B. Ligand-based receptor identification on living cells and tissues using TRICEPS. *Nature protocols* **8**, 1321-1336, doi:10.1038/nprot.2013.072 (2013).
199 Fleige, S. & Pfaffl, M. W. RNA integrity and the effect on the real-time qRT-PCR performance. *Molecular aspects of medicine* **27**, 126-139, doi:10.1016/j.mam.2005.12.003 (2006).
200 Hennersdorf, F. *et al.* Identification of CD13, CD107a, and CD164 as novel basophil-activation markers and dissection of two response patterns in time kinetics of IgE-dependent upregulation. *Cell research* **15**, 325-335, doi:10.1038/sj.cr.7290301 (2005).
201 Nomenclature for clusters of differentiation (CD) of antigens defined on human leukocyte populations. IUIS-WHO Nomenclature Subcommittee. *Bulletin of the World Health Organization* **62**, 809-815 (1984).

202 Pennartz, S., Reiss, S., Biloune, R., Hasselmann, D. & Bosio, A. Generation of single-cell suspensions from mouse neural tissue. *Journal of visualized experiments : JoVE*, doi:10.3791/1267 (2009).
203 Kokovay, E. *et al.* VCAM1 is essential to maintain the structure of the SVZ niche and acts as an environmental sensor to regulate SVZ lineage progression. *Cell stem cell* **11**, 220-230, doi:10.1016/j.stem.2012.06.016 (2012).
204 Bayraktar, O. A., Fuentealba, L. C., Alvarez-Buylla, A. & Rowitch, D. H. Astrocyte Development and Heterogeneity. *Cold Spring Harbor perspectives in biology*, doi:10.1101/cshperspect.a020362 (2014).
205 Chaboub, L. S. & Deneen, B. Developmental origins of astrocyte heterogeneity: the final frontier of CNS development. *Developmental neuroscience* **34**, 379-388, doi:10.1159/000343723
000343723 (2012).
206 Brooks, P. C., Lin, J. M., French, D. L. & Quigley, J. P. Subtractive immunization yields monoclonal antibodies that specifically inhibit metastasis. *The Journal of cell biology* **122**, 1351-1359 (1993).
207 Reyes-Haro, D., Mora-Loyola, E., Soria-Ortiz, B. & Garcia-Colunga, J. Regional density of glial cells in the rat corpus callosum. *Biological research* **46**, 27-32, doi:10.4067/S0716-97602013000100004 (2013).
208 Moransard, M. *et al.* NG2 expressed by macrophages and oligodendrocyte precursor cells is dispensable in experimental autoimmune encephalomyelitis. *Brain : a journal of neurology* **134**, 1315-1330, doi:10.1093/brain/awr070 (2011).
209 Baumann, N. & Pham-Dinh, D. Biology of oligodendrocyte and myelin in the mammalian central nervous system. *Physiological reviews* **81**, 871-927 (2001).
210 Kohwi, M. *et al.* A subpopulation of olfactory bulb GABAergic interneurons is derived from Emx1- and Dlx5/6-expressing progenitors. *J Neurosci* **27**, 6878-6891 (2007).
211 Soltani, M. H. *et al.* Microtubule-associated protein 2, a marker of neuronal differentiation, induces mitotic defects, inhibits growth of melanoma cells, and predicts metastatic potential of cutaneous melanoma. *The American journal of pathology* **166**, 1841-1850 (2005).
212 Sehgal, A. *et al.* Cell adhesion molecule Nr-CAM is over-expressed in human brain tumors. *International journal of cancer. Journal international du cancer* **76**, 451-458 (1998).
213 Lein, E. S. *et al.* Genome-wide atlas of gene expression in the adult mouse brain. *Nature* **445**, 168-176, doi:10.1038/nature05453 (2007).
214 Minelli, A., Barbaresi, P. & Conti, F. Postnatal development of high-affinity plasma membrane GABA transporters GAT-2 and GAT-3 in the rat cerebral cortex. *Brain research. Developmental brain research* **142**, 7-18 (2003).
215 Minelli, A., DeBiasi, S., Brecha, N. C., Zuccarello, L. V. & Conti, F. GAT-3, a high-affinity GABA plasma membrane transporter, is localized to astrocytic processes, and it is not confined to the vicinity of GABAergic synapses in the cerebral cortex. *J Neurosci* **16**, 6255-6264 (1996).
216 Aub, J. C., Tieslau, C. & Lankester, A. Reactions of Normal and Tumor Cell Surfaces to Enzymes. I. Wheat-Germ Lipase and Associated Mucopolysaccharides. *Proceedings of the National Academy of Sciences of the United States of America* **50**, 613-619 (1963).

217 Wright, C. S. Structural comparison of the two distinct sugar binding sites in wheat germ agglutinin isolectin II. *Journal of molecular biology* **178**, 91-104 (1984).
218 Rothwangl, K. B., Manicassamy, B., Uprichard, S. L. & Rong, L. Dissecting the role of putative CD81 binding regions of E2 in mediating HCV entry: putative CD81 binding region 1 is not involved in CD81 binding. *Virology journal* **5**, 46, doi:10.1186/1743-422X-5-46 (2008).
219 Orentas, D. M. & Miller, R. H. A novel form of migration of glial precursors. *Glia* **16**, 27-39, doi:10.1002/(SICI)1098-1136(199601)16:1<27::AID-GLIA4>3.0.CO;2-8 (1996).
220 Lee, J. C., Mayer-Proschel, M. & Rao, M. S. Gliogenesis in the central nervous system. *Glia* **30**, 105-121 (2000).
221 Stallcup, W. B. & Beasley, L. Bipotential glial precursor cells of the optic nerve express the NG2 proteoglycan. *The Journal of neuroscience : the official journal of the Society for Neuroscience* **7**, 2737-2744 (1987).
222 Chang, M. Y., Park, C. H., Son, H., Lee, Y. S. & Lee, S. H. Developmental stage-dependent self-regulation of embryonic cortical precursor cell survival and differentiation by leukemia inhibitory factor. *Cell death and differentiation* **11**, 985-996, doi:10.1038/sj.cdd.4401426 (2004).
223 Fernandez, M. E., Croce, S., Boutin, C., Cremer, H. & Raineteau, O. Targeted electroporation of defined lateral ventricular walls: a novel and rapid method to study fate specification during postnatal forebrain neurogenesis. *Neural development* **6**, 13, doi:10.1186/1749-8104-6-13 (2011).
224 Pastrana, E., Cheng, L. C. & Doetsch, F. Simultaneous prospective purification of adult subventricular zone neural stem cells and their progeny. *Proceedings of the National Academy of Sciences of the United States of America* **106**, 6387-6392, doi:10.1073/pnas.0810407106 (2009).
225 Harada, T. *et al.* Functions of the two glutamate transporters GLAST and GLT-1 in the retina. *Proceedings of the National Academy of Sciences of the United States of America* **95**, 4663-4666 (1998).
226 Lehre, K. P., Davanger, S. & Danbolt, N. C. Localization of the glutamate transporter protein GLAST in rat retina. *Brain Res* **744**, 129-137 (1997).
227 Reichenbach, A., Derouiche, A. & Kirchhoff, F. Morphology and dynamics of perisynaptic glia. *Brain research reviews* **63**, 11-25, doi:10.1016/j.brainresrev.2010.02.003 (2010).
228 Tuppen, H. A., Blakely, E. L., Turnbull, D. M. & Taylor, R. W. Mitochondrial DNA mutations and human disease. *Biochimica et biophysica acta* **1797**, 113-128, doi:10.1016/j.bbabio.2009.09.005 (2010).
229 Consalez, G. G. & Hawkes, R. The compartmental restriction of cerebellar interneurons. *Frontiers in neural circuits* **6**, 123, doi:10.3389/fncir.2012.00123 (2012).
230 Takayasu, Y. *et al.* Differential roles of glial and neuronal glutamate transporters in Purkinje cell synapses. *J Neurosci* **25**, 8788-8793, doi:10.1523/JNEUROSCI.1020-05.2005 (2005).
231 Yamada, K. *et al.* Dynamic transformation of Bergmann glial fibers proceeds in correlation with dendritic outgrowth and synapse formation of cerebellar Purkinje cells. *The Journal of comparative neurology* **418**, 106-120 (2000).
232 Fletcher, C., Norman, D. J. & Heintz, N. Genetic mapping of meander tail, a mouse mutation affecting cerebellar development. *Genomics* **9**, 647-655 (1991).

233 Koepsell, H., Lips, K. & Volk, C. Polyspecific organic cation transporters: structure, function, physiological roles, and biopharmaceutical implications. *Pharmaceutical research* **24**, 1227-1251, doi:10.1007/s11095-007-9254-z (2007).
234 Sato, T. & Nakamura, H. The Fgf8 signal causes cerebellar differentiation by activating the Ras-ERK signaling pathway. *Development* **131**, 4275-4285, doi:10.1242/dev.01281 (2004).
235 Logan, C. Y. & Nusse, R. The Wnt signaling pathway in development and disease. *Annual review of cell and developmental biology* **20**, 781-810, doi:10.1146/annurev.cellbio.20.010403.113126 (2004).
236 Machold, R. P., Kittell, D. J. & Fishell, G. J. Antagonism between Notch and bone morphogenetic protein receptor signaling regulates neurogenesis in the cerebellar rhombic lip. *Neural development* **2**, 5, doi:10.1186/1749-8104-2-5 (2007).
237 Sivakumar, K. C., Dhanesh, S. B., Shobana, S., James, J. & Mundayoor, S. A systems biology approach to model neural stem cell regulation by notch, shh, wnt, and EGF signaling pathways. *Omics : a journal of integrative biology* **15**, 729-737, doi:10.1089/omi.2011.0011 (2011).
238 Barker, N. *et al.* Identification of stem cells in small intestine and colon by marker gene Lgr5. *Nature* **449**, 1003-1007, doi:10.1038/nature06196 (2007).
239 Barker, N., Tan, S. & Clevers, H. Lgr proteins in epithelial stem cell biology. *Development* **140**, 2484-2494, doi:10.1242/dev.083113 (2013).
240 Alenina, N., Bashammakh, S. & Bader, M. Specification and differentiation of serotonergic neurons. *Stem cell reviews* **2**, 5-10, doi:10.1007/s12015-006-0002-2 (2006).
241 Leto, K., Carletti, B., Williams, I. M., Magrassi, L. & Rossi, F. Different types of cerebellar GABAergic interneurons originate from a common pool of multipotent progenitor cells. *J Neurosci* **26**, 11682-11694, doi:10.1523/JNEUROSCI.3656-06.2006 (2006).
242 Pascual, M. *et al.* Cerebellar GABAergic progenitors adopt an external granule cell-like phenotype in the absence of Ptf1a transcription factor expression. *Proceedings of the National Academy of Sciences of the United States of America* **104**, 5193-5198, doi:10.1073/pnas.0605699104 (2007).
243 Kim, E. J., Battiste, J., Nakagawa, Y. & Johnson, J. E. Ascl1 (Mash1) lineage cells contribute to discrete cell populations in CNS architecture. *Molecular and cellular neurosciences* **38**, 595-606, doi:10.1016/j.mcn.2008.05.008 (2008).
244 Leto, K., Bartolini, A. & Rossi, F. The prospective white matter: an atypical neurogenic niche in the developing cerebellum. *Archives italiennes de biologie* **148**, 137-146 (2010).
245 Chung, S. *et al.* Wnt1-lmx1a forms a novel autoregulatory loop and controls midbrain dopaminergic differentiation synergistically with the SHH-FoxA2 pathway. *Cell stem cell* **5**, 646-658, doi:10.1016/j.stem.2009.09.015 (2009).
246 Yuasa, S. Bergmann glial development in the mouse cerebellum as revealed by tenascin expression. *Anatomy and embryology* **194**, 223-234 (1996).
247 Rash, J. E. *et al.* Identification of cells expressing Cx43, Cx30, Cx26, Cx32 and Cx36 in gap junctions of rat brain and spinal cord. *Cell communication & adhesion* **8**, 315-320 (2001).
248 Gazit, R., Krizhanovsky, V. & Ben-Arie, N. Math1 controls cerebellar granule cell differentiation by regulating multiple components of the Notch signaling pathway. *Development* **131**, 903-913, doi:10.1242/dev.00982 (2004).

249 Fleming, J. T. *et al.* The Purkinje neuron acts as a central regulator of spatially and functionally distinct cerebellar precursors. *Developmental cell* **27**, 278-292, doi:10.1016/j.devcel.2013.10.008 (2013).
250 Kimelberg, H. K. Supportive or information-processing functions of the mature protoplasmic astrocyte in the mammalian CNS? A critical appraisal. *Neuron glia biology* **3**, 181-189, doi:10.1017/S1740925X08000094 (2007).
251 Cai, J. *et al.* A crucial role for Olig2 in white matter astrocyte development. *Development* **134**, 1887-1899, doi:10.1242/dev.02847 (2007).
252 Sauvageot, C. M. & Stiles, C. D. Molecular mechanisms controlling cortical gliogenesis. *Current opinion in neurobiology* **12**, 244-249 (2002).
253 Hochstim, C., Deneen, B., Lukaszewicz, A., Zhou, Q. & Anderson, D. J. Identification of positionally distinct astrocyte subtypes whose identities are specified by a homeodomain code. *Cell* **133**, 510-522, doi:10.1016/j.cell.2008.02.046 (2008).
254 Cammer, W. Glutamine synthetase in the central nervous system is not confined to astrocytes. *Journal of neuroimmunology* **26**, 173-178 (1990).
255 Rothstein, J. D. *et al.* Localization of neuronal and glial glutamate transporters. *Neuron* **13**, 713-725 (1994).
256 Takumi, T. *et al.* A novel ATP-dependent inward rectifier potassium channel expressed predominantly in glial cells. *The Journal of biological chemistry* **270**, 16339-16346 (1995).
257 Lee, Y., Messing, A., Su, M. & Brenner, M. GFAP promoter elements required for region-specific and astrocyte-specific expression. *Glia* **56**, 481-493, doi:10.1002/glia.20622 (2008).
258 Schwandt, E. [Protides of biological fluids. Report on the 19th colloquium Brugge-Belgium]. *Fortschritte der Medizin* **89**, 8-13 (1971).
259 Corver, W. E., Cornelisse, C. J., Hermans, J. & Fleuren, G. J. Limited loss of nine tumor-associated surface antigenic determinants after tryptic cell dissociation. *Cytometry* **19**, 267-272, doi:10.1002/cyto.990190311 (1995).
260 Shen, Q. *et al.* Adult SVZ stem cells lie in a vascular niche: a quantitative analysis of niche cell-cell interactions. *Cell stem cell* **3**, 289-300, doi:10.1016/j.stem.2008.07.026 (2008).
261 Beurel, E. & Jope, R. S. Differential regulation of STAT family members by glycogen synthase kinase-3. *The Journal of biological chemistry* **283**, 21934-21944, doi:10.1074/jbc.M802481200 (2008).
262 Daley, D. O. The assembly of membrane proteins into complexes. *Current opinion in structural biology* **18**, 420-424, doi:10.1016/j.sbi.2008.04.006 (2008).
263 Matesic, D. F., Manning, D. R., Wolfe, B. B. & Luthin, G. R. Pharmacological and biochemical characterization of complexes of muscarinic acetylcholine receptor and guanine nucleotide-binding protein. *The Journal of biological chemistry* **264**, 21638-21645 (1989).
264 Kaboord, B. & Perr, M. Isolation of proteins and protein complexes by immunoprecipitation. *Methods in molecular biology* **424**, 349-364, doi:10.1007/978-1-60327-064-9_27 (2008).
265 Birikh, K. R., Sklan, E. H., Shoham, S. & Soreq, H. Interaction of "readthrough" acetylcholinesterase with RACK1 and PKCbeta II correlates with intensified fear-induced conflict behavior. *Proceedings of the National Academy of Sciences of the United States of America* **100**, 283-288, doi:10.1073/pnas.0135647100 (2003).

266 Walsh, C. Posttranslational modification of proteins: Expanding nature's inventory. *Roberts and Co. Publishers, Englewood, CO. ISBN 0974707732.* (2006).
267 Bleckmann, C. *et al.* O-glycosylation pattern of CD24 from mouse brain. *Biological chemistry* **390**, 627-645, doi:10.1515/BC.2009.044 (2009).
268 Stanley, P. & Cummings, R. D. in *Essentials of Glycobiology* (eds A. Varki *et al.*) (2009).
269 Merkle, F. T., Tramontin, A. D., Garcia-Verdugo, J. M. & Alvarez-Buylla, A. Radial glia give rise to adult neural stem cells in the subventricular zone. *Proceedings of the National Academy of Sciences of the United States of America* **101**, 17528-17532, doi:10.1073/pnas.0407893101 (2004).
270 Hockfield, S. & McKay, R. D. Identification of major cell classes in the developing mammalian nervous system. *The Journal of neuroscience : the official journal of the Society for Neuroscience* **5**, 3310-3328 (1985).
271 Obermair, F. J. *et al.* A novel classification of quiescent and transit amplifying adult neural stem cells by surface and metabolic markers permits a defined simultaneous isolation. *Stem cell research* **5**, 131-143, doi:10.1016/j.scr.2010.05.001 (2010).
272 Stump, G. *et al.* Notch1 and its ligands Delta-like and Jagged are expressed and active in distinct cell populations in the postnatal mouse brain. *Mechanisms of development* **114**, 153-159 (2002).
273 Kero, D. *et al.* Expression of Ki-67, Oct-4, gamma-tubulin and alpha-tubulin in human tooth development. *Archives of oral biology* **59**, 1119-1129, doi:10.1016/j.archoralbio.2014.05.025 (2014).
274 Leto, K., Rolando, C. & Rossi, F. The genesis of cerebellar GABAergic neurons: fate potential and specification mechanisms. *Frontiers in neuroanatomy* **6**, 6, doi:10.3389/fnana.2012.00006 (2012).
275 Naruse, M., Shibasaki, K., Yokoyama, S., Kurachi, M. & Ishizaki, Y. Dynamic changes of CD44 expression from progenitors to subpopulations of astrocytes and neurons in developing cerebellum. *PloS one* **8**, e53109, doi:10.1371/journal.pone.0053109 (2013).
276 Cai, N., Kurachi, M., Shibasaki, K., Okano-Uchida, T. & Ishizaki, Y. CD44-positive cells are candidates for astrocyte precursor cells in developing mouse cerebellum. *Cerebellum* **11**, 181-193, doi:10.1007/s12311-011-0294-x (2012).
277 Leto, K. *et al.* Laminar fate and phenotype specification of cerebellar GABAergic interneurons. *J Neurosci* **29**, 7079-7091, doi:10.1523/JNEUROSCI.0957-09.2009 (2009).
278 Corbeil, D. *et al.* Expression of distinct splice variants of the stem cell marker prominin-1 (CD133) in glial cells. *Glia* **57**, 860-874, doi:10.1002/glia.20812 (2009).
279 Alcock, J. & Sottile, V. Dynamic distribution and stem cell characteristics of Sox1-expressing cells in the cerebellar cortex. *Cell research* **19**, 1324-1333, doi:10.1038/cr.2009.119 (2009).
280 Alvarez-Dolado, M., Gonzalez-Sancho, J. M., Bernal, J. & Munoz, A. Developmental expression of the tenascin-C is altered by hypothyroidism in the rat brain. *Neuroscience* **84**, 309-322 (1998).
281 Grimaldi, P., Parras, C., Guillemot, F., Rossi, F. & Wassef, M. Origins and control of the differentiation of inhibitory interneurons and glia in the cerebellum. *Developmental biology* **328**, 422-433, doi:10.1016/j.ydbio.2009.02.008 (2009).

282 Lee, E. Y. *et al.* Hedgehog pathway-regulated gene networks in cerebellum development and tumorigenesis. *Proceedings of the National Academy of Sciences of the United States of America* **107**, 9736-9741, doi:10.1073/pnas.1004602107 (2010).
283 Corrales, J. D., Rocco, G. L., Blaess, S., Guo, Q. & Joyner, A. L. Spatial pattern of sonic hedgehog signaling through Gli genes during cerebellum development. *Development* **131**, 5581-5590, doi:10.1242/dev.01438 (2004).
284 Lutz, S. E. *et al.* Deletion of astrocyte connexins 43 and 30 leads to a dysmyelinating phenotype and hippocampal CA1 vacuolation. *J Neurosci* **29**, 7743-7752, doi:10.1523/JNEUROSCI.0341-09.2009 (2009).
285 Larsen, K., Momeni, J., Farajzadeh, L. & Bendixen, C. Porcine SLITRK1: Molecular cloning and characterization. *FEBS open bio* **4**, 872-878, doi:10.1016/j.fob.2014.10.001 (2014).

IV Acknowledgement

I am very grateful to Prof. Dr. Elena I. Rugarli and Prof. Dr. Thomas Langmann for taking over university supervision of my PhD project. Thank you very much for your help and support. In addition, I would like to thank Stefan Miltenyi for the possibility to perform my PhD project at Miltenyi Biotec. At this point I would also like to thank Dr. Andreas Bosio and Dr. Melanie Jungblut for the initiation of this project, their support and advice throughout this study.

Besides, I would like to thank Dr. Harold Cremer and Dr. Marie-Catherine Tiveron for their supervision during my internships at the IBDM. In addition, I am grateful to Dr. Marie-Catherine Tiveron and Dr. Philipp Follert for teaching me the *in vivo* electroporation technique and in company with Dr. Serena Barral for teaching me IHC stainings.

In addition, I would like to thank Dr. Annalisa Buffo and Dr. Elena Parmigiani from the NICO in Turin for their support in previous and ongoing collaborations.

I am grateful to all people that further supported me during my PhD project at Miltenyi Biotec including: Dr. Stefan Tomiuk and Michail Knauel for bioinformatic support, Dr. Frank Single, Paul Colesar and Merlin Siewert for providing animals and supporting breeding and animal shipping. Thanks to all members of the Neuroscience group (Ina Herzig, Sandy Reiß and Katrin Portugall), to supervisors and (former) students at Miltenyi Biotec for great discussion at Studi Clubs and symposia. I thank Dr. Eva Almajan and Prof. Dr. Elena Rugarli for providing sections of their mouse model. I thank Dr. Bernd Wollscheid, Dr. Andreas Frei, Dr. Jens Hellmer as well as Dr. Tobias Haas for their support on proteome analysis, immunoprecipitation and mass spectrometry analysis. In addition, I'd like to thank Dr. Thomas Rockel and Jan Drewes for help with the MICS experiments.

I am very grateful to all people involved in the proofreading process, especially Dr. Tilo Eichler. Next, I have to mention two people that became really good friends during my PhD and I don't want to miss any day we spend together:

Dr. Andrea (Fratelli) Aloia and Daniela Lehnen.

Last but not least, I would like to thank my mother for her support – Although, she never really knew what my work is all about.

Erklärung

Ich versichere, dass ich die von mir vorgelegte Dissertation selbständig angefertigt, die benutzten Quellen und Hilfsmittel vollständig angegeben und die Stellen der Arbeit − einschließlich Tabellen, Karten und Abbildungen −, die anderen Werken im Wortlaut oder dem Sinn nach entnommen sind, in jedem Einzelfall als Entlehnung kenntlich gemacht habe; dass diese Dissertation noch keiner anderen Fakultät oder Universität zur Prüfung vorgelegen hat; dass sie − abgesehen von unten angegebenen Teilpublikationen − noch nicht veröffentlicht worden ist sowie, dass ich eine solche Veröffentlichung vor Abschluss des Promotionsverfahrens nicht vornehmen werde. Die Bestimmungen der Promotionsordnung sind mir bekannt. Die von mir vorgelegte Dissertation ist von Frau Prof. Dr. Elena I. Rugarli betreut worden.

Köln, den 23.04.2015

Christina Kantzer

~~Teilpublikationen:~~

Die vorliegende Arbeit wurde in der Zeit von Oktober 2011 bis April 2015 unter der Betreuung von Frau Prof. Dr. Elena I. Rugarli, Institut für Genetik der Universität zu Köln angefertigt. Dabei wurden die zugrunde liegenden Experimente in der Forschungs- und Entwicklungsabteilung der Miltenyi Biotec GmbH in Bergisch Gladbach durchgeführt.
Betreuer dieser Arbeit innerhalb der Firma Miltenyi Biotec GmbH waren:
Dr. Andreas Bosio und Dr. Melanie Jungblut.